HIGH TEMPERATURE (800° TO 1600° F) MAGNETIC MATERIALS

by P. E. Kueser, K. Detert, J. W. Toth, and R. J. Towner

Prepared by
WESTINGHOUSE ELECTRIC CORPORATION
Lima, Ohio
for Lewis Research Center

NATIONAL AERONAUTICS AND SPACE ADMINISTRATION • WASHINGTON, D. C. • MARCH 1970

1. Report No. NASA CR-1460	2. Government Accession No.	3. Recipient's Catalog No.
4. Title and Subtitle HIGH TEMPERATURE (800° TO 1600° F) MAGNETIC MATERIALS		5. Report Date March 1970 6. Performing Organization Code
7. Author(s) P. E. Kueser, K. Detert, J. W. Toth, and R. J. Towner		8. Performing Organization Report No. WAED 67.34E
9. Performing Organization Name and Address Westinghouse Electric Corporation Lima, Ohio		10. Work Unit No. 11. Contract or Grant No. NAS 3-6465
12. Sponsoring Agency Name and Address National Aeronautics and Space Administration Washington, D. C. 20546		13. Type of Report and Period Covered Contractor Report 14. Sponsoring Agency Code

15. Supplementary Notes

16. Abstract

An experimental investigation was performed to improve the performance of magnetic materials suitable for application in advanced rotating machinery. Four major areas were investigated: (1) Precipitation hardened magnetic materials; (2) Raising the alpha to gamma transformation temperature in cobalt-iron alloys; (3) Dispersion strengthened magnetic materials; and (4) Creep testing of Nivco alloys. The equipment and experimental results and conclusions are presented. Materials are described that are suitable for operation in the 800° to 1600° F range. Comparisons are made between the magnetic properties for the new alloys and existing alloys. Application temperatures for the various materials are summarized.

17. Key Words *(Suggested by Author(s))*	18. Distribution Statement Unclassified - unlimited

19. Security Classif. (of this report)	20. Security Classif. (of this page)	21. No. of Pages	22. Price*
Unclassified	Unclassified	342	$3.00

*For sale by the Clearinghouse for Federal Scientific and Technical Information Springfield, Virginia 22151

Distribution of this report is provided in the interest of information exchange. Responsibility for the contents resides in the author or organization that prepared it.

FOREWORD

The work described herein was done by the Westinghouse Electric Corporation under NASA contract NAS 3-6465. Mr. R. A. Lindberg of the Space Power Systems Division of the Lewis Research Center was the Project Manager for the program. The report was originally issued as Westinghouse report WAED 67.34E

The Westinghouse Electric Corporation Aerospace Electrical Division (WAED) performed the work reported in section IV and was responsible for the overall technical direction of the program. The Westinghouse Research and Development Center (WR&D) performed the work reported in sections II, III, and V. Mr. P. E. Kueser, Manager, Materials Development, (WAED) was the Program Manager.

In a program of this magnitude, a large group of engineers and scientists is involved. The principal investigators and the sections of the report in which their work is reported are as follows:

Section II - Optimized Precipitation Hardened Magnetic Alloys for Application in the 1000° to 1200° F Range: Dr. K. Detert (WR&D); J. W. Toth (WAED).

Section III - Investigation for Raising the Alpha to Gamma Transformation Temperature in Iron-Cobalt Alloys: Dr. K. Detert (WR&D); J. W. Toth (WAED).

Section IV - Dispersion-Strengthened Magnetic Materials for Application in the 1200° to 1600° F Range: Dr. R. J. Towner (WAED).

Section V - Vacuum Creep Test of Nivco Alloy: M. Spewock (WR&D); D. H. Lane (WAED).

Other contributors and consultants who actively participated in this project are the following: from WAED, Dr. A. C. Beiler (consultant), Dr. D. M. Pavlovic, H. W. Banks, and R. P. Shumate; from WR&D, Dr. G. W. Wiener (consultant), Dr. D. M. Moon, Dr. R. Stickler, B. M. Ballough, R. B. Hewlett, and E. H. Van Antwerp.

TABLE OF CONTENTS

TABLE OF CONTENTS - CONTINUED

TABLE OF CONTENTS - CONTINUED

TABLE OF CONTENTS - CONTINUED

TABLE OF CONTENTS - CONCLUDED

LIST OF FIGURES

LIST OF FIGURES - CONTINUED

LIST OF TABLES

LIST OF TABLES - CONTINUED

LIST OF TABLES - CONCLUDED

SECTION I

INTRODUCTION AND SUMMARY

This topical report presents the results of work accomplished on one portion of the program conducted under NASA contract NAS3-6465 concerned with the Development and Evaluation of Magnetic and Electrical Materials Capable of Operating in the 800° to 1600°F Temperature Range. The contract comprises three parts as follows:

Program I - Magnetic Materials for High Temperature Operation.

Program II - High Temperature Capacitor Feasibility.

Program III- Bore Seal Development and Combined Material Investigation Under a Space Simulated Environment.

This report is one of three reports prepared under contract NAS3-6465. The others are High Temperature Capacitor Topical Report (WAED 67.24E) and Bore Seal and High Temperature Electrical Materials and Components Endurance Test Topical Report (WAED 67.46E).

Program I, the subject of this topical report, is directed toward the improvement and further understanding of magnetic materials suitable for application in the rotor of a generator or motor in advanced space electric power systems.

This topical report is divided into four technical discussion sections representing four areas of investigation.

Section II - Precipitation Hardened Magnetic Materials for Application in the 1000° to 1200°F Range.

Section III - Investigation for Raising the Alpha to Gamma Transformation Temperature in Cobalt-Iron Alloys.

Section IV - Dispersion Strengthened Magnetic Materials for Application in the 1200° to 1600°F Range.

Section V - Creep Testing of Nivco Alloy.

Each section includes a discussion of equipment and experimental procedures utilized during that particular investigation, a pre-
References are listed in Section VI of this report and are numbered chronologically for each technical discussion section (program task).

The appendix contains procurement information for the Nivco alloy used in the work described in section V.

The investigation reported in section II is concerned with precipitation hardened magnetic materials in the 1000° to 1200°F range. Two areas of specific interest are alloys from the iron and cobalt corners of the ternary iron-cobalt-nickel-system.

The objective of this investigation is to find and evaluate an alloy composition that displays high-creep strength at elevated temperature as well as useful ferromagnetic properties. The target tensile strength for the alloy at 1100°F is 125,000 psi or higher. The target stress to produce 0.4 percent creep strain in 1000 hours at 1100°F is 76,000 psi or greater. The target magnetic saturation for the developmental alloy is 13,000 gauss or better at 1100°F.

Section III presents the results of a limited investigation for determining the feasibility of raising the alpha to gamma transformation temperatures in the iron-cobalt system; thereby increasing the useful magnetic applications temperature of the system.

Section IV reports on an investigation to determine the feasibility of applying the dispersion-strengthening mechanism to magnetic materials and then to achieve useful mechanical and magnetic properties in the 1200° to 1600°F range. Because these properties are influenced differently by dispersoid particle size and spacing, a compromise is sought which will accommodate the requirements of high-temperature dynamic electric machines.

The objective of this investigation is to develop a dispersion-strengthened magnetically soft material for use in the 1200° to 1600°F temperature range for rotor applications. As a goal, the material should have the following properties at a temperature in the range of 1200° to 1600°F preferably at the upper end of the range:

Magnetic Saturation - 12,000 gauss, minimum

Coercive Force - 25 oersteds, maximum

Creep Strain in 10,000
hours at 10,000 psi - 0.4 percent, maximum

Section V presents the results of a creep program on Nivco alloy which generated 10,000-hour data in a vacuum environment (less than 1×10^{-6} torr). Nivco alloy (72% cobalt, 23% nickel, and certain other elements) is a presently available material having the highest useful application temperature for stressed magnetic applications.

The high-strength magnetic materials discussed in this report are suitable for operation in the 800° to 1600°F range. In determining the applicability of the new alloys identified, a comparison between existing alloys is of interest. Figure I-1 compares the 10,000-hour creep properties of three experimental alloys from Larson-Miller extrapolations with two commercially available alloys which are H-11 (5Cr-1Mo-1V-Fe) and Nivco alloy (Co-23Ni-1.7Ti-0.4Al-0.2Zr). For the same stress, the experimental precipitation hardened (PH) martensitic alloy 1-A-S-2 (Fe-12Ni-30Co-1W-3Ta-0.4Al-0.4Ti) has higher temperature capabilities than the H-11 and is a logical replacement. The same is true of the precipitation hardened cobalt-base alloy 1-B-S-1 (Co-5Fe-15Ni-1.25Al-5.0Ta-0.2Zr) which has greatly improved creep resistance over that exhibited by Nivco alloy.

The dispersion strengthened (DS) alloys of either cobalt-iron or cobalt are shown as an area on the curve, and their preliminary data suggests that they are candidates above 1200°F where precipitation hardened cobalt-base rotor material becomes marginal in long-term stability.

A comparison of the magnetic induction of the various magnetic materials is shown in figure I-2. It shows that a magnetic induction improvement is available in both of the new precipitation hardened alloys 1-A-S-2 and 1-B-S-1 over that found in H-11 and Nivco alloy. It also indicates the magnetic induction possible in alloys strengthened by dispersion-strengthened mechanisms. These alloys exhibit very good magnetic properties because the non-magnetic strengthening phase is minimized. They are limited to higher temperature (>1200°F) because their rate of increasing strength with decreasing temperature is lower than the precipitation hardened alloys which are stronger at the lower temperatures.

In applying these materials to a wide variety of high-temperature designs, a number of tradeoffs are followed which necessitate quite complicated geometric programing using a computer. This was beyond the scope of this program, but an attempt has been made to identify application temperatures for various materials based upon a general observation in the design of high-temperature inductor alternators where creep resistance and magnetic induction, in that order, set the weight of a generator. Electric motors or lower-stressed magnetic applications may alter this observation. Table I-1 presents the suggested magnetic material for various temperatures and includes the present commercial material suitable for this range. The advantage of the newer, replacement alloy is summarized in a remarks column.

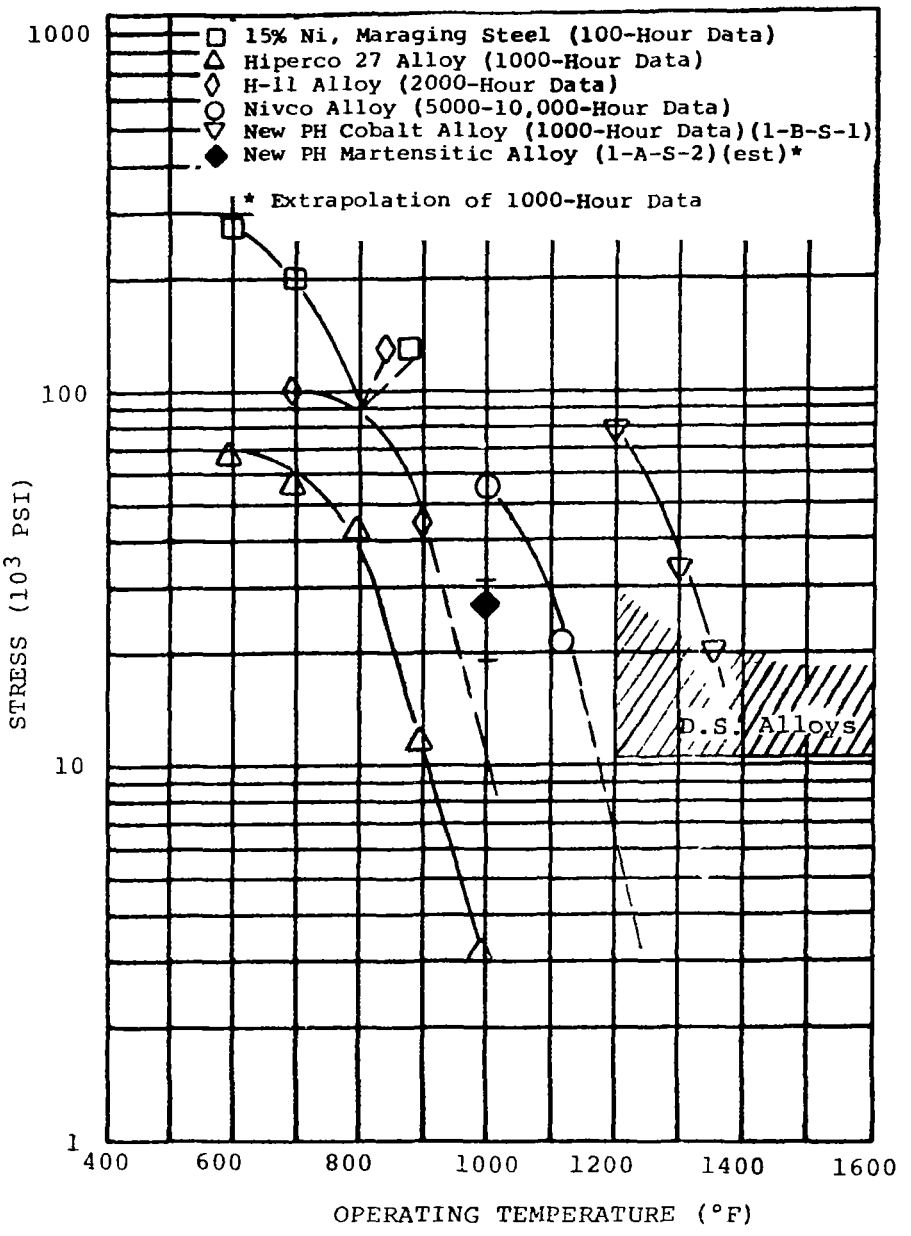

FIGURE I-1. Stress to Produce 0.4 Percent Creep Strain in 10,000 Hours Based Upon Extrapolations Using the Larson-Miller Parameter

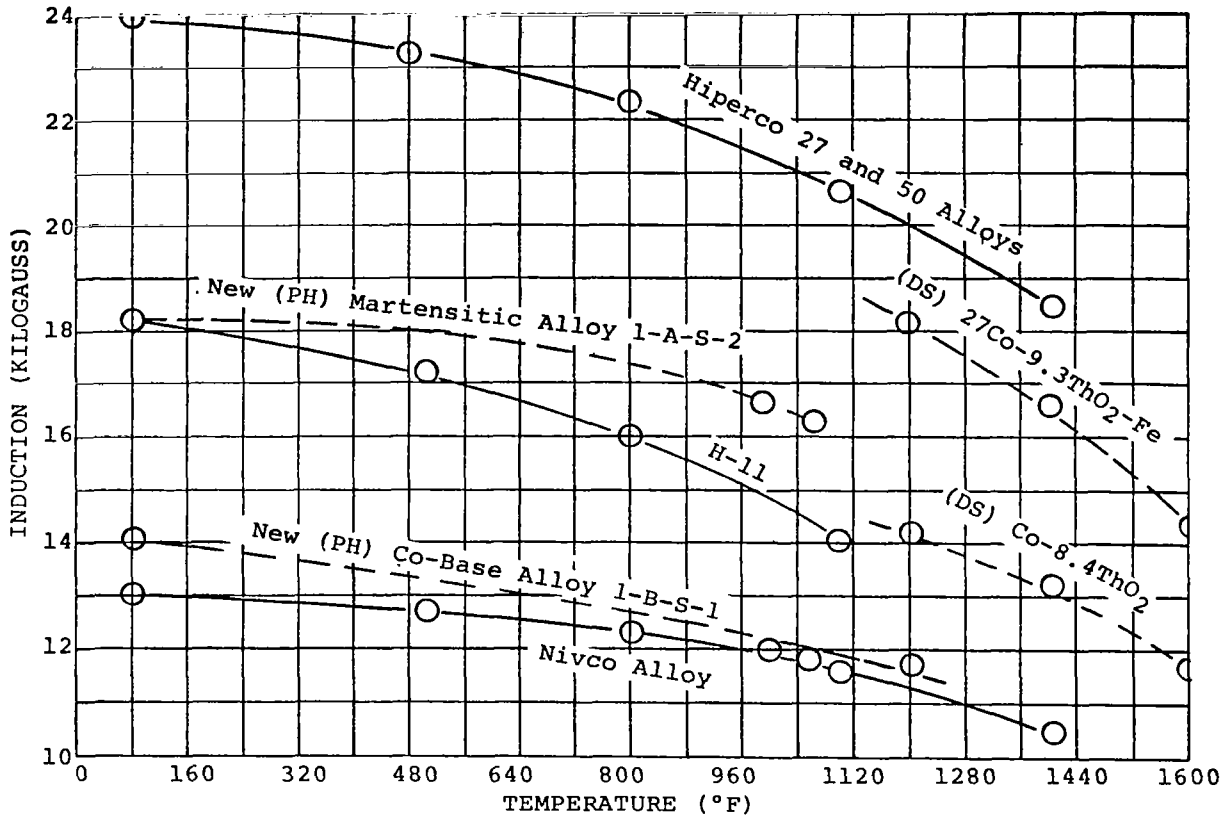

FIGURE I-2. Magnetic Induction Versus Temperature at a Magnetization of 250 to 300 Oersteds for High Temperature Magnetic Alloy Developed on this Program Compared to Existing Alloys

TABLE I-1. Application Temperatures for Potential High Temperature Rotor Magnetic Materials

Temperature Range (°F)	Existing Commercial Material	Alloys Evaluated	Remarks
800 to 1000	H-11 (Fe-5Cr-1Mo-1V)	1-A-S-2 (Fe-12Ni-30Co-1W-3Ta-0.4Al-0.4Ti)	Improved Electrical Overload Capability, Higher Creep Resistance, Better Stability
1000 to 1200	Nivco Alloy (Co-23Ni-1.7Ti-0.4Al-0.2Zr)	1-B-S-1 (Co-5Fe-15Ni-1.25Al-5Ta-0.2Zr)	Greatly Improved Creep Resistance, Better Stability
1200 to 1350	None	DS 27Co-9.3 ThO_2-Fe	Provides a High-Temperature, Stable Material Not Now Available
1350 to 1600	None	DS 8.4ThO_2-Co	Provides a High-Temperature, Stable Material Not Now Available

SECTION II

OPTIMIZED PRECIPITATION HARDENED MAGNETIC ALLOYS FOR APPLICATION IN THE 1000° TO 1200°F RANGE

By K. Detert

A. INTRODUCTION

The objective of this effort was to find and evaluate an alloy composition which displays high-creep strength as well as useful ferromagnetic properties in the temperature range of 1000° to 1200°F. The target tensile strength for the alloy at 1100°F is 125,000 psi or better. The target stress to produce 0.4 percent creep strain in 1000 hours at 1100°F is 76,000 psi or greater. The 10,000-hour stress target for 0.4 percent total creep strain at 1100°F is 80 to 90 percent of that at 1000 hours. The target magnetic saturation for the developmental alloy is 13,000 gauss or better at 1100°F and a coercive force less than 25 oersteds.

Alloys in the iron and cobalt corners of the Fe-Co-Ni system were investigated on this program. Ternary alloy compositions in these areas should have the best magnetic properties. Certain elements were added to the iron and cobalt base alloys to produce precipitation hardening in each system. Details of melting practices and test methods used during this program are described in later sections.

A screening program of a variety of alloy compositions was conducted as the first step in attaining this goal. The purpose of the screening program was to find a certain region of alloy composition where an optimum combination of high strength and magnetic saturation, low coercivity, and stability of structure during exposure at temperature could be attained. Hardness tests, coercivity measurements and saturation measurements, after a suitable heat treatment, and dilatometer tests were made to provide the data for the properties and thermal stability of the structure.

As a second phase in the screening program, six alloys of the ferritic type and six of the cobalt-base type were prepared in a larger button size of ~300 grams. These alloys were melted and tested to confirm the results of the screening program, define the suitable range of alloy composition within narrow limits, and extend the measurements of mechanical and magnetic properties.

In the final phase of the program, two ferritic alloy compositions and two cobalt-base compositions were selected and vacuum-induction melted in the form of 15-pound ingots. Hardness, coercivity and saturation measurements were conducted which verified the results obtained on previous tests. Then creep tests, ac and dc

magnetic tests and a kinetics study, were conducted on samples of the ingots and the final evaluations were made.

Two general areas of basic alloy composition are regarded as the most promising for providing alloys with the desired properties. First, body-centered ferritic alloys of iron and cobalt containing additional alloying elements for strengthening by a precipitation hardening mechanism. Second, cobalt-base alloys with alloying additions to obtain precipitation strengthening. The basic composition must provide magnetic saturation which is still adequate between 1000° and 1200°F. The known data in literature which are best reviewed in Bozorth, Ferromagnetism (ref. II-1)[1], were considered in the selection of the two areas of interest:

1) a ferritic or martensitic iron-cobalt alloy

2) a cobalt alloy

Iron-cobalt alloys with cobalt between 30 and 50 percent appear to be the most suitable insofar as a high value of magnetization is concerned. The magnetization dependence of iron-cobalt compositions on the cobalt content is plotted in figure II-1 from data remeasured at the Westinghouse Laboratories. The values differ slightly from earlier results published in the literature (refs. II-2, II-3, and II-4). These differences are discussed and resolved in section III of this topical report. Although peak room temperature magnetic saturation is attained at 30 percent cobalt and the 1112°F (600°C) magnetic saturation at 30 to 40 percent cobalt, it was believed desirable to hold the cobalt content well below 30 percent to avoid embrittling effects. For a similar reason, compositions in which phase transformation results in a hexagonal phase, as in pure cobalt, must be avoided. This may be accomplished by the addition of at least five weight percent iron.

The basic alloy compositions which provide the required magnetic saturation at service temperature do not possess the required strength. Therefore, suitable alloying elements must be added to provide a useful precipitation hardening reaction. R. F. Decker recently presented a review of potent precipitation hardening reactions in high temperature alloys and in steel (refs. II-5 and II-6). It is generally accepted that a precipitation process involving intermetallic compounds is preferred to carbide formation when stability at temperature is required. Of all known precipitation phases which occur, only precipitation of an A_3B phase appears to lead to a potent precipitation strengthening process.

This process, however, never occurs in ferritic iron-cobalt or in face-centered cubic cobalt alloys unless a substantial amount of nickel is present.

[1] References are listed separately for each section of this topical report in section VI.

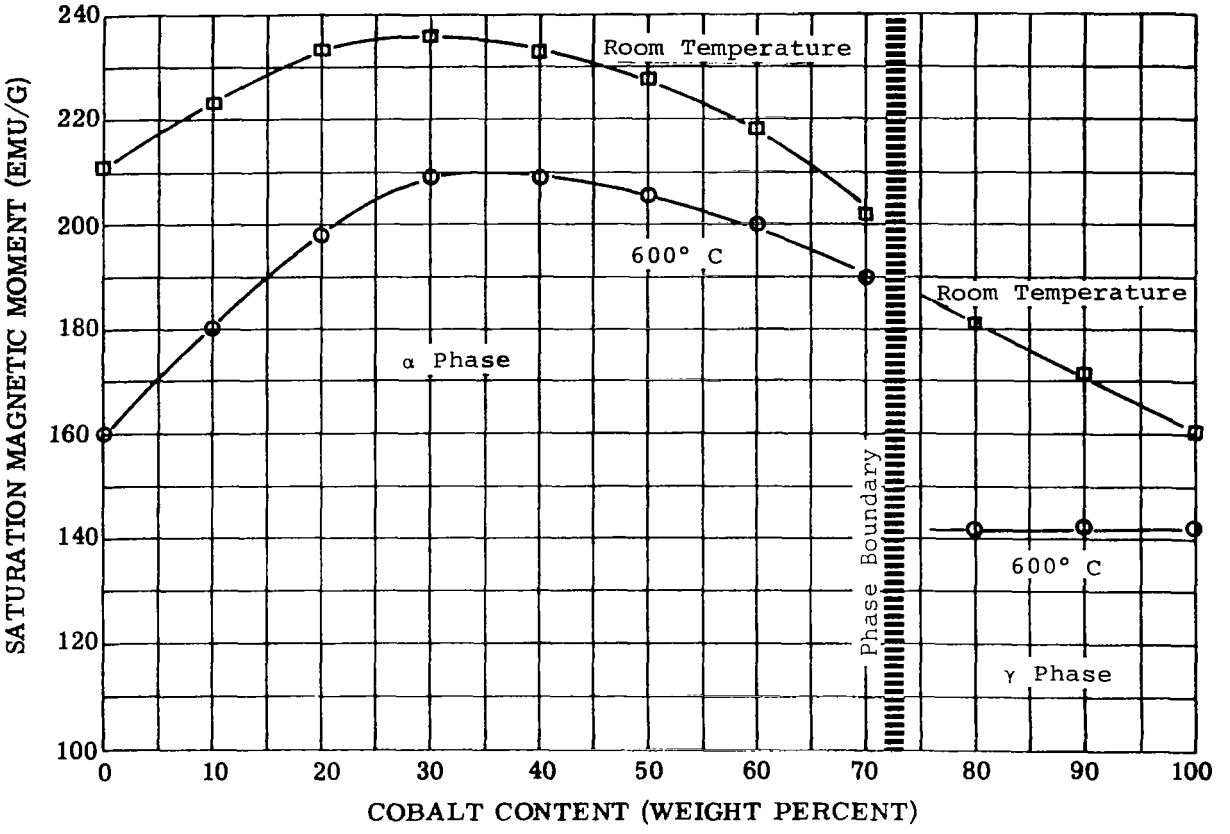

FIGURE II-1. Influence of Cobalt Content on the Saturation Magnetic Moment in the Iron-Cobalt System

In the ferritic alloys, the maraging treatment produces high strength. This treatment also requires the presence of a certain amount of nickel in the alloy. It has been shown that martensitic alloys containing between 12 and 15 percent nickel respond to the maraging treatment, providing very high strength and good toughness (refs. II-7, II-8, II-9, and II-10). The limitation of the commercial maraging steels, with regard to service temperature, is caused by the instability of the parent phase which reverts to austenite at temperatures exceeding 662° to 932°F (350° to 500°C) depending on alloy composition. This results in the loss of magnetic properties and a decrease in strength (ref. II-11). One goal of the screening program conducted during initial phase of this program was to find a suitable Fe-Co alloy composition which responded to the maraging treatment and maintained sufficient temperature stability of the alpha phase. Stated more specifically, the purpose of the screening program was to select a ferritic composition fulfilling the following requirements:

1) High magnetic saturation (B_s) at the service temperature ($B_s \geq 13{,}000$ gauss.) Or, since saturation magnetic moments (σ) was more readily measured on small specimens, $\sigma \geq 130$ emu/gram at 1112°F (600°C).

2) The alpha to gamma transformation should start during slow heating ($\leq$90°F(50°C)/min) above 1112°F (600°C).

3) A precipitation reaction occurs such that a hardness of more than 500 VHN can be achieved during aging at 1022°F (550°C) to 1112°F (600°C).

A large variety of cobalt base alloys have been developed as high temperature materials (refs. II-12 and II-13). These alloys are either non-magnetic or have very poor magnetic saturation although the range of service temperature might be well above the 1022° to 1202°F (550° to 650°C) range. A few investigations have been made to study precipitation hardening in ferromagnetic alloys (refs. II-13, II-14, II-15, and II-16). It appears that one can expect very potent precipitation hardening in cobalt-base alloys only when a face centered cubic phase in the form A_3B is formed (ref. II-6). This again requires a substantial amount of nickel present. To obtain good creep strength, discontinuous precipitation, which will be favored in cobalt-base alloys (refs. II-16 and II-17), must be avoided.

The first step in the screening of the cobalt-base alloys was a study of the influence of iron and nickel on the saturation of binary cobalt alloys. The purpose of the screening program was to select a cobalt-base composition fulfilling the following requirements.

1) Magnetic saturation (B_s) at 1100°F ($B_s \geq 11{,}000$ gauss), or saturation magnetic moment (σ) equal to or greater than 100 emu/gram at 1100°F.

2) A minimum hardness of 350 VHN

3) No discontinuous precipitate forms after 100 hours aging at 1292°F (750°C)

The screening of cobalt-base alloys was carried on simultaneously with the screening of the martensitic type alloy. During the first phase of the program, a total of more than 100 alloy compositions were melted by the levitation melting technique. The ingots cast by this technique were small; therefore, complete evaluation of mechanical and magnetic properties were not attempted. However, a number of simple tests which could be performed on very small specimens were adequate for the screening of alloys. The coercive force and magnetic saturation were measured on the levitation melted samples and were sufficient

for characterizing magnetic properties. The magnetic saturation measurements were made at room temperature and at 1112°F (600°C). Coercivity tests were made only at room temperature. In most cases coercivity will be less at higher test temperatures than at room temperature. Table II-1 shows a comparison of saturation, coercive force and induction at 100 oersteds for several commercially available alloys. These alloys have been the prime candidates for rotor applications in high temperature alternators.

If, in the course of testing new alloys on the screening program, higher values of magnetic saturation and lower values of coercivity are determined, then the permeability of the new alloy will be better than that listed for the commercial alloys in table II-1.

Unfortunately, there exists no simple method of testing to predict creep properties, for creep strength is a very complex property. High yield stress is a desirable though insufficient requirement for high creep strength. Hardness measurements allow prediction of yield strength within certain limits.

In order to obtain a high yield strength, precipitation hardening was evaluated on this project. Isochronal aging with successively increasing increments in temperature was used to determine whether age-hardening by a precipitation reaction occurred in a specific alloy. After a homogenization annealing treatment, the

TABLE II-1. Magnetic Properties of Several High Strength Commercial Alloys

Material	Test Temperature	Induction at 100 Oersteds (gauss)	Coercivity (oersteds)	Saturation (gauss)	Hardness (VHN)
H-11 (Fe-5Cr-1.3Mo-0.5V-0.40C)	Room	16,400	23.9	18,000	560
	792°F(425°C)	14,800	18.4	15,000	
	1112°F(600°C)(a)	12,500	14.1	13,500	
15% Ni Maraging Steel (Fe-9Co-5Mo-0.70Ti-0.70Al-15Ni)	Room	16,500	22.6	18,500	580
	792°F(425°C)	14,400	19.6	15,800	
	1112°F(600°C)(b)	10,000	38.1	13,000	
Nivco Alloy (Co-23Ni-1Zr-2Ti)	Room	10,800	11.46	12,500	360
	792°F(425°C)	10,200	8.43	12,000	
	1112°F(600°C)	9,800	6.31	11,000	

(a) - Carbide precipitate not stable at 600°C.
(b) - Matrix not stable at 600°C.

samples were aged for one hour at a temperature which was increased by 90°F (50°C) increments after each aging step. The room temperature Vickers hardness was measured after each aging step. A plot of hardness as a function of aging temperature was made. If precipitation hardening does occur in a particular alloy, a maximum hardness will be obtained. The temperature at which maximum hardness occurs represents a suitable range for age hardening that alloy. The maximum hardness value obtained represents the level of strength which may be achieved in the alloy.

If creep strength at a certain temperature is desired, a second requirement is that the age-hardened structure must remain essentially stable. It is possible to estimate the temperature range where structural stability can be expected by determining the temperature where overaging occurs. Overaging is a definite indication that the structure is changing. In many cases the temperature range at which overaging is likely to occur is somewhat higher than the temperature range of maximum hardness determined by the isochronal testing method. However, many instances are known in which a decrease in yield strength occurs at a very low or negligible rate after initial rearrangement of the metallurgical structure. A better indication of the rate of overaging may be obtained by isothermal aging at a specified temperature.

Isothermal aging was also applied to alloy specimens on this program. Specimens were aged at a constant temperature at varying periods of time. The time intervals were chosen to approximate a logarithmic sequence. Vickers pyramid hardness was measured at room temperature after each isothermal aging period. The maximum hardness was often attained in the initial stages of aging.

The hardness when plotted on a logarithmic scale may be extrapolated to indicate the decrease of hardness at time intervals beyond the measured periods. However, the extrapolated values may be considered reliable estimates only for time periods which are no more than 10 times larger than the measured periods. Coercivity, as a structure sensitive property will also be influenced by the change of structure during overaging. Therefore, coercivity was measured during the aging schedules. In most cases, overaging is caused by coagulation of precipitate particles. However, it may also be caused, in some instances as in maraging steel, by a diffusion controlled decomposition of the ground matrix when phase transformation is to be expected. A dilatometer test was applied to establish the temperature range of a possible phase transformation. By heating at a rather slow rate during the dilatometer test, a good estimate of the transformation temperature may be obtained even when the transformation reaction is very sluggish.

B. EXPERIMENTAL PROCEDURE AND TESTING

1. Levitation Melting

The experimental screening alloys were prepared by the levitation melting technique. In general, a cylindrical compaction was made about 5/8-inch diameter and 3/4-inch high with a weight of 20 to 25 grams. A pressure of 220,000 psi was applied for one minute. Very small chips of electrolytic grade nickel, cobalt, and iron were used. Table II-2 lists the metals used according to supplier, trade name, and the supplier analysis. The alloying elements present in smaller percentages were added as small chips tightly wrapped in cobalt or nickel foil. The small wrapped package was inserted in the center of the compaction.

The levitation melting was performed in a chamber which was first pumped down to less than 10^{-2} torr, then back-filled with pure argon (10 ppm O_2 max., 5 ppm H_2, 40 ppm H_2; -85°F dew point) to a pressure of about 700 mm mercury. The levitation melting technique was recently described in detail by W. A. Pfeifer (ref. II-18). For this study a funnel-shaped coil of five windings was used. The frequency was in the range of 550 kilocycles, the input energy in the range of 3 to 5 kilowatts, and the operating voltage was near 750 volts.

The procedure for melting consisted of heating the compactions to the melting temperature within 60 seconds. After five more seconds, the entire surface appeared molten. The sample was kept in the molten state for eight seconds. During this period, the temperature increased further; an indication that the sample was completely molten. Then the molten mass was dropped into a copper mold which was positioned beneath the coil. The mold was slightly tapered to provide a bar-shaped ingot with a 9/32-inch diameter on one end and 5/16-inch diameter on the upper end. The ingot was 1-7/8 inches long.

The cast structure always showed a homogeneous phase as shown in a typical photograph in figure II-2. A dendritic growth from the outside wall into the center may be noted. The appearance of rather large dendritic growth even after casting in a cold mold proves that the purity and homogenity of the material was very good.

A fraction of the added elements with higher vapor pressure such as manganese, chromium, and those with activity toward oxygen such as aluminum, titanium and beryllium, may be lost during melting. The method of compaction and the use of inert gas provided some protection against evaporation and

TABLE II-2. Analyses of Metals Used in Experimental Alloys (weight percent)

Material	Supplier	Designation	Fe	Co	Ni	Be	V	Ti
Iron [a]	The Glidden Co.	Electrolytic Iron Alloy	99.9	0.002	0.005	0.0005		0.001
Cobalt [a]	International Nickel Co.	Electrolytic Cobalt	0.0015	99.61	0.35			
Nickel [a]	International Nickel Co.	Electrolytic Nickel	0.04		99.95			
Beryllium [b]	Brush Beryllium Co.	Beryllium Pebbles				95		
Titanium [b]	Frankel Co.	Titanium Chips	0.25					99.1-99.3
Aluminum [b]	Alcoa	Pure Aluminum Bar	0.05					0.007
Manganese [b]	Foote Mineral Co.	Electrolytic Manganese	0.001					
			Cr	Sn	Sb	Si	Zn	Ge
Chromium [a]	Union Carbide Metals Co.	Elchrome HP	99.94			0.004		
Tin [a]	Fisher Scientific Co.	T-124 Tin Shot		99.9				
Antimony [a]	J. T. Baker Chemical Co.	Assay Sb 100			99.97			
Silicon [a]	Electro-Metallurgical Co.	Silicon Metal Low Al				98.64		
Zinc [a]	Fisher Scientific Co.	Granular Zinc Metal					99.97	
Germanium [b]	Westinghouse Electric Corp.	Semiconductor Grade						99.999
Niobium [a]	Electro-Metallurgical Co.	Roundals						
Tantalum [a]	Electro-Metallurgical Co.	Roundals						

(a) - Lot analysis provided by supplier.
(b) - Typical analysis provided by supplier.

Al	Mn	Si	C	Cu	S	V	H	N	O	Other
0.003	0.001	0.001	0.004	0.001	0.004	0.005				P-0.003
			0.016	0.005	0.001					Pb-0.00026
		Trace	Trace	0.03	Trace					
										Slag 4%
			0.10							Total < 0.6
	0.001	0.04	0.0039	0.011		0.01				Mg-0.002 Ga-0.01
	99.9 min.	Trace	0.004		0.024		0.015 max.	0.001 max.		P-Not detectable Heavy Metals 0.005 max.

Nb	Ta	Fe	C	As	Cu	Pb	H	N	O	Other
		0.004	0.007				0.0003	0.008	0.0089	S-0.006
		0.005		0.00005	0.001	0.020				Total foreign metals 0.05
		0.002		0.004	0.002	0.004				
		0.75								Al-0.05 Ca-0.01
		0.01		0.000001		0.010				
99.6 min.										
	99.6 min.									

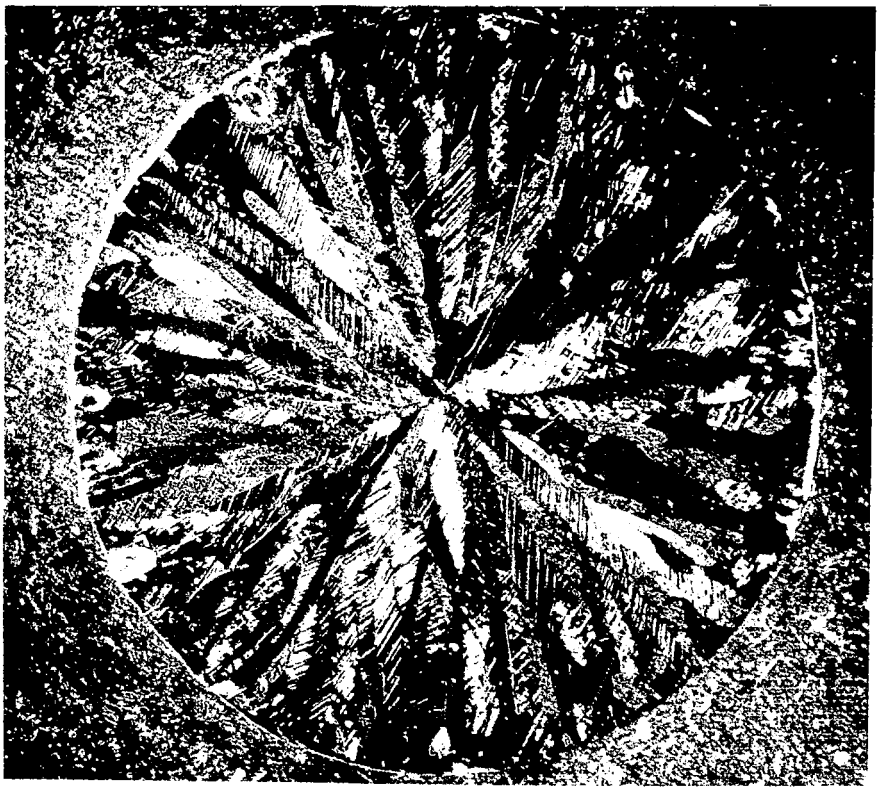

Photograph shows dendritic growth in the levitation melted ingot. The grains contain many twins.

FIGURE II-2. Photograph of As-Cast Structure of Cobalt-Base Alloy 1-B-4 (80Co-5Fe-15Ni) 14X

oxidation. Therefore, it may be expected, based on the experience gained in levitation melting practice, that less than 20 percent of the total amount of these elements would be lost during the melting procedure.

In a few cases when difficulties were encountered in cold rolling, master alloys were used in levitation melting the experimental alloys. The compositions of the master alloys, as specified by the supplier are given in table II-3. Analysis to determine the actual amount of alloying constituents in the melted ingots were not performed on the screening program. However, analyses were performed when selection of the better alloys were made later in the program.

TABLE II-3. Composition of Master Alloys[a] (weight percent)

Material Designation	Supplier	Fe	B	Nb	V	Si	Cr	Ti	W	Mo	Be	Ni	Al	C	P	S	Sn	Other
Ferro Boron Lot 20-150	Reading Alloys Inc.	Bal	18.54										0.52					
Ferro Columbium Lot 20-106	Reading Alloys Inc.	Bal		68.6		1.50		0.55					0.46	0.057	0.031	0.017	0.009	Mn-0.37 Ta-0.10
Ferro Vanadium Lot 20-106	Reading Alloys Inc.	Bal			52.71	1.11							0.38	0.11	0.03	0.03		
50% Ferrosilicon (Low aluminum)	Union Carbide Corp.	Bal				50.96							0.08					
Ferrochrome (Low carbon)	Union Carbide Corp.	Bal				0.23	72.53							0.019				
70% Ferrotitanium	Union Carbide Corp.	Bal				0.04		65.97					3.68	0.05				
Ucar Ferrotungsten	Union Carbide Corp.	Bal				0.02			79.84	0.01					<0.01		<0.01	Cu-0.02 Mn-0.05
Nickel Columbium Lot 20-140	Reading Alloys Inc.	0.43		59.8		0.22						39.18	0.21	0.034	0.028	0.009	<0.003	Ta-0.1
Nickel Molybdenum Lot 20-161	Reading Alloys Inc.	0.88				0.48				66.26		31.18	0.33	0.039				Cu-<0.01 Pb-<0.01
Beryllium Nickel	Brush Beryllium Co.	<0.12				<0.07					8-12%	Bal	<0.07	<0.2				

(a) Composition reported by the supplier.

2. Saturation Measurements

Specimens for saturation measurements were machined from the levitation-melted ingots. The specimens were 1/10 inch in diameter and 1/10 inch high.

Saturation was measured in a magnetic field with a gradient of 980 oersteds per centimeter. The mean values of the applied field was on the order of 10,000 oersteds. The accuracy was within one percent. For measuring the saturation at high temperature, a small electric resistance furnace was placed into the gap of the magnet which was double wound to avoid any additional field by the electric current passing through the windings. This technique reduced the residual field below 100 millioersteds. The measured saturation values are presented in this report as magnetic moment per gram (σ) which may be converted to the approximate saturation induction (B_S) by the equation

$$B_S = 4\pi\sigma\delta$$

The density δ was not determined for the experimental alloys. A value of 8g/cc was used for the density of the ferritic alloys and a density of 8.8g/cc was used for the cobalt-base alloys.

3. Dilatometer Tests (Transformation Temperature)

Dilatometer samples were machined to bars 1/4-inch in diameter and one inch long. A drilled hole was provided in the dilatometer specimens for thermocouple placement.

The dilatometer tests were made under high-purity argon by heating to 1832°F (1000°C), then cooling while recording the change in length at temperature. The heating rates applied were 90°F/min (50°C/min) or 1.8 to 3.6°F/min (1 to 2°C/min). The cooling rates were 90°F/min (50°C/min) or 9°F/min (5°C/min).

The beginning and end of a noticeable deviation in the slope of the thermal expansion curves were recorded at the beginning and end of transformation.

4. Aging Tests, Coercivity and Hardness Measurements

After dilatometer tests were performed, on the ferritic alloys, the cast rod samples were cold rolled (~50% reduction) on a two-high mill with eight-inch diameter rolls at a speed of one inch per second. The 95-mil-thick strips were used for the aging, hardness, and coercivity tests.

The ferritic alloy samples were homogenized and austenitized in an argon flushed tube furnace at 1832°F (1000°C) for 30 minutes. Then the samples underwent isochronal anneal as follows. The samples were held for one hour at temperature with intermittent increases of 90°F (50°C) between 842°F (450°C) and 1202°F (650°C). A flow chart for isochronal aging the ferritic alloys is shown in figure II-3. Aging at each temperature was performed in a salt bath using a neutral blend of alkali nitrates and nitrides at the lower temperatures and alkali or alkaline chlorides at the highest temperatures. (See table II-4 for details.) The furnace temperature was controlled within ± 9°F (±5°C). Room temperature hardness and coercive force were measured after each aging interval. The cobalt-base alloys were subjected to the isochronal aging sequence at slightly higher temperature intervals; the lowest aging temperature was 932°F (500°C) and the highest was 1382°F (750°C).

After isochronal aging, the samples were homogenized by a heat treatment with a slight (5%) cold reduction between anneals. The change in room temperature hardness and coercive force was measured after isothermal aging at 1022°F (550°C) for the ferritic alloys and at 1292°F (700°C) for the cobalt-base alloys. A flow chart showing the isothermal aging intervals is shown in figure II-4. The total aging time for ferritic and cobalt-base alloys was 100 hours.

TABLE II-4. Type of Salt Bath Used for the Aging Treatments

Temperature of Treatment	Salt Designation (a)	Main Constituents
842° to 1022°F (450° to 550°C)	Thermosalt #311	Blend of Alkali Nitrates and Nitrites
1112° to 1292°F (600° to 700°C)	Thermosalt #914	Ternary Mixture of Alkali and Alkaline Chlorides
1382°F (750°C)	Thermosalt #1018	Eutectic Mixture of Chlorides

(a) Carmac Chemical Company Designation

Vickers pyramid hardness was measured using a 50-kilogram load and a 15-second indentation time. Three indentations were made and the mean value determined. The coercivity was measured in the Koerzimeter made by the Förster Co., Reutlingen, Germany (figure II-5). This instrument is capable of measuring the coercive force of samples with small or unusual geometry. The sample was magnetized in a large field coil, the magnetizing field being 1300 oersteds. After switching off the field, the remanent field of the samples was determined by a very sensitive field probe as seen in figure II-6. A reverse field was then applied, increasing gradually from zero until the field probe did not indicate any remanent field from the sample. The measured value of coercivity was established by four readings. The direction of the applied magnetizing field was reversed between each reading. Coercive force measured by this method was accurate to two percent.

5. Preparation of Vacuum-Arc Melted Buttons

Vacuum-arc melted buttons were prepared for the second stage of the screening program. Three hundred-gram buttons of six cobalt-base and six ferritic type alloys were prepared. Composition limits were based on the evaluation of test results made on the levitation-melted alloys. Buttons were melted in a vacuum-arc furnace with non-consumable tungsten electrodes. Small pieces of the constituent metals and master alloys were placed in copper crucibles. All of the minor additions were added as master alloys. Table II-5 lists the metal and master alloy suppliers and the supplied material analysis.

The vacuum-arc furnace contained a turntable with six copper molds which were about three inches in diameter. These served simultaneously as crucibles for vacuum-arc melting. The furnace was evacuated to a pressure of less than 1×10^{-4} torr and then back-filled with high-purity argon to a pressure of <450 torr and evacuated again. The furnace was back-filled three times in this manner and evacuated to less than 1×10^{-4} torr. Finally, the furnace was back-filled with helium to a pressure of ~200 torr. The first alloy button was melted in about three minutes. The arc current was approximately 600 amps and the operating voltage was 30 volts. After melting six buttons, the furnace was opened and the buttons were inverted. The procedure of evacuating and back-filling was repeated and the buttons were remelted.

In general, the alloy buttons were remelted twice. In a few cases when the bottom of the button did not appear smooth, the buttons were remelted a third time. The 3-inch-diameter by 400-mil-thick buttons were then cleaned by abrasive blasting.

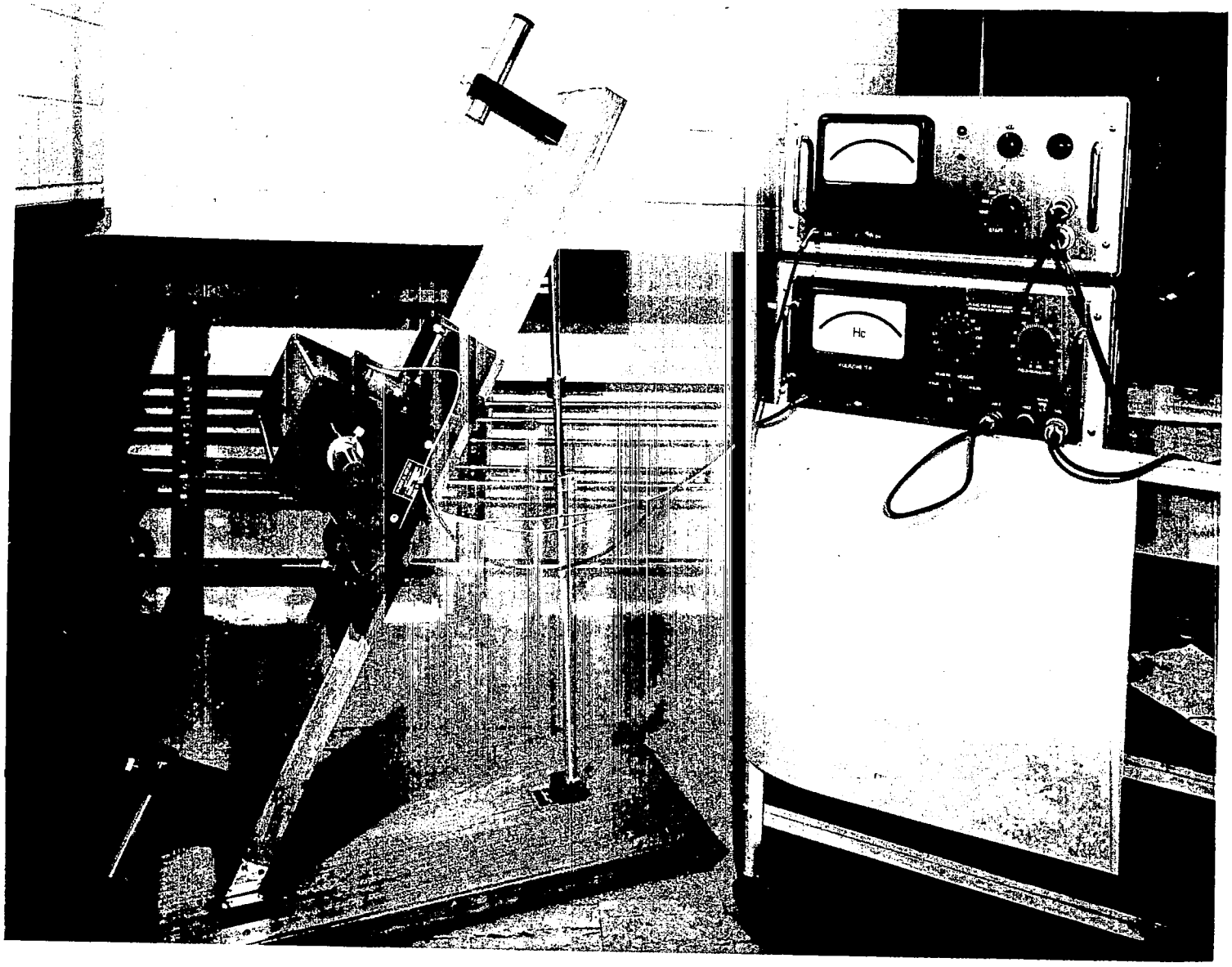

FIGURE II-5. Photograph of the Förster "Koerzimeter"

TABLE II-5. Compositions of Master Alloys Used in the 300-Gram Button Melts (weight percent) (a)

Material Designation	Supplier	Fe	Co	Ni	Ta	Cr	Ti	W	Al	Si	Mn	Cu	P	C	Other
Electrolytic 99.9 Iron	The Gidden Co.	99.9	0.002	0.005			0.001		0.003	0.001	0.001	0.001	0.003	0.004	S -0.004 V -0.005 Be -0.0005
Electrolytic 99.61 Cobalt	International Nickel Co.	0.0015	99.61	0.35								0.005		0.016	S -0.001 Pb -0.00026
Electrolytic 99.95 Nickel	International Nickel Co.	0.04		99.95						Trace		0.03		Trace	S -Trace
Nickel-Tantalum	Union Carbide Corp.	0.15		48.06	51.56				0.40	0.07	0.01			0.01	Nb -0.08
Low Carbon Ferrochrome	Union Carbide Corp.					72.53				0.23				0.019	
Ferrotitanium	Union Carbide Corp.	30.2(b)					65.97		3.68	0.04				0.05	
UCAV Ferro-tungsten	Union Carbide Corp.	20.0(b)						79.84		0.02	0.05	0.02	<0.01	0.04	P -0.01 Sn -<0.01
Nickel Aluminum	Reading Alloys Inc.	0.47		71.11					27.58	0.41					

(a) Analyses reported by supplier

(b) By Difference

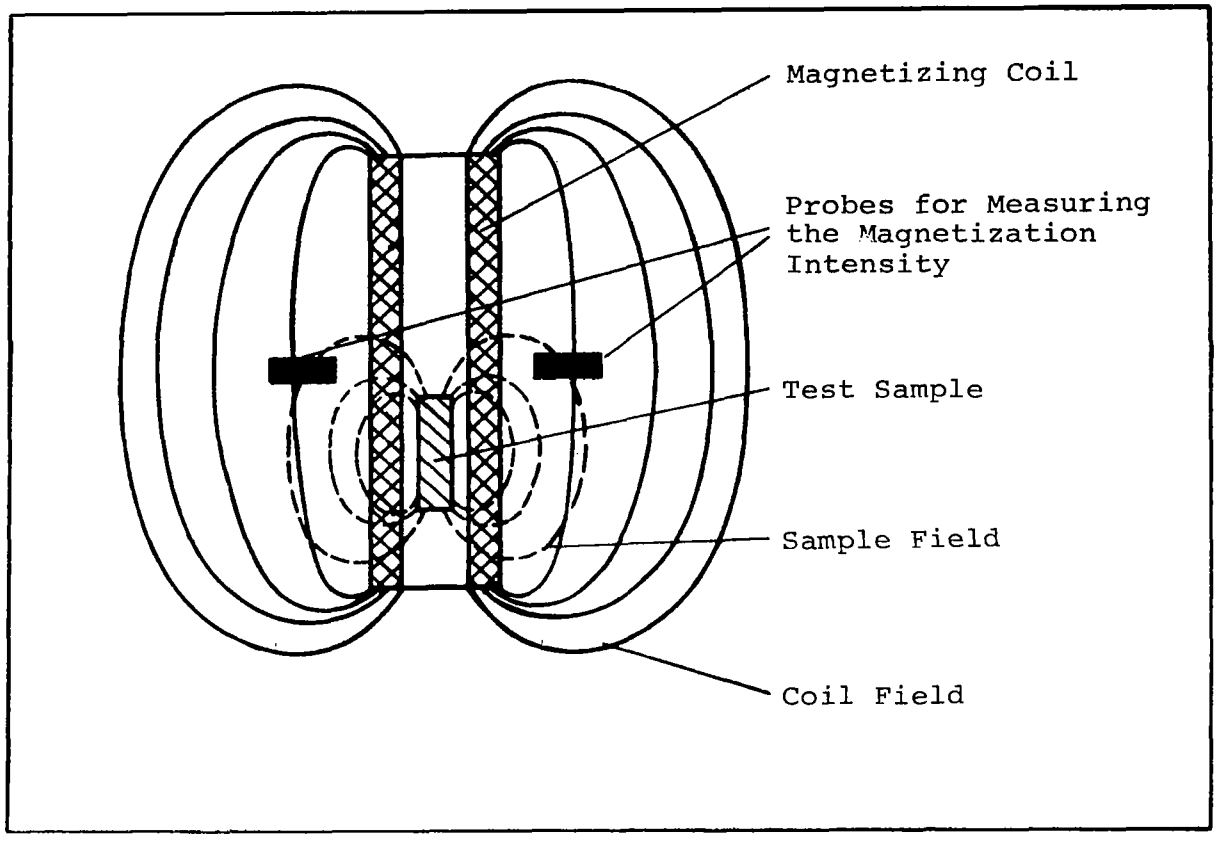

FIGURE II-6. Schematic of Sensitive Field Probe Used in the Coercive Force Meter Showing Coil and Sample Fields

The martensitic alloys were heated for 30 minutes at 1922°F (1050°C), then hot rolled in three passes to a thickness of 150 mils. After each pass, the slabs were put into the furnace for 15 minutes. After hot rolling, the slabs were sandblasted then cold rolled to 65-mil sheet.

The cobalt-base alloys were heated to 2012°F (1100°C) and soaked for one hour then hot rolled in three passes to 140 mils. After each pass the slabs were heated in a furnace for 15 minutes. After hot rolling, the slabs were reheated for 15 minutes at 2012°F (1100°C) and cooled in air. The slabs were then sandblasted and cold rolled to 65-mil sheet.

Samples for saturation measurements, dilatometer tests, hardness and coercivity measurements were prepared and tested in the same manner as the levitation melted alloys previously described. Isochronal and isothermal aging were performed as described previously with one exception. Isochronal aging of the martensitic type alloys was started at 932°F (500°C) instead of the 842°F (450°C) starting temperature applied to the levitation melted samples.

6. Preparation of Vacuum-Induction Melted Ingots

The four alloy compositions for the final evaluation were vacuum induction melted in the form of 15-pound ingots.

The charge used in melting each of two large ferritic alloy ingots weighed 8000 grams and the charge used in each of two cobalt-base alloys weighed 8500 grams. The metals used in the charges correspond to those listed in table II-2. The alloying additions were obtained from master alloys as specified in table II-5.

The alloy melting was started with the Fe-Ni-Co metals in an induction furnace using a heating coil of three windings operating at 10,000 cycles at a nominal 50 kVA. The molten material was held for about one hour at a vacuum of 2×10^{-4} torr, then one gram of Mischmetal was added. After the pressure returned to 2×10^{-4} torr, the furnace was back-filled with high purity argon to a pressure of 280 torr. The alloying elements were added as required. Nickel-zirconium and iron-boron were the last additions. The same magnesium oxide crucible was used for all melts. The alloys were then cast into an iron tube ten inches long with a two-inch inside diameter. The tube, coated with a zirconia wash, was positioned on a copper plate. A funnel shaped from refractory brick was placed on top of the tube. After cooling, the top of the ingots formed in this mold were cut off. After cutting, each ingot weighed 7000 to 7500 grams.

The 2-inch diameter rod-shaped ingots were then used as consumable electrodes in a vacuum-arc furnace at a pressure of 10^{-4} torr. Melting was performed at the rate of one inch per minute using an applied current of 1600 amperes. The mold had a 3-inch inside diameter. A 7-inch long melted ingot was obtained. After cutting the ends off, each ingot weighed 5000 grams. The ingots were machined to give a flaw-free finish. The ingots were placed in a furnace at 2102°F (1150°C) and soaked for one hour, then forged into one by 2-inch bars. The bars were reheated during forging when the temperature cooled below 1832°F (1000°C). After forging, the bars were 17 inches long and weighed 4500 grams

except for alloy 1-B-S-1, which had developed cracks during forging. The end of this bar was cut off. This bar was 11 inches long and weighed 3300 grams.

A 4-inch length of each bar was cut off and heated in an argon-filled retort for one hour at 1922°F (1050°C). The pieces were then hot rolled to 150-mil-thick slabs. The slabs were reheated for 15 minutes after each pass. After the last pass, the samples were soaked for one hour at 1922°F (1050°C) then air cooled. The slabs were then sand-blasted to remove the scale. Samples for magnetic saturation measurements were machined from the hot-rolled slabs. The slabs were then cold-rolled to 70-mil-thick strips and pickled in hydrochloric acid. Samples for hardness and coercive force were taken from these strips.

7. Hot Hardness and Tensile Tests on Samples From Vacuum Induction Melted Ingots

Hot hardness measurements were made at a pressure of 2×10^{-5} torr using a Vickers pyramid indenter. The applied load was 2.5 kG. Samples were held at temperature for one minute after heating to temperature within 15 minutes.

The tensile tests were performed on a hard-beam tensile tester at a strain rate of 5×10^{-5} in/in/sec using flat samples with a gage length of 1-1/4 inches and a cross section of 1/4 inch by 0.050 inch. Sensitivity was estimated at 5×10^{-5} inches strain and 500 psi stress. When measuring at elevated temperatures, the samples were held for 15 minutes at temperature. Test time was about 10 minutes. Annealing was done in helium or argon-flushed tube furnaces. Aging was performed in salt baths as described previously.

8. DC and AC Magnetic Properties

Tests were made on specimens of the final vacuum-induction melted alloys to determine dc and ac properties.

In order to produce the laminations for the magnetic test rings, 70-mil-thick sheet was annealed for one hour at 1922°F (1050°C) in helium and then cross rolled to 44-mil thickness to obtain the required 3-1/2-inch-wide strip. At this stage the martensitic alloy strips were annealed at 1832°F (1000°C) for one hour in a helium atmosphere. The 44-mil strips were then straight-rolled in the original rolling direction to a thickness of 26 mils. The strips were then annealed for one hour at 2012°F (1100°C) in helium and cold rolled to the final thickness of 25 mils. Rings having an outer diameter of three inches and an inner diameter of 2.5 inches were punched from the strip. Nine rings from

martensitic alloy 1-A-S-2 were aged three hours at 1022°F (550°C) in helium before testing. Ten rings punched from the cobalt-base alloy 1-B-S-1 were annealed one hour at 2012°F (1100°C) and aged one hour at 1382°F (750°C) in helium before magnetic testing.

The laminations were stacked and wound with Anadur[2] insulated nickel-clad silver wire. The dc and ac properties were determined according to a modified testing procedure specified in ASTM A341 and A343.

Hardness was measured as the Vickers hardness number under a load of 50 kG. The accuracy was two percent. The coercive force was measured in a Förster "Koerzimeter" as previously outlined (section II.B.4) with an accuracy of two percent. The electric resistivity was measured on strips about 2.5-mm wide, 0.5-mm thick, and 150-mm long by the standard four-blade resistance method. The temperature was kept constant at 77°F (25°C) within ±0.18°F (±0.1°C) by means of a coolant loop and a heater attached to a thermostat. The accuracy in determining specific resistivity was two percent, with the limitation set by the cross section measurements.

C. RESULTS AND EVALUATION

1. Ferritic Alloys

a. SCREENING OF LEVITATION MELTED ALLOYS

More than sixty ferritic alloy compositions were melted and tested on the screening program. The nominal compositions, in weight percent and atomic percent, are shown in table II-6. A series of ternary alloy compositions were melted and tested to determine the best composition range that would provide a matrix with satisfactory magnetic properties, good metallurgical stability and adequate composition for strengthening. Ferritic Alloys 1-A-11 to 1-A-20 were formulated for this purpose. Previous tests had been made on ternary alloys containing 15 weight percent cobalt. Alloys 1-A-1 to 1-A-10 and 1-A-26 to 1-A-61 were formulated to determine the simple and complex addition-element combinations which would produce precipitation hardening in the ferritic alloys. From these alloys, the approximate composition range that would provide a stable alloy with adequate magnetic properties and strength, could be selected. The ferritic

[2] Trade name of the Anaconda Wire and Cable Company.

TABLE II-6. Nominal Composition of Martensitic Alloys Used in the Screening Tests

Alloy Number	Nominal Alloy Composition (weight percent)	Nominal Alloy Composition (atomic percent)
1-A-1	55Fe-15Ni-25Co-5W	58.21Fe-15.10Ni-25.08Co-1.61W
1-A-2	58Fe-15Ni-25Co-2Nb	59.69Fe-14.69Ni-24.38Co-1.24Nb
1-A-3	58Fe-15Ni-25Co-2V	59.05Fe-14.54Ni-24.14Co-2.23V
1-A-4	58Fe-15Ni-25Co-2Cr	59.12Fe-14.54Ni-24.15Co-2.19Cr
1-A-5	59.5Fe-15Ni-25Co-0.5Al	60.41Fe-14.49Ni-24.05Co-1.05Al
1-A-6	58Fe-15Ni-25Co-2Be	53.53Fe-13.17Ni-21.86Co-11.44Be
1-A-6W	59.5Fe-15Ni-25Co-0.5Be	59.17Fe-14.19Ni-23.56Co-3.08Be
1-A-7	58Fe-15Ni-25Co-2Sb	59.87Fe-14.73Ni-24.45Co-0.95Sb
1-A-8	58Fe-15Ni-25Co-2Sn	59.85Fe-14.73Ni-24.45Co-0.97Sn
1-A-9	58Fe-15Ni-25Co-2Si	58.03Fe-14.28Ni-23.71Co-3.98Si
1-A-10	58Fe-15Ni-25Co-2Mn	59.19Fe-14.56Ni-24.18Co-2.07Mn
1-A-11	88Fe-12Ni	88.52Fe-11.48Ni
1-A-12	83Fe-12Ni-5Co	83.71Fe-11.51Ni-4.78Co
1-A-13	78Fe-12Ni-10Co	78.88Fe-11.54Ni-9.58Co
1-A-14	73Fe-12Ni-15Co	74.02Fe-11.57Ni-14.41Co
1-A-15	68Fe-12Ni-20Co	69.13Fe-11.60Ni-19.27Co
1-A-16	63Fe-12Ni-25Co	64.21Fe-11.64Ni-24.15Co
1-A-17	58Fe-12Ni-30Co	59.27Fe-11.67Ni-29.06Co
1-A-18	53Fe-12Ni-35Co	54.31Fe-11.70Ni-33.99Co
1-A-19	48Fe-12Ni-40Co	49.32Fe-11.73Ni-38.95Co
1-A-20	43Fe-12Ni-45Co	44.30Fe-11.76Ni-43.94Co
1-A-26	67Fe-12Ni-20Co-1Ti	68.01Fe-11.58Ni-19.23Co-1.18Ti
1-A-27	63Fe-12Ni-20Co-5Mo	65.43Fe-11.86Ni-19.69Co-3.02Mo
1-A-28	63Fe-12Ni-20Co-5Ta	66.37Fe-12.03Ni-19.97Co-1.63Ta
1-A-29	66Fe-12Ni-20Co-2Nb	67.65Fe-11.70Ni-19.42Co-1.23Nb
1-A-30	66Fe-12Ni-20Co-2W	68.06Fe-11.77Ni-19.54Co-0.63W
1-A-31	67.5Fe-12Ni-20Co-0.5Be	66.85Fe-11.31Ni-18.77Co-3.07Be
1-A-32	67.5Fe-12Ni-20Co-0.5Al	68.25Fe-11.54Ni-19.16Co-1.05Al

TABLE II-6. Nominal Composition of Martensitic Alloys Used in the Screening Tests (Continued)

Alloy Number	Nominal Alloy Composition (weight percent)	Nominal Alloy Composition (atomic percent)
1-A-21	54.5Fe-15Ni-25Co-0.5Ti-5Mo	56.74Fe-14.87Ni-24.69Co-0.67Ti-3.03Mo
1-A-22	54.5Fe-15Ni-25Co-0.5Ti-5Ta	57.61Fe-15.09Ni-25.05Co-0.62Ti-1.63Ta
1-A-23	54.5Fe-15Ni-25Co-0.5Ti-2Mo-3Ta	56Fe-15.22Ni-25.27Co-0.62Ti-1.24Mo-1.65Ta
1-A-24	54Fe-15Ni-25Co-1Nb-5Ta	57.38Fe-15.16Ni-25.18Co-0.64Nb-1.64Ta
1-A-25	52.5Fe-15Ni-25Co-5Ta-2Si-0.5Be	52.99Fe-14.40Ni-23.91Co-1.56Ta-4.01Si-3.13Be
1-A-33	54.4Fe-15Ni-25Co-0.5Be-5Ta-0.1Mn	56.03Fe-14.69Ni-24.40Co-3.19Be-1.59Ta-0.10Mn
1-A-34	53.9Fe-15Ni-25Co-1W-5Ta-0.1Mn	57.46Fe-15.21Ni-25.25Co-0.32W-1.65Ta-0.11Mn
1-A-35	54.4Fe-15Ni-25Co-0.5Al-5Ta-0.1Mn	57.24Fe-15.01Ni-24.93Co-1.09Al-1.62Ta-0.11Mn
1-A-36	53.9Fe-15Ni-25Co-0.5Al-0.5Ti-5Ta-0.1Mn	56.66Fe-15.00Ni-24.91Co-1.09Al-0.61Ti-1.62Ta-0.11Mn
1-A-37	53.9Fe-15Ni-25Co-0.5Al-0.5Ti-2Mo-3Ta-0.1Mn	56.34Fe-14.91Ni-24.76Co-1.08Al-0.61Ti-1.22Mo-0.97Ta-0.11Mn
1-A-43	55Fe-15Ni-25Co-2Mo-3Ta	57.87Fe-15.01Ni-24.92Co-1.23Mo-0.97Ta
1-A-44	53Fe-15Ni-25Co-2Cr-5Ta	56Fe-15.07Ni-25.03Cr-2.27Cr-1.63Ta
1-A-45	57.5Fe-15Ni-25Co-2Cr-0.5Be	57.10Fe-14.17Ni-23.52Co-2.13Cr-3.08Be
1-A-46	56Fe-15Ni-25Co-2Cr-2Si	55.95Fe-14.26Ni-23.67Co-2.15Cr-3.97Si
1-A-47	53Fe-15Ni-25Co-2V-5Ta	55.96Fe-15.07Ni-25.02Co-2.32Cr-1.63Ta
1-A-48	53Fe-15Ni-25Co-2Si-5Ta	54.75Fe-14.79Ni-24.56Co-4.12Si-1.60Ta
1-A-49	56Fe-15Ni-25Co-2Si-2W	56.82Fe-14.48Ni-24.04Co-4.04Si-0.62W
1-A-50	57Fe-15Ni-25Co-1Si-2V	57.49Fe-14.39Ni-23.90Co-2.01Si-2.21V
1-A-51	58Fe-15Ni-25Co-1Si-1Ti	58.51Fe-14.40Ni-23.90Co-2.01Si-1.18Ti
1-A-52	56Fe-15Ni-25Co-2Mo-2W	58.50Fe-14.90Ni-24.75Co-1.22Mo-0.63W
1-A-53	54.9Fe-15Ni-25Co-1Si-3Ta-0.5Al 0.5Ti-0.1Mn	56.31Fe-14.64Ni-24.30Co-2.04Si-0.95Ta-1.06Al-0.60Ti-0.10Mn

TABLE II-6. Nominal Composition of Martensitic Alloys Used in the Screening Tests (Concluded)

Alloy Number	Nominal Alloy Composition (weight percent)	Nominal Alloy Composition (atomic percent)
1-A-54	55.9Fe-12Ni-25Co-5Ta-2Si-0.1Mn	57.85Fe-11.81Ni-24.51Co-1.60Ta-4.12Si-0.11Mn
1-A-55	57Fe-12Ni-25Co-5Ta-0.5Ti-0.5Al	59.84Fe-11.98Ni-24.86Co-1.62Ta-0.61Ti-1.09Al
1-A-56	57Fe-12Ni-25Co-5Mo-0.5Ti-0.5Al	59.0Fe-11.81Ni-24.51Co-3.01Mo-0.60Ti-1.07Al
1-A-57	56Fe-12Ni-25Co-5Ta-2W	60.06Fe-12.24Ni-25.40Co-1.65Ta-0.65W
1-A-58	55.9Fe-12Ni-25Co-4Ta-2W-1Si-0.1Mn	58.89Fe-12.03Ni-24.95Co-1.30Ta-0.64W-2.09Si-0.10Mn
1-A-59	55.9Fe-12Ni-25Co-3Ta-2W-1Si-0.5Al-0.5Ti-0.1Mn	58.07Fe-11.86Ni-24.61Co-0.96Ta-0.63W-2.07Si-1.08Al-0.61Ti-0.11Mn
1-A-60	55 9Fe-12Ni-25Co-4Ta-2Si-0.5Al-0.5Ti-0.1Mn	57.1Fe-11.66Ni-24.18Co-1.26Ta-4.05Si 1.05Al-0.60Ti-0.10Mn
1-A-38	69.9Fe-25Co-5Ta-0.1Mn	73.39Fe-24.88Co-1.62Ta-0.11Mn
1-A-39	66.49Fe-5Ni-25Co-5Ta-0.1Mn	68.32Fe-5.01Ni-24.94Co-1.62Ta-0.11Mn
1-A-40	62Fe-5Ni-25Co-5Ta-3Mn	65.24Fe-5.01Ni-24.92Co-1.62Ta-3.21Mn
1-A-41	66Fe-25Co-5Ta-4Mn	69.26Fe-24.86Co-1.62Ta-4.26Mn
1-A-42	59.9Fe-5Ni-25Co-5Cr-5Ta-0.1Mn	62.81Fe-4.99Ni-24.84Co-5.63Cr-1.62Ta-0.11Mn
1-A-61	57.4Fe-5Ni-25Co-5Cr-5Ta-2Si-0.5Al-0.1Mn	58.64Fe-4.86Ni-24.21Co-5.49Cr-1.58Ta-4.06Si-1.06Al-0.10Mn

alloy series 1-A-V-1 to 1-A-V-6, shown in table II-7 was formulated from this screening evaluation. Additional mechanical and magnetic tests and analyses provided data for the selection of the final ferritic alloys 1-A-S-1 and 1-A-S-2 shown in table II-8.

The transformation temperatures of the ferritic alloys, shown in table II-9, indicates that nickel reduces the transformation temperature (note 1-A-48 versus 1-A-54). The addition of cobalt increases the transformation temperature (see 1-A-11 to 1-A-20); however, if the cobalt content becomes too large the transformation temperature decreases again. In the Fe-12Ni system an addition of ~30 weight percent cobalt results in the highest transformation temperature. It may be noted that the addition of Cr and Mn sharply reduce the transformation temperature of the Fe-Co-Ni alloy (alloys 1-A-4 and 1-A-10), exhibiting the same influence as Cr and Mn have on the phase transformation in iron. In nearly all cases of the alloys, shown in table II-9, the transformation during cooling started at temperatures below 932°F (500°C), which indicates that the transformation must be of the martensitic type since diffusion processes can play only minor roles within the time periods involved during cooling.

To determine the hardening response of alloys to which the various elements and combinations of elements were added, isochronal aging was performed as described in Section II.B.4. Vickers pyramid hardness and coercive force were determined at room temperature after each one-hour aging interval at temperatures to 1202°F (650°C).

Data obtained from the isochronal treatment of a number of representative alloys are plotted in figure II-7.

The data from 15% nickel maraging are plotted for comparison. The maximum values of room temperature hardness, which were measured during this aging sequence, are listed in table II-10 for the martensitic alloys, together with aging temperature where maximum hardness was obtained. The room temperature coercivity is listed for the same aging temperature. The addition of Ti, Mo, W, Nb, Ta, and Be had a strong effect on age hardening when added in sufficient quantity singly or in combination to the matrix composition. It should also be noted that the addition of either combination of Si+Cr (alloy 1-A-46) or Si+V (alloy 1-A-50) gave a strong hardening effect while no such response was obtained when the elements were added singly (alloys 1-A-3, 1-A-4, and 1-A-9).

TABLE II-7. Composition of 300-Gram Vacuum Arc Melted Martensitic Alloys 1-A-V-1 to 1-A-V-6

(a) Nominal Composition (weight percent)

Alloy Number	Fe	Co	Ni	Ta	Ti	Al	W	Cu	C	Cr
1-A-V-1	48	30	15	4	0.5	0.5	2	-	-	-
1-A-V-2	66	20	10	3	0.5	0.5	-	-	-	-
1-A-V-3	57.5	25	12	3.5	0.5	0.5	1	-	-	-
1-A-V-4	51	30	15	3	0.5	0.5	-	-	-	-
1-A-V-5	49	30	15	3	0.5	0.5	2	-	-	-
1-A-V-6	60	25	5	3	0.5	0.5	1	-	-	5

(b) Analyzed Composition (weight percent)

Alloy Number	Fe	Co	Ni	Ta	Ti	Al	W	Cu	C	Cr
1-A-V-1	47.4	29.2	14.6	4.50	0.49	0.56	2.15	0.005	0.0057	-
1-A-V-2	65.5	20.1	9.57	3.56	0.53	0.63	<0.2	0.020	0.0034	-
1-A-V-3	57.2	25.0	11.4	4.06	0.52	0.61	1.00	0.005	0.0028	-
1-A-V-4	52.2	29.4	14.8	3.48	0.52	0.64	<0.2	0.006	0.0029	-
1-A-V-5	48.6	29.8	14.5	3.48	0.54	0.62	2.10	0.005	0.0032	-
1-A-V-6	59.8	25.7	4.66	3.56	0.49	0.64	1.18	0.058	0.015	5.19

(c) Analyzed Composition (atomic percent)

Alloy Number	Fe	Co	Ni	Ta	Ti	Al	W	Cu	C	Cr
1-A-V-1	bal	29.49	14.80	1.48	0.61	1.24	0.70	-	-	-
1-A-V-2	bal	19.68	9.41	1.14	0.64	1.35	-	-	-	-
1-A-V-3	bal	24.84	11.37	1.31	0.64	1.32	0.32	-	-	-
1-A-V-4	bal	28.99	14.65	1.12	0.66	1.38	-	-	-	-
1-A-V-5	bal	29.85	14.58	1.14	0.67	1.36	0.67	-	-	-
1-A-V-6	bal	25.29	4.60	1.14	0.59	1.38	0.37	-	-	5.79

TABLE II-8. Composition of Final Martensitic Alloys Vacuum Induction Melted as 15-Pound Ingots

(a) Nominal Composition (weight percent)

Alloy Number	Fe	Ni	Co	W	Ta	Al	Ti	Zr	Be	B	C
1-A-S-1	50.3	15	30	1	3	0.3	0.4	0.003	-	0.001	-
1-A-S-2	53.2	12	30	1	3	0.4	0.4	0.003	-	0.001	-

(b) Analyzed Composition (weight percent)

Alloy Number	Fe	Ni	Co	W	Ta	Al	Ti	Zr	Be	B	C
1-A-S-1	50.2	15.3	29.1	0.92	2.90	0.27	0.42	0.006	-	0.002	0.0039
1-A-S-2	52.4	12.2	29.5	0.96	2.95	0.38	0.41	0.006	-	0.002	0.0022

(c) Analyzed Composition (atomic percent)

Alloy Number	Fe	Ni	Co	W	Ta	Al	Ti	Zr	Be	B	C
1-A-S-1	bal	15.25	28.89	0.29	0.94	0.59	0.51	-	-	-	-
1-A-S-2	bal	12.14	29.23	0.30	0.95	0.82	0.50	-	-	-	-

After completion of isochronal aging, the alloy samples that indicated a hardening response were homogenized by a double heat treatment as indicated in figure II-4. The samples were then subjected to isothermal aging at 1022°F (550°C) for various times up to 100 hours. The room temperature hardness and coercive force were measured after certain aging periods. Typical curves obtained by plotting these data are shown in figure II-8. Generally, the hardness curve passes a maximum and the coercive force curve passes a minimum during the 100-hour aging period.

The measured values of hardness and coercive force of the ferritic alloys after 100 hours aging at 1022°F (550°C) are also shown in table II-10. The change in hardness from the maximum values obtained during the 100-hour aging at 1022°F (550°C) and the values after 100-hour aging is also given, expressed as a percentage of the maximum.

TABLE II-9. Transformation Temperature of the Martensitic Alloys

Alloy Number	Nominal Alloy Composition (weight percent)	Transformation On Heating $\alpha \longrightarrow \gamma$				Transformation On Cooling $\gamma \longrightarrow \alpha$			
		90°F/Min (°F)	50°C/Min (°C)	1.8 to 3.6°F/Min (°F)	1 to 2°C/Min (°C)	90°F/Min (°F)	50°C/Min (°C)	9°F/Min (°F)	5°C/Min (°C)
1-A-1	55Fe-15Ni-25Co-5W	1425 - 1551	774 - 844	1087 - 1450	586 - 788	752 - 572	400 - 300	721 - 554	383 - 290
1-A-2	58Fe-15Ni-25Co-2Nb	1472 - 1634	800 - 890	1193 - 1542	645 - 839	916 - 662	491 - 350	891 - 680	477 - 360
1-A-3	58Fe-15Ni-25Co-2V	1472 - 1603	800 - 873	1112 - 1530	600 - 832	878 - 678	470 - 359	948 - 783	509 - 417
1-A-4	58Fe-15Ni-25Co-2Cr	1450 - 1587	788 - 864	1065 - 1472	574 - 800	828 - 628	442 - 331	863 - 680	462 - 360
1-A-5	59.5Fe-15Ni-25Co-0.5Al	1521 - 1652	827 - 900	1164 - 1515	629 - 824	986 - 781	530 - 416	1033 - 839	556 - 448
1-A-6	58Fe-15Ni-25Co-2Be	1548 - 1666	842 - 908	1447 - 1630	786 - 888	1326 - 1207	719 - 653	1517 - 1265	825 - 685
1-A-7	58Fe-15Ni-25Co-2Sb	1515 - 1634	824 - 890	1175 - 1490	635 - 810	846 - 631	452 - 333	903 - 729	484 - 387
1-A-8	58Fe-15Ni-25Co-2Sn	1456 - 1594	791 - 868	1112 - 1515	600 - 824	932 - 709	500 - 376	966 - 752	519 - 400
1-A-9	58Fe-15Ni-25Co-2Si	1434 - 1612	779 - 878	1195 - 1503	646 - 817	815 - 572	435 - 300	855 - 669	457 - 354
1-A-10	58Fe-15Ni-25Co-2Mn	1472 - 1618	800 - 881	1058 - 1450	570 - 788	786 - 545	419 - 285	842 - 610	450 - 321
1-A-11	88Fe-12Ni	1240 - 1328	671 - 720	1143 - 1261	617 - 683	657 - 829	347 - 443	984 - 721	529 - 383
1-A-12	83Fe-12Ni-5Co	1323 - 1386	717 - 752	1207 - 1384	653 - 751	952 - 779	511 - 415	943 - 779	506 - 415
1-A-13	78Fe-12Ni-10Co	1386 - 1441	752 - 783	1207 - 1463	653 - 795	984 - 815	529 - 435	997 - 826	536 - 441
1-A-14	73Fe-12Ni-15Co	1459 - 1530	793 - 832	1249 - 1521	676 - 827	1089 - 914	587 - 490	1072 - 896	578 - 480
1-A-15	68Fe-12Ni-20Co	1494 - 1573	812 - 856	1175 - 1560	635 - 849	1157 - 972	625 - 522	1143 - 1006	617 - 541
1-A-16	63Fe-12Ni-25Co	1551 - 1639	844 - 893	1193 - 1585	645 - 863	1173 - 984	634 - 529	1170 - 952	632 - 500
1-A-17	58Fe-12Ni-30Co	1515 - 1634	824 - 890	1249 - 1582	676 - 861	1177 - 975	636 - 524	1182 - 945	639 - 508
1-A-18	53Fe-12Ni-35Co	1481 - 1625	805 - 885	1227 - 1594	664 - 868	1130 - 952	610 - 511	1155 - 1009	624 - 543
1-A-19	48Fe-12Ni-40Co	1472 - 1625	800 - 885	1157 - 1618	625 - 881	1107 - 921	597 - 494	1173 - 993	634 - 534
1-A-20	43Fe-12Ni-45Co	1463 - 1643	795 - 895	1130 - 1594	610 - 868	1085 - 905	585 - 485	1107 - 968	597 - 520

TABLE II-9. Transformation Temperature of the Martensitic Alloys (Continued)

Alloy Number	Nominal Alloy Composition (weight percent)	Transformation On Heating α → γ				Transformation On Cooling α → γ			
		90 F Min (°F)	50 C Min (°C)	1.8 to 3.6 F. Min (°F)	1 to 2 C Min (°C)	90 F Min (°F)	50 C Min (°C)	9 F/Min (°F)	5 C/Min (°C)
1-A-21	54.5Fe-15Ni-25Co-0.5Ti-5Mo	1391 - 1569	755 - 854	1148 - 1508	620 - 820	603 - 324	317 - 162	597 - 356	314 - 180
1-A-22	54.5Fe-15Ni-25Co-0.5Ti-5Ta	1499 - 1600	815 - 871	1242 - 1551	672 - 844	775 - 480	413 - 249	775 - 572	413 - 300
1-A-23	54.5Fe-15Ni-25Co-0.5Ti-2Mo-3Ta	1434 - 1594	779 - 868	1224 - 1560	662 - 849	730 - 435	388 - 224	718 - 496	381 - 258
1-A-24	54Fe-15Ni-25Co-1Nb-5Ta	1438 - 1603	781 - 873	1249 - 1530	676 - 832	763 - 532	406 - 278	783 - 635	417 - 335
1-A-25	52.5Fe-15Ni-25Co-0.5Be-5Ta-2Si	1472 - 1582	800 - 861	1276 - 1508	691 - 820	682 - 471	361 - 244	752 - 514	400 - 268
1-A-26	67Fe-12Ni-20Co-1Ti	1454 - 1609	790 - 876	1317 - 1569	714 - 854	1006 - 829	541 - 443	1026 - 880	552 - 471
1-A-27	63Fe-12Ni-20Co-5Mo	1425 - 1560	774 - 849	1233 - 1501	667 - 816	788 - 555	420 - 263	768 - 451	409 - 283
1-A-28	63Fe-12Ni-20Co-5Ta	1494 - 1612	812 - 878	1310 - 1573	710 - 856	975 - 770	524 - 410	981 - 813	527 - 434
1-A-29	66Fe-12Ni-20Co-2Nb	1490 - 1569	810 - 854	1330 - 1585	721 - 863	968 - 795	520 - 424	984 - 820	529 - 438
1-A-30	66Fe-12Ni-20Co-2W	1472 - 1533	800 - 834	1224 - 1542	662 - 839	1029 - 829	554 - 443	855 - 788	557 - 420
1-A-31	67.5Fe-12Ni-20Co-0.5Be	1494 - 1585	812 - 863	1332 - 1598	722 - 870	984 - 817	529 - 436	1036 - 901	558 - 483
1-A-32	67.5Fe-12Ni-20Co-0.5Al	1483 - 1560	806 - 849	1411 - 1591	766 - 866	1126 - 955	608 - 513	1159 - 1038	626 - 559
1-A-33	54.4Fe-15Ni-25Co-0.5Be-5Ta-0.1Mn	1472 - 1617	800 - 881	1292 - 1553	700 - 845	720 - 509	383 - 265	786 - 545	419 - 285
1-A-34	53.9Fe-15Ni-25Co-1W-5Ta-0.1Mn	1566 - 1668	852 - 909	1260 - 1542	682 - 839	721 - 487	383 - 253	774 - 597	412 - 314
1-A-35	54.4Fe-15Ni-25Co-0.5Al-5Ta-0.1Mn	1485 - 1607	807 - 875	1270 - 1542	688 - 839	786 - 527	419 - 275	799 - 667	426 - 353
1-A-36	53.9Fe-15Ni-25Co-0.5Al-0.5Ti-5Ta-0.1Mn	1485 - 1600	807 - 871	1292 - 1539	700 - 837	748 - 475	398 - 246	748 - 536	398 - 280
1-A-37	53.9Fe-15Ni-25Co-0.5Al-0.5Ti-2Mo-3Ta-0.1Mn	1438 - 1593	781 - 867	1256 - 1553	680 - 845	671 - 369	355 - 187	673 - 430	356 - 221
1-A-38	69.9Fe-25Co-5Ta-0.1Mn	1764 - 1780	962 - 971	1740 - 1764	949 - 962	1587 - 1521	864 - 827	1726 - 1713	941 - 934
1-A-39	64.9Fe-5Ni-25Co-5Ta-0.1Mn	1659 - 1740	904 - 949	1517 - 1717	825 - 936	1227 - 1072	664 - 578	1351 - 1218	733 - 659
1-A-40	62Fe-5Ni-25Co-3Mn-5Ta	1584 - 1706	862 - 930	1292 - 1645	700 - 896	1053 - 837	567 - 447	1155 - 972	624 - 522
1-A-41	66Fe-25Co-4Mn-5Ta	1622 - 1735	884 - 946	1416 - 1699	769 - 926	1231 - 1053	666 - 567	1330 - 1166	721 - 630
1-A-42	59.9Fe-5Ni-25Co-5Cr-5Ta-0.1Mn	1530 - 1681	832 - 916	1222 - 1589	661 - 865	833 - 640	445 - 338	937 - 752	503 - 400

TABLE II-9. Transformation Temperature of the Martensitic Alloys (Concluded)

Alloy Number	Nominal Alloy Composition (weight percent)	Transformation On Heating α → γ				Transformation On Cooling γ → α			
		90°F/Min (°F)	50°C/Min (°C)	1.8 to 3.6°F/Min (°F)	1 to 2°C/Min (°C)	90°F/Min (°F)	50°C/Min (°C)	9°F/Min (°F)	5°C/Min (°C)
1-A-43	55Fe-15Ni-25Co-2Mo-3Ta	1411 - 1578	766 - 859	1222 - 1535	661 - 835	712 - 475	378 - 246	747 - 518	397 - 270
1-A-44	53Fe-15Ni-25Co-2Cr-5Ta	1425 - 1584	774 - 862	1112 - 1465	600 - 807	622 - 306	328 - 152	622 - 392	328 - 200
1-A-45	57.5Fe-15Ni-25Co-2Cr-0.5Be	1521 - 1652	827 - 900	1069 - 1398	576 - 759	675 - 448	357 - 231	622 - 378	328 - 192
1-A-46	56Fe-15Ni-25Co-2Cr-2Si	1490 - 1609	810 - 876	1041 - 1420	560 - 771	619 - 345	326 - 174	649 - 351	343 - 177
1-A-47	53Fe-15Ni-25Co-2V-5Ta	1551 - 1652	844 - 900	1222 - 1508	661 - 820	693 - 369	367 - 187	705 - 478	374 - 248
1-A-48	53Fe-15Ni-25Co-2Si-5Ta	1569 - 1652	854 - 900	1265 - 1521	685 - 827	734 - 475	390 - 246	766 - 597	408 - 314
1-A-49	56Fe-15Ni-25Co-2Si-2W	1503 - 1652	817 - 900	1218 - 1472	659 - 800	727 - 482	386 - 250	752 - 509	400 - 265
1-A-50	57Fe-15Ni-25Co-1Si-2V	1459 - 1652	793 - 900	1337 - 1499	725 - 815	705 - 437	374 - 225	775 - 545	413 - 285
1-A-51	58Fe-15Ni-25Co-1Si-1Ti	1528 - 1652	831 - 900	1308 - 1615	709 - 880	837 - 572	447 - 300	894 - 709	479 - 376
1-A-52	56Fe-15Ni-25Co-2Mo-2W	1404 - 1526	762 - 830	1175 - 1472	635 - 800	721 - 558	383 - 292	743 - 572	395 - 300
1-A-53	54.9Fe-15Ni-25Co-3Ta-1Si-0.5Al-0.5Ti-0.1Mn	1575 - 1679	857 - 915	1260 - 1553	682 - 845	752 - 491	400 - 255	777 - 572	414 - 300
1-A-54	55.9Fe-12Ni-25Co-5Ta-2Si-0.1Mn	1569 - 1704	854 - 929	1310 - 1605	710 - 874	811 - 631	433 - 333	900 - 712	482 - 378
1-A-55	57Fe-12Ni-25Co-5Ta-0.5Ti-0.5Al	1596 - 1677	869 - 914	1382 - 1641	750 - 894	905 - 684	485 - 362	963 - 786	517 - 419
1-A-56	57Fe-12Ni-25Co-5Mo-0.5Ti-0.5Al	1501 - 1652	816 - 900	1233 - 1551	667 - 844	705 - 419	374 - 215	730 - 505	388 - 263
1-A-57	56Fe-12Ni-25Co-5Ta-2W	1535 - 1670	835 - 910	1292 - 1617	700 - 881	815 - 644	435 - 340	918 - 777	492 - 414
1-A-58	55.9Fe-12Ni-25Co-4Ta-2W-1Si-0.1Mn	1517 - 1652	825 - 900	1242 - 1620	672 - 882	809 - 637	432 - 336	900 - 718	482 - 381
1-A-59	55.9Fe-12Ni-25Co-3Ta-2W-1Si-0.5Al-0.5Ti-0.1Mn	1584 - 1681	862 - 916	1301 - 1602	705 - 872	802 - 585	428 - 307	871 - 669	466 - 354
1-A-60	55.9Fe-12Ni-25Co-4Ta-2Si-0.5Al-0.5Ti-0.1Mn	1542 - 1670	839 - 910	1303 - 1600	706 - 871	820 - 628	438 - 331	887 - 709	475 - 376
1-A-61	57.4Fe-5Ni-25Co-5Cr-5Ta-0.5Al-0.1Mn-2Si	1564 - 1695	851 - 924	1220 - 1587	660 - 864	727 - 549	386 - 287	799 - 572	426 - 300

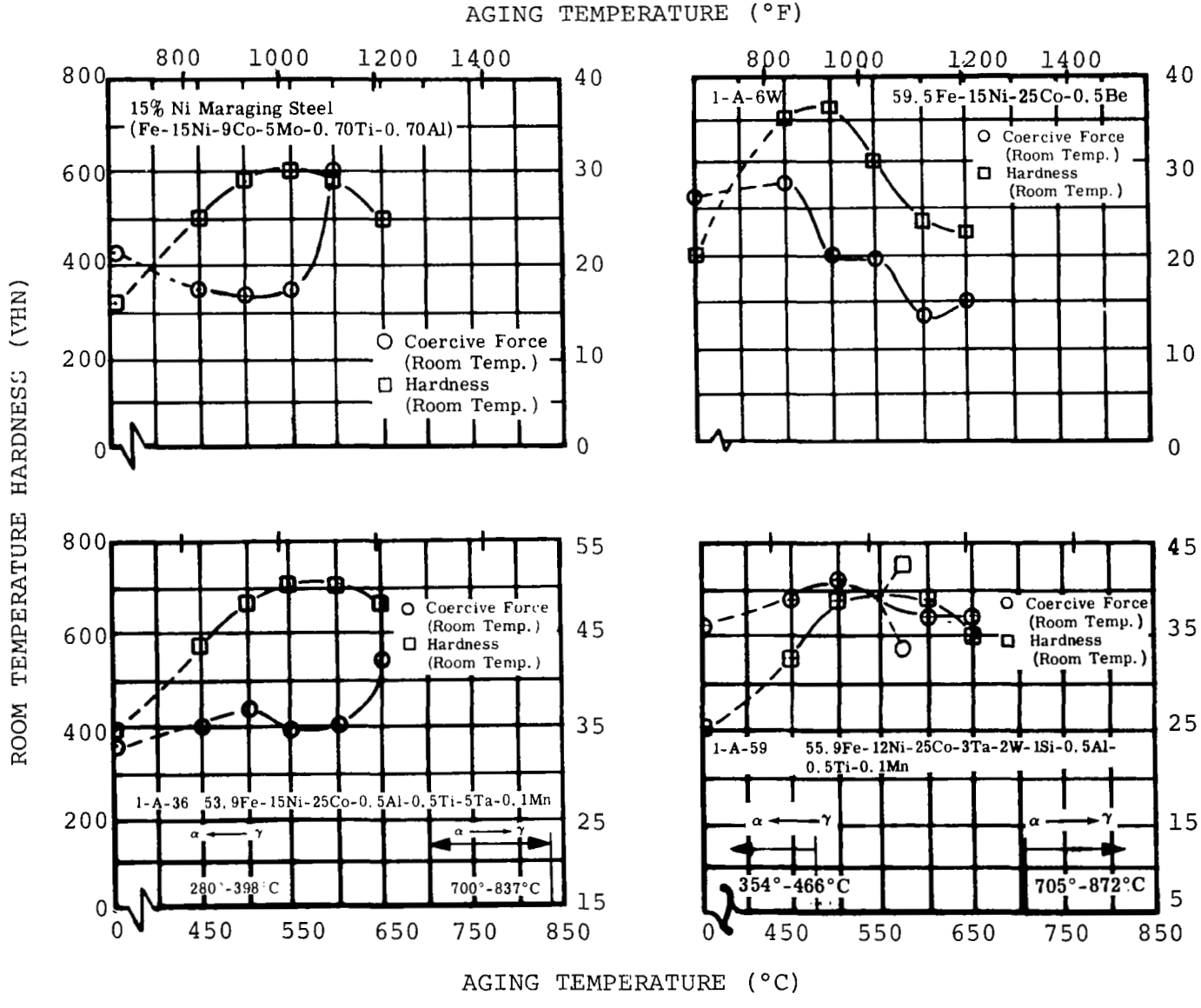

FIGURE II-7. Hardness and Coercive Force of Representative Ferritic Alloys and 15% Ni Maraging Steel at Room Temperature after Aging One Hour at Temperature

The results indicated that all of the tested alloys exhibited overaging at 1022°F (550°C). However, the degree varied among the alloys. The coercive force behaved in a manner similar to that shown in the 15 percent or 18 percent nickel maraging steels (refs. II-19 and II-20). The increase in coercive force, after extended aging in the experimental alloys, was substantially less than that of the commercial maraging steels. In general, the strong influence of increasing cobalt content on overaging was noted. Alloys containing Ta, W, or Nb showed less tendency to overage than alloys containing Ti or Mo when a similar hardness was attained in each case. Alloys containing a suitable combination of Ta+Al+Ti showed a small degree of overaging.

Results of the saturation measurements on ferritic alloys combining addition elements are shown in table II-11. The method of testing was described in section II.B.2. The alloys containing modifier additions were first measured in a condition where no precipitation had occurred. Samples from the levitation melts were measured in the as-cast condition.

The room temperature magnetic saturation differed in only a few cases before and after aging. The saturation test results, shown in figure II-9, for the ternary alloys (1-A-11 to 1-A-20) indicate agreement with the well known behavior of the binary alloys where the increase in cobalt content to a certain level increases the magnetic saturation especially at elevated temperatures. In the ternary alloys containing 12 weight percent nickel, the maximum magnetic saturation at 1112°F (600°C) was obtained when the cobalt content was near 35 weight percent. However, the influence of cobalt on magnetic saturation is less between 20 and 45 weight percent than at levels between 0 and 20 percent. All of the alloying additions shown in table II-11 reduced the magnetic saturation at room and elevated temperatures. However, the influence of Ti and Be are quite low. On the other hand, Mo, Cr, and Mn appear to have a marked effect in reducing the magnetic saturation at elevated temperature, while the depressing effect of Si, W, or V is less severe though noticeable when the alloying addition is expressed in weight percent.

A comparison was made of the influence of the modifying elements based on atomic percent on the room temperature magnetic saturation of samples in the annealed condition. Table II-12 shows the change in saturation

TABLE II-10. Results of Isochronal and Isothermal Aging Tests on Levitation-Melted Martensitic Alloys

Alloy Number	Nominal Alloy Composition (weight percent)	Isochronal Tests: Aging Temperature at which Maximum Hardness[c] was obtained (°F)	Isochronal Tests: Aging Temperature at which Maximum Hardness[c] was obtained (°C)	Isochronal Tests: Maximum Room Temperature Hardness[b] (VHN_m)	Isochronal Tests: Room Temperature Coercivity at Maximum Hardness (Oe)	Isothermal Tests (After 100 Hours at 1022°F (550°C)): Room Temperature Hardness (VHN_{100})	Isothermal Tests (After 100 Hours at 1022°F (550°C)): Room Temperature Coercivity H_{c100} (Oe)	Isothermal Tests (After 100 Hours at 1022°F (550°C)): ΔVHN[d] (%)
For Comparison								
15% Ni Maraging Steel	71.1Fe-15Ni-8Co-4.5Mo-0.7Al-0.7Ti	1022	550	607	17.5	539	60	10
LM10[a]	55Fe-15Ni-25Co-5Ta	1022	550	632	29	557	32.0	11
1-A-1	55Fe-15Ni-25Co-5W	932	500	610	33.5	511	27.5	10
1-A-2	58Fe-15Ni-25Co-2Nb	932	500	558	27.4	494	21.0	10
1-A-3	58Fe-15Ni-25Co-2V	932	500	390	18.3	363	21.0	10
1-A-4	58Fe-15Ni-25Co-2Cr	1022	550	391	20.1	-	-	-
1-A-5	59.5Fe-15Ni-25Co-0.5Al	1022	550	412	14.7	351	150	15
1-A-6W	59.5Fe-15Ni-25Co-0.5Be	932	500	717	19.1	451	20.0	22
1-A-7	58Fe-15Ni-25Co-2Sb			brittle, no test			brittle, no test	
1-A-8	58Fe-15Ni-25Co-2Sn			brittle, no test			brittle, no test	
1-A-9	58Fe-15Ni-25Co-2Si	842	450	468	24.2	-	-	-
1-A-10	58Fe-15Ni-25Co-2Mn	932	500	482	16.3	-	-	-
1-A-26	67Fe-12Ni-20Co-1Ti	1022	550	502	18.0	413	20	11
1-A-27	63Fe-12Ni-20Co-5Mo	1022	550	629	26.0	488	20	21
1-A-28	63Fe-12Ni-20Co-5Ta	1022	550	541	24	452	23	19
1-A-29	66Fe-12Ni-20Co-2Nb	1022	550	538	20.5	425	21	20
1-A-30	66Fe-12Ni-20Co-2W	1112	600	354	16	-	-	-
1-A-31	67.5Fe-12Ni-20Co-0.5Be	932	500	639	21.5	372	21	22
1-A-32	67.5Fe-12Ni-20Co-0.5Al	1022	550	337	11.0	-	-	-
1-A-21	54.5Fe-15Ni-25Co-0.5Ti-5Mo	932	500	684	29.3	553	36.7	23
1-A-22	54.5Fe-15Ni-25Co-0.5Ti-5Ta	1022	550	682	30.1	598	37.8	10
1-A-23	54.5Fe-15Ni-25Co-0.5Ti-2Mo-3Ta	1022	550	664	30.0	577	43.2	11
1-A-24	54Fe-15Ni-25Co-1Nb-5Ta	932	500	649	36.0	533	34.1	11
1-A-25	52.5Fe-15Ni-25Co-0.5Be-5Ta-2Si			brittle, no test			brittle, no test	
1-A-33	54.4Fe-15Ni-25Co-0.5Be-5Ta-0.1Mn	1022	550	810	44.5	673	45.0	19
1-A-34	53.9Fe-15Ni-25Co-1W-5Ta-0.1Mn	1022	550	642	31.0	617	32.0	11
1-A-35	54.4Fe-15Ni-25Co-0.5Al-5Ta-0.1Mn	1022	550	649	31.0	646	40.5	4
1-A-36	53.9Fe-15Ni-25Co-0.5Al-0.5Ti-5Ta-0.1Mn	1022	550	687	34.0	696	46.0	2
1-A-37	53.9Fe-15Ni-25Co-0.5Al-0.5Ti-2Mo-3Ta-0.1Mn	1022	550	674	32.0	688	57.0	4

(a) Alloy LM10 was melted and tested on a previous Westinghouse program.

(b) VHN hardness obtained using a load of 50 kilograms (see Section II.B.4).

(c) The total aging time that a isochronal aging specimen encountered during a test may be determined by adding one hour aging time for each 90°F (50°C) increment in temperature starting at 842°F (450°C); e.g., for 550°C total aging time is three hours.

(d) ΔVHN, the change in hardness during aging at 1022°F (550°C) or $\frac{VHN_1 - VHN_{100}}{VHN_1} \times 100$.

TABLE II-10. Results of Isochronal and Isothermal Aging Tests on Levitation-Melted Martensitic Alloys (Continued)

Alloy Number	Nominal Alloy Composition (weight percent	Isochronal Tests: Aging Temperature at which Maximum Hardness[c] was obtained (°F)	Isochronal Tests: Aging Temperature at which Maximum Hardness[c] was obtained (°C)	Isochronal Tests: Maximum Room Temperature Hardness[b] (VHN_m)	Isochronal Tests: Room Temperature Coercivity at Maximum Hardness (Oe)	Isothermal Tests (After 100 Hours at 1022°F (550°C)): Room Temperature Hardness (VHN_{100})	Isothermal Tests (After 100 Hours at 1022°F (550°C)): Room Temperature Coercivity H_{c100} (Oe)	ΔVHN[d] (%)
For Comparison								
15% Ni Maraging Steel	71.1Fe-15Ni-8Co-4.5Mo-0.7Al-0.7Ti	1022	550	607	17.5	539	60	10
1-A-43	55Fe-15Ni-25Co-2Mo-3Ta	1022	550	695	31.0	534	40.0	14
1-A-44	53Fe-15Ni-25Co-2Cr-5Ta	1022	550	663	35.0	574	53.0	14
1-A-45	57.5Fe-15Ni-25Co-2Cr-0.5Be	842	450	757	39.0	466	33.0	24
1-A-46	56Fe-15Ni-25Co-2Cr-2Si	842	450	568	29.5	446	37.0	18
1-A-47	53Fe-15Ni-25Co-2V-5Ta	1022	550	677	31.0	607	56.0	10
1-A-48	53Fe-15Ni-25Co-2Si-5Ta	1022	550	663	30.5	565	30.0	10
1-A-49	56Fe-15Ni-25Co-2Si-2W	932	500	572	30.5	452	26.5	10
1-A-50	57Fe-15Ni-25Co-1Si-2V	842	450	546	29.5	450	27.5	10
1-A-51	58Fe-15Ni-25Co-1Si-1Ti	932	500	616	29.5	523	23.0	15
1-A-52	56Fe-15Ni-25Co-2Mo-2W	932	500	577	30.0	502	25.0	11
1-A-53	54.9Fe-15Ni-25Co-1Si-3Ta-0.5Al-0.5Ti-0.1Mn	1022	550	732	30.0	670	46.0	5
1-A-54	55.9Fe-12Ni-25Co-5Ta-2Si-0.1Mn			brittle, no test			brittle, no test	
1-A-55	57Fe-12Ni-25Co-5Ta-0.5Ti-0.5Al	1022	550	663	33.5	629	43.0	6
1-A-56	57Fe-12Ni-25Co-5Mo-0.5Ti-0.5Al	1022	550	732	25.0	660	51.0	13
1-A-57	56Fe-12Ni-25Co-5Ta-2W	1022	550	629	35.0	570	33.0	11
1-A-58	55.9Fe-12Ni-25Co-4Ta-2W-1Si-0.1Mn	1022	550	649	39.0	557	33.0	13
1-A-59	55.9Fe-12Ni-25Co-3Ta-2W-1Si-0.5Ti-0.1Mn-0.5Al	1022	550	692	39.0	697	48.5	2.3
1-A-60	55.9Fe-12Ni-25Co-4Ta-2Si-0.5Al-0.5Ti-0.1Mn			brittle, no test			brittle, no test	
1-A-38	69.9Fe-25Co-5Ta-0.1Mn	1022	550	259	14.0	-	-	-
1-A-41	66Fe-25Co-5Ta-4Mn			brittle, no test			brittle, no test	
1-A-40	62Fe-5Ni-25Co-5Ta-3Mn			brittle, no test			brittle, no test	
1-A-39	64.9Fe-5Ni-25Co-5Ta-0.1Mn			brittle, no test			brittle, no test	
1-A-42	59.9Fe-5Ni-25Co-5Cr-5Ta-0.1Mn	1022	550	533	36.0	518	37.0	8
1-A-61	57.4Fe-5Ni-25Co-5Cr-5Ta-0.5Al-2Si-0.1Mn	1022	550	616	40.0	571	38.0	7

(a) Alloy LM10 was melted and tested on a previous Westinghouse program.
(b) VHN hardness obtained using a load of 50 kilograms (see section II. B. 4).
(c) The total aging time that a isochronal aging specimen encountered during a test may be determined by adding one hour aging time for each 90°F (50°C) increment in temperature starting at 842°F (450°C); e.g., for 550°C total aging time is three hours.
(d) Δ VHN, the change in hardness during aging at 1022°F (550°C) or $\frac{VHN_1 - VHN_{100}}{VHN_1} \times 100$.

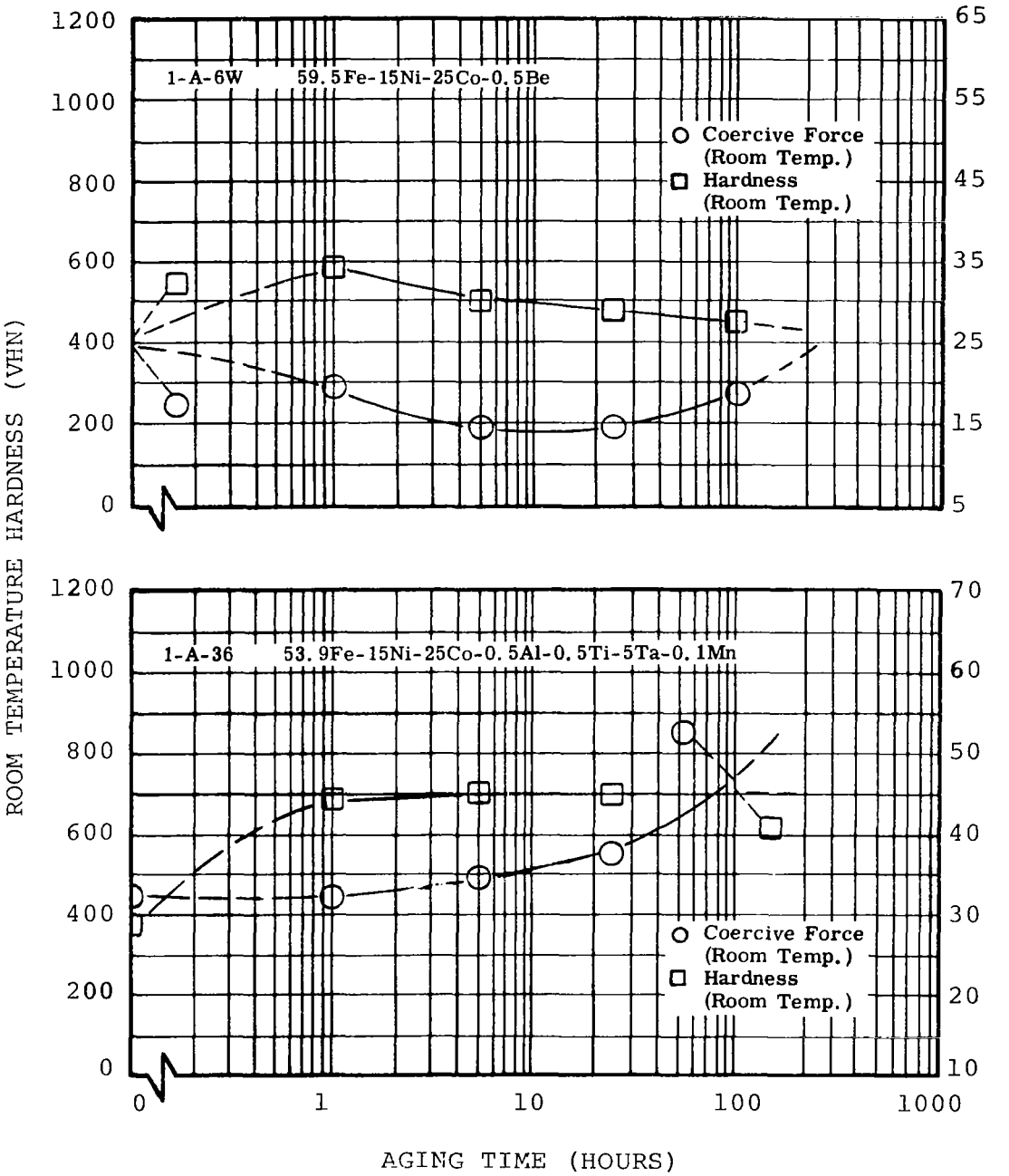

FIGURE II-8. Change in Room Temperature Hardness and Coercive Force of Representative Ferritic Alloys During Isothermal Aging at 1022° F (550° C)

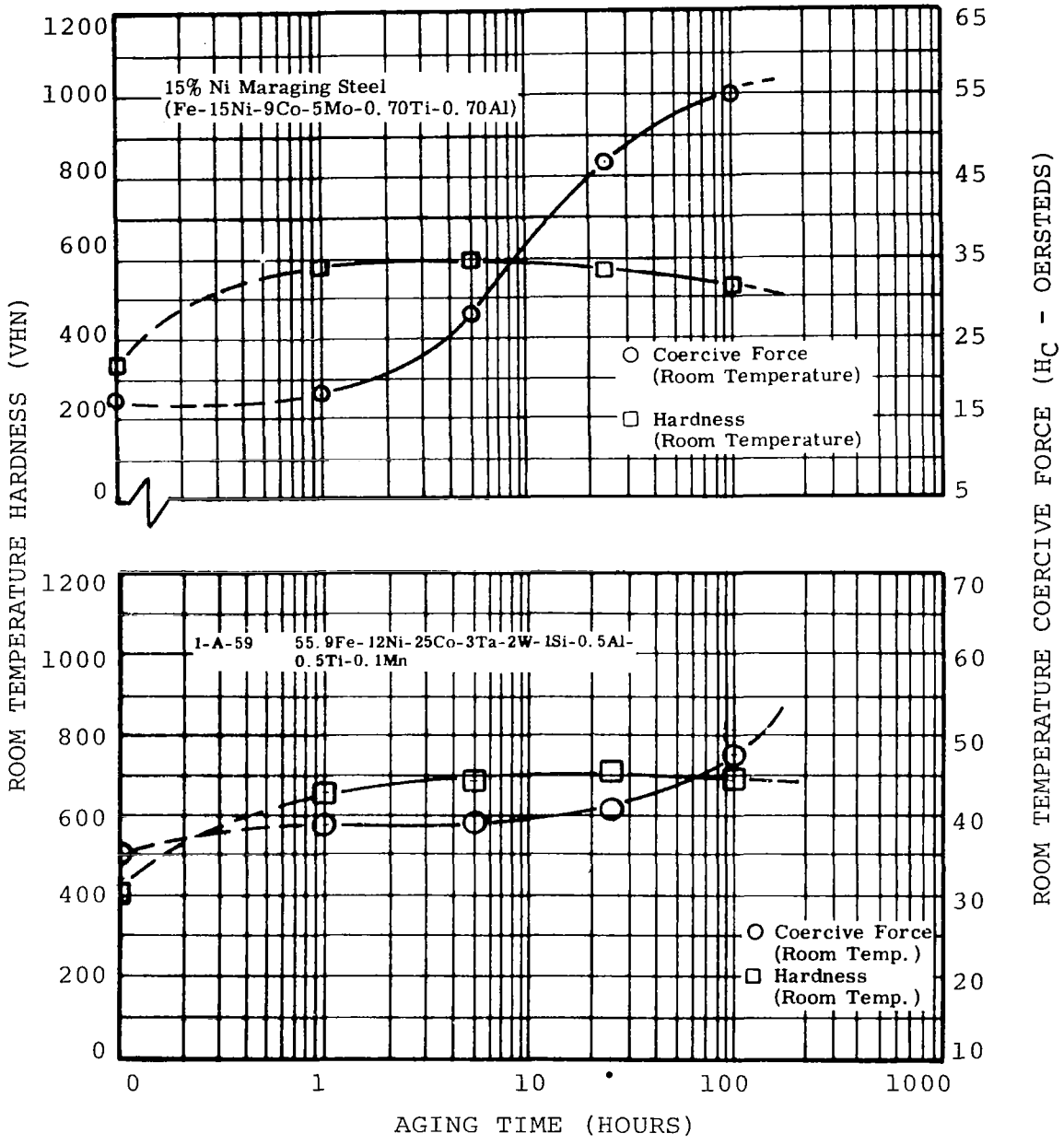

FIGURE II-8. (Continued) Change in Room Temperature Hardness and Coercive Force of Representative Ferritic Alloys During Isothermal Aging at 1022°F (550°C)

TABLE II-11. Saturation Magnetic Moment of Martensitic Alloys(a) Containing Addition Elements

Alloy Number	Nominal Alloy Composition (weight percent)	Saturation Magnetic Moment (emu/g)(c)		
		After Annealing One Hour at 1832°F (1000°C)	After Aging One Hour at 1112°F (600°C)	
		Tested at Room Temperature	Tested at Room Temperature	Tested at 1112°F (600°C)
1-A-1	55Fe-15Ni-25Co-5W	197.6(b)	198.9	152.7
1-A-2	58Fe-15Ni-25Co-2Nb	208.4(b)	211.0	167.8
1-A-3	58Fe-15Ni-25Co-2V	206.4(b)	206.5	158.4
1-A-4	58Fe-15Ni-25Co-2Cr	204.8(b)	202.8	149.8
1-A-5	59.5Fe-15Ni-25Co-0.5Al	212.0(b)	204.4	168.9
1-A-6	58Fe-15Ni-25Co-2Be	194.8(b)	195.1	162.2
1-A-7	58Fe-15Ni-25Co-2Sb	210.8(b)	208.1	163.2
1-A-8	58Fe-15Ni-25Co-2Sn	210.8(b)	195.7	166.1
1-A-9	58Fe-15Ni-25Co-2Si	202.0(b)	201.6	154.1
1-A-10	58Fe-15Ni-25Co-2Mn	214.0(b)	205.5	151.0
1-A-21	54.5Fe-15Ni-25Co-0.5Ti-5Mo	189	188	143
1-A-22	54.5Fe-15Ni-25Co-0.5Ti-5Ta	191	192	158
1-A-23	54.5Fe-15Ni-25Co-0.5Ti-2Mo-3Ta	191	191	156
1-A-24	54Fe-15Ni-25Co-1Nb-5Ta	191	193	161
1-A-25	52.5Fe-15Ni-25Co-0.5Be-5Ta-2Si	176	181	148
1-A-26	67Fe-12Ni-20Co-1Ti	217	217	181
1-A-27	63Fe-12Ni-20Co-5Mo	200	200	161
1-A-28	63Fe-12Ni-20Co-5Ta	205	205	171
1-A-29	66Fe-12Ni-20Co-2Nb	212	213	175
1-A-30	66Fe-12Ni-20Co-2W	215	215	174
1-A-31	67.5Fe-12Ni-20Co-0.5Be	217	219	179
1-A-32	67.5Fe-12Ni-20Co-0.5Al	220	220	177
1-A-33	54.4Fe-15Ni-25Co-0.5Be-5Ta-0.1Mn	191	193	160
1-A-34	53.9Fe-15Ni-25Co-1W-5Ta-0.1Mn	192	193	156
1-A-35	54.4Fe-15Ni-25Co-0.5Al-5Ta-0.1Mn	193	194	161
1-A-36	53.9Fe-15Ni-25Co-0.5Al-0.5Ti-5Ta-0.1Mn	188	189	156
1-A-37	53.9Fe-15Ni-25Co-0.5Al-0.5Ti-2Mo-3Ta-0.1Mn	187	186	150
1-A-38	69.9Fe-25Co-5Ta-0.1Mn	222	221	192
1-A-39	64.9Fe-5Ni-25Co-5Ta-0.1Mn	215	214	182
1-A-40	62Fe-5Ni-25Co-3Mn-5Ta	212	209	171
1-A-41	66Fe-25Co-4Mn-5Ta	211	213	174
1-A-42	59.9Fe-5Ni-25Co-5Cr-5Ta-0.1Mn	190	192	152
1-A-43	55Fe-15Ni-25Co-2Mo-3Ta	194	192	147
1-A-44	53Fe-15Ni-25Co-2Cr-5Ta	184	176	122
1-A-45	57.5Fe-15Ni-25Co-2Cr-0.5Be	198	190	137
1-A-46	56Fe-15Ni-25Co-2Cr-2Si	190	177	119
1-A-47	53Fe-15Ni-25Co-2V-5Ta	186	185	145
1-A-48	53Fe-15Ni-25Co-2Si-5Ta	186	190	147
1-A-49	56Fe-15Ni-25Co-2Si-2W	182	181	129
1-A-50	57Fe-15Ni-25Co-1Si-2V	196	192	133
1-A-51	58Fe-15Ni-25Co-1Si-1Ti	204	206	166
1-A-52	56Fe-15Ni-25Co-2Mo-2W	198	197	143
1-A-53	54.9Fe-15Ni-25Co-3Ta-1Si-0.5Al-0.5Ti-0.1Mn	190	192	157
1-A-54	55.9Fe-12Ni-25Co-5Ta-2Si-0.1Mn	188	192	159
1-A-55	57Fe-12Ni-25Co-5Ta-0.5Ti-0.5Al	196	197	167
1-A-56	57Fe-12Ni-25Co-5Mo-0.5Ti-0.5Al	192	192	160
1-A-57	56Fe-12Ni-25Co-5Ta-2W	195	195	165
1-A-58	55.9Fe-12Ni-25Co-4Ta-2W-1Si-0.1Mn	191	195	161
1-A-59	55.9Fe-12Ni-25Co-3Ta-2W-1Si-0.5Al-0.5Ti-0.1Mn	189	192	160
1-A-60	55.9Fe-12Ni-25Co-4Ta-2Si-0.5Al-0.5Ti-0.1Mn	186	191	158
1-A-61	57.4Fe-5Ni-25Co-5Cr-5Ta-0.5Al-0.1Mn-2Si	172	176	136

(a) All specimens were machined from cast ingots.
(b) Tested in the as cast condition.
(c) To convert Saturation Magnetic Moment to the approximate induction in gauss, multiply the listed value by 100.

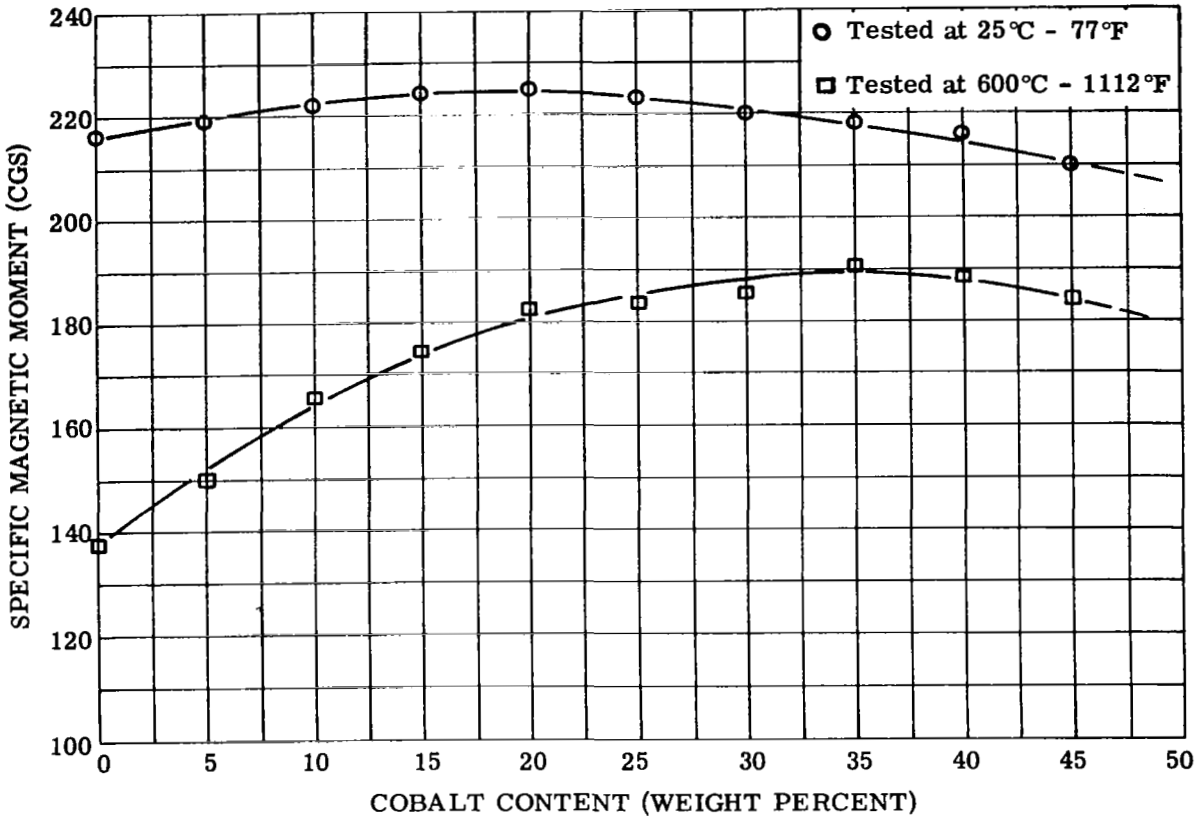

FIGURE II-9. Influence of Cobalt Content on Saturation in a Ternary Alloy with 12 Percent Nickel in Iron, (Alloys 1-A-11 to 1-A-20)

for one atomic percent of the element added to the Fe-15Ni-25Co matrix and to the Fe-12Ni-20Co matrix. These values must be considered with caution since the atomic percent was calculated from the nominal composition. The latter may deviate as much as 20% of the true value of some elements, especially those very active to oxygen and nitrogen (see section II.B.1.). There is good agreement between the values derived from the two groups of alloys.

One notices that the influence of transition metals on magnetic saturation increases generally with the distance in row and column from the ferromagnetic metals Fe, Ni, and Co in the periodic table. The metals, Si, Al, and Be behaved in a similar manner, though Be deviates to some degree. It is clear that the influence of the alloying additions is not merely a dilution effect.

TABLE II-12. Reduction of Magnetic Saturation (emu/g) Per Unit Atomic Percent Addition Element in 12 and 15 Percent Nickel Iron Matrices[a]

Addition Element	Change in Room Temperature Magnetic Saturation Per Unit Atomic Percent Expressed in emu/g	
	60Fe-15Ni-25Co Matrix (weight percent) 61.25Fe-14.57Ni-24.18Co (atomic percent)	63Fe-12Ni-25Co Matrix (weight percent) 64.21Fe-11.64Ni-24.15Co (atomic percent)
Ti	- 6.8	- 6.8
Mo	- 8.5	- 8.2
Ta	-11.0	-12.2
W	-11.2	-15.9
Nb	- 6.5	-10.5
Be	- 1.95	- 2.6
Al	- 3.8	- 4.75
V	- 4.4	
Cr	- 4.6	
Si	- 3.5	
Mn	- 0.97	

(a) Based on nominal compositions. See discussion on page 45.

b. SELECTION AND EVALUATION OF INTERMEDIATE VACUUM ARC MELTED ALLOYS

As an additional step in the screening program, six alloys of the martensitic type and six of the cobalt-base type were prepared by vacuum-arc melting in a larger button size of ~300 grams. Testing of these alloys would verify the results of the previous screening effort, define the suitable range of alloy composition within narrow limits, and extend the measurements of mechanical and magnetic measurements. The selection of compositions for these alloys were made on the basis of results from the screening tests performed on the levitation melted alloys and described in the preceding section. The results used for the selection of the martensitic alloys are listed in tables II-9, II-10 and II-11.

In the case of the martensitic alloys, the following criteria were used in screening the alloys:

1) Transformation should not start at a temperature below the upper limit of the anticipated range of service temperature. Therefore, all of the alloys which showed the start of transformation during a slow rate of heating (1.8° to 3.6°F), lower than 1202°F (650°C), were eliminated.

2) The magnetic saturation at 1112°F (600°C) should be well in excess of the saturation of the best available material (B_s = 13,000 gauss at 1112°F in H-11 steel and 15 percent nickel maraging steel). Attention was therefore focused only on those alloys in which the measured magnetic moment per gram at 1112°F (600°C) was higher than 150 (equivalent to B_s = 15,000 gauss).

3) Only those alloys which exhibited substantial age hardening were considered. In order to be comparable with commercially available materials such as H-11 steel or 15 percent nickel maraging steel, the hardness measured at room temperature during isochronal or isothermal aging was required to be at least 550 VHN.

4) The values of coercivity associated with these hardness measurements should be relatively low. It is difficult to select a definite limit on the measured room temperature values. The coercive force will decrease at elevated temperatures (ref. II-21). Since it is difficult to predict the amount of decrease, an arbitrary room temperature value of H_c = 50 oersteds was selected as the limit which should not be exceeded even after 100 hours aging at 1022°F (550°C).

5) The most important criterion is the stability of the structure. Yet, there is no such stability in its genuine meaning, which would forbid any diffusion controlled process to proceed in measurable times. In all of the alloys tested, age hardening was promoted in the temperature range between the 842° and 1202°F (450° and 650°C). This indicated that

the diffusion controlled precipitation - reaction proceeds in measurable times. Therefore, it is desirable to find conditions which establish a certain state of structure defined as dynamically stable. Such a state requires that hardness and strength remain nearly at a constant level during exposure at temperature while some diffusion controlled process may continue. Practically all creep resistant alloys make use of such state of structure.

It is common experience that such behavior is related to the temperature at which the maximum hardness is obtained during isochronal aging. The anticipated service temperature may be higher than the temperature at which maximum hardness is attained; however, in those cases one has to anticipate that overaging will occur at prolonged exposure times at temperature.

Therefore, it appeared reasonable to focus attention only on those alloys exhibiting a maximum hardness temperature of at least 1022°F (550°C). In addition, the decrease of hardness from the maximum value obtained during the isothermal aging at 1022°F (550°C) to the value obtained after 100 hours should be less than 10 percent.

In applying the listed criteria, one notices that the commercially available 15 percent nickel maraging steel does not fulfill or even approach these requirements. The screened alloys 1-A-22, 1-A-35, 1-A-36, 1-A-53, 1-A-55 and 1-A-59 fulfill all of the requirements simultaneously. The alloys LM10, 1-A-23, 1-A-34, 1-A-48, 1-A-57, and 1-A-61 very nearly fulfill the requirements. These results enable us to derive a most suitable alloy composition.

However, some ambiguity remained regarding the exact amount of added elements to use for the best combination. Furthermore, one should be cautioned in assuming that the nominal weight percent is the actual amount present in the 20-gram ingots. As stated previously, deviations of 20 percent may be expected based on previous experience with levitation melts. The results of the screening tests obtained from the levitation melts provided certain ranges of the most suitable composition and it was the purpose of the next step to

narrow the limits of these ranges still further. The limits of the most suitable nickel content may be defined as 10 to 15 weight percent. The cobalt content may vary between 20 and 30 weight percent. As far as the beneficial additions of Ta, W, Si, Cr, Al, and Ti in the above listed test alloys are concerned, Si may be eliminated, even in advantageous combination with other elements, for the following reasons: silicon addition has an embrittling effect, as noted in many cases and reduces the magnetic saturation. In comparing alloy 1-A-53 with 1-A-36, the former did not show improvement in other properties when silicon was added in similar combinations (see table II-10). Comparing 1-A-48 with LM10 (see table II-10) shows that the addition of silicon produced only marginal benefits as far as hardness and stability were concerned.

The addition of chromium has a very detrimental effect on stability of the α phase and on the magnetic saturation. Therefore, chromium can only be tolerated as an addition when a substantial reduction in nickel compensates for the detrimental effects of chromium.

The addition of tantalum has proven beneficial in nearly any combination tested. It should be restricted to between 3 and 4 weight percent in combination with aluminum and titanium at ~0.5 weight percent. There is some doubt whether an increase in tungsten content to two weight percent will provide enough improvement to compensate its more drastic effect in reducing the transformation temperature and magnetic saturation.

Because of the previously mentioned uncertainties in the actual composition of the levitation melts, it appeared impractical to try to reproduce specific alloy composition of the levitation melts as 300-gram buttons made by vacuum-arc melting. It appeared to be more useful to design the alloy compositions for the 300-gram buttons to obtain information about the optimum composition and its limits. Therefore, six alloys were melted (see section II.B.5. for details) containing variations of composition within the above specified limits. Ni content was between 10 and 15 weight percent; Co between 20 and 30 weight percent (Cr, 1 weight percent substituting ~2 weight percent Ni); Ta between 3 and 4 weight percent; W between 0 and 2 weight percent. Al and Ti 0.5 weight percent each. The nominal compositions of the alloys are listed in table II-7.a. The first five alloys were designed to obtain equations for the properties expressed as independent linear relationships with the weight percent of the components Ni, Ta, W, and Co. It was assumed that within the narrow limits

defined, the independent linear relationship is a justified approximation. The common rule for such a procedure was followed by placing the composition of the experimental alloys at the range limit except for one alloy. The composition of the latter corresponded to the mid-range quantity of each component. However, nickel was reduced to five weight percent while introducing five weight percent chromium as in alloy 1-A-61.

The (aging response, hardness and coercive force) results (table II-13) obtained from the 300-gram vacuum arc melted buttons indicate that this approach placed the results in agreement with the properties anticipated on the basis of results obtained on the levitation melts.

The analyzed compositions of the six martensitic alloys (see table II-7.b) were very near the nominal compositions (table II-7.a). The only noticeable differences were the tantalum and aluminum contents; generally, about 0.5 and 0.1 weight percent higher respectively than expected.

Test results of magnetic saturation measurements made on samples from the 300-gram buttons are listed in table II-14. Saturation of the aged samples was measured at room temperature, 1112°F (600°C), and at 1202°F (650°C). Samples of the martensitic alloys were annealed for one hour at 1832°F (1000°C) then aged for one hour at 1112°F (600°C) before testing.

TABLE II-13. Maximum Hardness Obtained by the Isochronal Aging of Vacuum Arc Melted Martensitic Alloys 1-A-V-1 to 1-A-V-6

Alloy Number	Nominal Alloy Composition (weight percent)	Aging Temperature at Which Maximum Room Temperature Hardness was Obtained (°F)	(°C)	Total Aging Time[a] (hours)	Maximum Room Temperature Hardness (VHN)	Room Temperature Coercivity at Maximum Hardness (oersteds)
1-A-V-1	48Fe-15Ni-30Co-2W-4Ta-0.5Al-0.5Ti	1112	600	4	732	39
1-A-V-2	66Fe-10Ni-20Co-3Ta-0.5Al-0.5Ti	1022	550	3	570	22
1-A-V-3	57.5Fe-12Ni-25Co-1W-3.5Ta-0.5Al-0.5Ti	1022	550	3	641	30.5
1-A-V-4	51Fe-15Ni-30Co-3Ta-0.5Al-0.5Ti	1112	600	4	670	35
1-A-V-5	49Fe-15Ni-30Co-2W-3Ta-0.5Al-0.5Ti	1112	600	4	704	37
1-A-V-6	60Fe-5Ni-5Cr-25Co-1W-3Ta-0.5Al-0.5Ti	1022	550	3	553	34

(a) Total aging time may be determined by adding one hour aging time for each 90°F (50°C) increment in temperature starting at 842°F (450°C).

Results obtained from coercive force measurements on samples of the 300-gram buttons are shown in table II-15. Coercive force was measured at several temperatures. Two samples were taken from each of the ferritic alloys for measurements. One sample was aged for one hour at 1112°F (600°C), the other sample was subjected to isothermal aging for 100 hours at 1022°F (550°C) before testing. In the case of the isothermally aged samples, coercive force was remeasured at room temperature after measurements at higher temperatures. The results indicate a slight reduction of coercive force value due to the tests at temperature.

Results of tensile tests, which were obtained on samples from the 300-gram buttons, are shown in table II-16. The ferritic samples were annealed one hour at 1832°F (1000°C), then machined to size and aged for one hour at 1112°F (600°C) before testing. The hardness of each sample was measured at room temperature before the test. This value is also shown in table II-16. The table lists yield stress at 0.2 percent plastic elongation, the ultimate tensile stress the uniform elongation, and the reduction of area at fracture. Tests were performed at room temperature and at 1112°F (600°C). Samples were held for 15 minutes at temperature before the start of testing. Tests at 1112°F (600°C) were conducted in argon. In the room temperature tests tensile specimens of the ferritic alloys with the exception of alloy 1-A-V-6 failed in a brittle manner at the radius of the fillet before 0.2 percent plastic elongation was reached. The stress at fracture is listed in those cases. Ferritic tensile specimens showed some necking when tested in 1112°F (600°C).

Hot-hardness values for samples from the 300-gram buttons are shown in table II-17. Samples of the ferritic alloys were annealed one hour at 1832°F (1000°C) and then aged for one hour at 1112°F (600°C) before testing. The temperature dependence of hardness of alloys 1-A-V-4 is shown in figure II-10.

The following requirements were set previously for selecting suitable alloys from the screening program and were applied to the selection of the final alloys for investigation:

1) Magnetic saturation at 1112°F (600°C) equal to or greater than 150 emu/g (15,000 guass).

2) Maximum room temperature hardness during isochronal aging equal to or greater than 550 VHN.

TABLE II-14. Saturation Magnetic Moment of 300-Gram Vacuum Arc Melted Martensitic Alloys 1-A-V-1 to 1-A-V-6

Alloy Number	Nominal Alloy Composition (weight percent)	Saturation Magnetic Moment (emu/g)[a]			
		After Annealing One Hour at 1832°F (1000°C)	After Annealing One Hour at 1832°F (1000°C) and Aging One Hour at 1112°F (600°C)		
		Tested at Room Temperature	Tested at Room Temperature	Tested at 1112°F (600°C)	Tested at 1202°F (650°C)
1-A-V-1	48Fe-15Ni-30Co-2W-4Ta-0.5Al-0.5Ti	181	183	160	149
1-A-V-2	66Fe-10Ni-20Co-3Ta-0.5Al-0.5Ti	208	206	172	165
1-A-V-3	57.5Fe-12Ni-25Co-1W-3.5Ta-0.5Al-0.5Ti	196	196	166	150
1-A-V-4	51Fe-15Ni-30Co-3Ta-0.5Al-0.5Ti	192	195	168	151
1-A-V-5	49Fe-15Ni-30Co-2W-3Ta-0.5Al-0.5Ti	185	187	161	153
1-A-V-6	60Fe-5Ni-5Cr-25Co-1W-3Ta-0.5Al-0.5Ti	184	186	150	139

(a) To convert the saturation magnetic moment to the approximate induction in gauss, multiply the listed value by 100.

TABLE II-15. Coercive Force Measurements on 300-Gram Vacuum Arc Melted Martensitic Alloys 1-A-V-1 to 1-A-V-6 at Different Temperatures

Alloy Number	Nominal Alloy Composition (weight percent)	Coercive Force (Oersteds)				
		Annealed One Hour at 1832°F (1000°C); Then Aged One Hour at 1112°F (600°C) Before Testing				
		Test Temperature				
		Room Temp.	1022°F (550°C)	1112°F (600°C)	1202°F (650°C)	Room[a] Temp.
1-A-V-1	48Fe-15Ni-30Co-2W-4Ta-0.5Al-0.5Ti	42.5	--	39.0	31.0	--
1-A-V-2	66Fe-10Ni-20Co-3Ta-0.5Al-0.5Ti	24.0	--	17.6	15.8	--
1-A-V-3	57.5Fe-12Ni-25Co-1W-3.5Ta-0.5Al-0.5Ti	32.8	--	25.0	22.5	--
1-A-V-4	51Fe-15Ni-30Co-3Ta-0.5Al-0.5Ti	37.0	--	30.0	26.0	--
1-A-V-5	49Fe-15Ni-30Co-2W-3Ta-0.5Al-0.5Ti	43.0	--	37.0	31.0	--
1-A-V-6	60Fe-5Ni-5Cr-25Co-1W-3Ta-0.5Al-0.5Ti	37.0	--	24.5	20.0	--
		Annealed One Hour at 1832°F (1000°C); Then Aged 100 Hours at 1022°F (550°C) Before Testing				
1-A-V-1	48Fe-15Ni-30Co-2W-4Ta-0.5Al-0.5Ti	62.5	56.0	51.0	48.0	63.0
1-A-V-2	66Fe-10Ni-20Co-3Ta-0.5Al-0.5Ti	30.0	22.0	20.0	20.0	28.0
1-A-V-3	57.5Fe-12Ni-25Co-1W-3.5Ta-0.5Al-0.5Ti	42.5	33.0	30.0	29.0	41.5
1-A-V-4	51Fe-15Ni-30Co-3Ta-0.5Al-0.5Ti	48.5	48.0	45.5	42.0	48.0
1-A-V-5	49Fe-15Ni-30Co-2W-3Ta-0.5Al-0.5Ti	62.5	58.0	53.0	48.5	62.0
1-A-V-6	60Fe-5Ni-5Cr-25Co-1W-3Ta-0.5Al-0.5Ti	37.0	22.0	20.0	18.1	32.0

(a) Room temperature results shown in the last column were measured after elevated temperature measurements were made.

TABLE II-16. Tensile Tests[a] of 300-Gram Vacuum Arc Melted Martensitic 1-A-V-1 to 1-A-V-6

Alloy Number	Nominal Alloy Composition (weight percent)	Room Temperature Hardness 50 k G Load (VHN)	Test Temperature °F	Test Temperature °C	0.2% Yield Strength (psi)	Ultimate Tensile Strength (psi)	Uniform Elongation (percent)	Reduction of Area (percent)
1-A-V-1	48Fe-15Ni-30Co-2W-4Ta-0.5Al-0.5Ti	747	77	25	71 650[b]	-	-	(c)
1-A-V-2	66Fe-10Ni-20Co-3Ta-0.5Al-0.5Ti	547	77	25	153 000[b]	-	-	(c)
1-A-V-3	57.5Fe-12Ni-25Co-1W-3.5Ta-0.5Al-0.5Ti	642	77	25	148 000[b]	-	-	(c)
1-A-V-4	51Fe-15Ni-30Co-3Ta-0.5Al-0.5Ti	687	77	25	140 500[b]	-	-	(c)
1-A-V-5	49Fe-15Ni-30Co-2W-3Ta-0.5Al-0.5Ti	685	77	25	131 800[b]	-	-	(c)
1-A-V-6	60Fe-5Ni-5Cr-25Co-1W-3Ta-0.5Al-0.5Ti	503	77	25	229 650	239 850	2.11	16.26
1-A-V-1	48Fe-15Ni-30Co-2W-4Ta-0.5Al-0.5Ti	747	1112	600	147 600	158 750	1.00	4.0
1-A-V-2	66Fe-10Ni-20Co-3Ta-0.5Al-0.5Ti	540	1112	600	101 200	115 050	1.93	43.9
1-A-V-3	57.5Fe-12Ni-25Co-1W-3.5Ta-0.5Al-0.5Ti	636	1112	600	115 300	129 050	1.43	30.6
1-A-V-4	51Fe-15Ni-30Co-3Ta-0.5Al-0.5Ti	685	1112	600	115 750	133 850	1.60	4.0
1-A-V-5	49Fe-15Ni-30Co-2W-3Ta-0.5Al-0.5Ti	723	1112	600	130 250	152 800	1.30	5.6
1-A-V-6	60Fe-5Ni-5Cr-25Co-1W-3Ta-0.5Al-0.5Ti	510	1112	600	97 950	104 650	1.06	76.4

(a) Samples were annealed one hour at 1832°F (1000°C), machined to size and then aged one hour at 1112°F (600°C) before testing.

(b) Fracture stress

(c) Broke at radius of fillet in a brittle manner

TABLE II-17. Hot Hardness Measurements[a] on Samples of 300-Gram Vacuum-Arc Melted Martensitic Alloys 1-A-V-1 to 1-A-V-6 after Annealing One Hour at 1832°F (1000°C) and Aging One Hour at 1112°F (600°C).

Alloy Number	Nominal Alloy Composition (weight percent)	Hot Hardness (VHN) Test Temperature 1112°F (600°C)	1202°F (650°C)	ΔVHN (b)
1-A-V-1	48Fe-15Ni-30Co-2W-4Ta-0.5Al-0.5Ti	340	267	-73
1-A-V-2	66Fe-10Ni-20Co-3Ta-0.5Al-0.5Ti	268	193	-75
1-A-V-3	57.5Fe-12Ni-25Co-1W-3.5Ta-0.5Al-0.5Ti	322	252	-70
1-A-V-4	51Fe-15Ni-30Co-3Ta-0.5Al-0.5Ti	338	215	-125
1-A-V-5	49Fe-15Ni-30Co-2W-3Ta-0.5Al-0.5Ti	355	250	-105
1-A-V-6	60Fe-5Ni-5Cr-25Co-1W-3Ta-0.5Al-0.5Ti	242	157	-85

(a) All measurements were made under vacuum of 2×10^{-5} torr at a load of 2.5 kG.
(b) $\Delta VHN = VHN_{650} - VHN_{600}$

3) Temperature at which maximum hardness was obtained equal to or greater than 1022°F (550°C).

4) Room temperature coercive force even after 100 hours aging at 1022°F (550°C) equal to or less than 50 oersteds.

5) The decrease in hardness during isothermal aging at 1022°F (550°C) from the maximum value should be less than 10 percent.

The requirements listed in 1, 2, and 3 were fulfilled by all selected alloys. Alloys 1-A-V-1 and 1-A-V-5 did not fulfill requirement 4. This may be due to the higher amount of tantalum and aluminum additions than expected. Alloy 1-A-V-2 does not meet requirement 5. The results very clearly show the influence of cobalt on stability and coercive force. The higher cobalt content produces better thermal stability, but the coercive force increases. Chromium addition resulted in lower coercive force.

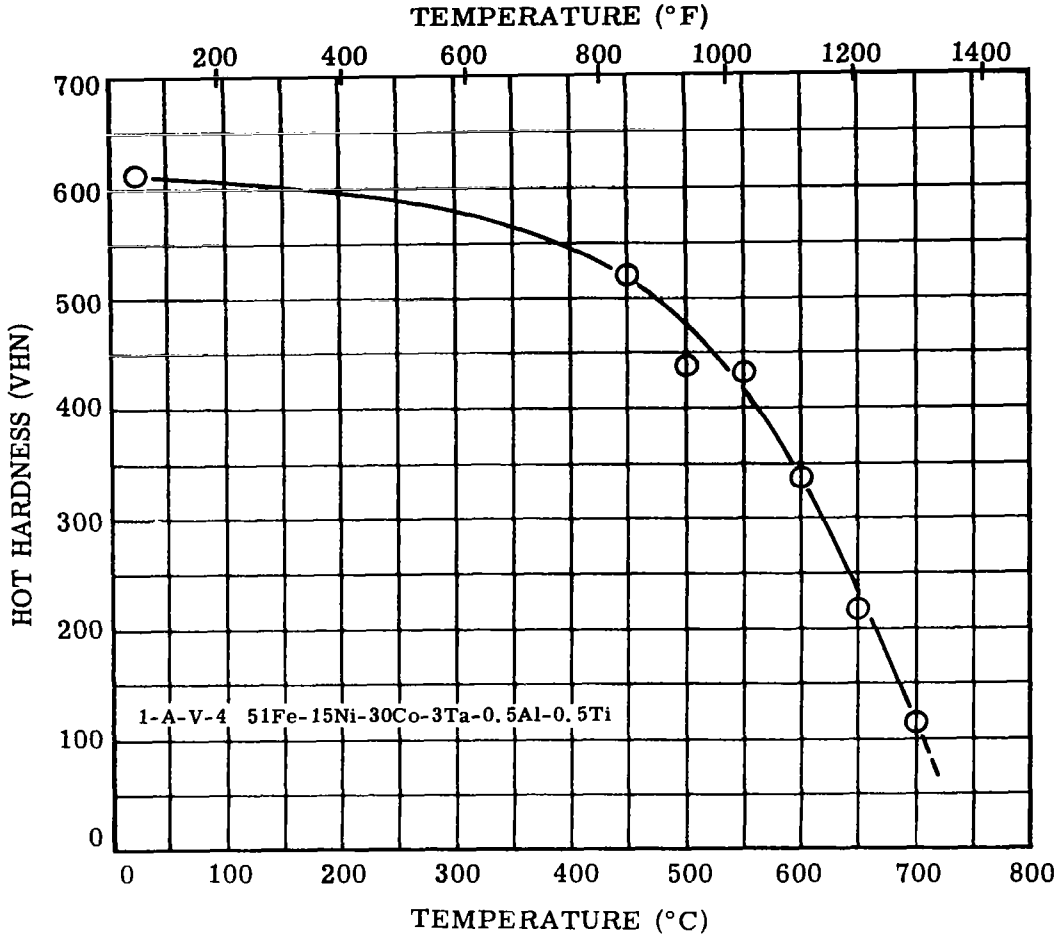

FIGURE II-10. Hot Hardness vs. Temperature of Alloy 1-A-V-4 After Annealing One Hour at 1382°F (1000°C) and Aging at 1112°F (600°C). Test Load 2.5 kG.

However, stability of hardness and saturation of alloy 1-A-V-6 is less than alloys 1-A-V-3 and 1-A-V-4. The latter two alloys were selected for the final alloy compositions with some minor adjustments. Cobalt was chosen at 30 percent to give better stability. Ta, Al, and Ti were reduced to decrease that coercive force.

The coercive force measurements at elevated temperature show that in the case of the iron-base alloys containing 30 percent cobalt (1-A-V-1, 1-A-V-4, 1-A-V-5), the reduction of coercive force from room temperature to 1112°F

(600°C) is between 15 and 20 percent; while in alloy 1-A-V-6 which contains chromium, the reduction is more than 30 percent. One may conclude that a further refinement in alloy development would be a suitable balance between tolerable coercive force and stability in strength. This balance may be obtained by adjusting the cobalt content versus aluminum and chromium content. An additional measure to keep the coercive force down would be the application for ~5 percent plastic strain prior to aging.

2. Cobalt-Base Alloys

a. SCREENING OF LEVITATION MELTED ALLOYS

More than forty cobalt-base alloys were melted and tested during the first portion of the screening program. Nominal compositions of the cobalt-base alloys are shown in table II-18. No tests were made on binary Co-Ni alloys because of the existence of the hexagonal phase at room temperature which prevents achievement of magnetic saturation with the available magnetizing field. Alloys 1-B-1 to 1-B-12 were formulated to determine the relative effect of iron and nickel on the room and elevated temperature magnetic saturation of the ternary cobalt-base alloys; thereby establishing the range of useful matrix compositions for precipitation hardening and fix the approximate range of composition which would provide a stable alloy with adequate strength and magnetic properties. Alloys 1-B-13 to 1-B-15 were formulated to determine the effect of precipitation hardening elements on several matrix compositions. Alloys 1-B-21 to 1-B-32 were formulated to determine the effect of iron, zirconium, and the aluminum to titanium ratio on the precipitation hardening process. Alloys 1-B-33 to 1-B-46 were tested to determine the effect of addition elements on the precipitation hardened matrix containing Al+Ti+Zr. The series 1-B-V-1 to 1-B-V-6 shown in table II-19 were melted in larger size buttons. Additional mechanical and magnetic tests and analyses on alloys 1-B-V-1 to 1-B-V-6 provided data for the selection of the final alloys 1-B-S-1 and 1-B-S-2 (compositions shown in table II-20).

The results from alloy 1-B-1 to 1-B-12 show (see figure II-11) that increasing nickel content decreases magnetic saturation values at room temperature and even more so at 1112°F (600°C). Iron increases the magnetic saturation at room temperature as reported in the literature (ref. II-22). However, the influence of iron on magnetic saturation is negligible at 1112°F (600°C).

TABLE II-18. Nominal Compositions of Cobalt-Base Alloys Used in the Screening Tests(a)

Alloy Number	Nominal Alloy Composition (weight percent)	Nominal Alloy Composition (atomic percent)
1-B-1	95Co-5Fe	94.74Co-5.26Fe
1-B-2	90Co-5Ni-5Fe	84.52Co-4.99Ni-10.49Fe
1-B-3	85Co-10Ni-5Fe	84.73Co-10.01Ni-5.26Fe
1-B-4	80Co-15Ni-5Fe	79.73Co-15.01Ni-5.26Fe
1-B-5	75Co-20Ni-5Fe	74.73Co-20.01Ni-5.26Fe
1-B-6	70Co-25Ni-5Fe	69.74Co-25.0Ni-5.26Fe
1-B-7	65Co-30Ni-5Fe	64.74Co-30.0Ni-5.26Fe
1-B-8	85Co-5Ni-10Fe	84.52Co-4.99Ni-10.49Fe
1-B-9	80Co-5Ni-15Fe	79.32Co-4.98Ni-15.70Ni
1-B-10	75Co-5Ni-20Fe	74.17Co-4.96Ni-20.87Fe
1-B-11	70Co-5Ni-25Fe	69.0Co-4.96Ni-26.0Fe
1-B-12	65Co-5Ni-30Fe	64.2Co-4.96Ni-31.1Fe
1-B-13	86Co-5Fe-5Ni-3Ti-1Al	84.18Co-5.16Fe-4.91Ni-3.61Ti-2.14Al
1-B-14	81Co-5Fe-10Ni-3Ti-1Al	79.27Co-5.16Fe-9.82Ni-3.61Ti-2.14Al
1-B-15	76Co-5Fe-15Ni-3Ti-1Al	74.36Co-5.16Fe-14.73Ni-3.61Ti-2.14Al
1-B-21	76.5Co-20Ni-2Ti-0.5Al-1.0Zr	75.92Co-19.92Ni-2.44Ti-1.08Al-0.64Zr
1-B-22	77.3Co-20Ni-2Ti-0.5Al-0.2Zr	76.49Co-19.87Ni-2.43Ti-1.08Al-0.13Zr
1-B-23	77.5Co-20Ni-2Ti-0.5Al	76.64Co-19.85Ni-2.43Ti-1.08Al
1-B-24	76Co-20Ni-3Ti-1Al	74.55Co-19.69Ni-3.62Ti-2.14Al
1-B-25	71Co-5Fe-20Ni-3Ti-1Al	69.45Co-5.16Fe-19.64Ni-3.61Ti-2.14Al
1-B-26	66Co-10Fe-20Ni-3Ti-1Al	64.39Co-10.29Fe-19.59Ni-3.60Ti-2.13Al
1-B-27	81Co-15Ni-3Ti-1Al	79.47Co-14.77Ni-3.62Ti-2.14Al
1-B-28	71Co-10Fe-15Ni-3Ti-1Al	69.28Co-10.30Fe-14.69Ni-3.60Ti-2.13Al
1-B-29	75.7Co-5Fe-15Ni-3.8Ti-0.5Al	74.37Co-5.18Fe-14.79Ni-4.59Ti-1.07Al
1-B-30	76.3Co-5Fe-15Ni-2.2Ti-1.5Al	74.36Co-5.14Fe-14.67Ni-2.64Ti-3.19Al
1-B-31	76.6Co-5Fe-15Ni-1.4Ti-2.0Al	74.35Co-5.12Fe-14.62Ni-1.67Ti-4.24Al

(a) All alloys listed in this table were made by the levitation melting technique as described in Section II-B. 1.

TABLE II-18. Nominal Compositions of Cobalt-Base Alloys Used in the Screening Tests(a) (Continued)

Alloy Number	Nominal Alloy Composition (weight percent)	Nominal Alloy Composition (atomic percent)
1-B-32	75.8Co-5Fe-15Ni-2.2Ti-1.5Al-0.5Zr	73.99Co-5.15Fe-14.70Ni-2.64Ti-3.20Al-0.32Zr
1-B-33	70.8Co-5Fe-15Ni-2.2Ti-1.5Al-0.5Zr-5Cu	69.36Co-5.17Fe-14.75Ni-2.65Ti-3.21Al-0.32Zr-4.54Cu
1-B-34	70.8Co-5Fe-15Ni-2.2Ti-1.5Al-0.5Zr-5Mn	68.87Co-5.13Fe-14.65Ni-2.63Ti-3.19Al-0.31Zr-5.22Mn
1-B-35	73.8Co-5Fe-15Ni-2.2Ti-1.5Al-0.5Zr-2Si	70.47Co-5.04Fe-14.39Ni-2.59Ti-3.13Al-0.31Zr-4.07Si
1-B-36	75.3Co-5Fe-15Ni-2.2Ti-1.5Al-0.5Zr-0.5Be	71.57Co-5.02Fe-14.31Ni-2.57Ti-3.11Al-0.31Zr-3.11Be
1-B-37	70.8Co-5Be-15Ni-2.2Ti-1.5Al-0.5Zr-5Cr	68.66Co-5.12Fe-14.60Ni-2.63Ti-3.18Al-0.31Zr-5.50Cr
1-B-38	70.8Co-5Fe-15Ni-2.2Ti-1.5Al-0.5Zr-5W	71.48Co-5.33Fe-15.20Ni-2.73Ti-3.31Al-0.33Zr-1.62W
1-B-39	70.8Co-5Fe-15Ni-2.2Ti-1.5Al-0.5Zr-5Ta	71.46Co-5.33Fe-15.20Ni-2.73Ti-3.31Al-0.33Zr-1.64Ta
1-B-40	70.8Co-5Fe-15Ni-2.2Ti-1.5Al-0.5Zr-5Mo	70.44Co-5.25Fe-14.98Ni-2.69Ti-3.26Al-0.32Zr-3.06Mo
1-B-41	70.8Co-5Fe-15Ni-2.2Ti-1.5Al-0.5Zr-5V	68.6Co-5.11Fe-14.59Ni-2.62Ti-3.17Al-0.31Zr-5.60V
1-B-42	70.8Co-5Fe-15Ni-2.2Ti-1.5Al-0.5Zr-5Nb	70.37Co-5.24Fe-14.97Ni-2.69Ti-3.26Al-0.32Zr-3.15Nb
1-B-43	71Co-5Fe-15Ni-2.2Ti-1.5Al-0.3Zr-5Ta	71.62Co-5.32Fe-15.19Ni-2.73Ti-3.30Al-0.20Zr-1.64Ta
1-B-44	73Co-5Fe-15Ni-2.2Ti-1.5Al-0.3Zr-3Ta	72.66Co-5.25Fe-14.98Ni-2.69Ti-3.26Al-0.19Zr-0.97Ta
1-B-45	71.7Co-5Fe-15Ni-1.5Ti-1.5Al-0.3Zr-5Ta	72.44Co-5.33Fe-15.21Ni-1.86Ti-3.31Al-0.20Zr-1.65Ta
1-B-46	76Co-5Fe-10Ni-2.2Ti-1.5Al-0.3Zr-5Ta	76.67Co-5.32Fe-10.13Ni-2.73Ti-3.31Al-0.20Zr-1.64Ta

(a) All alloys listed in this table were made by the levitation melting technique as described in Section II-B.1.

TABLE II-19. Composition of 300-Gram Vacuum Arc Melted Cobalt-Base Alloys 1-B-V-1 to 1-B-V-6

(a) Nominal Composition (weight percent)

Alloy Number	Fe	Co	Ni	Ta	Ti	Al	W	Cu	C	Zr
1-B-V-1	5	71.7	15	5	1.5	1.5	-	-	-	0.3
1-B-V-2	5	80.5	10	3	-	1.2	-	-	-	0.3
1-B-V-3	5	76.3	12	4	1.0	1.4	-	-	-	0.3
1-B-V-4	5	73.5	15	5	-	1.2	-	-	-	0.3
1-B-V-5	5	78.2	10	5	-	1.5	-	-	-	0.3
1-B-V-6	5	74.0	15	3	1.5	1.2	-	-	-	0.3

(b) Analyzed Composition (weight percent)

Alloy Number	Fe	Co	Ni	Ta	Ti	Al	W	Cu	C	Zr
1-B-V-1	5.0	71.4	14.6	5.20	1.66	1.44	0.010	0.29	0.0030	0.27
1-B-V-2	4.8	79.2	10.3	3.07	<0.2	1.19	0.008	0.018	0.0036	0.27
1-B-V-3	4.9	76.0	11.9	4.05	1.07	1.40	0.029	0.087	0.0039	0.26
1-B-V-4	5.1	72.8	14.8	5.19	<0.2	1.25	<0.005	0.018	0.0045	0.26
1-B-V-5	5.0	77.0	9.85	5.30	0.2	1.60	0.11	0.023	0.0047	0.27
1-B-V-6	4.8	73.8	15.0	3.10	1.66	1.19	0.12	0.013	0.0046	0.24

(c) Analyzed Composition (atomic percent)

Alloy Number	Fe	Co	Ni	Ta	Ti	Al	W	Cu	C	Zr
1-B-V-1	5.34	bal	14.83	1.71	2.07	3.18	-	-	-	0.18
1-B-V-2	5.09	bal	10.39	1.00	-	2.61	-	-	-	0.19
1-B-V-3	5.20	bal	12.02	1.33	1.32	3.08	-	-	-	0.17
1-B-V-4	5.48	bal	15.12	1.72	-	2.78	-	-	-	0.17
1-B-V-5	5.35	bal	10.03	1.75	-	3.55	-	-	-	0.18
1-B-V-6	5.02	bal	14.92	1.00	2.02	4.31	-	-	-	0.15

TABLE II-20. Composition of Final Cobalt-Base Alloys Vacuum Induction Melted as 15-Pound Ingots

(a) Nominal Composition (weight percent)

Alloy Number	Fe	Ni	Co	W	Ta	Al	Ti	Zr	Be	B	C	Ce
1-B-S-1	5	15	73.55	-	5.0	1.25	-	0.2	-	0.001	-	-
1-B-S-2	5	15	73.55	-	5.0	1.25	-	0.1	0.1	0.001	-	-

(b) Analyzed Composition (weight percent)

Alloy Number	Fe	Ni	Co	W	Ta	Al	Ti	Zr	Be	B	C	Ce
1-B-S-1	5.8	15.3	71.3	-	4.98	1.28	-	0.21	-	0.003	0.0062	-
1-B-S-2	5.2	15.2	72.4	-	4.98	1.36	-	0.12	0.065	0.002	0.0062	0.006

(c) Analyzed Composition (atomic percent)

Alloy Number	Fe	Ni	Co	W	Ta	Al	Ti	Zr	Be	B	C	Ce
1-B-S-1	6.22	15.60	bal	-	1.65	2.84	-	0.14	-	-	-	-
1-B-S-2	5.55	15.43	bal	-	1.64	3.00	-	0.08	0.43	-	-	-

The alloys containing addition elements were subjected to magnetic saturation measurements (see table II-21) at room temperature after annealing for one hour and quenching in oil. Then the samples were aged for one hour at 1292°F (700°C) to provide precipitation hardening and tested again at room temperature and at 1112°F (600°C). The measured saturation values are presented in this report as magnetic moment per gram (σ) which may be converted to the approximate saturation induction (B_S) by the equation $B_S = 4\pi\sigma\delta$. The density δ was not determined for the experimental alloys. A value of 8.8g/cc was used for the cobalt-base alloys. In only a few cases did the values of magnetic saturation differ noticeably when measured at room temperature before and after aging. The results (table II-21) show that in the more complex alloys, nickel and iron have the same relative influence on magnetic saturation as they have in the ternary alloys. All other elements

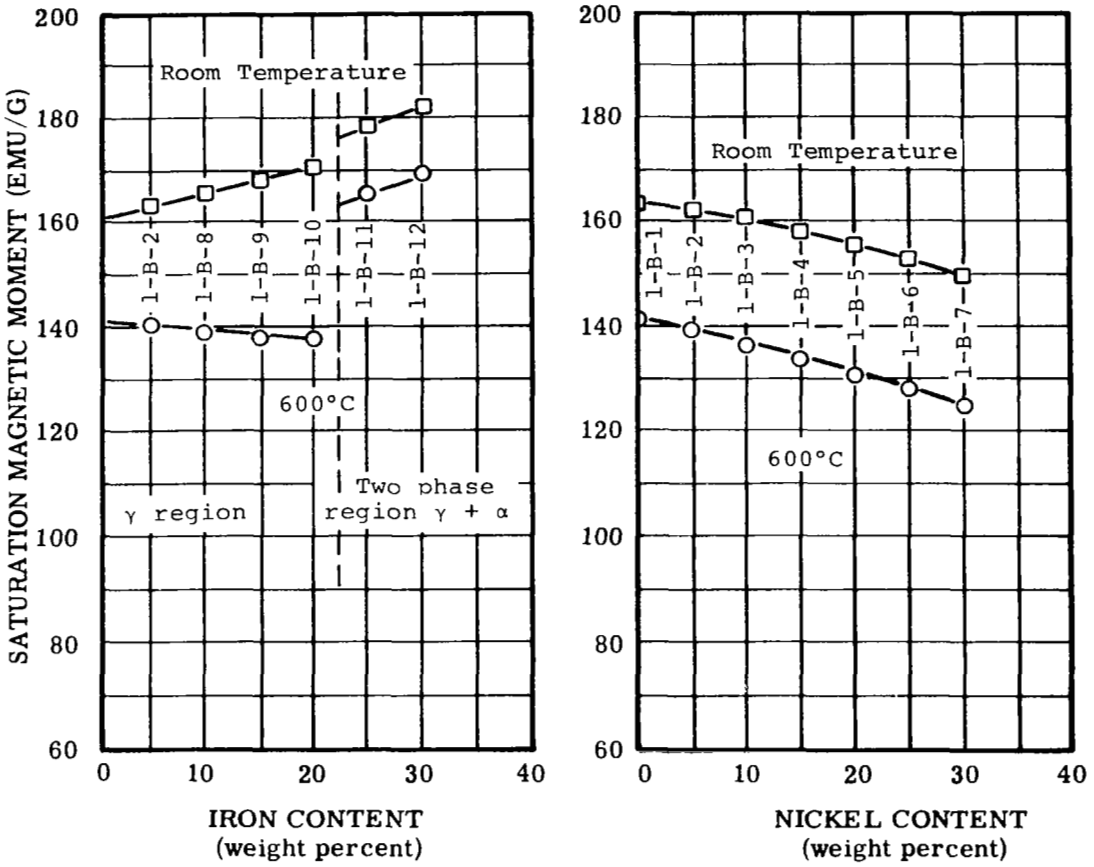

FIGURE II-11. Influence of Iron and Nickel on the Magnetic Saturation of Cobalt-5% Nickel and Cobalt-5% Iron Alloys Respectively (Alloys 1-B-2, 1-B-8 1-B-12 and 1-B-1 to 1-B-7)

TABLE II-21. Saturation Magnetic Moment of Cobalt-Base Alloys with Additions[a]

Alloy Number	Nominal Alloy Composition (weight percent)	Saturation Magnetic Moment (emu/g)[b]		
		After Annealing One Hour at 2012°F (1100°C)	After Aging One Hour at 1292°F (700°C)	
		Tested at Room Temperature	Tested at Room Temperature	Tested at 1112°F (600°C)
1-B-13	86Co-5Fe-5Ni-3Ti-1Al	146	142	109
1-B-14	81Co-5Fe-10Ni-3Ti-1Al	142	137	106
1-B-15	76Co-5Fe-15Ni-3Ti-1Al	136	132	102
1-B-21	76.5Co-20Ni-2Ti-1Zr-0.5Al	128	128	105
1-B-22	77.3Co-20Ni-2Ti-0.2Zr-0.5Al	131	132	108
1-B-23	77.5Co-20Ni-2Ti-0.5Al	132	132	102
1-B-24	76Co-20Ni-3Ti-1Al	124	123	100
1-B-25	71Co-20Ni-3Ti-1Al-5Fe	128	128	100
1-B-26	66Co-20Ni-3Ti-1Al-10Fe	134	134	100
1-B-27	81Co-15Ni-3Ti-1Al	128	128	103
1-B-28	71Co-15Ni-3Ti-1Al-10Fe	137	137	102
1-B-29	75.7Co-15Ni-3.8Ti-0.5Al-5Fe	132	131	104
1-B-30	76.3Co-15Ni-2.2Ti-1.5Al-5Fe	134	133	103
1-B-31	76.6Co-15Ni-1.4Ti-2.0Al-5Fe	136	136	104
1-B-32	75.8Co-15Ni-5Fe-2.2Ti-1.5Al-0.5Zr	133	132	103
1-B-33	70.8Co-15Ni-5Fe-2.2Ti-1.5Al-0.5Zr-5Cu	124	125	93
1-B-34	70.8Co-15Ni-5Fe-2.2Ti-1.5Al-0.5Zr-5Mn	122	122	65
1-B-35	73.8Co-15Ni-5Fe-2.2Ti-1.5Al-0.5Zr-2Si	120	118	79
1-B-36	75.3Co-15Ni-5Fe-2.2Ti-1.5Al-0.5Zr-0.5Be	128	128	97
1-B-37	70.8Co-15Ni-5Fe-2.2Ti-1.5Al-0.5Zr-5Cr	99	99	32
1-B-38	70.8Co-15Ni-5Fe-2.2Ti-1.5Al-0.5Zr-5W	117	115	84
1-B-39	70.8Co-15Ni-5Fe-2.2Ti-1.5Al-0.5Zr-5Ta	116	116	90
1-B-40	70.8Co-15Ni-5Fe-2.2Ti-1.5Al-0.5Zr-5Mo	110	107	70
1-B-41	70.8Co-15Ni-5Fe-2.2Ti-1.5Al-0.5Zr-5V	103	97	62
1-B-42	70.8Co-15Ni-5Fe-2.2Ti-1.5Al-0.5Zr-5Nb	109	108	82
1-B-43	71Co-15Ni-5Fe-2.2Ti-1.5Al-0.3Zr-5Ta	119	117	90
1-B-44	73Co-15Ni-5Fe-2.2Ti-1.5Al-0.3Zr-3Ta	124	122	95
1-B-45	71.7Co-15Ni-5Fe-1.5Ti-1.5Al-0.3Zr-5Ta	122	122	94
1-B-46	76Co-10Ni-5Fe-2.2Ti-1.5Al-0.3Zr-5Ta	123	122	93

(a) For the saturation magnetic moment of binary and ternary cobalt alloys see Figure II-11.
(b) To convert saturation magnetic moment to the approximate induction in gauss, multiply the listed value by 110.

added to form the complex alloy reduce the magnetic saturation at both room and elevated temperatures as compared to the simple ternary alloys. At room temperature, the influence of chromium, columbium and vanadium are most pronounced in reducing the magnetic saturation (see table II-21). At 1112°F (600°C), the influence of chromium is by far the greatest of all addition elements. Manganese and vanadium have a strong influence at this temperature. The effect of the other elements on magnetic saturation were balanced against their effect on strength for the analytical evaluation.

The hardening response of alloys to which the various elements and combinations of elements were added was determined by isochronal aging (see section II.B.4.). Samples were aged for one hour at each 90°F aging interval from 932°F (in the case of the levitation melts) or 1202°F (for the larger melts) to 1382°F or 1472°F. Vickers pyramid hardness and coercive force were measured at room temperature after each one-hour aging interval.

Data obtained from several representative cobalt-base alloys are plotted in figure II-12. The maximum values of room temperature hardness, which were measured during this aging sequence, are listed in table II-22 together with the aging temperature where maximum hardness was obtained. The room temperature coercivity is listed for the same aging temperature. The data indicate that higher nickel content, when addition elements remain constant result in higher hardness values. A decrease in the aluminum to titanium ratio, when total Al+Ti expressed in atomic percent stays constant, also results in an increase in hardness. This agrees with the results obtained by Mihalisin and Decker for ternary Ni-Al-Ti alloys (ref. II-23). The addition of iron decreases the hardness if the other additions remain constant. Addition of zirconium also increases hardness. Evaluation of the results from alloys 1-B-32 to 1-B-42 show that additions of Be, W, Ta, Mo, and Nb increase the maximum hardness value substantially. On the other hand the additions of Cu, Si, and V produce only a moderate increase of hardness. If Mn or Cr are added to a similar Co-Ni-Fe matrix with the Al and Ti additions, lower hardness values are obtained than the compositions in the absence of Mn or Cr.

It may be noted in table II-22 that the temperature at which maximum hardness was obtained during isochronal aging changed as the alloying additions were changed.

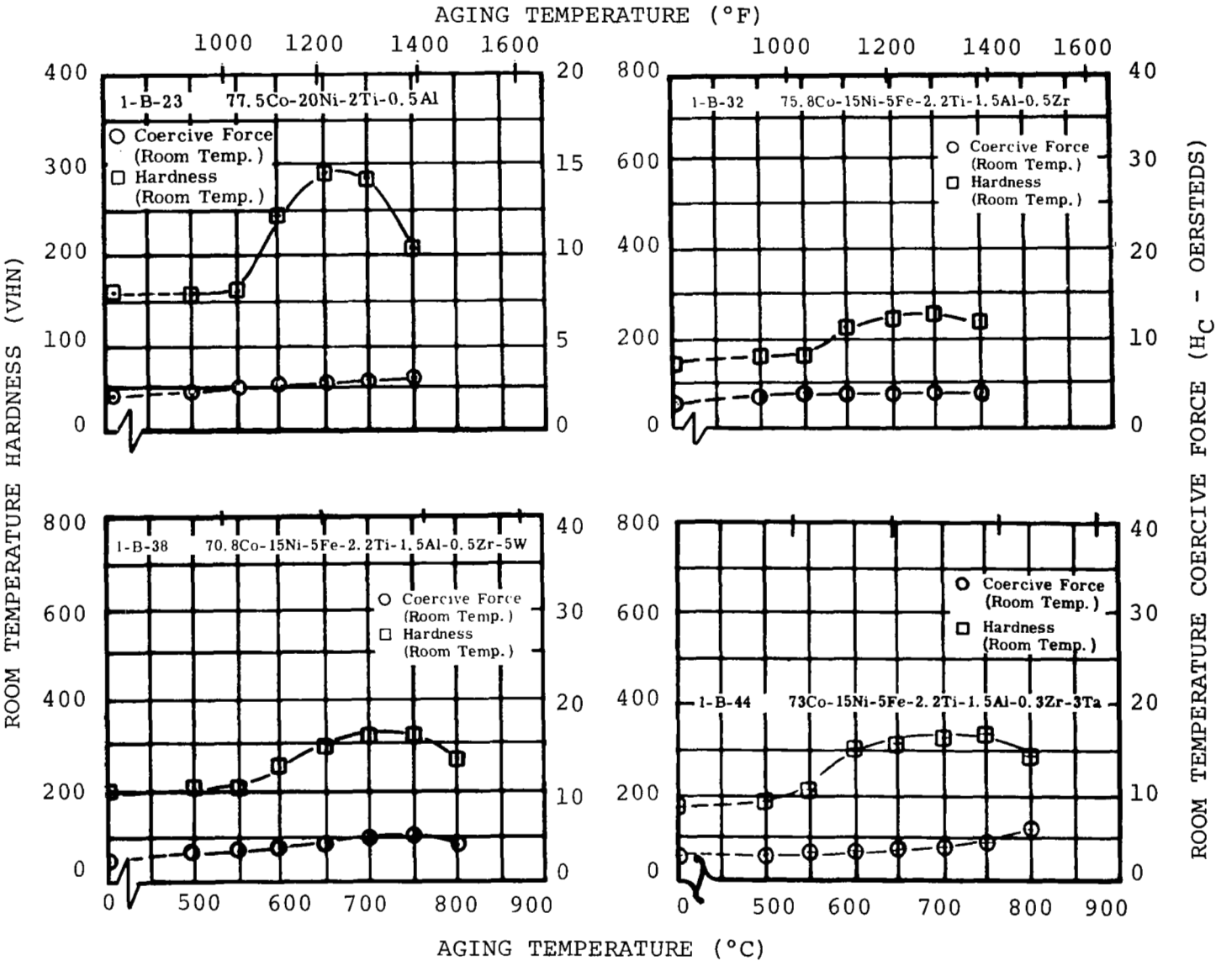

FIGURE II-12. Hardness and Coercive Force of Representative Cobalt-Base Alloys at Room Temperature After Aging One Hour at Temperature

TABLE II-22. Results of Isochronal and Isothermal Aging Tests on Levitation-Melted Cobalt Base Alloys

Alloy Number	Nominal Alloy Composition (weight percent)	Isochronal Tests: Aging Temperature at which Maximum Hardness was obtained (°F)	Isochronal Tests: Aging Temperature at which Maximum Hardness was obtained (°C)	Isochronal Tests: Maximum Room Temperature Hardness[b] (VHN_m)	Isochronal Tests: Room Temperature Coercivity at Maximum Hardness (Oe)	Isothermal Tests (After 100 hours) 1292 (700°C): Room Temperature Hardness (VHN_{100})	Isothermal Tests (After 100 hours) 1292 (700°C): Room Temperature Coercivity H_{c100} (Oe)	Isothermal Tests (After 100 hours) 1292 (700°C): Discontinuous Precipitate (volume percent)
Nivco Alloy	73.4Co-23.4Ni-0.3Fe-1.7Ti-0.4Al-0.2Zr-0.3Si-0.3Mn	1202	650	272	3.9	303	17.0	10
1-B-13	86Co-5Ni-5Fe-3Ti-1Al	1112	600	218	1.62	220	7	4
1-B-14	81Co-10Ni-5Fe-3Ti-1Al	1292	700	239	2.45	260	8.5	4
1-B-15	76Co-15Ni-5Fe-3Ti-1Al	1292	700	273	3.36	290	10.5	5
1-B-21	76.5Co-20Ni-2Ti-0.5Al-1Zr	1292	700	329	7.65	346	15.1	4
1-B-22	77.3Co-20Ni-2Ti-0.5Al-0.2Zr	1292	700	309	5.00	331	11.0	3
1-B-23	77.5Co-20Ni-2Ti-0.5Al	1202	650	280	3.03	325	10.8	13
1-B-24	76Co-20Ni-3Ti-1Al	1292	700	327	6.41	351	15.2	17
1-B-25	71Co-20Ni-5Fe-3Ti-1Al	1292	700	290	4.3	332	7.8	6
1-B-26	66Co-20Ni-10Fe-3Ti-1Al	1292	700	270	3.3	310	5.0	2
1-B-27	81Co-15Ni-3Ti-1Al	1292	700	310	3.8	325	15.1	9
1-B-28	71Co-15Ni-10Fe-3Ti-1Al	1292	700	258	3.4	289	4.7	1
1-B-29	75.7Co-15Ni-5Fe-3.8Ti-0.5Al	1292	700	303	3.5	340	10.0	5
1-B-30	76.3Co-15Ni-5Fe-2.2Ti-1.5Al	1292	700	239	3.1	269	4.6	1
1-B-31	76.6Co-15Ni-5Fe-1.4Ti-2.0Al	1202	650	209	1.9	221	3.0	0
1-B-32	75.8Co-15Ni-5Fe-2.2Ti-1.5Al-0.5Zr	1292	700	264	3.8	297	8.7	0
1-B-33	70.8Co-15Ni-5Fe-2.2Ti-1.5Al-0.5Zr-5Cu	1202	650	280	4.0	301	17.0	0
1-B-44	70.8Co-15Ni-5Fe-2.2Ti-1.5Al-0.5Zr-5Mn	1112	600	224	2.5	-	-	-
1-B-35	73.8Co-15Ni-5Fe-2.2Ti-1.5Al-0.5Zr-2Si	1112	600	293	5.0	282	29.0	0
1-B-36	75.3Co-15Ni-5Fe-2.2Ti-1.5Al-0.5Zr-0.5Be	1382	750	353	42.0	377	82.0	1
1-B-37	70.8Co-15Ni-5Fe-2.2Ti-1.5Al-0.5Zr-5Cr	1202	650	256	3.0	269	8.4	0
1-B-38	70.8Co-15Ni-5Fe-2.2Ti-1.5Al-0.5Zr-5W	1382	750	328	5.3	378	10.5	1
1-B-39	70.8Co-15Ni-5Fe-2.2Ti-1.5Al-0.5Zr-5Ta	1382	750	383	7.1	420	19.0	0
1-B-40	70.8Co-15Ni-5Fe-2.2Ti-1.5Al-0.5Zr-5Mo	1292	700	330	5.85	389	32.0	0
1-B-41	70.8Co-15Ni-5Fe-2.2Ti-1.5Al-0.5Zr-5V	1202	650	287	3.3	337	38.0	0
1-B-42	70.8Co-15Ni-5Fe-2.2Ti-1.5Al-0.5Zr-5Nb	1382	750	433	20.0	440	93.0	0
1-B-43	71Co-15Ni-5Fe-2.2Ti-1.5Al-0.3Zr-5Ta	1382	750	393	7.2	422	34.0	0
1-B-44	73Co-15Ni-5Fe-2.2Ti-1.5Al-0.3Zr-3Ta	1382	750	339	4.9	402	21.0	0
1-B-45	71.7Co-15Ni-5Fe-1.5Ti-1.5Al-0.3Zr-5Ta	1382	750	385	6.8	420	22.0	0
1-B-46	76Co-10Ni-5Fe-2.2Ti-1.5Al-0.3Zr-5Ta	1382	750	380	6.9	431	28.5	0

Additions of Mn, Si, Cr, and V reduced this temperature, while Be, W, Ta and Nb additions increased this temperature to 1382°F (750°C). A very large coercive force value is associated with the maximum hardness values in alloys with Be and Nb additions. One might conclude that these effects depend on the solubilities of the added elements which are in turn dependent on the various combinations of elements. However, a contribution arises from the change in strength and coherency strains of the precipitate when its composition is altered by the presence of different elements.

After isochronal aging, most of the samples were homogenized by a double heat-treatment and isothermally aged as described in section II.B.4. The samples were aged at 1292°F (700°C) for 100 hours. Room temperature hardness and coercive force were measured at several intervals and after 100 hours. Plots of the results from several typical alloys are shown in figure II-13. The long aging treatments produce higher hardness and coercive force values. In the case of Ta and Nb additions hardness in excess of 400 VHN was attained. The room temperature coercive force of the alloys containing Be or Nb additions were as high as 82 or 93 oersteds. No overaging was observed in any of those alloys during aging at 1292°F (700°C).

b. SELECTION AND EVALUATION OF INTERMEDIATE VACUUM ARC MELTED ALLOYS

A comparison of the data obtained from the screening tests of the cobalt-base alloys, listed in tables II-21 and II-22 with those from the screening tests of the martensitic iron-base alloys (tables II-10 and II-11) showed that hardness values and values of magnetic saturation of the cobalt-base alloys were substantially lower. However, the temperature at which the maximum hardness was obtained was much higher; in some instances even 1382°F (750°C), which indicates that the permissible service temperature in this type of alloy may be 270°F higher than the martensitic alloys. Under these circumstances, it appeared fruitful to study this system further in spite of the inferior values of magnetic saturation and hardness compared to the martensitic alloys.

If a superficial comparison of hardness and magnetic saturation values obtained in the experimental alloys is made with those of the final commercial Nivco alloy, one might conclude that no substantial improvement was obtained in the experimental alloys. The value of magnetic saturation induction of Nivco alloy at 1112°F (600°C) was B_s = 11,000 gauss (σ = 100 emu/g).

The hardness value in the final heat treatment condition was about 320 to 340 VHN. No experimental alloys attained hardness and saturation values which were simultaneously larger than these values for Nivco alloy. However, such a comparison neglects two important facts. First, the hardness in the Nivco alloy material is obtained by a lengthy heat treatment and can in no way be compared to hardness values obtained by the rather simple aging treatment applied during this study. Therefore, a sample of Nivco alloy was heat treated according to the aging routine used throughout the present program. In this case the hardness obtained in Nivco alloy reached only 300 VHN after the isothermal aging of 100 hours at 1292°F (700°C). Secondly, one should not neglect the fact that Nivco alloy contains about 15 percent discontinuous precipitate after its final heat treatment. Such discontinuous precipitate contributes to the measured values of hardness and short time tensile strength (refs. II-24 and II-25). It is, however, detrimental to long-term creep strength.

A requirement was established during the development of the screening program. No discontinuous precipitate was tolerated after isothermal aging for 100 hours at 1292°F (700°C). A simple comparison of the hardness of an alloy having no discontinuous precipitate to a Nivco alloy sample with 10 or 15 percent discontinuous precipitate is therefore meaningless. However, the creep strength of an alloy with the same or even lower hardness with no discontinuous precipitate may be far superior to the creep strength obtained in Nivco alloy provided that the other parameters are similar.

A further improvement of some of the experimental alloys is indicated by the temperature at which the maximum hardness was obtained during the isochronal aging. A temperature of 1202°F (650°C) was obtained for the Nivco alloy sample. In some of the experimental alloys, this temperature was as high as 1382°F (750°C). Using this temperature parameter as the criterion, alloy selection was confirmed to 1-B-36, 1-B-38, 1-B-39, and 1-B-42 to 1-B-46.

These alloys exhibited high hardness values. However, the magnetic saturation values at 1112°F (600°C) were less than that of Nivco alloy. The coercive force values measured in alloys 1-B-36 and 1-B-42 after isothermal aging at 1292°F (700°C) were high. The data indicates that the addition of Ta+Ti+Al to the cobalt-base alloys were the most beneficial. It is interesting to note that a combination of the same elements produced the best results in the martensitic alloys.

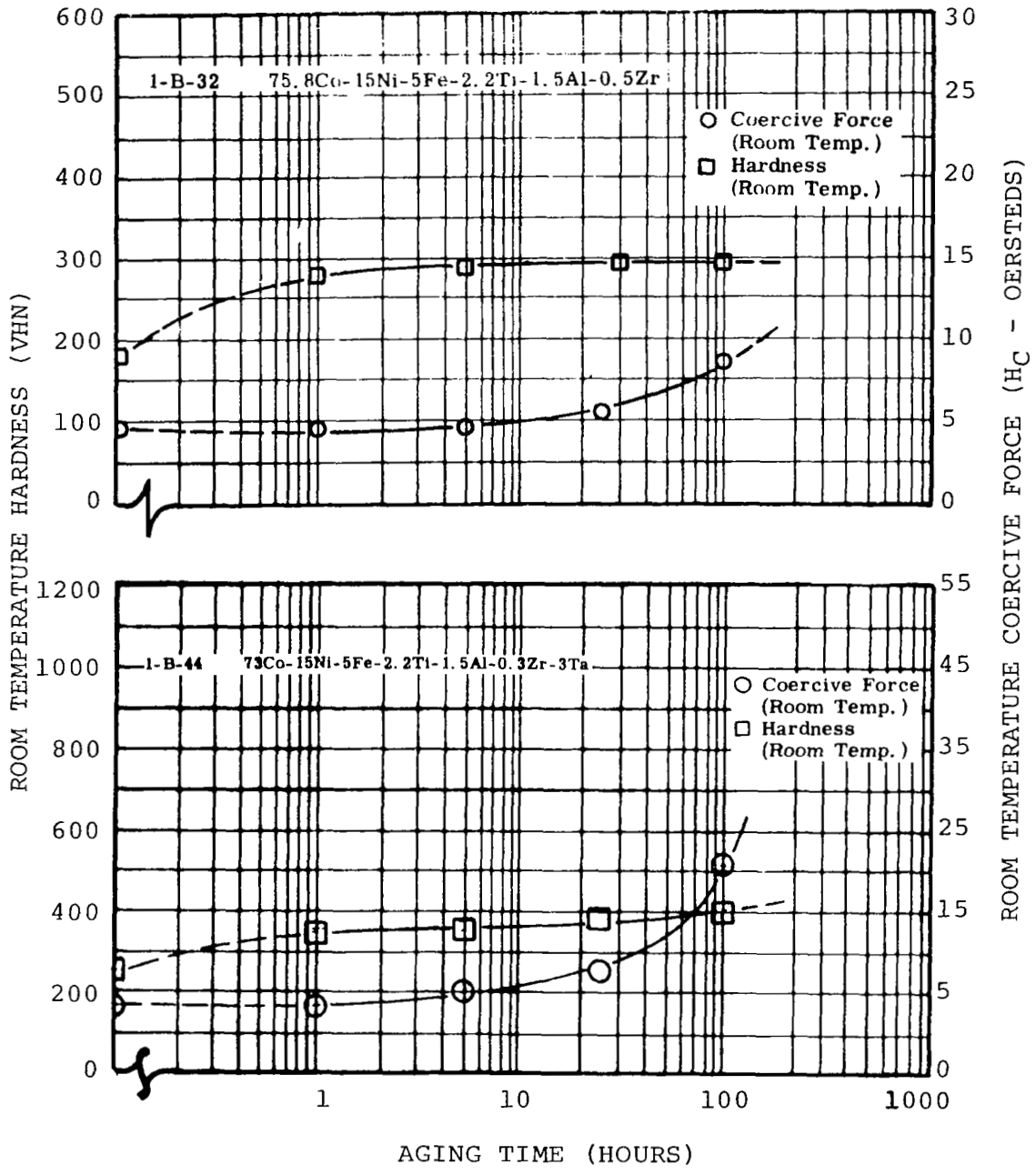

FIGURE II-13. Change in Room Temperature Hardness and Coercive Force of Representative Cobalt-Base Alloys During Isothermal Aging at 1292°F (700°C)

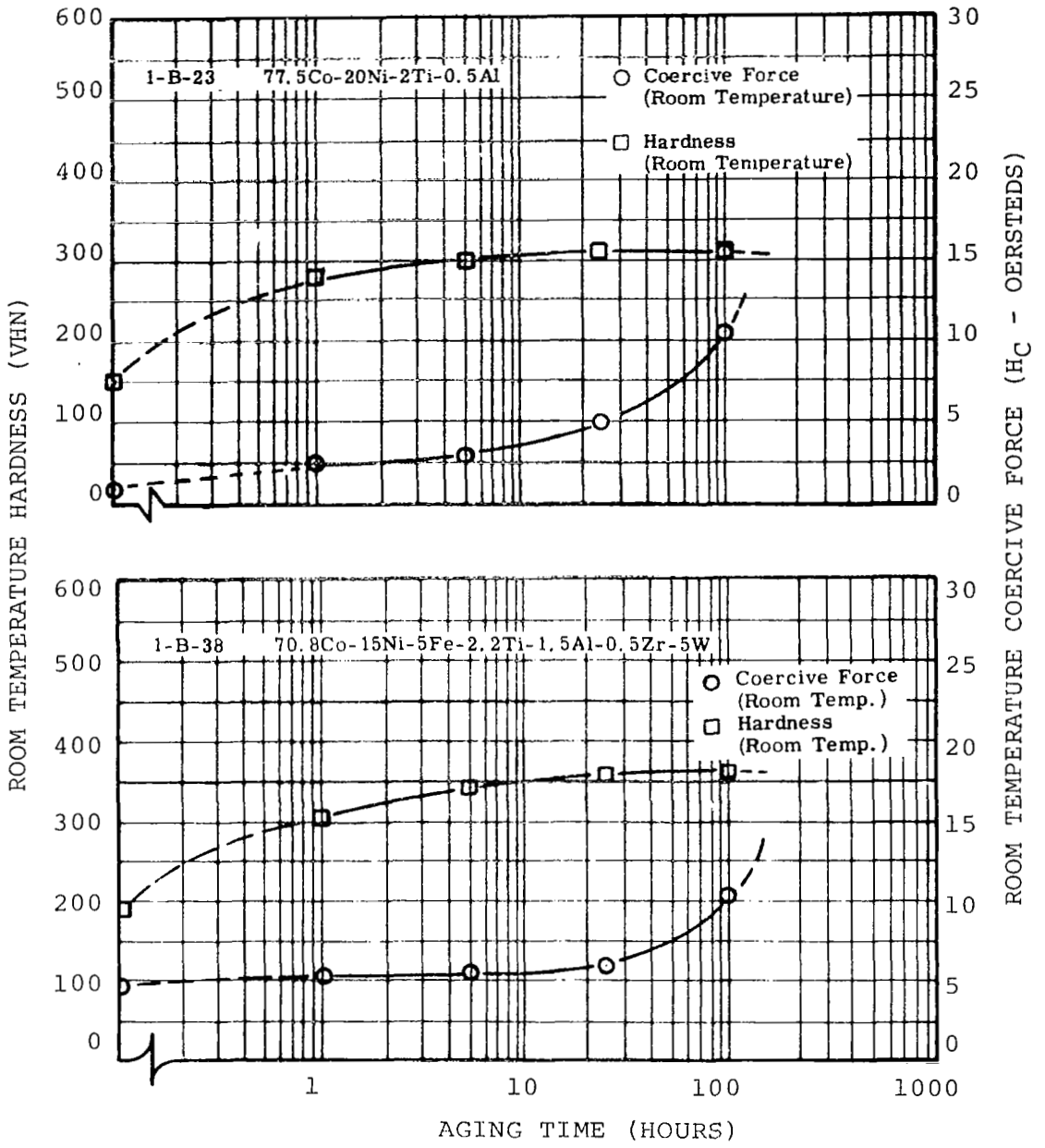

FIGURE II-13. (Continued) Change in Room Temperature Hardness and Coercive Force of Representative Cobalt-Base Alloys During Isothermal Aging at 1292°F (700°C)

This result warrants more careful analysis. A more detailed analysis of this observation follows.

The addition of 2.2Ti+1.5Al+0.3 to 0.5Zr (nominal weight percent) to the cobalt-base alloys was the most effective for providing high-hardness without discontinuous precipitate. The further addition of 0.5Be, 5W, 5Ta, or 5Nb increased maximum hardness and temperature during isochronal aging and also increased the hardness after isothermal aging for 100 hours 1292°F (700°C). The increments in hardness, together with the associated increment in coercive force and decrement in magnetic saturation with reference to alloy 1-B-32, are listed in table II-23. In order to learn which of the additions increase hardness with the least reduction of magnetic saturation and with the least increase of coercive force, the ratios of the increments are also listed in this table. The highest ratio of hardness increment to saturation decrement was obtained for the beryllium addition. Tantalum showed the next highest ratio and the tungsten addition was the lowest. The highest ratio of hardness increment to coercive force increment was obtained for the tungsten addition; tantalum was next and beryllium was by far the lowest. The tantalum addition, therefore, is the best choice. These ratio values definitely depend on the amount of the alloying additions. For this reason extrapolation of this type of preference must be made with caution if an appreciable change is made in the amount of the alloying addition.

The 1-B-39 alloy remains too low in magnetic saturation - about 10 percent lower than Nivco alloy, while its hardness values appear quite high. The results obtained from alloys 1-B-43 to 1-B-46 should show which element might be reduced to give the largest increase in magnetic saturation associates with the smallest sacrifice in hardness. These results were analyzed in a manner similar to that described above for alloys 1-B-36, 1-B-38, 1-B-39, and 1-B-42. The increments and decrements for alloys 1-B-44 to 1-B-46 with reference to alloy 1-B-43 and the various ratios are listed in table II-23. In this case, the reduction of elements which produces the lowest values in ratios was required. It was shown that the reduction of the titanium content increased the saturation with the smallest sacrifice in strength.

With these results the alloy compositions for the 300-gram button melts could be chosen. As mentioned above,

TABLE II-23. Increments and Decrements of Room Temperature Properties of Alloys 1-B-36, 1-B-38, 1-B-39, 1-B-42, and 1-B-44 to 1-B-46

Alloy Number	Change In Composition (Δ Comp. in nominal weight percent)	Change in Saturation (Δ σ)	Effect of Isochronal Aging One Hour at 1382°F(750°C)				Effect of Isothermal Aging 100 Hours at 1292°F(700°C)			
			Change in Hardness After Aging 1 Hour (ΔH_1)	Change in Coercive Force After Aging 1 Hour (ΔH_{c1})	$\left(\frac{\Delta H_1}{\Delta \sigma}\right)$ (a)	$\left(\frac{\Delta H_1}{\Delta H_{c1}}\right)$ (b)	Change in Hardness After Aging 100 Hours (ΔH_{100})	Change in Coercive Force After Aging 100 Hours (ΔH_{c100})	$\frac{\Delta H_{100}}{\Delta \sigma}$	$\frac{\Delta H_{100}}{\Delta H_{c100}}$
Changes in Selected Alloys Relative to Alloy 1-B-32 (75.8Co-15Ni-5Fe-2.2Ti-1.5Al-0.5Zr)										
1-B-36	+0.5Be	- 6	+ 89	+38.2	14.8	2.33	80	73.3	13.3	1.1
1-B-38	+5W	-19	+ 64	+ 1.5	3.4	42.8	81	1.8	3.4	45
1-B-39	+5Ta	-13	+119	+ 3.3	9.1	36.0	123	10.3	9.5	12
1-B-42	+5Nb	-21	+169	+16.2	8.1	10.5	143	84.3	6.9	1.7
Changes in Selected Alloys Relative to Alloy 1-B-43 (71Co-15Ni-5Fe-2.2Ti-1.5Al-0.3Zr-5Ta)										
1-B-44	-2Ta	+ 5	- 54	- 2.3	10.8	23	-20	-13	4	1.5
1-B-45	-0.7Ti	+ 4	- 8	- 0.4	2	20	- 2	-12	0.5	0.17
1-B-46	-5Ni	+ 3	- 13	- 0.3	4.3	43	+ 9	- 5.5	3	1.63

(a) Increment in hardness per unit decrement in saturation. (Indication of hardening effectiveness of element compared its reducing action on saturation.)

(b) Increment in hardness per unit decrement in coercive force. (To determine which element promotes hardening with the smallest increase in coercive force.)

some uncertainties existed concerning the actual amount of alloy composition of the levitation melts; and secondly, some adjustment of composition appeared desirable to obtain an even better balance of magnetic saturation and hardness than obtained in alloy 1-B-45. Therefore, the six alloys for the larger melts were chosen to cover a range of composition with the composition of 1-B-45 as the upper limit. From these compositions equations were obtained to define the linear relationship between properties and the weight percent additions of Ni, Al, Ti, and Ta while keeping Fe fixed at five weight percent and Zr at 0.3 weight percent nominal addition. The limits listed below were chosen on the assumption that within these narrow limits the independent linear relationship was a justified approximation. Furthermore, the previous results indicated that this range is sufficient to vary the saturation by more than 20 percent: nickel, 10 to 15 weight percent; titanium, 0 to 15 weight percent; aluminum, 1.2 to 1.5 weight percent; and tantalum, 3 to 5 weight percent. Again the values of element additions in the alloys correspond with the limits of variation except for one alloy which has a composition corresponding to the center of the ranges of variation. The compositions of the vacuum-arc melted cobalt-base alloys, 1-B-V-1 through 1-B-V-6, are listed in table II-19.

The hardness and coercive force (table II-24) results obtained from these 300-gram button vacuum-arc melts indicate that the alloys were chosen successfully.

The analyzed compositions of the six vacuum-arc melted cobalt-base alloys (table II-19.b) were in close agreement with the nominal compositions. The only exceptions were tantalum which was generally 0.1 to 0.2 weight percent higher than expected and titanium which was generally about 0.1 weight percent higher.

The results of magnetic saturation measurements made on samples from the 300-gram buttons are listed in table II-25. Saturation of the aged samples was measured at room temperature, 1112°F (600°C) and 1202°F (650°C). Samples of the cobalt alloys were annealed for one hour at 2012°F (1100°C) and aged for one hour at 1292°F (700°C) before testing.

Results obtained from coercive force measurements on samples of the 300-gram buttons are shown in table II-26. Coercive force was measured at several temperatures. Two samples were taken from each of the cobalt alloys for measurements. One sample was aged for one

TABLE II-24. Maximum Hardness Obtained by the Isochronal Aging of Vacuum Arc Melted Cobalt-Base Alloys 1-B-V-1 to 1-B-V-6

Alloy Number	Nominal Alloy Composition (weight percent)	Aging Temperature at Which Maximum Room Temperature Hardness was Obtained (°F)	(°C)	Total Aging Time[a] (hours)	Maximum Room Temperature Hardness (VHN)	Room Temperature Coercivity at Maximum Hardness (oersteds)
1-B-V-1	71.7Co-5Fe-15Ni-1.5Ti-1.5Al-0.3Zr-5Ta	1382	750	6	354	4.7
1-B-V-2	80.5Co-5Fe-10Ni-1.2Al-0.3Zr-3Ta	1382	750	6	248	3.1
1-B-V-3	76.3Co-5Fe-12Ni-1.0Ti-1.4Al-0.3Zr-4Ta	1382	750	6	307	3.6
1-B-V-4	73.5Co-5Fe-15Ni-1.2Al-0.3Zr-5Ta	1382	750	6	323	3.6
1-B-V-5	78.2Co-5Fe-10Ni-1.5Al-0.3Zr-5Ta	1382	750	6	303	3.9
1-B-V-6	74Co-5Fe-15Ni-1.5Ti-1.2Al-0.3Zr-3Ta	1382	750	6	313	3.4

(a) Total aging time may be determined by adding one hour time for each 90°F (50°) increment in temperature starting at 842°F ( )0°C).

TABLE II-25. Magnetic Moment of 300-Gram Vacuum Arc Melted Cobalt-Base Alloys 1-B-V-1 to 1-B-V-6

Alloy Number	Nominal Alloy Composition (weight percent)	Saturation Magnetic Moment (emu/g)[a]			
		After Annealing One Hour at 2012°F (1100°C)	After Annealing one Hour at 2012°F (1100°C) and Aging One Hour at 1292°F (700°C)		
		Tested at Room Temperature	Tested at Room Temperature	Tested at 1112°F (600°C)	Tested at 1202°F (650°C)
1-B-V-1	71.7Co-5Fe-15Ni-1.5Ti-1.5Al-0.3Zr-5Ta	123	119	91	87
1-B-V-2	80.5Co-5Fe-10Ni-1.2Al-0.3Zr-3Ta	144	144	114	108
1-B-V-3	76.3Co-5Fe-12Ni-1.0Ti-1.4Al-0.3Zr-4Ta	132	130	102	97
1-B-V-4	73.5Co-5Fe-15Ni-1.2Al-0.3Zr-5Ta	133	134	106	101
1-B-V-5	78.2Co-5Fe-10Ni-1.5Al-0.3Zr-5Ta	135	135	105	100
1-B-V-6	74Co-5Fe-15Ni-1.5Ti-1.2Al-0.3Zr-3Ta	130	128	100	94

(a) To convert the saturation magnetic moment to the approximate induction in gauss, multiply the listed value by 110.

TABLE II-26. Coercive Force Measurements on 300-Gram Vacuum-Arc Melted Cobalt-Base Alloys 1-B-V-1 to 1-B-V-6 at Different Temperatures

Alloy Number	Nominal Alloy Composition (weight percent)	Coercive Force (Oersteds)				
		Annealed One Hour at 1832°F (1000°C); Then Aged One Hour at 1382°F (750°C) Before Testing				
		Test Temperature				
		Room Temp.	1022°F (550°C)	1112°F (600°C)	1202°F (650°C)	Room[a] Temp.
1-B-V-1	71.7Co-5Fe-15Ni-1.5Ti-1.5Al-0.3Zr-5Ta	3.4	2.2	1.6	1.5	--
1-B-V-2	80.5Co-5Fe-10Ni-1.2Al-0.3Zr-3Ta	3.0	1.4	1.2	0.95	--
1-B-V-3	76.3Co-5Fe-12Ni-1.0Ti-1.4Al-0.3Zr-4Ta	2.8	1.5	1.0	0.85	--
1-B-V-4	73.5Co-5Fe-15Ni-1.2Al-0.3Zr-5Ta	2.9	1.4	0.90	0.65	--
1-B-V-5	78.2Co-5Fe-10Ni-1.5Al-0.3Zr-5Ta	2.6	1.3	0.88	0.77	--
1-B-V-6	74Co-5Fe-15Ni-1.5Ti-1.2Al-0.3Zr-3Ta	2.8	1.5	0.99	0.88	--
		Annealed One Hour at 1832°F (1000°C); Then Aged 100 Hours at 1292°F (700°C) Before Testing				
1-B-V-1	71.7Co-5Fe-15Ni-1.5Ti-1.5Al-0.3Zr-5Ta	26.0	11.0	9.2	8.3	25.0
1-B-V-2	80.5Co-5Fe-10Ni-1.2Al-0.3Zr-3Ta	6.7	3.4	2.5	2.3	6.3
1-B-V-3	76.3Co-5Fe-12Ni-1.0Ti-1.4Al-0.3Zr-4Ta	12.4	5.6	4.8	3.7	12.2
1-B-V-4	73.5Co-5Fe-15Ni-1.2Al-0.3Zr-5Ta	10.6	5.0	3.4	2.8	10.3
1-B-V-5	78.2Co-5Fe-10Ni-1.5Al-0.3Zr-5Ta	9.3	4.2	4.3	2.7	9.0
1-B-V-6	74Co-5Fe-15Ni-1.5Ti-1.2Al-0.3Zr-3Ta	14.2	6.5	5.0	4.1	13.6

(a) Room temperature results shown in the last column were measured after elevated temperature measurements were made.

hour at 1392°F (750°C) before testing; the other sample was subjected to isothermal aging for 100 hours at 1292°F (700°C) before testing. In the case of the isothermally aged samples, coercive force was remeasured at room temperature after measurements at higher temperatures. The results indicate a slight reduction of coercive force value due to the tests at temperature.

Results of tensile tests which were obtained on samples from the 300-gram buttons are shown in table II-27. Cobalt alloys were annealed one hour at 1832°F (1000°C); then machined to size and aged for one hour at 1382°F (750°C) before testing. The hardness of each sample was measured at room temperature before the test. This value is also shown in table II-27. The table lists yield stress at 0.2 percent plastic elongation, the ultimate tensile stress, the uniform elongation, and the reduction of area at fracture. Tensile tests were performed at room temperature and at 1112°F (600°C). Samples were held for 15 minutes at temperature before the start of testing. Tests at 1112°F (600°C) were

TABLE II-27. Tensile Tests[a] of 300-Gram Vacuum Arc Melted Cobalt Base Alloys 1-B-V-1 to 1-B-V-6

Alloy Number	Nominal Alloy Composition (weight percent)	Room Temperature Hardness[b] 50 kg Load (VHN)	Test Temperature °F	Test Temperature °C	0.2% Yield Strength (psi)	Ultimate Tensile Strength (psi)	Uniform Elongation (percent)	Reduction of Area (percent)
1-B-V-1	71.7Co-5Fe-15Ni-1.5Ti-1.5Al-0.3Zr-5Ta	305	77	25	120 800	178 000	19.3	41.6
1-B-V-2	80.5Co-5Fe-10Ni-1.2Al-0.3Zr-3Ta	230	77	25	68 800	115 200	36.5	54.1
1-B-V-3	76.3Co-5Fe-12Ni-1.0Ti-1.4Al-0.3Zr-4Ta	317	77	25	106 800	160 000	22.7	42.7
1-B-V-4	73.5Co-5Fe-15Ni-1.2Al-0.3Zr-5Ta	327	77	25	110 800	158 800	19.7	41.0
1-B-V-5	78.2Co-5Fe-10Ni-1.5Al-0.3Zr-5Ta	313	77	25	110 000	155 600	22.3	49.3
1-B-V-6	74Co-5Fe-15Ni-1.5Ti-1.2Al-0.3Zr-3Ta	323	77	25	111 200	166 800	23.3	42.7
1-B-V-1	71.7Co-5Fe-15Ni-1.5Ti-1.5Al-0.3Zr-5Ta	361	1112	600	102 400	141 600	12.2	29.1
1-B-V-2	80.5Co-5Fe-10Ni-1.2Al-0.3Zr-3Ta	226	1112	600	46 400	84 000	14.9	17.0
1-B-V-3	76.3Co-5Fe-12Ni-1.0Ti-1.4Al-0.3Zr-4Ta	317	1112	600	91 200	127 600	13.9	35.4
1-B-V-4	73.5Co-5Fe-15Ni-1.2Al-0.3Zr-5Ta	325	1112	600	93 200	128 400	11.5	32.3
1-B-V-5	78.2Co-5Fe-10Ni-1.5Al-0.3Zr-5Ta	316	1112	600	89 200	122 000	11.9	28.0
1-B-V-6	74Co-5Fe-15Ni-1.5Ti-1.2Al-0.3Zr-3Ta	320	1112	600	92 400	126 000	13.0	25.0

(a) Samples were annealed one hour at 1832 F (1000°C), machined to size and aged for one hour at 1382°F (750°C) before testing.
(b) Measured at room temperature after the thermal treatment, but before the tensile test.

conducted in argon. The cobalt-base samples were quite ductile at both room temperature and at elevated temperature.

Hot-hardness values for samples from the 300-gram buttons are shown in table II-28. Samples of the cobalt alloys were annealed one hour at 1832°F (1000°C) and aged for one hour at 1382°F (750°C) prior to testing. The temperature dependence of hardness of alloy 1-B-V-4 is shown in figure II-14.

The cobalt-base alloys, which were melted in the form of 300-gram buttons, were chosen from the range of compositions as outlined previously.

The following requirements were set previously for the selection of suitable alloys from the screening program and applicable in the selection of the final alloys:

1) No discontinuous precipitate should occur during isothermal aging of 100 hours at 1292°F (700°C).

TABLE II-28. Hot Hardness Measurements[a] on Samples of 300-Gram Vacuum-Arc Melted Cobalt-Base Alloys 1-B-V-1 to 1-B-V-6 after Annealing One Hour at 1832°F (1000°C) and Aging One Hour at 1382°F (750°C)

Alloy Number	Nominal Alloy Composition (weight percent)	Hot Hardness (VHN) Test Temperature	
		1112°F (600°C)	1202°F (650°C)
1-B-V-1	71.7Co-5Fe-15Ni-1.5Ti-1.5Al-0.3Zr-5Ta	192	270
1-B-V-2	80.5Co-5Fe-10Ni-1.2Al-0.3Zr-3Ta	106	132
1-B-V-3	76.3Co-5Fe-12Ni-1.0Ti-1.4Al-0.3Zr-4Ta	246	249
1-B-V-4	73.5Co-5Fe-15Ni-1.2Al-0.3Zr-5Ta	292	257
1-B-V-5	78.2Co-5Fe-10Ni-1.5Al-0.3Zr-5Ta	229	242
1-B-V-6	74Co-5Fe-15Ni-1.5Ti-1.2Al-0.3Zr-3Ta	156	248

(a) All measurements were made under vacuum of 2×10^{-5} torr at a load of 2.5 kG.

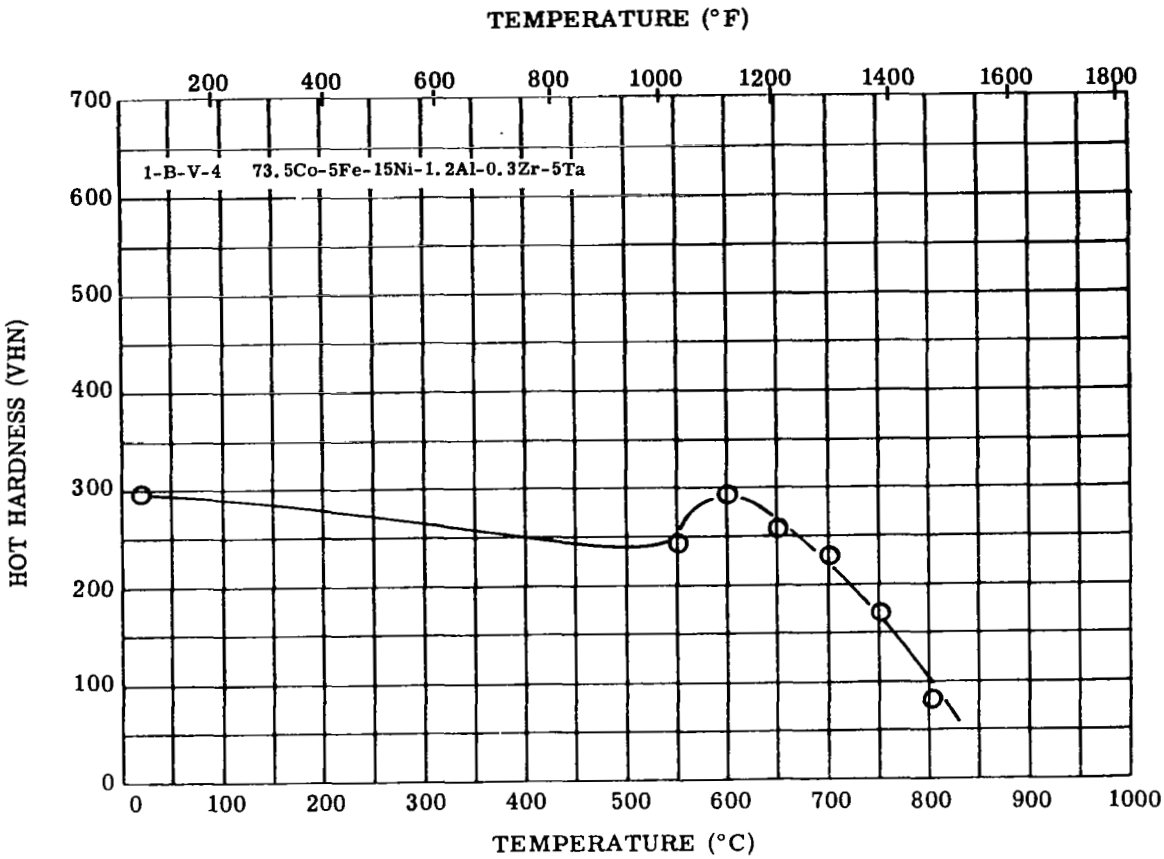

FIGURE II-14. Hot Hardness vs. Temperature of Alloy 1-B-V-4 After Annealing One Hour at 1832°F (1000°C) and Aging at 1112°F (600°C). Test Load 2.5 kG.

2) The temperature at which maximum hardness is obtained during isochronal aging should be 1382°F (750°C) or higher.

The listed requirements were fulfilled in all the 300-gram cobalt-base alloys except 1-B-V-2 which did not meet requirement 2. Apparently, the alloying content was too low in that alloy. Within the given range of additions; Ta: 3 to 5 weight percent, Al: 1.2 to 1.5 weight percent, Ti: 0 to 1.7 weight percent, the most suitable combination that produces the best balance of

magnetic saturation, hardness, and coercive force must be found. Alloy 1-B-V-4 exhibits a good combination of properties. Among the 300-gram experimental alloys, the hardness data from alloy 1-B-V-4 were second best; the magnetic properties were also second best.

The results confirm the previous results from the 25-gram ingots that showed the addition of Al+Ta gave a better balance of hardness, yield strength, and magnetic properties than those including Ti in the alloying content.

The influence of alloying elements may be expressed analytically in the following equation:

Magnetic saturation (σ) expressed as emu/g
= 102-0.5(%Ni)+3.6(%Al)-7.0(%Ti)-3.0(%Ta)
Hardness expressed in VHN = 120+6(%Ni)+80
(%Al)+16(%Ti)+9(%Ta)

However, these expressions must be considered with some caution. The number of alloys tested before deriving the equation was not large enough to provide adequate significance to the results. In addition, the variation of aluminum content in the test alloys is too small to place any significance to the coefficients obtained for aluminum content. The standard error for this coefficient is greater than 100 percent. The computer analysis would indicate that an alloy with no Ti, but containing Ni, Al, and Ta at the upper limit, would produce the best balance of hardness and saturation.

3. Selection and Evaluation of the Final Vacuum Induction Melted Alloys

a. ALLOY SELECTION

The exploratory study on this program defined the final ferritic alloy composition in the following manner:

Ni: 11 to 13 weight percent, Co: 25 to 35 weight percent, Cr: up to two weight percent by replacing two weight percent Ni with one weight percent Cr, Ta: 2 to 3 weight percent, W: up to one weight percent, Ti: 0.3 to 0.4 weight percent, Al: 0.3 to 0.5 weight percent, Fe: balance.

Alloys 1-A-V-3 and 1-A-V-4 (table II-7a) were selected for the final alloys with some minor modifications. The alloys were vacuum induction melted in the form of 15-pound ingots (see section II.A.6).

Alloy 1-B-V-4 (table II-19a) was selected as the composition having the best combination of properties among the cobalt-base alloys. Alloy 1-B-S-1 was vacuum induction melted to duplicate that alloy. Alloy 1-B-S-2 was a modification of alloy 1-B-S-1 obtained by adding a small amount of beryllium. The nominal and analyzed compositions of the four final alloys are shown in table II-20. The analyzed compositions were very near the nominal compositions.

Results of the isochronal aging of samples made from the four final ferritic and cobalt alloys are plotted in figure II-15. The two ferritic samples (1-A-S-1 and 1-A-S-2) were annealed one hour at 1832°F (1000°C). The isochronal aging sequence started at 932°F (500°C). Aging time was one hour with 90°F (50°C) increments in temperature. The highest isochronal aging temperature for the ferritic alloys was 1202°F (650°C). Both cobalt-base samples (1-B-S-1 and 1-B-S-2) were annealed one hour at 1832°F (1000°C). The isochronal aging sequence started at 1202°F (650°C), with an aging time of one hour. The temperature was then successively increased in increments of 90°F (50°C) to 1472°F (800°C) which was the highest aging temperature applied to the cobalt-base alloys.

The maximum values of room temperature hardness measured during the isochronal aging sequence are listed in table II-29 together with the aging temperature, where maximum hardness was attained. The room temperature coercivity is listed for the same aging temperature.

Results of the isothermal aging tests of the final alloys are plotted in figures II-16, II-17, and II-18. The samples for isothermal aging tests were annealed one hour at 1832°F (1000°C) before testing.

Two samples were taken from each of the ferritic alloys. One sample was aged at 1012°F (550°C) after annealing; the other sample was five percent cold reduced after annealing. Then aging at 1012°F (550°C) was started. The results are compared for alloy 1-A-S-1 in figure II-16 and alloy 1-A-S-2 in figure II-17. Five percent reduction by cold rolling had reduced the value of coercive force between 10 and 15 oersteds. After isothermal aging 100 hours, the values of coercive force increased, but the value of the five percent cold rolled sample was still 10 oersteds lower. The change of hardness was not influenced by cold working. The influence of the small plastic strain is similar to the behavior observed in 15 percent Nickel maraging steel.

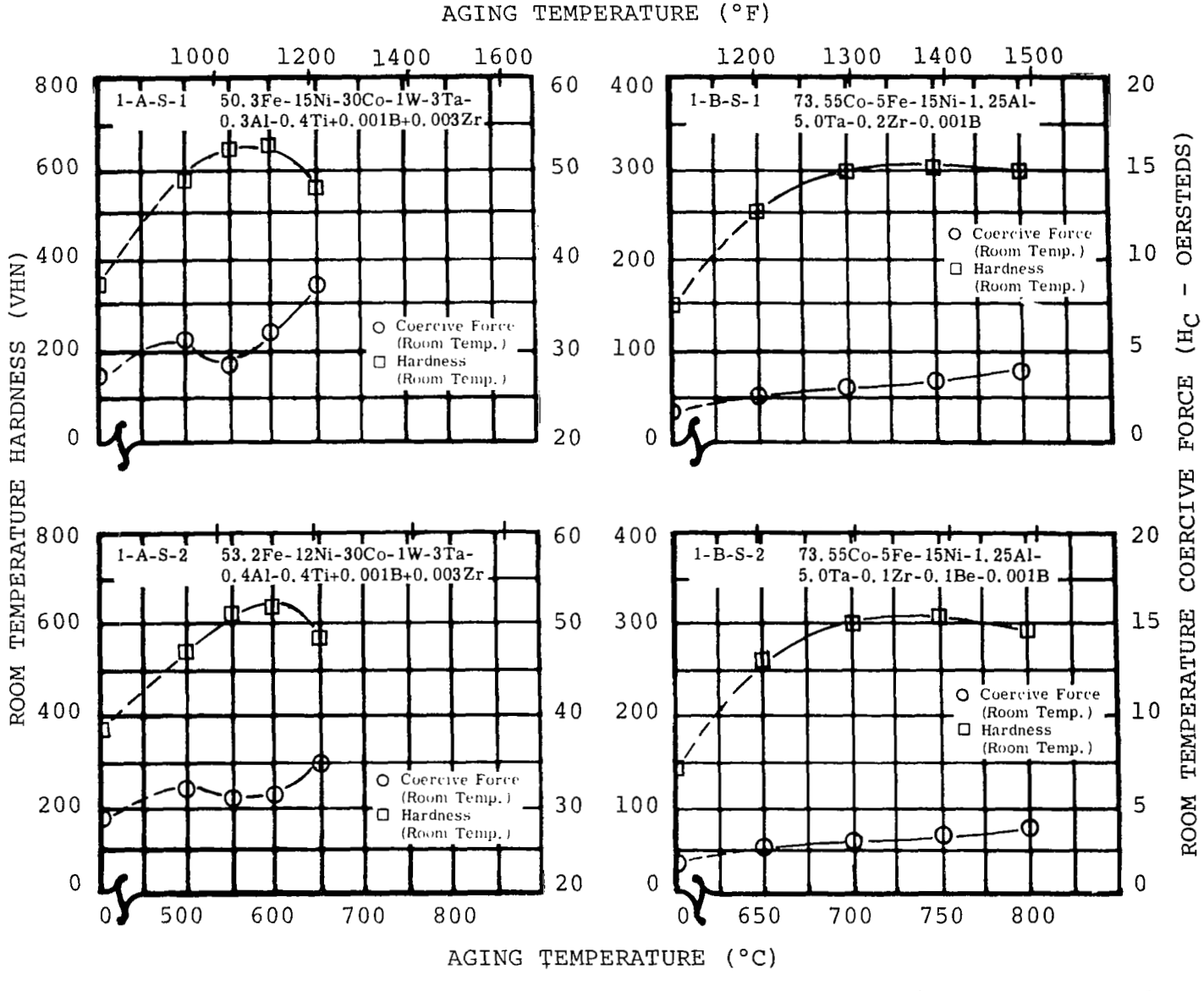

FIGURE II-15. Hardness and Coercive Force of Alloys 1-A-S-1, 1-A-S-2, 1-B-S-1, and 1-B-S-2 at Room Temperature After Aging One Hour at Temperature. (See Page 79 for Annealing and Aging Sequences.)

TABLE II-29. Maximum Hardness Obtained by the Isochronal Aging of the Final Alloys Vacuum Induction Melted as 15-Pound Ingots[a]

Alloy Number	Nominal Alloy Composition (weight percent)	Aging Temperature At Which Maximum Room Temperature Hardness Was Obtained °F	°C	Total Aging Time[b] (hours)	Maximum Room Temperature Hardness (VHN)	Room Temperature Coercivity At Maximum Hardness (oersteds)
1-A-S-1	50.3Fe-15Ni-30Co-1W-3Ta-0.3Al-0.4Ti+0.001B+0.003Zr	1112	600	4	664	32
1-A-S-2	53.2Fe-12Ni-30Co-1W-3Ta-0.4Al-0.4Ti+0.001B+0.003Zr	1112	600	4	643	31
1-B-S-1	73.55Co-5Fe-15Ni-1.25Al-5.0Ta-0.2Zr-0.001B	1382	750	6	311	3.3
1-B-S-2	73.55Co-5Fe-15Ni-1.25Al-5.0Ta-0.1Zr-0.1Be-0.001B	1382	750	6	313	3.1

(a) See Figure II-15

(b) Total aging time may be determined by adding one hour aging time for each 90°F (50°C) increment in temperature starting at 932°F (500°C).

Results of isothermal aging at 1292°F (700°C) of the cobalt-base alloys are plotted in figure II-18. The results of magnetic saturation measurements on the final four alloys are listed in table II-30.

A comparison of test results obtained on samples of the 300-gram vacuum-arc melted buttons and the final 15-pound vacuum induction melted ingots are shown in tables II-31 and II-32. The results from the ferritic alloys are shown in table II-31. The results on alloys 1-A-S-1 and 1-A-S-2 were similar to that obtained on alloys 1-A-V-3 and 1-A-V-4. However, alloy 1-A-V-3 and 1-A-V-4 showed better stability than the final alloys. The lower aluminum content in the final alloys can be regarded as responsible for this behavior. The coercive force of 1-A-V-3 was lower than the final alloys which is due to the lower cobalt content. Therefore, the 15-pound heats of the alloys cannot be regarded as optimum alloys. However, they give a good combination of properties well within the established range of requirements. The alloy 1-A-S-2 is superior to alloy 1-A-S-1 as far as high magnetic saturation, low coercive force, and stability are concerned. Alloy 1-A-S-2 was therefore selected for the final evaluation.

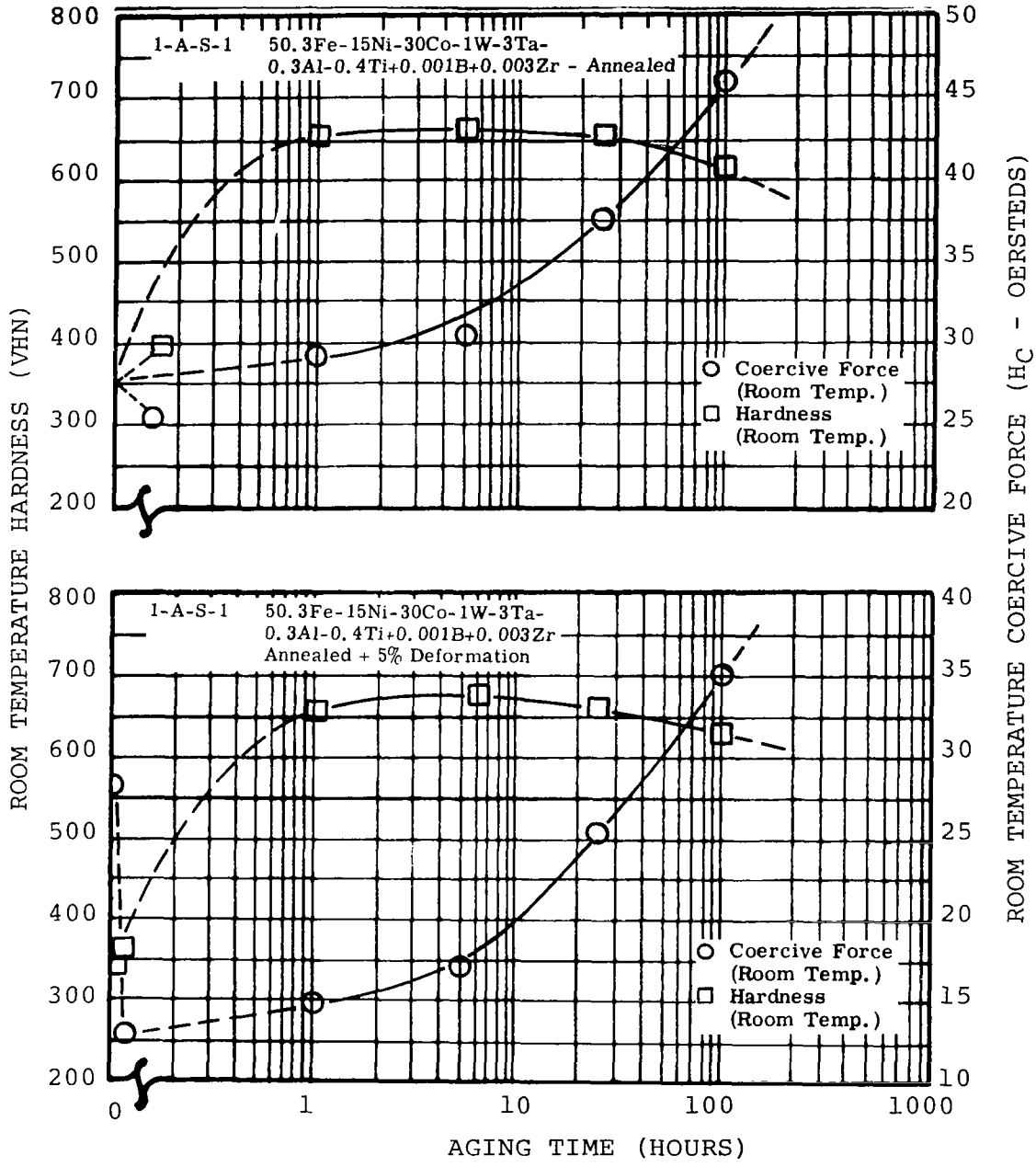

FIGURE II-16. Change in Room Temperature Hardness and Coercive Force During Isothermal Aging at 1022°F (550°C) of Alloy 1-A-S-1 Annealed, and Annealed and Five Percent Deformed

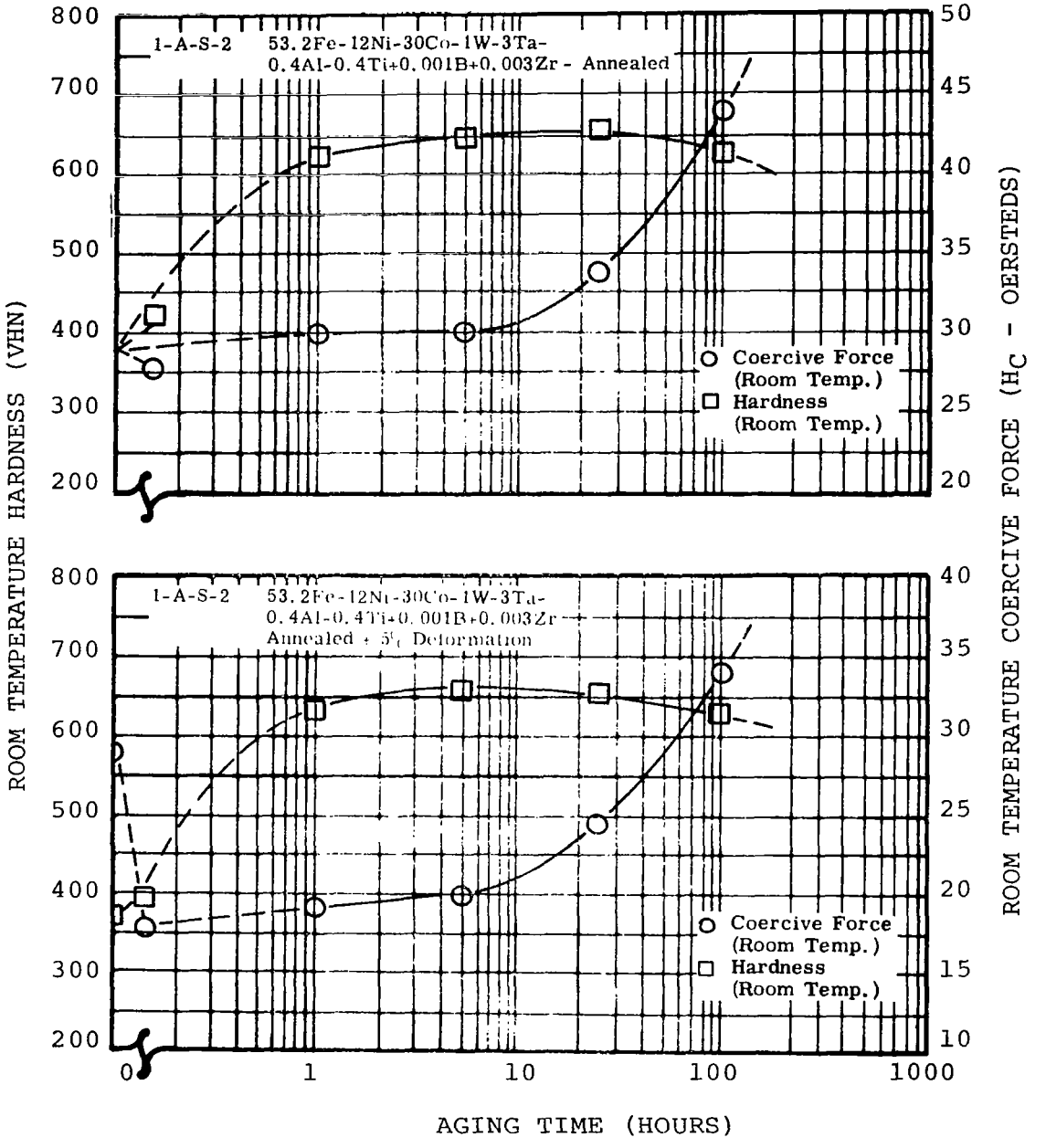

FIGURE II-17. Change in Room Temperature Hardness and Coercive Force During Isothermal Aging at 1022°F (550°C) of Alloy 1-A-S-2 Annealed, and Annealed and Five Percent Deformed

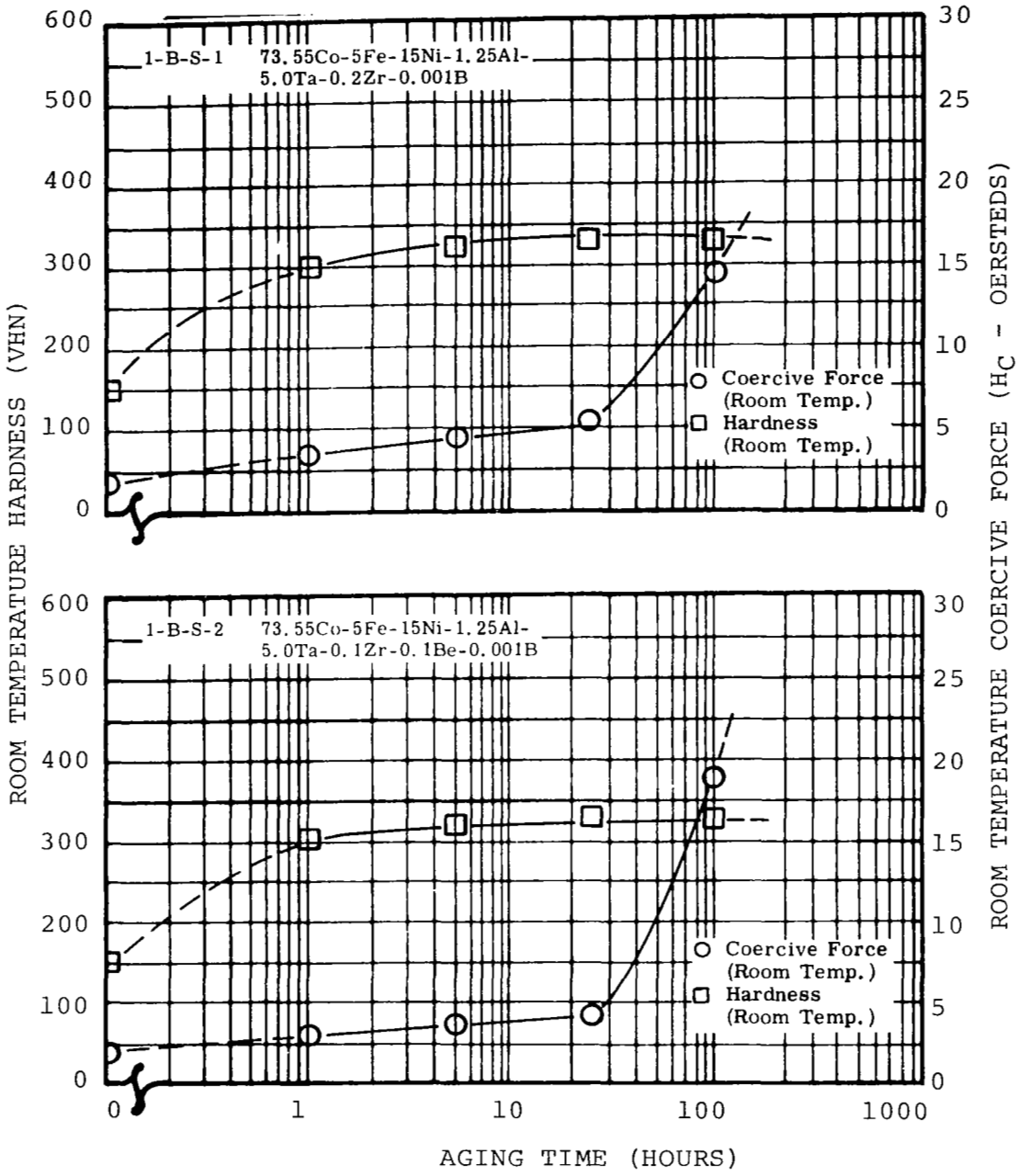

FIGURE II-18. Change in Room Temperature Hardness and Coercive Force of Alloys 1-B-S-1 and 1-B-S-2 During Isothermal Aging at 1022°F (550°C)

TABLE II-30. Saturation Magnetic Moment of the Final Alloys Vacuum Induction Melted as 15-Pound Ingots

Alloy Number	Nominal Alloy Composition (weight percent)	Treatment Before Testing	Saturation Magnetic Moment (emu/g)[a] Tested at Room Temperature	Treatment Before Testing	Saturation Magnetic Moment (emu/g) Tested at Room Temperature	Tested at 1112°F (600°C)
1-A-S-1	50.3Fe-15Ni-30Co-1W-3Ta-0.3Al-0.4Ti+0.001B+0.003Zr	Annealed one hour at 1832°F (1000°C)	192	Annealed then aged one hour at 1112°F (600°C)	195	162
1-A-S-2	53.2Fe-12Ni-30Co-1W-3Ta-0.4Al-0.4Ti+0.001B+0.003Zr		197		200	171
1-B-S-1	73.55Co-5Fe-15Ni-1.25Al-5.0Ta-0.2Zr-0.001B	Annealed one hour at 2012°F (1100°C)	138	Annealed then aged one hour at 1292°F (700°C)	135	104
1-B-S-2	73.55Co-5Fe-15Ni-1.25Al-5.0Ta-0.1Zr-0.1Be-0.001B		132		134	102

(a) To convert the saturation magnetic moment to the approximate induction in gauss, multiply the listed values for alloys 1-A-S-1 and 1-A-S-2 by 100 and alloys 1-B-S-1 and 1-B-S-2 by 110.

TABLE II-31. Properties of Ferritic Alloys 1-A-V-1 to 1-A-V-6 and 1-A-S-1 and 1-A-S-2

Alloy Number	Analyzed Composition (weight percent)	Aged One Hour at 1112°F(600°C) Measured at 1112°F(600°C) Saturation Magnetic Moment[a] (emu/g)	Temperature at Which Maximum Room Temperature Hardness[b] Was Obtained (°F)	(°C)	Maximum Room Temperature Hardness (VHN)	Room Temperature Coercivity At Maximum Hardness (oersteds)	Aged 100 Hours at 1022°F(550°C) Room Temperature Hardness (VHN)	Room Temperature Coercivity (oersteds)	Change in Hardness After 100 Hours Aging (percent)
1-A-V-1	Fe-14.6Ni-29.2Co-0.56Al-0.49Ti-2.15W-4.5Ta	160	1112	600	732	35	746	62.5	-0.5
1-A-V-2	Fe-9.57Ni-20.1Co-0.63Al-0.53Ti-3.56Ta	172	1022	550	570	22	512	30	-13.5
1-A-V-3	Fe-11.4Ni-25.0Co-0.61Al-0.52Ti-1.00W-4.06Ta	166	1022	550	641	30.5	630	42.5	-4.1
1-A-V-4	Fe-14.8Ni-29.4Co-0.64Al-0.52Ti-3.48Ta	168	1112	600	670	35	683	48.5	-2.3
1-A-V-5	Fe-14.5Ni-29.8Co-0.62Al-0.54Ti-2.10W-3.48Ta	161	1112	600	704	37	721	62.5	-0.4
1-A-V-6	Fe-4.66Ni-5.19Cr-25.7Co-0.64Al-0.49Ti-1.18W-3.56Ta	150	1022	550	553	33	540	37	-7.0
1-A-S-1	Fe-15.3Ni-29.1Co-2.90Ta-0.92W-0.42Ti-0.27Al	162	1112	600	664	32	625	46	-7.5
1-A-S-2	Fe-12.2Ni-29.5Co-2.95Ta-0.96W-0.41Ti-0.38Al	171	1112	600	643	31	630	44	-5.5

(a) To convert saturation magnetic moment per gram to the approximate saturation induction in gauss, multiply the listed value by 100.
(b) Total aging time may be determined by adding one hour aging time for each 90°F (50°C) increment in temperature starting at 842°F (450°C); e.g., at 600°C total time is four hours.

TABLE II-32. Properties of Cobalt-Base Alloys 1-B-V-1 to 1-B-V-6 and 1-B-S-1 and 1-B-S-2

Alloy Number	Analyzed Composition (weight percent)	Aged One Hour at 1382°F(750°C) Measured at 1112°F(600°C) Saturation Magnetic Moment[a] (emu/g)	Temperature at Which Maximum Room Temperature Hardness[b] Was Obtained (°F)	(°C)	Maximum Room Temperature Hardness (VHN)	Room Temperature Coercivity At Maximum Hardness (oersteds)	Aged 100 Hours at 1292°F(700°C) Room Temperature Hardness (VHN)	Room Temperature Coercivity (oersteds)	Discontinuous Precipitate
1-B-V-1	Co-5.0Fe-0.27Zr-14.6Ni-1.44Al-1.66Ti-5.20Ta	91	1382	750	354	4.7	388	26	None
1-B-V-2	Co-4.8Fe-0.27Zr-10.3Ni-1.19Al-3.07Ta	114	1292	700	248	3.1	255	6.7	None
1-B-V-3	Co-4.9Fe-0.26Zr-11.9Ni-1.40Al-1.07Ti-4.05Ta	102	1382	750	307	3.6	333	12.4	None
1-B-V-4	Co-5.1Fe-0.26Zr-14.8Ni-1.25Al-5.19Ta	106	1382	750	323	3.6	343	10.6	None
1-B-V-5	Co-5.0Fe-0.27Zr-9.85Ni-1.60Al-5.3Ta	105	1382	750	303	3.9	320	9.3	None
1-B-V-6	Co-4.8Fe-0.24Zr-15.0Ni-1.19Al-1.66Ti-3.1Ta	100	1382	750	313	3.4	338	14.2	None
1-B-S-1	Co-5.8Fe-15.3Ni-4.98Ta-1.28Al-0.21Zr	104	1382	750	311	3.3	331	14.7	None
1-B-S-2	Co-5.2Fe-15.2Ni-4.98Ta-1.36Al-0.12Zr-0.065Be	102	1382	750	313	3.1	336	14.8	None

(a) To convert saturation magnetic moment per gram to the approximate saturation induction in gauss, multiply the listed value by 110.
(b) Total aging time may be determined by adding one hour aging time for each 90°F (50°C) increment in temperature starting at 932°F (500°C); e.g., at 700°C total time is five hours.

The test results obtained on the vacuum arc melted cobalt-base alloys and the vacuum induction melted cobalt-base alloys are shown in table II-32. The results are comparable. There are differences in chemical composition. Although very small, they may account for the observed differences in properties. The alloy 1-B-S-2 had been slightly modified by a minor addition of beryllium. The stability and saturation of this alloy were not as good as alloy 1-B-S-1. Therefore, the latter was selected for further evaluation of properties. It is believed that the composition Co-5Fe-15Ni-5Ta-(1.2-1.5)Al-0.25Zr, provides a very good balance of magnetic and mechanical properties. An optimum composition can only be defined if one knows the desired balance of both properties required in the electrical generator design. On the other hand, some adjustment of the composition and some minor additions up to 1.1 weight percent, may become necessary during a development program for creep properties. The upper service temperature limit for this alloy is expected to be in the 1292° to 1382°F (700° to 750°C) range.

The four final vacuum induction melted alloys were subjected to additional magnetic and mechanical tests. Then short-term creep tests and kinetics study were conducted on two alloys; one cobalt-base and one ferritic type.

b. MAGNETIC TEST RESULTS

The magnetic test data are shown in table II-33 and II-34. Sample preparation and testing procedures were outlined in sections II.B.7 and 8. Figures II-19 and II-20 show the dc magnetization curves of the final ferritic and cobalt alloys compared to 15% Ni maraging and H-11 alloys (figure II-19) and to Nivco alloy (figure II-20) respectively. The improvement achieved in the experimental alloys is readily evident.

The ac properties shown in tables II-33 and II-34 also indicate definite improvement over the available commercial alloys. When coupled with the lower coercive force values, especially at temperature or after aging, the superiority of these alloys for alternator rotors in the 900° to 1200°F range is evident.

c. TENSILE TEST RESULTS

Tensile test data are shown in table II-35. Sample preparation and test methods were reported in section II.B.7. The ferritic alloys have considerably higher strength at 1112°F (600°C) than the cobalt-base alloys.

TABLE II-33. Magnetic Properties of Ferritic Alloy 1-A-S-2[a]

DC Properties							
Alloy Number	Test Temperature (°F)	Test Temperature (°C)	Induction at Magnetizing Force Indicated (kilogauss) 10 Oe	100 Oe	250 Oe	Coercive Force from 200 Oe (oersteds)	Residual Induction at Magnetizing Force of 200 Oe (kilogauss)
1-A-S-2	77	25	--	14.4	18.2	27.3	9.07
1-A-S-2	1004	540	--	14.0	16.8	20.1	8.25
1-A-S-2	1103	595	--	13.6	16.2	22.2	8.20
For Comparison							
H-11 Alloy[b]	77	25	--	16.2	17.9	23.1	11.75
H-11 Alloy[b]	1103	595	--	12.5	13.0	14.1	7.35

AC Properties								
Alloy Number	Induction (kilogauss)	Frequency (cps)	Core Loss (watts per pound)	Apparent Core Loss (exciting volt-amps per pound)	Core Loss (watts per pound)	Apparent Core Loss (exciting volt-amps per pound)	Core Loss (watts per pound)	Apparent Core Loss (exciting volt-amps per pound)
			At 77°F (25°C)		At 1004°F (540°C)		At 1103°F (595°C)	
1-A-S-2	10	60	19.73	38.04	14.90	32.75	15.59	32.25
1-A-S-2	15	60	31.20	139.0	19.77	182.0	19.99	195.0
1-A-S-2	10	400	156.0	276.0	110.0	233.0	111.0	241.0
1-A-S-2	15	400	252.0	940.0	162.0	950.0	162.0	1010.0
For Comparison								
H-11 Alloy[b]	10	400	115.0	179.0	--	--	87.0	185.0

(a) Test specimen consisted of 0.025 inch thick rings (3 inch O.D. by 2-1/2 inch I.D.) which had been annealed one hour at 2012°F(1100°C) cold rolled (5% reduction) and then aged 3 hours at 1022°F(550°C) before testing.

(b) Data from Magnetic Materials Topical Report by P. E. Kueser et al, NASA-CR-54091, Contract NAS3-4162, 1964.

TABLE II-34. Magnetic Properties of Cobalt-Base Alloy 1-B-S-1[a]

DC Properties

Alloy Number	Test Temperature (°F)	Test Temperature (°C)	Induction at Magnetizing Force Indicated (kilogauss) 10 Oe	100 Oe	250 Oe	Coercive Force from 200 Oe (oersteds)	Residual Induction at Magnetizing Force of 200 Oe (kilogauss)
1-B-S-1	77	25	9.6	12.8	14.0	2.43	5.8
1-B-S-1	1004	540	8.8	10.9	12.0	0.88	7.8
1-B-S-1	1103	595	8.3	10.3	11.3	0.72	7.8
1-B-S-1	1202	650	8.3	10.3	11.3	0.72	8.3
For Comparison							
Nivco Alloy[b]	77	25	1.0	10.9	13.6	35.5	8.0
Nivco Alloy[b]	1103	595	2.0	10.3	11.6	20.9	7.8

AC Properties

Alloy Number	Induction (kilogauss)	Frequency (cps)	Core Loss (watts per pound)	Apparent Core Loss (exciting volt-amps per pound)	Core Loss (watts per pound)	Apparent Core Loss (exciting volt-amps per pound)	Core Loss (watts per pound)	Apparent Core Loss (exciting volt-amps per pound)	Core Loss (watts per pound)	Apparent Core Loss (exciting volt-amps per pound)
			At 77°F (25°C)		At 1004°F (540°C)		At 1103°F (595°C)		At 1202°F (650°C)	
1-B-S-1	6	60	1.31	2.72	0.67	1.29	0.56	0.86	0.55	0.86
1-B-S-1	6	400	16.80	23.74	8.10	11.25	7.98	9.12	7.74	8.66
For Comparison										
Nivco Alloy[b]	6	400	80.0	149.0	--	--	41.3	77.0	--	--

(a) Test specimen consisted of 0.025 inch thick rings (3 inch O.D. by 2-1/2 inch I.D.) which had been annealed one hour at 2012°F (1100°C) and then aged one hour at 1382°F (750°C).

(b) Data from Magnetic Materials Topical Report by P. E. Kueser et al, NASA-CR-54091, Contract NAS3-4162, 1964.

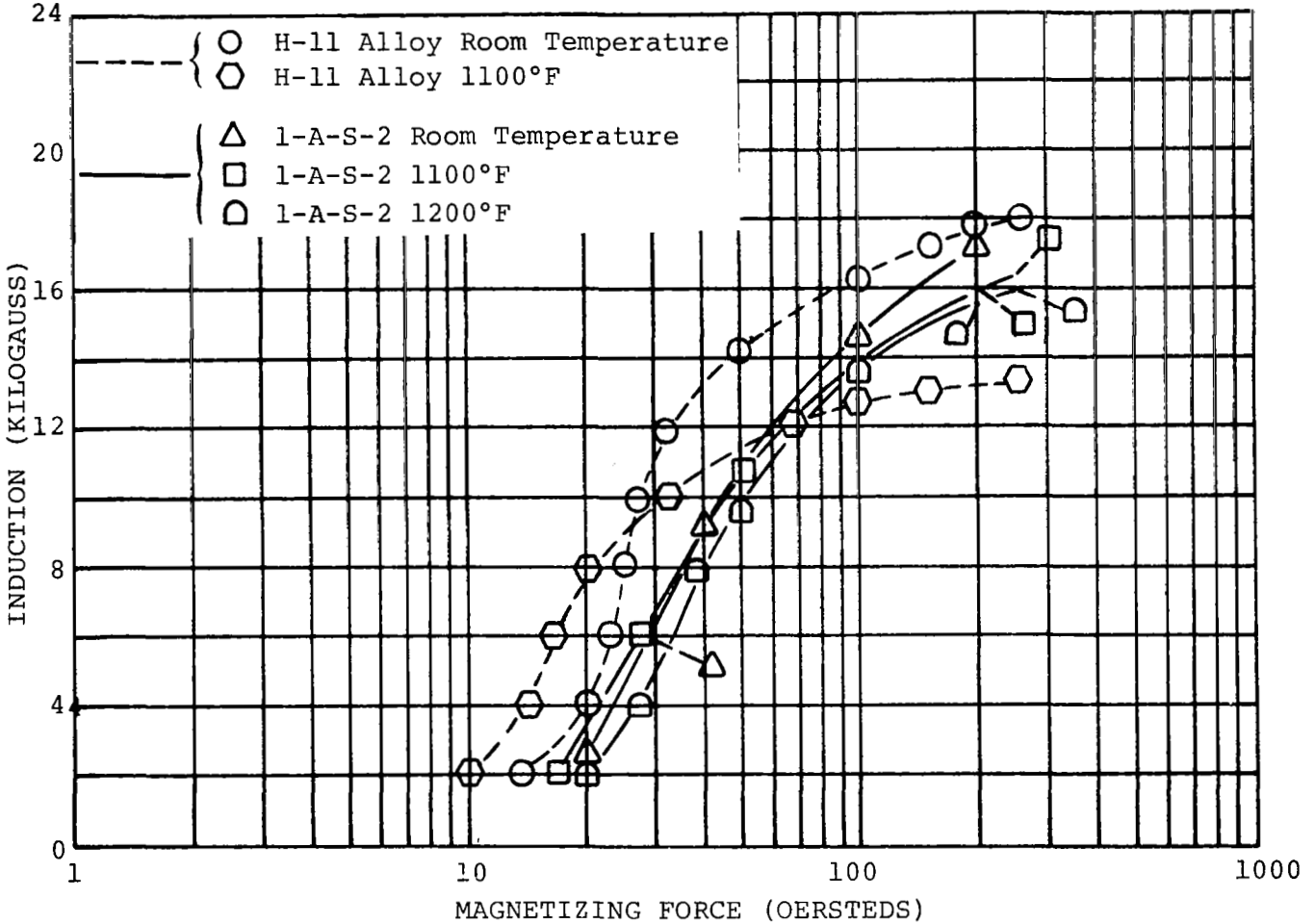

FIGURE II-19. DC Magnetization Curves of Alloy 1-A-S-2 (Fe-12Ni-30Co-1W-3Ta-0.4Al-0.4Ti) and H-11 (Fe-5Cr-1.3Mo-0.5V-0.4C) Alloy at Room Temperature and Elevated Temperature, 0.025-inch Laminations. Data for H-11 Alloy from Reference II-11.

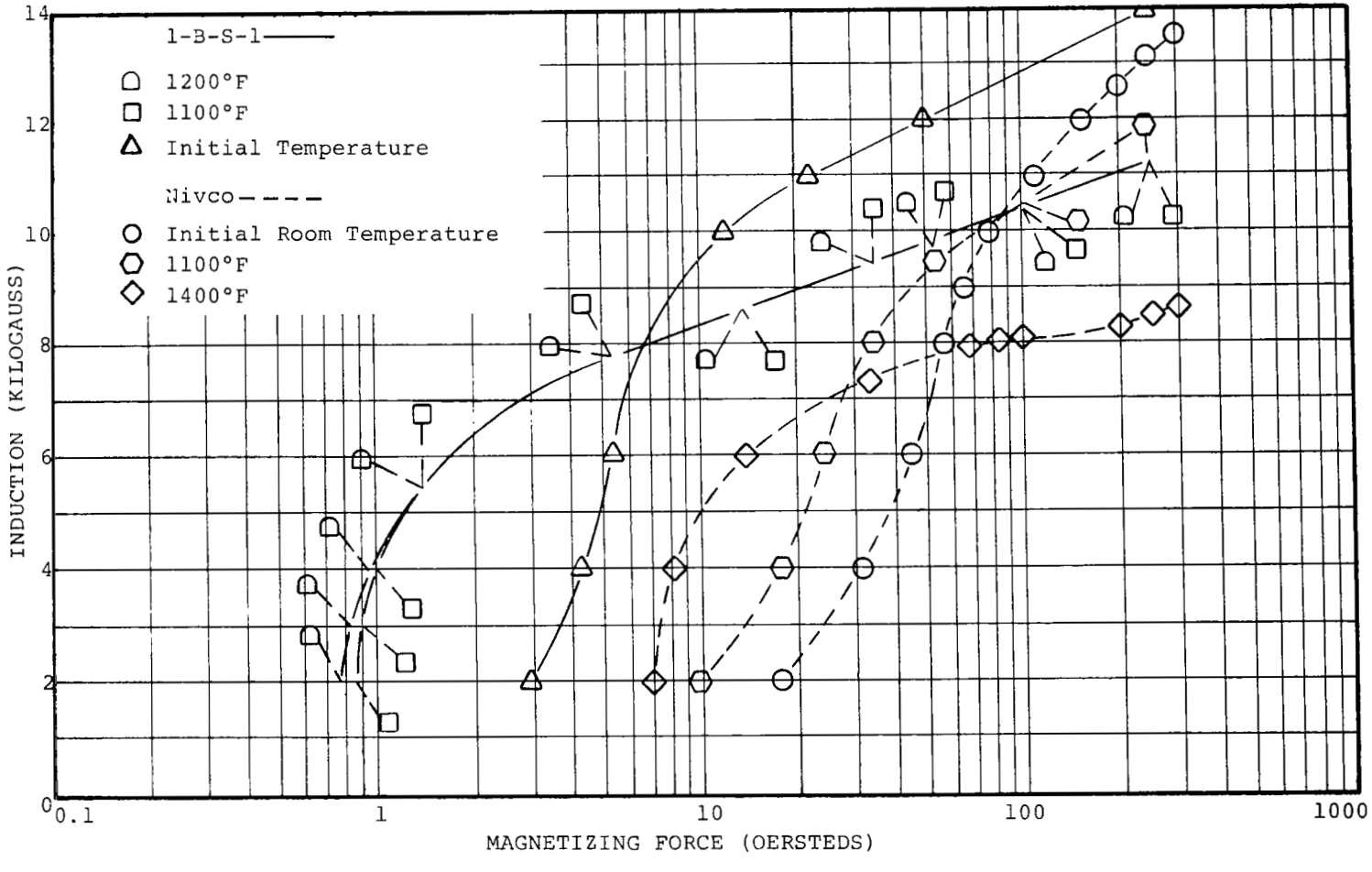

FIGURE II-20. DC Magnetization Curves of Alloy 1-B-S-1 (Co-15Ni-5Fe-5Ta-1.25Al-0.2Zr) and Nivco Alloy (Co-23Ni-1Zr-2Ti) at Room Temperature and Elevated Temperature, 0.025-inch Laminations. Data for Nivco Alloy from Reference II-11.

TABLE II-35. Tensile Test Data of 300-Gram Vacuum-Arc Melted Martensitic Alloys 1-A-S-1 and 1-A-S-2, and Cobalt Alloys 1-B-S-1 and 1-B-S-2

Alloy Number	Nominal Alloy Composition (weight percent)	Room Temperature Hardness 50 kg Load VHN	Temperature °F	Temperature °C	0.2% Yield Strength (psi)	Ultimate Tensile Strength (psi)	Uniform Elongation (percent)	Reduction of Area (percent)
Martensitic Alloys								
1-A-S-1[a]	Fe-15Ni-30Co-1W-3Ta-0.3Al-0.4Ti	-	77	25	Specimen failed at 182 000 psi with no elongation			
1-A-S-2[a]	Fe-12Ni-30Co-1W-3Ta-0.4Al-0.4Ti	-	77	25	Specimen failed at 182 000 psi with no elongation			
1-A-S-1[a]	Fe-15Ni-30Co-1W-3Ta-0.3Al-0.4Ti	674	1112	600	139 000	165 200	6.0	4.8
1-A-S-1[a]	Fe-15Ni-30Co-1W-3Ta-0.3Al-0.4Ti	669	1112	600	130 000	164 800	9.0	20.8
1-A S-2[a]	Fe-12Ni-30Co-1W-3Ta-0.4Al-0.4Ti	671	1112	600	141 700	169 000	2.0	0.8
1-A-S-2[a]	Fe-12Ni-30Co-1W-3Ta-0.4Al-0.4Ti	666	1112	600	158 700	171 000	3.5	2.4
For Comparison:								
H-11 Alloy[b]	Fe-5Cr-1.3Mo-0.5V-0.4C	-	77	25	180 000	215 000	15.2	29.0
H-11 Alloy[b]	Fe-5Cr-1.3Mo-0.5V-0.4C	-	800	427	144 000	174 000	15.0	40.0
15%Ni Maraging Steel[c]	Fe-9Co-15Ni-5Mo-0.7Al-0.7Ti	613	77	25	282 000	296 000	4.9	31.7
15%Ni Maraging Steel[c]	Fe-9Co-15Ni-5Mo-0.7Al-0.7Ti	619	1112	600	110 000	117 000	10.5	61.5
Cobalt-Base Alloys								
1-B-S-1[d]	Co-15Ni-5Fe-5Ta-1.25Al-0.2Zr	316	77	25	105 500	152 800	33.0	39.4
1-B-S-1[d]	Co-15Ni-5Fe-5Ta-1.25Al-0.2Zr	318	77	25	108 500	153 600	33.0	39.4
1-B-S-2[d]	Co-15Ni-5Fe-5Ta-1.25Al-0.1Zr-0.1Be	321	77	25	105 400	154 700	33.6	42.5
1-B-S-2[d]	Co-15Ni-5Fe-5Ta-1.25Al-0.1Zr-0.1Be	319	77	25	104 200	153 600	33.8	41.7
1-B-S-1[d]	Co-15Ni-5Fe-5Ta-1.25Al-0.2Zr	323	1112	600	88 700	125 600	19.0	24.8
1-B-S-1[d]	Co-15Ni-5Fe-5Ta-1.25Al-0.2Zr	329	1112	600	87 100	126 800	18.0	20.8
1-B-S-2[d]	Co-15Ni-5Fe-5Ta-1.25Al-0.1Zr-0.1Be	325	1112	600	89 500	123 800	19.5	32.0
1-B-S-2[d]	Co-15Ni-5Fe-5Ta-1.25Al-0.1Zr-0.1Be	322	1112	600	86 400	122 800	20.5	37.6
1-B-S-1[e]	Co-15Ni-5Fe-5Ta-1.25Al-0.2Zr	351	77	25	114 300	166 400	23.6	39.3
1-B-S-1[e]	Co-15Ni-5Fe-5Ta-1.25Al-0.2Zr	358	1112	600	99 200	132 000	13.6	20.5
1-B-S-1[e]	Co-15Ni-5Fe-5Ta-1.25Al-0.2Zr	354	1202	650	85 900	117 300	10.0	14.2
For Comparison:								
Nivco Alloy[b]	Co-23Ni-1Zr-2Ti	-	77	25	112 400	165 400	30.7	43.6
Nivco Alloy[b]	Co-23Ni-1Zr-2Ti	-	1100	593	89 900	124 600	24.3	47.0

(a) Sheet specimens annealed one hour at 1832°F(1000°C) and aged one hour at 1112°F(600°C) before testing.
(b) Round bar specimens. Data from Magnetic Materials Topical Report by P. E. Kueser et al, NASA-CR-54091, Contract NAS3-4162.
(c) Sheet specimens; source same as note (b).
(d) Sheet specimens annealed one hour at 1832°F(1000°C) and aged one hour at 1382°F(750°C) before testing.
(e) Sheet specimens annealed one hour at 1832°F(1000°C); then aged one hour at 1382°F(750°C) and 10 hours at 1202°F(650°C) before testing.

However, they are brittle at room temperature. These data also show the effect of a different heat treatment on the tensile strength of cobalt-base alloy 1-B-S-1. Test data from commercially available alloys of similar type such as H-11 alloy, 15 percent nickel maraging steel, and Nivco alloy are also listed in table II-35 for comparison (ref. II-11). One can see the improvement of high temperature strength obtained in the experimental alloys. Alloy 1-B-S-1 tested at 1100°F after aging one hour at 1380°F and ten hours at 1200°F shows a six percent improvement in strength over Nivco alloy.

The tensile tests indicate that room temperature ductility will present a problem in the ferritic alloys, although heat treatment holds promise for improvement.

It was also demonstrated previously on this program that the presence of chromium improves room temperature ductility (see table II-16). Floreen's work indicated that the absence of molybdenum in the alloys he studied greatly reduced ductility (refs. II-26 and II-27). Therefore, it may prove necessary to add molybdenum or chromium to the alloys under study here in order to improve room temperature ductility. The results from this program show the molybdenum may be tolerated up to a 2 weight percent addition. Above this amount the degrading influence on stability becomes serious. Since chromium has a detrimental effect on the stability of the alpha phase and on magnetic saturation (see tables II-9 and II-11; i.e., alloys 1-A-44, 1-A-45, 1-A-46) it should be added by replacing 2 weight percent nickel with one weight percent chromium. This will compensate for the otherwise detrimental effects of chromium.

d. KINETICS STUDY

A kinetics study was conducted on two final candidate alloys; one ferritic type, alloy 1-A-S-2, (Fe-12Ni-30Co-1W-3Ta-0.4Al-0.4Ti) and one cobalt type alloy 1-B-S-1 (Co-15Ni-5Fe-5Ta-1.25Al-0.2Zr). By this study of the precipitation process as reflected by a change in properties, time-temperature limits were obtained to provide guidelines for long-term applications. The change in hardness, coercive force, and electrical resistivity were measured during isothermal aging at several temperatures for periods to 1000 hours. Prior to testing, the martensitic alloys were subjected to a one-hour homogenization and austenitizing anneal at 1832°F in a helium-flushed tube furnace.

The subsequent aging was performed in neutral salt baths containing the appropriate mixture of nitrites and nitrates or chlorides as required by the aging temperature. The aging technique was described in section II.B.4. The temperature of the baths was maintained within 9°F (5°C). The properties were always measured at room temperature; therefore, the isothermal aging was interrupted for the test. Previous experience had shown that this interruption for the test did not produce any noticeable difference in the rate of change or in the absolute values of properties when measured at the same time and temperature.

This result was confirmed by a few spot checks. In some cases, different test samples were used for measuring the change of properties at various times. The measured values coincided within the limit of accuracy in spite of the fact that the time sequence for the test was different. These checks on different samples also confirmed reproducibility in the case of martensitic alloys. However, reproducibility in different samples of the cobalt-base alloy was poor because of apparent inhomogeneities of the alloy.

Hardness was measured as the Vickers hardness number under a load of 50kG. The accuracy was two percent. The coercive force was measured in a Förster "Koerzimeter" as previously outlined (section II.B.4.) with an accuracy of two percent. The electric resistivity was measured on strips about 2.5-mm wide, 0.5-mm thick, and 150-mm long by the standard four-blade resistance method. The temperature was kept constant at 77°F (25°C) within $\pm$0.18°F (0.1°C) by means of a coolant loop and a heater attached to a thermostat. The accuracy in determining specific resistivity was two percent, with the limitation set by the cross section measurements.

Test results of property changes during isothermal aging are shown in figures II-21 through II-27. The plot of hardness change for alloy 1-A-S-2 in figure II-21 shows that sufficient overaging to drop the room temperature hardness below 500 VHN occurs only at temperatures in excess of 1022°F (550°C). The measured change of coercive force (figure II-22) indicates a considerable increase (~60 oersteds) at an aging time of 1000 hours at 1022°F (550°C). The electrical resistivity decreases (figure II-23) during aging as one expects for a precipitation process. If a noticeable amount of reverted austenite had formed, one would expect the electrical resistivity to increase again after prolonged aging as had been observed in 15 percent

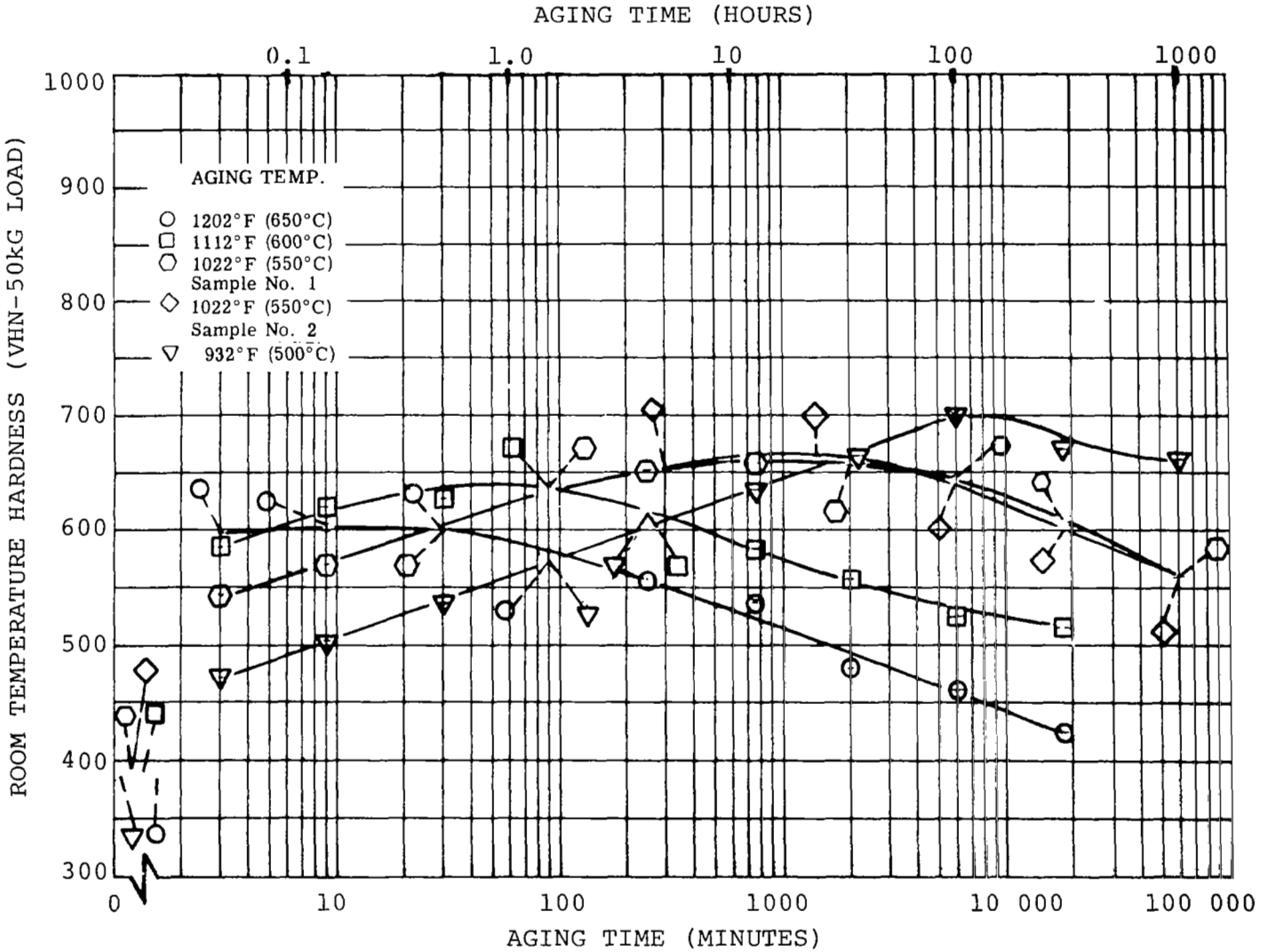

FIGURE II-21. Change in Room Temperature Hardness of Alloy 1-A-S-2 (Fe-12Ni-30Co-1W-3Ta-0.4Al-0.4Ti) During Isothermal Aging at Various Temperatures

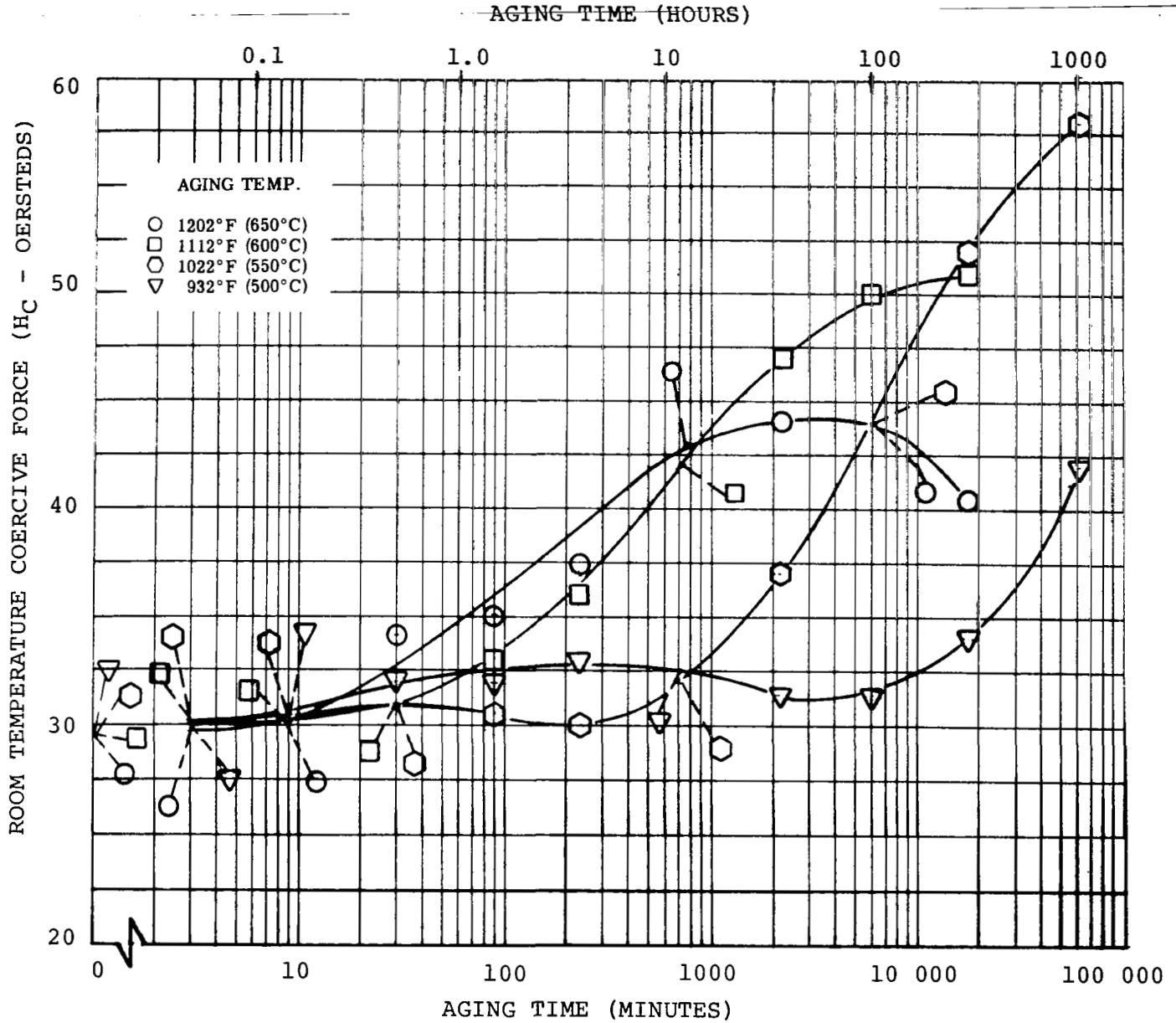

FIGURE II-22. Change in Room Temperature Coercive Force of Alloy 1-A-S-2 (Fe-12Ni-30Co-1W-3Ta-0.4Al-0.4Ti) During Isothermal Aging at Various Temperatures

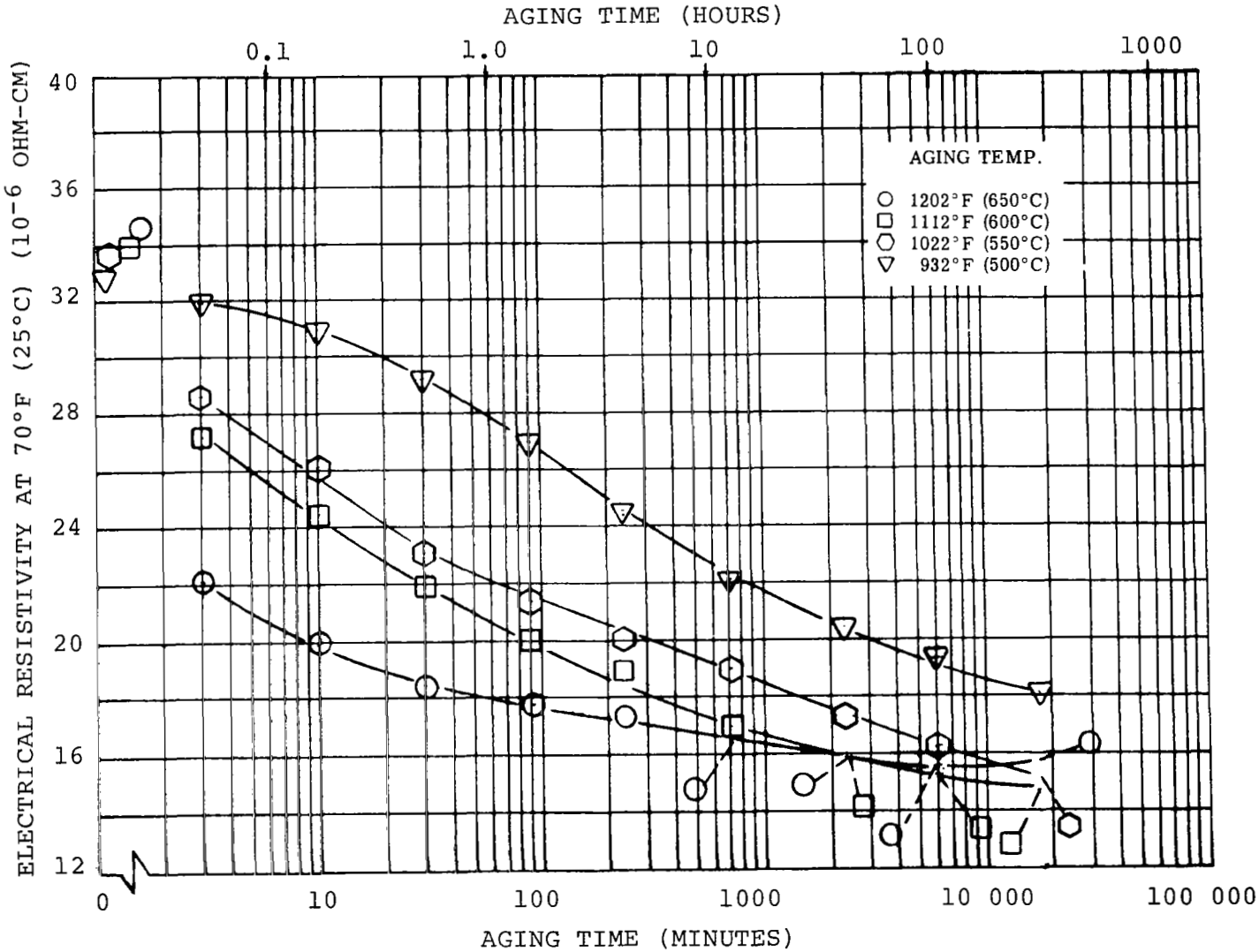

FIGURE II-23. Change in Room Temperature Electrical Resistivity of Alloy 1-A-S-2 (Fe-12Ni-30Co-1W-3Ta-0.4Al-0.4Ti) During Isothermal Aging at Various Temperatures

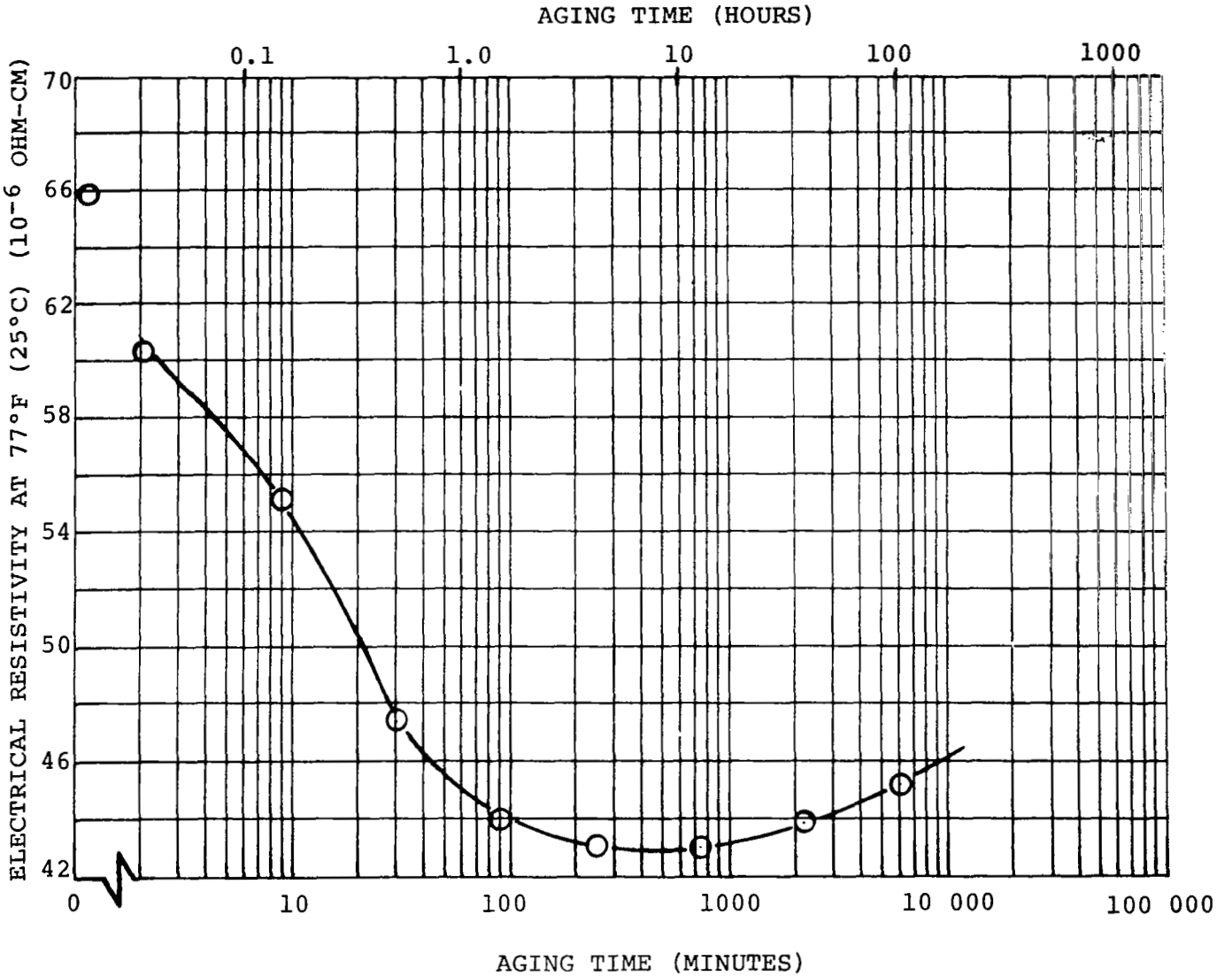

FIGURE II-24. Change in Room Temperature Electrical Resistivity of 15% Ni Maraging Steel (Fe-9Co-15Ni-5Mo-0.7Al-0.7Ti) During Isothermal Aging at 1112°F (600°C)

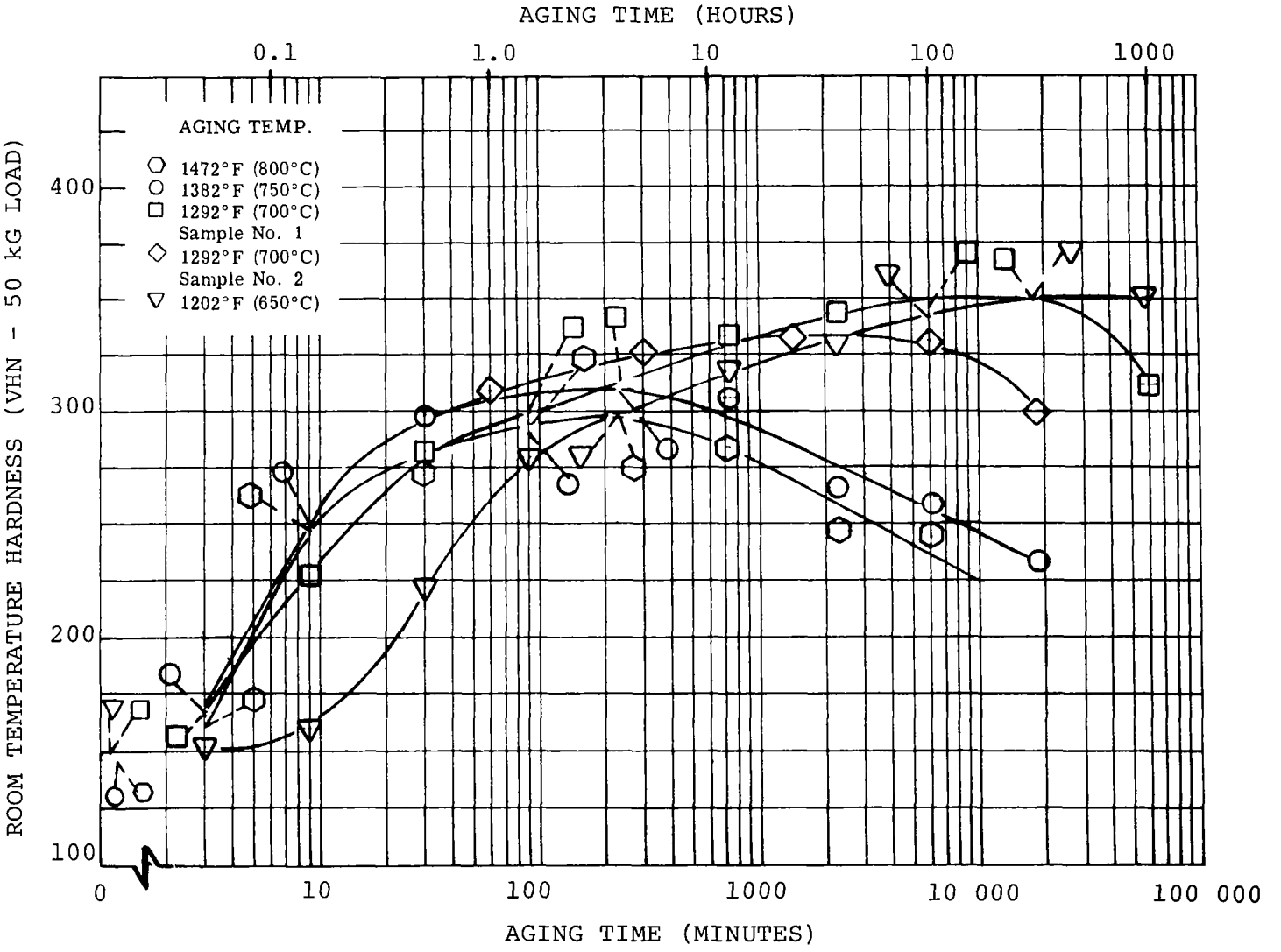

FIGURE II-25. Change in Room Temperature Hardness of Alloy 1-B-S-1 (Co-15Ni-5Fe-5Ta-1.25Al-0.2Zr-0.001B) During Isothermal Aging at Various Temperatures

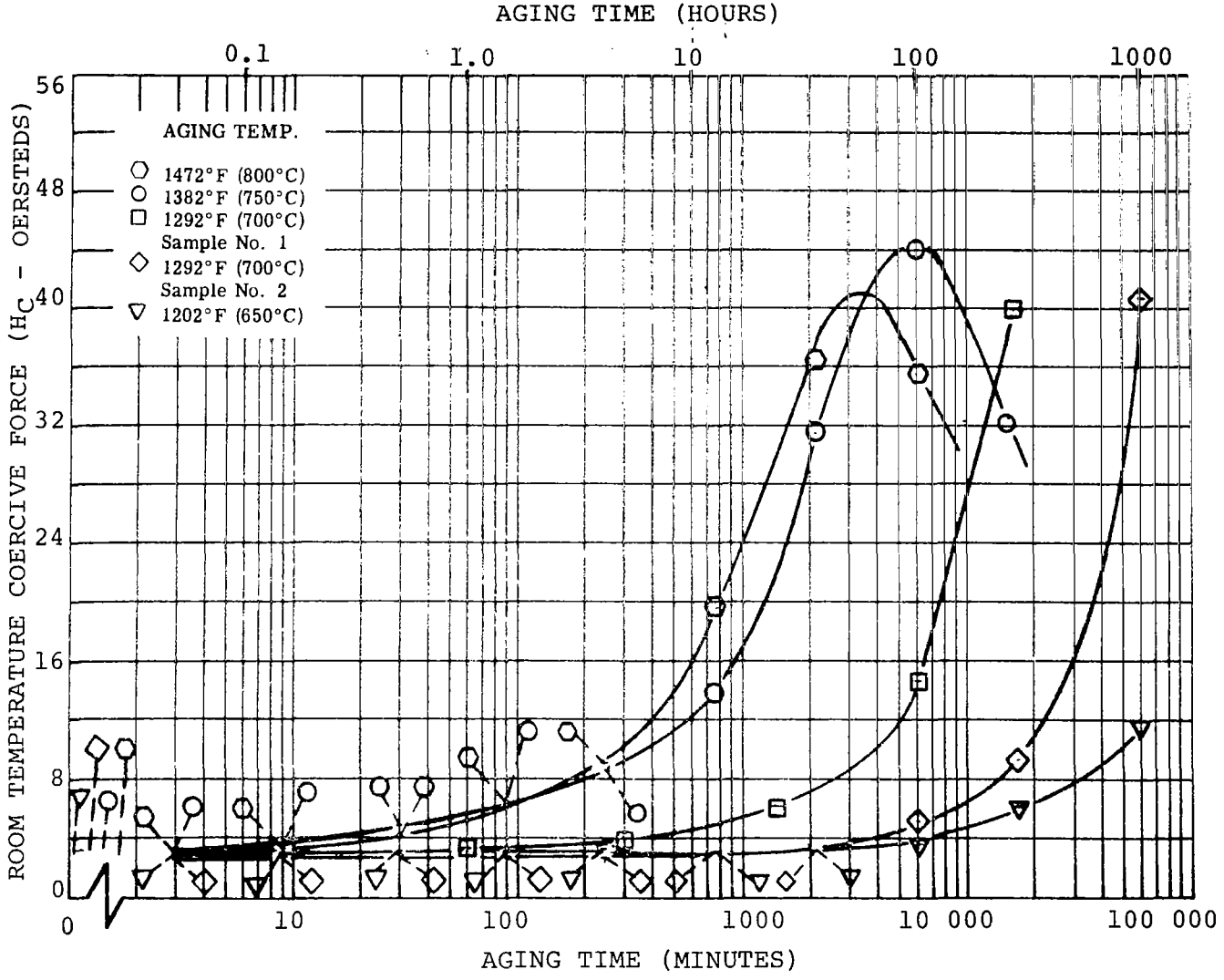

FIGURE II-26. Change in Room Temperature Coercive Force of Alloy 1-B-S-1 (Co-15Ni-5Fe-5Ta-1.25Al-0.2Zr-0.001B) During Isothermal Aging at Various Temperatures

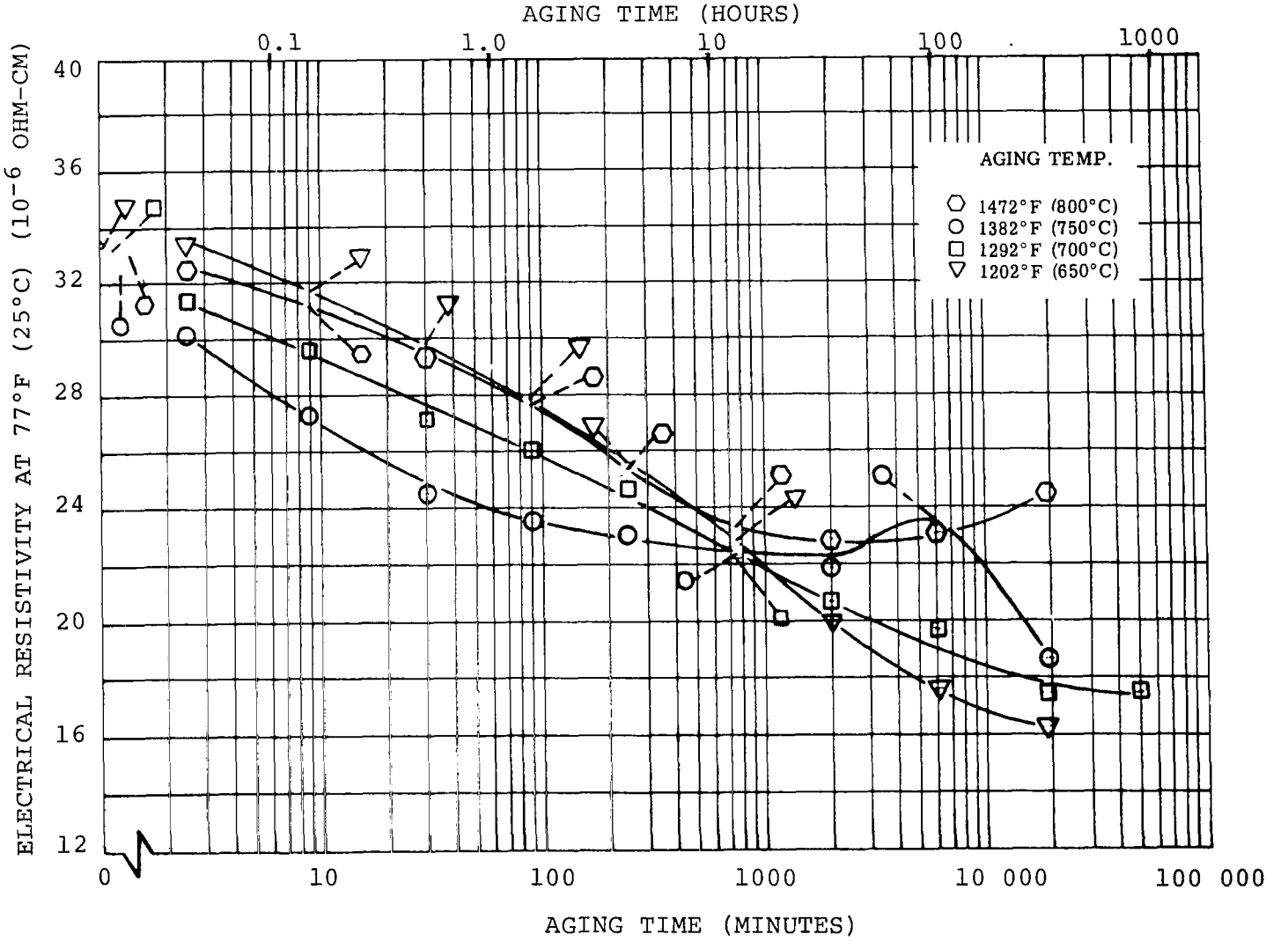

FIGURE II-27. Change in Room Temperature Electrical Resistivity of Alloy 1-B-S-1 (Co-15Ni-5Fe-5Ta-1.25Al-0.2Zr-0.001B) During Isothermal Aging At Various Temperatures

nickel maraging steel (figure II-24). One may therefore conclude that no measurable amount of reverted austenite formed in the present martensitic alloy during aging as high as 1112°F (600°C) within the measured periods of time. This is a significant indication of matrix stability achieved in the experimental alloy.

The plot of change of hardness for the cobalt-base alloy 1-B-S-1 in figure II-25 shows that sufficient overaging to drop the room temperature hardness below 300 VHN occurs within 1000 hours only at temperatures above 1292°F (700°C). The plot of the change in coercive force (figure II-26) shows that a strong increase of coercive force is also associated with overaging in the cobalt alloys. After 1000 hours at 1292°F (700°C) the room temperature coercive force was higher than 40 oersteds. The coercive force values were substantially lower when measured at higher temperatures (table II-36). The change of electrical resistivity of alloy 1-B-S-1, plotted in figure II-27 shows the decrease is probably due to a precipitation process. At aging temperatures below 1202°F (650°C) the resistivity increased slightly before it dropped. This increase of resistivity was observed previously in cobalt-base alloys with γ' precipitate (ref. II-28). It occurs also in nickel alloys with additions which produce γ' precipitate (refs. II-29 and II-30). One notices that an increase of electrical resistivity occurred with long aging times at temperatures higher than 1292°F (700°C). This resistivity increase occurs at aging times when the coercive force reaches its maximum and the hardness is already decreasing with aging time. It is perhaps associated with a transition of the precipitate from a metastable γ' phase into a more stable phase. Such transition has been reported in nickel alloys with additions of Al+Ti and Al+Ti+Nb (refs. II-31 and II-32). Such a transition can be observed in alloy 1-B-S-1 containing Al+Ta after aging at 1472°F (800°C) for 200 hours (see figure II-27). The increase in electrical resistivity at 1292°F (700°C) and a subsequent change in slope, simulates that observed for the coercive force (see figure II-26).

A light micrograph and electron micrograph replica showed that in addition to the grain boundary precipitate the matrix contains two types of precipitate within the grains. Fine cubes representing the γ' phase form first. There are also larger needle-like precipitate particles which have been identified as a hexagonal phase with a_o=9.41Å, c=15.50Å which is in agreement with the hexagonal phase Co_3Ta found by Dragsdorf and Forgeny (ref. II-33).

TABLE II-36. Coercive Force of Samples of Alloy 1-B-S-1 at Long Aging Times

Alloy Number	Aging Time and Temperature	Coercive Force (oersteds)	
		At Room Temperature	At 1112°F (600°C)
1-B-S-1	1000 hours at 1292°F (700°C)	41.0	19.0
1-B-S-1	300 hours at 1382°F (750°C)	32.5	20.0

It may well be that in the observed overaging at temperatures above 1292°F (700°C), the increase of coercive force and the irregularity of the resistivity change at long aging times, depend on this transition of the precipitate phase rather than on the growth of the original γ' particles. If this is the case, one should be able to suppress this transition by increasing the aluminum to tantalum ratio and hence increase the thermal stability of this alloy.

e. APPLICATION CONSIDERATIONS

The determination of relatively short term aging characteristics on both the ferritic base (1-A-S-2) and cobalt-base (1-B-S-1) alloys is of value in anticipating potential changes in the magnetic and mechanical behavior which these alloys may undergo due to diffusion kinetics.

An analysis of the time to reach the first coercive force inflection point (figure II-22) or time to reach maximum hardness in the ferritic alloy (figure II-21) suggests that these time periods (tm) obey an Arrhenius type relation,

$$t_m = t_{mo} \exp Q/RT,$$

where T is absolute temperature, R is the universal gas constant, t_{mo} is a constant, and Q is the activa-

tion energy produced by a diffusion-controlled, precipitation process. The activation energy observed in the ferritic alloy was approximately 65 kcal/mole as found by reviewing figure II-28. This is in some agreement with bulk diffusion of iron, nickel or cobalt in the alloy. Utilizing a 65 kcal/mole value, table II-37 estimates the times at which the coercive force inflection point and the maximum hardness occur at several temperatures for alloy 1-A-S-2. The coercive force inflection point was selected since it represents the condition prior to that when the precipitate size is of the same dimension as a magnetic domain. A maximum coercive force is attained when the precipitate size is the same as the domain wall thickness. Maximum hardness occurs earlier and suggests that the alloy will begin overaging almost an order of magnitude in time before the coercive force inflection point is reached.

The utilization of this method for the cobalt-base alloy 1-B-S-1 was not as straightforward because inhomogeneities in the alloy caused variations in the rate of changes in properties from sample to sample. Applying an activation energy of 70,000 to the longer time data, an approximate fit is observed between adjacent points. Using this value for activation energy and applying it to an Arrhenius type relation as before, table II-38 estimates the times at several temperatures when maximum hardness or the first coercive force inflection point will be reached.

The values observed in tables II-37 and II-38 alert the designer to conditions where more thorough data may be required to fully identify long-term performance.

f. MICROSTRUCTURE OF PRECIPITATION-HARDENED MAGNETIC ALLOYS

(1) Ferritic Alloys

The microstructure of several experimental alloys obtained by light microscopy are shown in figures II-29.a, II-29.b, and II-29.c. Specimens were aged for 100 hours at 1022°F (550°C) before the micrographs were made. A fine precipitate which delineates the grain boundaries and substructure may be seen in the micrographs. In some cases as in figure II-29.b inclusions may be noted. These inclusions had been present prior to rolling indicating that the alloy had not been completely homogenized during the previous heat treatment.

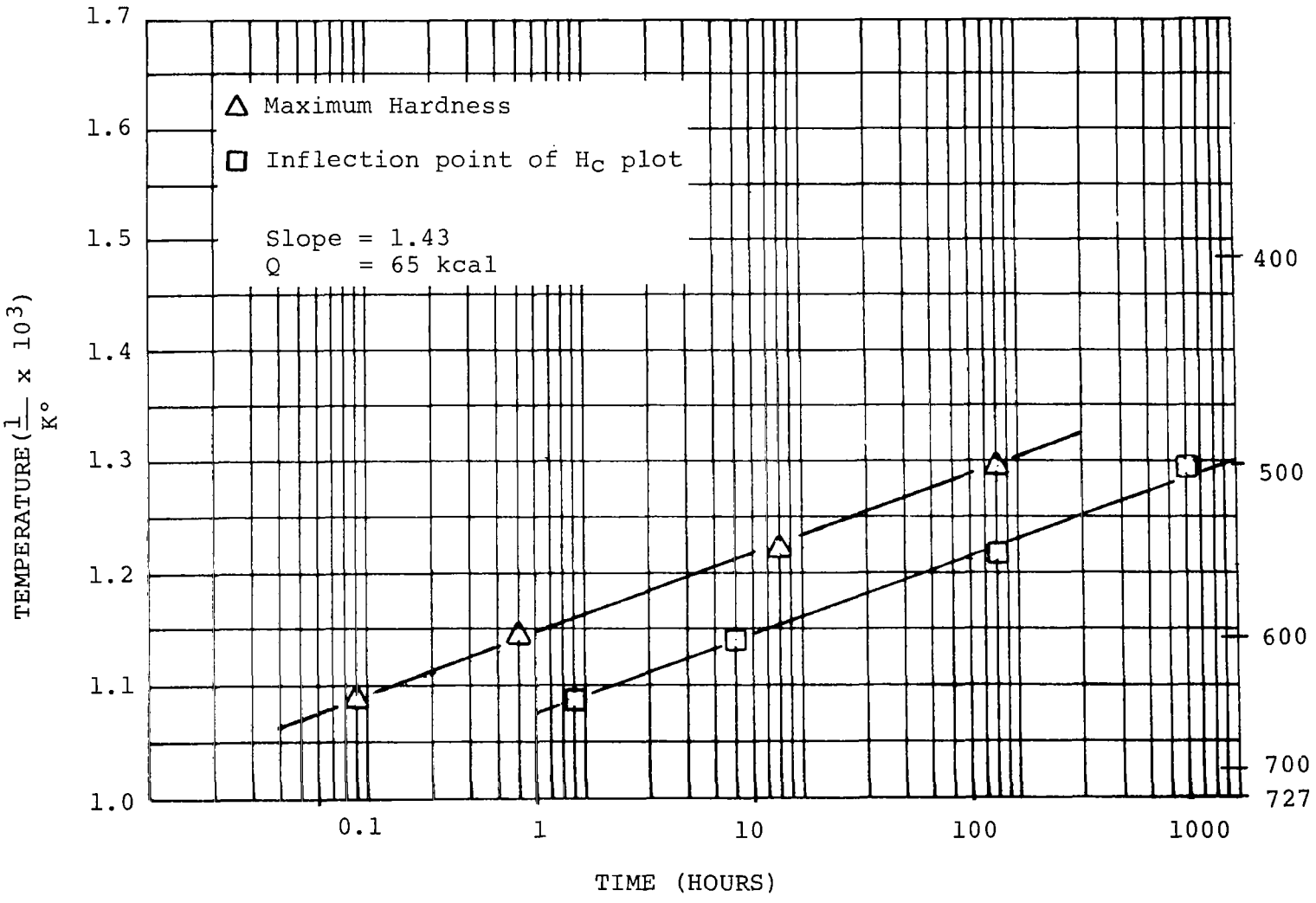

FIGURE II-28. Time-Temperature Plot of Hardness and Coercive Force of Alloy 1-A-S-2 (Fe-12Ni-30Co-1W-3Ta-0.4Al-0.4Ti)

TABLE II-37. Estimated Time to Reach Coercive Force Inflection Point or Maximum Hardness at the Indicated Temperature for Alloy 1-A-S-2

Temperature		Time at Which Coercive Force Inflection is Reached (hours)	Time at Which Maximum Hardness is Reached (hours)
(°C)	(°F)		
450	842	25,000	2,500
500	932	1,000	133
550	1022	133	13
600	1112	8	0.8

TABLE II-38. Estimated Time to Reach Coercive Force Inflection Point or Maximum Hardness at the Indicated Temperature for Alloy 1-B-S-1

Temperature		Time at Which Coercive Force Inflection is Reached (hours)	Time at Which Maximum Hardness is Reached (hours)
(°C)	(°F)		
550	1022	300,000	75,000
600	1112	30,000	7,500
650	1202	4,150	1,000
700	1282	835	166

(a)
Alloy 1-A-46
(56Fe-15Ni-25Co-2Cr-2Si)

(b)
Alloy 1-A-V-1
(48Fe-15Ni-30Co-2W-4Ta-
0.5Al-0.5Ti)

(c)
Alloy 1-A-S-1
(50.3Fe-15Ni-30Co-1W-3Ta-
0.3Al-0.4Ti+0.001B+0.003Zr)

20
10
0
Microns

Electrolytically etched in 10 percent chromic acid.

FIGURE II-29. Light Micrographs of Several Ferritic Alloys Annealed One Hour at 1832°F (1000°C) and Aged 100 Hours at 1022°F (550°C) 500X

The structure observed by light microscopy appears similar to that of nickel maraging steel after cooling. This appearance if regarded as an indication (refs. II-34 and II-35) that transformation after cooling resembles a structure produced by massive transformation (ref. II-36), which is believed to be typical for binary Fe-Ni alloys containing 8 to 20 weight percent nickel.

Figure II-30 shows the microstructure of alloy 1-A-S-2 obtained by electron transmission microscopy. The sequence is shown in the development and growth of precipitate during aging of this alloy at 1022°F (550°C). Many of the particles are formed at the dislocations. Then the precipitate grows to needles which are oriented according to the matrix orientation. A phase, probably austenite, appears in the form of long stringers at the boundaries of the lathes. Electron micrographs of replicas of several alloys after aging for 100 hours at 1022°F (550°C) are shown in figures II-31.a to II-31.d. Regularly oriented needles appear in the Fe-Ni-Co with titanium added. Needles also occur in the alloys containing tantalum or niobium, but are less regularly oriented. Spherical particles formed in the alloy containing molybdenum.

Electron diffraction patterns were obtained from replicas of samples which were aged for 100 hours at 1022°F (550°C). At this time some overaging had occurred. There was a possibility that the phases detected after 100 hours are not the same as that precipitating at the start of aging. The alloys containing molybdenum were studied at times starting at one hour. The results verified that the type of precipitate is the same as that found after 100 hours, but the particles are much smaller. Table II-39 shows the electron diffraction patterns obtained for a number of experimental alloys. Tentative identification of the patterns are also given in table II-39. The precipitate pattern for a given element was the same in the Fe-Co base containing either 12 or 15 percent Ni. Varying the cobalt content between 8 and 30 weight percent apparently did not change the type of precipitate. The identification of precipitate in alloys containing molybdenum was determined to be the Fe_2Mo Laves phase. Electron diffraction results on this program are in agreement with Fleetwood's results (ref. II-37) in similar molybdenum

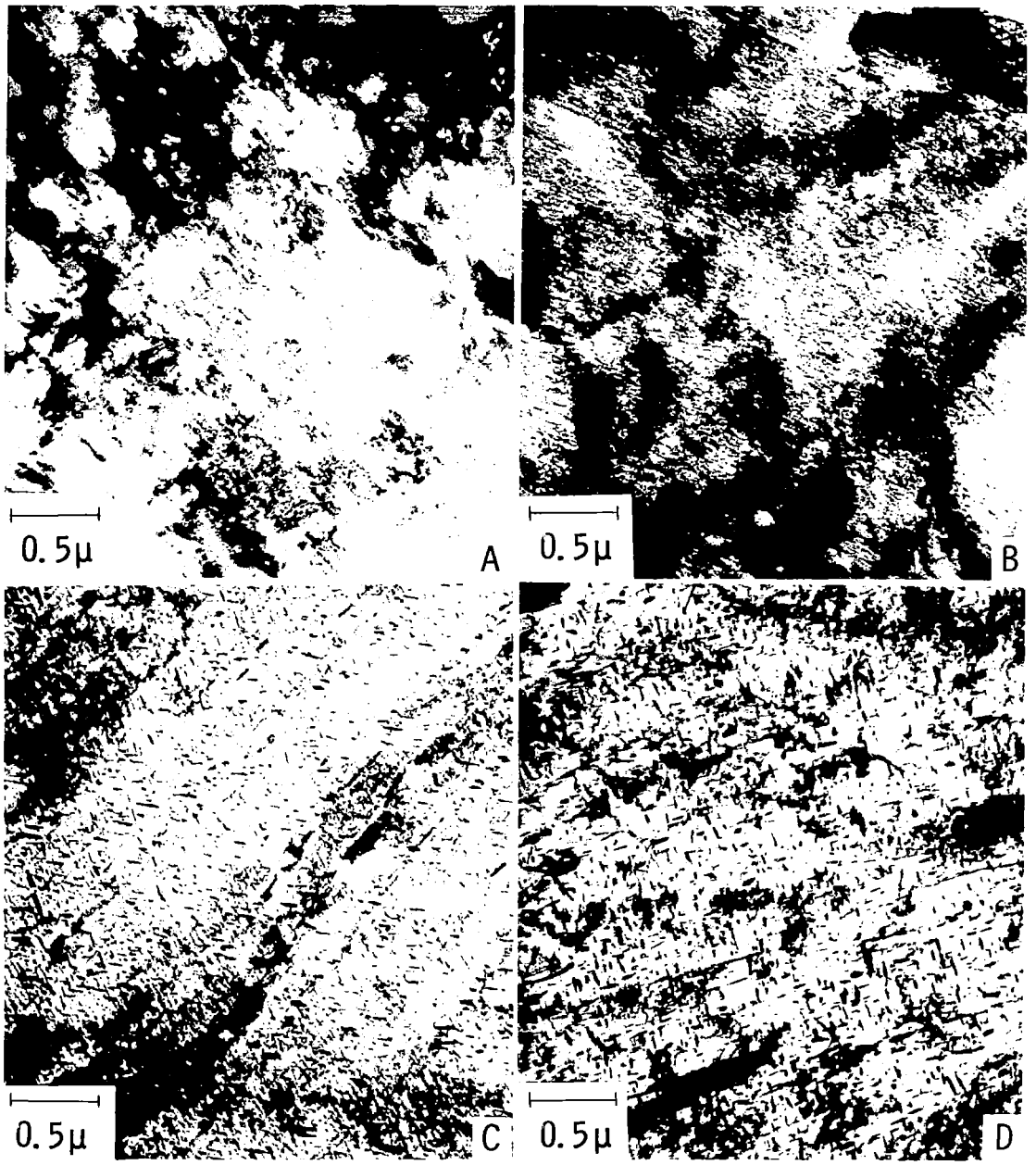

A. Annealed One Hour at 1832°F (1000°C)
B. Annealed and Aged Three Hours at 1022°F (550°C)
C. Annealed and Aged 100 Hours at 1022°F (550°C)
D. Annealed and Aged 1000 Hours at 1022°F (550°C)

FIGURE II-30. Electron Transmission Micrographs of Alloy 1-A-S-2 (Fe-12Ni-30Co-1W-3Ta-0.4Al-0.4Ti).

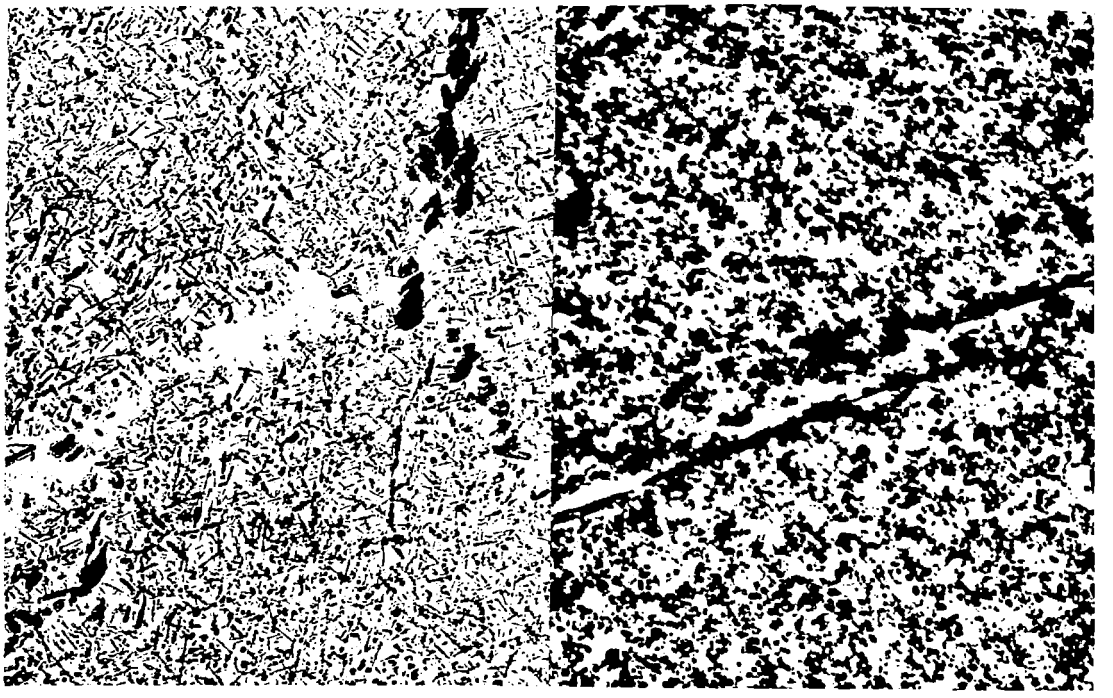

30,000X 22,400X

(a)
Alloy 1-A-26
(67Fe-12Ni-20Co-1Ti)

(b)
Alloy 1-A-27
(63Fe-12Ni-20Co-5Mo)

FIGURE II-31. Electron Microscope Replica of Ferritic Alloys. Annealed One Hour at 1832°F (1000°C) Then Aged 100 Hours at 1022°F (550°C).

TABLE II-39. Phases Detected in Alloys 1-A-26, 1-A-27, 1-A-28 After Aging 100 Hours at 1022°F (550°C) and in Alloy 1-A-V-4 After Aging 100 Hours at 1022°F (550°C)

Shape of Phases	Lattice	Probable Identification
1-A-26 (67Fe-12Ni-20Co-1Ti)		
Needles ~100 Å diam ~1000Å long	hexagonal a_o = 5.1Å, c = 8.3Å	Ni_3Ti Do_{24}
Dark globular particles at grain boundaries	cubic a_o = 4.6 Å	Ti(C, N)
Bright particles at boundaries	face centered cubic a_o = 3.6 Å	Austenite Al
1-A-27 (63Fe-12Ni-20Co-5Mo)		
Discs 200 Å diam (some as large as 1000 Å)	tetragonal a_o = 9.2 Å	FeMo $D8_6$
	or	or
Black Stringers 500 Å diam 3 μ long	hexagonal a_o = 4.7 Å, c = 7.7 Å	Fe_2Mo C14
	or both	
Large particles 1 μ diam	cubic a_o = 4.6 Å	Ti carbonitrides γ'
Large white elongated particles	face centered cubic a_o = 3.6 Å	Austenite Al
1-A-28 (63Fe-12Ni-20Co-5Ta)		
Large particles 0.5 μ diam	hexagonal a_o = 4.8 Å, c = 7.8 Å	Fe_2Ta C14
1-A-V-4 (Fe-14.8Ni-29.4Co-0.64Al-0.52Ti-3.48Ta) (electron diffraction analysis)		
Needles ~100 Å diam ~1000 Å long	hexagonal a ~ 4.5 Å, c ~ 4.0 Å	Similar to Ni_3Ta but 10% smaller containing Ta+Ti and Ni
Black small stringer 300 to 500 Å diam 1 to 3 μ long	face centered cubic a ~ 3.6 Å	Austenite
A few larger globular precipitate at grain boundaries	cubic	Ta or Ti carbonitrides

hardened maraging steels. With the addition of tantalum to the Fe-Ni-Co matrix, the Ni_3Ta-η phase precipitates with the addition of Ti the Ni_3Ti-η precipitates. While the Ni_3Ti-η phase lattice parameters are similar to the orthagonal Ni_3Ta-η phase, the former is indexed as a hexagonal structure. The addition of small amounts of Ti and Al in combination with Ta results in a similar η type structure, although the lattice parameters are significantly reduced, and the intensity changes noticeably. In alloys containing either Cr+Si or Si+V additions, a $Ni_3Si\gamma'$ type phase precipitates; however, it should be noted that the addition of Si alone did not produce a precipitation hardening effect. Beryllium also precipitated as a similar γ type structure of Ni_3Be with an identical lattice parameter.

(2) Cobalt-Base Alloys

Typical results obtained from the study of microstructure by light microscopy are shown in figures II-32.a, II-32.b, II-32.c. All light micrographs were made after aging the specimen for 100 hours at 1292°F (700°C). In some of the alloys, discontinuous or cellular precipitation has occurred as shown in figure II-32.a. The amount of discontinuous precipitate occurring in the cobalt alloys is listed in table II-22. It may be noted that the amount of discontinuous precipitate increases as the amount of Ti and Al increases. A change in the Ti and Al ratio also influences the amount of discontinuous precipitate: more discontinuous precipitate appears with higher Ti content. These results confirm earlier work (refs. II-28 and II-38). This phenomenon has been explained in terms of coherency strains between the continuous precipitate and the matrix. With higher disregistry, which is increased by higher Ti in the Ti to Al ratio (ref. II-23), discontinuous precipitation form preferentially to continuous precipitation. The addition of zirconium appears to reduce the amount of discontinuous precipitate sharply. The effect may be due to the segregation of zirconium which is in solution to the grain boundary; thereby changing the nucleation behavior of the discontinuous precipitate. The addition of iron also reduces the quantity of discontinuous precipitate. The alloying content of all alloys starting with 1-B-32 is apparently balanced in such a way that formation of discontinuous precipitation is minimized.

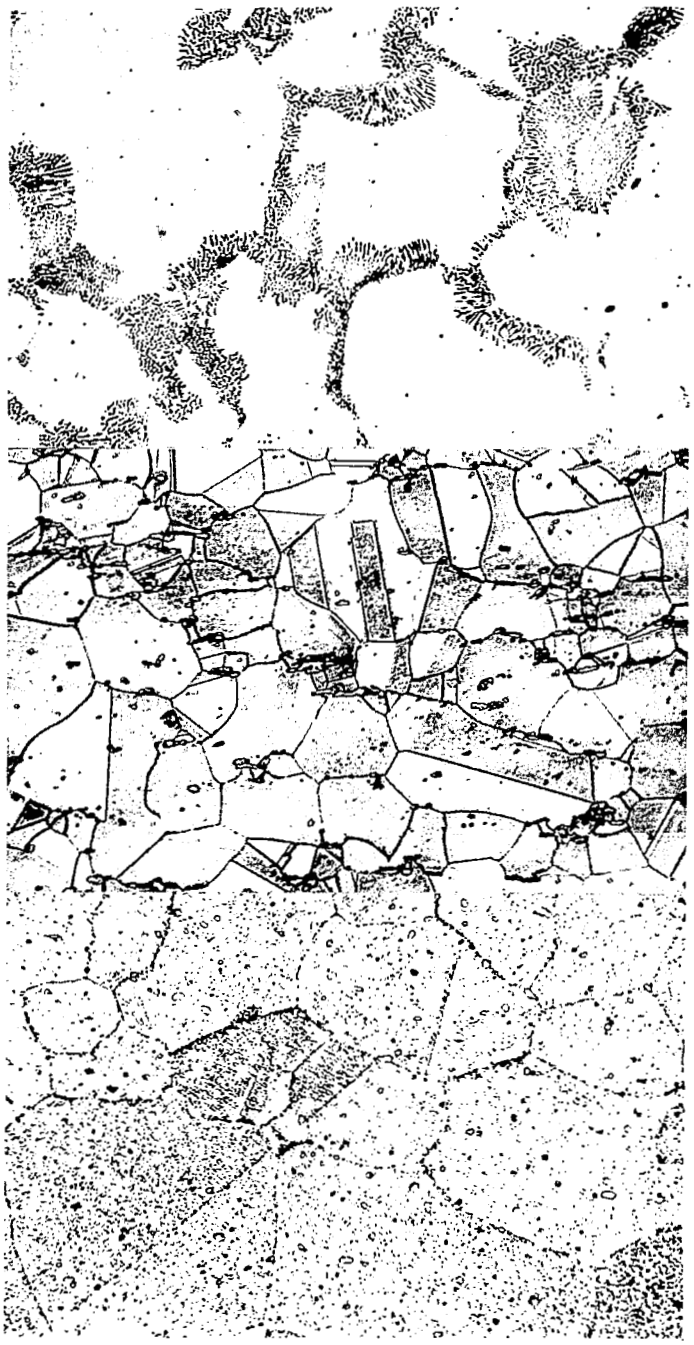

(a)
Alloy 1-B-24
(76Co-20Ni-3Ti-1Al)

(b)
Alloy 1-B-V-4
(73.5Co-5Fe-15Ni-1.2Al-
0.3Zr-5Ta)

(c)
Alloy 1-B-36
(75.3Co-15Ni-5Fe-2.2Ti-
1.5Al-0.5Zr-0.5Be)

20
10
0
Microns

Etchant: 20 ml HCl, 40 ml HNO_3, 60 ml glycerin

FIGURE II-32. Light Micrographs of Typical Cobalt Base Alloys
500X

In all alloys containing zirconium, small inclusions of a second phase were observed (see figure II-32.b) which indicate the Zr content is too high to be entirely dissolved in the lattice: a zirconium compound possibly formed during solidification. Microprobe analysis showed that these particles were contained in nickel as well as zirconium. The precipitate within the grains could not be observed by light microscopy after annealing and aging at 1292°F (700°C). In only a few cases (see figure II-32.c) did the etching behavior indicate a submicroscopic precipitate. However, when the samples were cold-rolled (~50% reduction) after annealing, but before aging, a heterogenized structure appeared. Examination by electron microscopy revealed the existence of cube-shaped precipitate particles 200 to 300 angstroms in size. These cubes were aligned in rows within the grains as shown in figures II-33.a and 33.b. The precipitate appears to be preferentially oriented with respect to the parent matrix. Electron and x-ray diffraction of the replica indicate that these particles represent the γ' phase of the Ll_2 type. The precipitate therefore resembles that found in aged Ni-Al and Ni-Al-Ti alloys (ref. II-23). The microprobe studies confirmed, however, that the particles contain not only Ti and Al but Co, Fe, Ti, and further additional elements such as Ta. This confirms the results reported by Westbrook (ref. II-39). The lattice constant of the γ' phase with regard to the matrix was determined in several cases after heterogenizing the alloys in order to concentrate the γ' phase. Results are reported in table II-40. The difference in lattice constant appears to correlate with the maximum hardness obtained for an alloy (table II-22). However, it is still possible that a considerable contribution to hardness results from solid solution hardening rather than from coherency strain due to disregistry.

g. CREEP RESISTANCE

The foregoing portions of section II have detailed the screening, testing, and evaluation of magnetic, hardness and tensile properties and metallurgical stability that led to the selection of four alloy compositions for final evaluation. Short term creep (<1000 hours) tests were scheduled at the end of the program for these alloys having the following nominal compositions in weight percent:

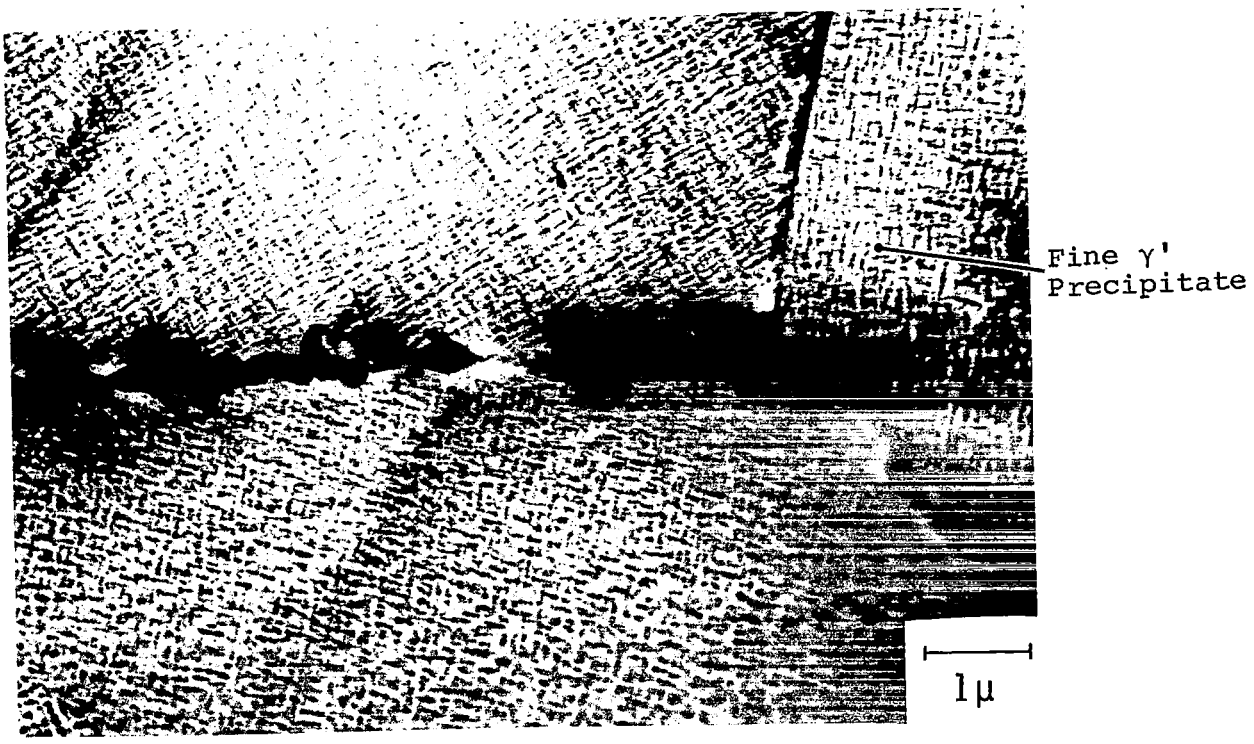

(a) Electron Transmission Micrograph 14,000X

(b) Carbon Replica of Etched Surface 17,500X

FIGURE II-33. Electron Micrographs of the Microstructure of Alloy 1-B-V-4 (73.5Co-5Fe-15Ni-1.2Al-0.3Zr-5Ta) After Aging 100 Hours at 1292°F (700°C)

TABLE II-40. Phases Detected in Alloy 1-B-39, After Aging 100 Hours at 1292°F (700°C) and in Alloy 1-B-V-4, After Aging 100 Hours at 1292°F (700°C) With and Without a Previous Deformation by 50 Percent Cold Rolling

Shape of Phases	Lattice	Probable Identification
1-B-39 (70.8Co-15Ni-5Fe-2.2Ti-1.5Al-0.5Zr-5Ta)		
Fine precipitate Larger lamellae	face centered cubic a_o = 3.62	γ' similar to Ni_3Al L_2 a_o = 3.561
Coarse particles		
Matrix	face centered cubic a_o = 3.55	
		(The presence of M_6C or $M_{23}C_6$ and M_2C was detected)
1-B-V-4 (Co-5.1Fe-0.26Zr-14.8Ni-1.25Al-5.19Ta) aged without deformation (electron diffraction analysis)		
Small particles cubic shape 100 to 200 Å width arranged in chains	face centered cubic	Gamma prime γ'
Coarser grain boundary precipitate particles	face centered cubic	Gamma prime γ'
1-B-V-4 (Co-5.1Fe-0.26Zr-14.8 Ni-1.25Al-5.19Ta) aged with previous deformation (X-ray diffraction)		
Heterogenized matrix	face centered cubic a_o = 3.552 Å	Matrix
	face centered cubic Ll_2 a_o = 3.612 Å	Gamma prime γ'

Ferritic Type

1-A-S-1 (Fe-15Ni-30Co-1W-3Ta-0.3Al-0.4Ti)

1-A-S-2 (Fe-12Ni-30Co-1W-3Ta-0.4Al-0.4Ti)

Cobalt Base

1-B-S-1 (Co-5Fe-15Ni-5Ta-1.25Al-0.2Zr)

1-B-S-2 (Co-5Fe-15Ni-5Ta-1.25Al-0.1Zr-0.1Be)

The creep tests were conducted in vacuum at a pressure less than $1x10^{-6}$ torr. The stress and temperature were selected on the basis of the tensile tests results previously described. It was believed that the creep strain in 1000 hours would be less than one percent for the ferritic alloys when tested at 1000°F under a load of about 80,000 psi and for the cobalt alloys when tested at 1200°F under a load of 40,000 psi. Alloys 1-A-S-2 and 1-B-S-1 were the first to be creep-tested under the conditions described above. Alloy 1-B-S-1 performed satisfactorily. Alloy 1-A-S-2 broke in a brittle manner after a short time at the prescribed conditions. A second specimen broke in the same manner. The creep performance of alloy 1-A-S-1 was better.

It should be mentioned that the experimental ferritic alloys, although possessing high strength, exhibited low ductility in the room temperature tensile tests. On the other hand, both cobalt-base alloys 1-B-S-1 and 1-B-S-2 performed well, indicating early in the creep testing their superiority over the commercially available Nivco alloy. The creep test results are compiled in table II-41. Because specimens of alloy 1-B-S-1 exhibited slightly higher creep resistance than those of alloy 1-B-S-2, effort was concentrated on the former alloy. This alloy continued to show a creep strain about one-third that of Nivco alloy when tested under similar conditions. Beginning with specimen No. 4 of alloy 1-B-S-1 (table II-41), the creep testing was altered to provide data for a Larson-Miller creep plot. Although these tests were of relatively short time for this treatment, the Larson-Miller curve substantiated the high creep resistance of the experimental cobalt alloy when compared to Nivco alloy (figure II-34).

TABLE II-41. Creep Test Results on Precipitation-Hardened Magnetic Alloys

	Specimen					
	1-A-S-2 #1	1-A-S-2 #2	1-A-S-1 #1	1-B-S-2 #1	1-B-S-1 #1	1-B-S-1 #2
Test Temperature (°F)	1000	1000	1000	1200	1200	1200
Stress (psi)	80000	80000	60000	60000	40000	60000
Test Duration (hours)	27[a]	55[a]	1015	1002	1008	1016
Total Creep Strain (%)	0.8	0.66	1.33	0.059	0.007	0.028
Plastic Strain on Loading (%)	0	0	0	0	0	0
Minimum Creep Rate; by Head Travel Measurement (%/hr)	(b)	(b)	(b)	0.0000378	(b)	(b)
Time to Reach 0.2% Creep Strain (hours)	(b)	(b)	(b)	4732[e]	(b)	(b)
Time to Reach 0.4% Creep Strain (hours)	(b)	(b)	(b)	10023[e]	(b)	(b)
Pressure Limits During Test (torr)	6.0×10^{-7} 3.4×10^{-7}	8.8×10^{-7} 2.7×10^{-7}	6.8×10^{-7} 4.7×10^{-8}	4.9×10^{-7} 1.1×10^{-7}	1.4×10^{-6} 1.0×10^{-7}	8.5×10^{-7} 1.3×10^{-7}

	Specimen					
	1-B-S-1 #3	1-B-S-1 #4	1-B-S-1 #5	1-B-S-1 #6	1-B-S-1 #7	1-B-S-1 #8
Test Temperature (°F)	1300	1200	1200	1200	1300	1350
Stress (psi)	60000	80000	85000	84500	50000	20000
Test Duration (hours)	246[c]	1001	500	1100	1004	1033
Total Creep Strain (%)	8.5	0.13	0.95	0.13	0.213	0.08
Plastic Strain on Loading (%)	0	0	0.36	0.10	0	0
Minimum Creep Rate; by Head Travel Measurement (%/hr)	(b)	0.000126	0.00042	0.00012	0.00018	0.00007
Time to Reach 0.2% Creep Strain (hours)	(b)	1557[e]	0.6[e]	1683[e]	928[d]	2748[e]
Time to Reach 0.4% Creep Strain (hours)	(b)	3144[e]	1.0[d]	3350[e]	2043[e]	5606[e]
Pressure Limits During Test (torr)	4.9×10^{-7} 1.4×10^{-7}	7.0×10^{-7} 1.7×10^{-7}	7.5×10^{-7} 1.1×10^{-7}	7.1×10^{-7} 1.5×10^{-7}	5.2×10^{-7} 1.0×10^{-7}	6.0×10^{-7} 2.0×10^{-7}

(a) Specimen broke at the fillet in a brittle manner
(b) Not determined
(c) Specimen failed
(d) Interpolated Value
(e) Extrapolated Value

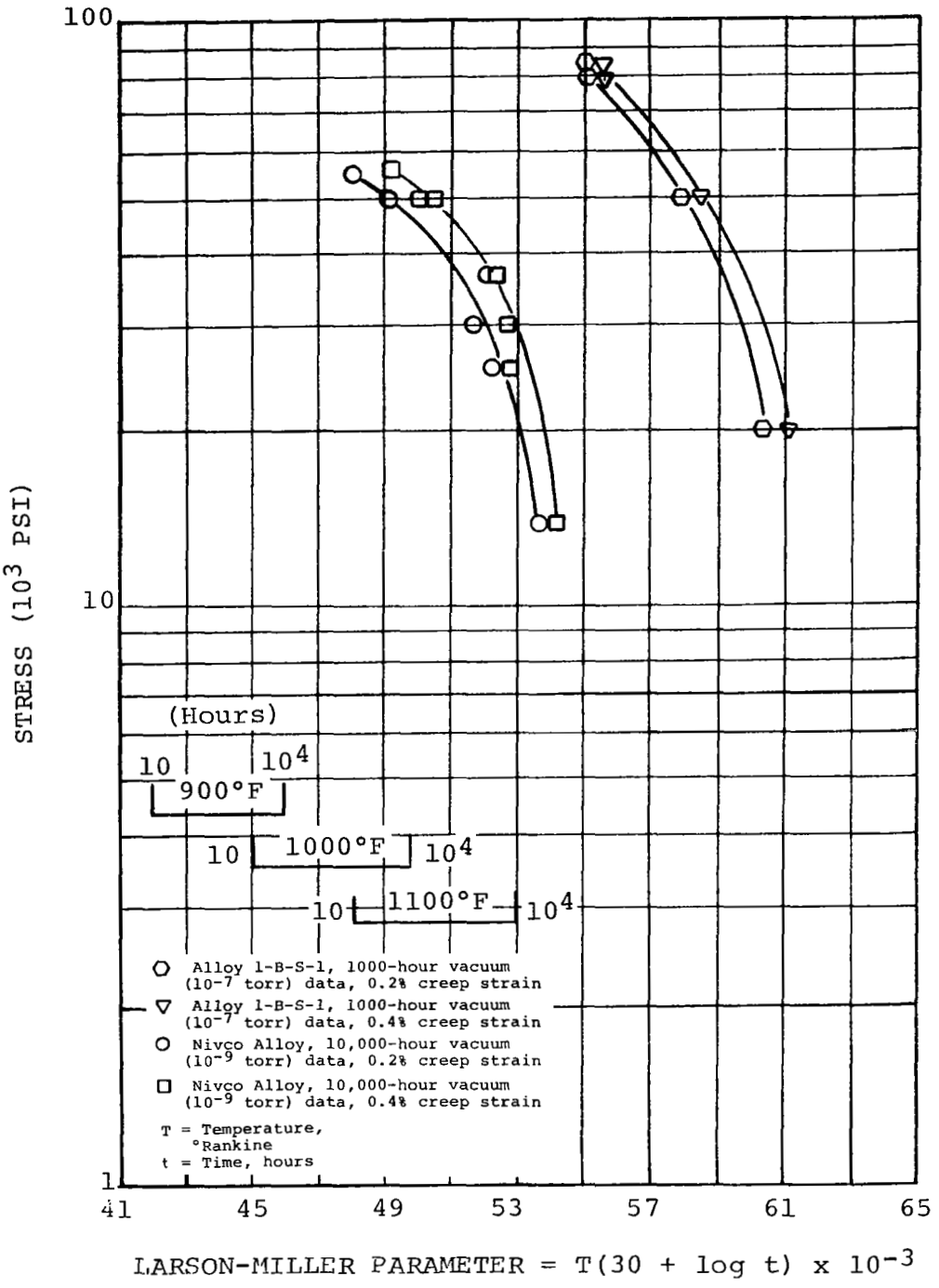

FIGURE II-34. Larson-Miller Plot of Experimental Alloy 1-B-S-1 Based on 1000-Hour Tests in Vacuum, Compared to Nivco Alloy

D. CONCLUSIONS AND RECOMMENDATIONS

1. Conclusions

a) Two precipitation hardened magnetic alloys appear applicable to rotating electrical apparatus operating in the 1000° to 1200°F range. One experimental martensitic type alloy and one cobalt-base alloy surpassed the magnetic and mechanical properties of their counterpart commercially available alloys, particularly in the 1000° to 1200°F temperature range.

b) The greatest improvement exhibited by the precipitation hardened magnetic alloys developed on this program over present candidate alloys is in thermal stability. The reversion to austenite (nonmagnetic) in the experimental martensitic alloys begins about 150°F higher than in 15 percent nickel maraging steel.

In the cobalt-base alloy no discontinuous precipitate formed after 100 hours isothermal aging or after 1000 hours creep testing at 1200°F. This is at least partially responsible for the superior creep resistance shown by the cobalt-base alloy. The total creep strain measured on the experimental alloy 1-B-S-1 was one-third that of Nivco alloy tested under similar conditions.

2. Recommendations

a) Although the ferritic type alloy exhibited excellent magnetic properties and high temperature strength, it proved to have low room temperature ductility. Modifications should be made by the minor additions of molybdenum, chromium or other elements to improve the ductility. At the same time creep strength should be optimized by minor alloy modification.

b) The creep strength of the cobalt-base alloys could be optimized by minor changes in alloy chemistry.

c) Both alloys should be made in larger ingot sizes using production techniques. These alloys could be worked to a greater degree, and combined with different annealing procedures, would yield a more homogeneous, higher strength magnetic alloy.

SECTION III

INVESTIGATION FOR RAISING THE ALPHA TO GAMMA TRANSFORMATION TEMPERATURE IN IRON-COBALT ALLOYS

By K. Detert

A. INTRODUCTION

Alloys having appreciable magnetic saturation at temperatures above 1652°F (900°C) can be found only in the iron-cobalt system. Figure III-1 shows the dependence of magnetic saturation on the composition in iron-cobalt alloys at room temperature and at 1652°F (refs. III-1 and III-2). The highest magnetic saturation at 1652°F (900°C) is found in the 50 weight percent iron - 50 weight percent cobalt alloy.

In the Fe-Co alloys containing between 20 and 80 weight percent cobalt, the upper temperature limit at which ferromagnetism disappears is set by the phase transformation of the ferromagnetic bcc α phase into the paramagnetic fcc γ phase; see figure III-2 (ref. III-3). Up to this temperature of phase transformation at 1778°F (970°C), iron-50 weight percent cobalt alloys have much better magnetic saturation than pure cobalt; see figure III-3.

If some means could be found to increase the phase transformation temperature in the iron-cobalt alloys containing approximately 50 weight percent Co, the material could have ferromagnetic properties superior to pure cobalt to temperatures higher than the existing limit.

The phase transformation temperature can be influenced by applying hydrostatic pressure or by minor alloying additions. The application of hydrostatic pressure increases the stability of the more densely packed γ phase, thereby reducing the temperature of phase transformation. Alloying additions appear to be the only way to obtain an increase in the transformation temperature. However, alloying additions will also influence the magnetic saturation and the Curie Temperature of the binary alloys. A detrimental effect is expected in most cases.

It was, therefore, the object of this investigation, to determine which alloying elements lead to an increase of transformation temperature and to determine the effect of those additions on the magnetic saturation of the resulting alloy.

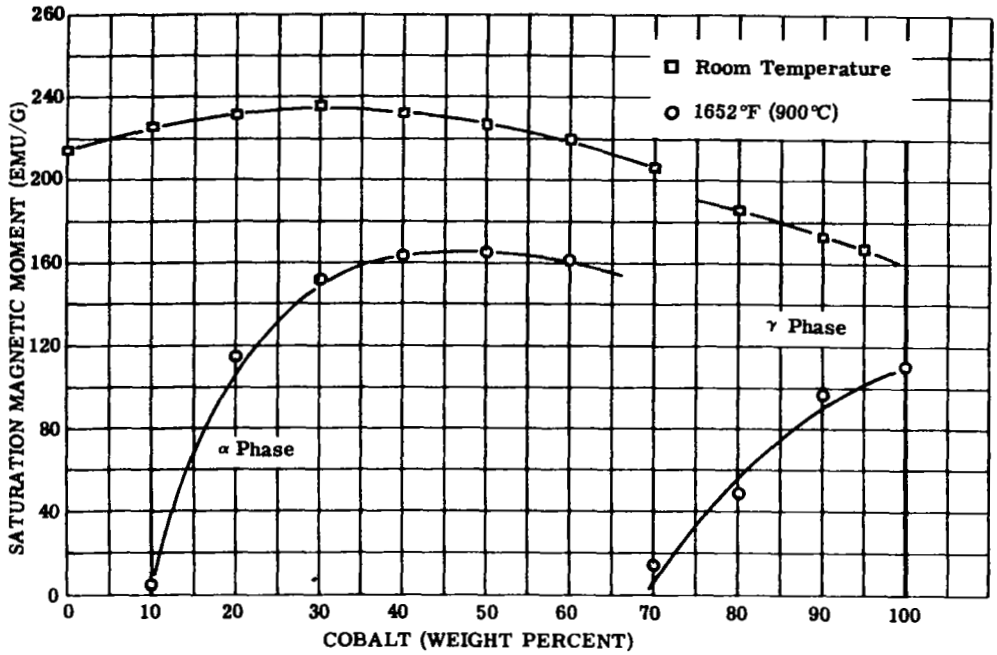

FIGURE III-1. The Influence of Cobalt Content on Saturation Magnetic Moment in Iron-Cobalt Alloys at Room Temperature and 1652°F (900°C). (References III-1 and III-2)

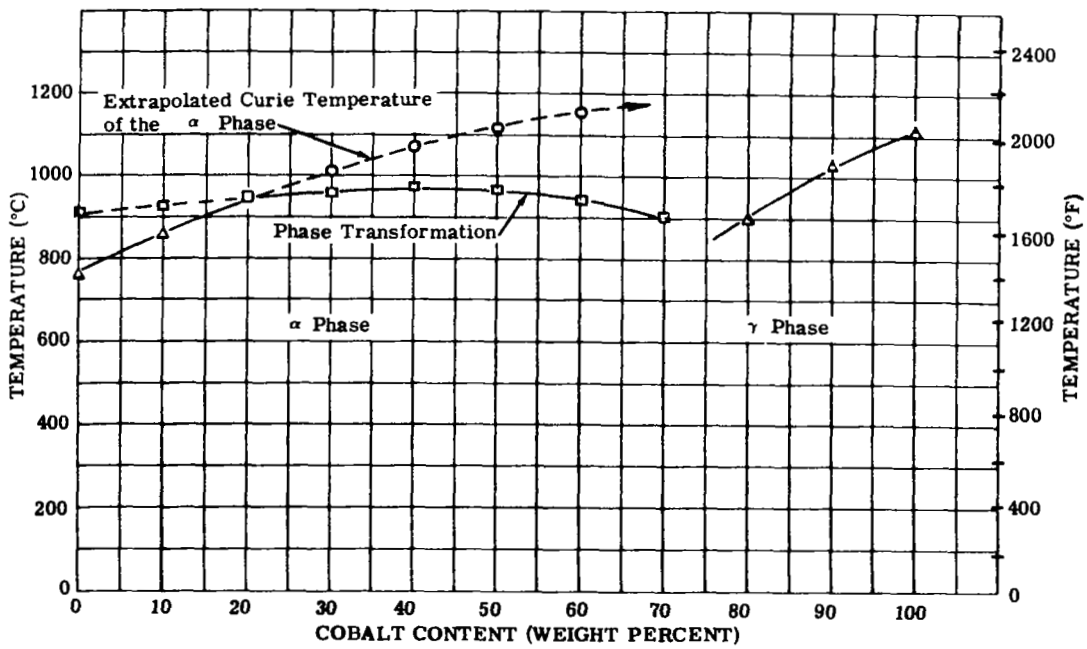

FIGURE III-2. Curie Temperature of the Iron-Cobalt Binary Alloys. (References III-3 and III-7).

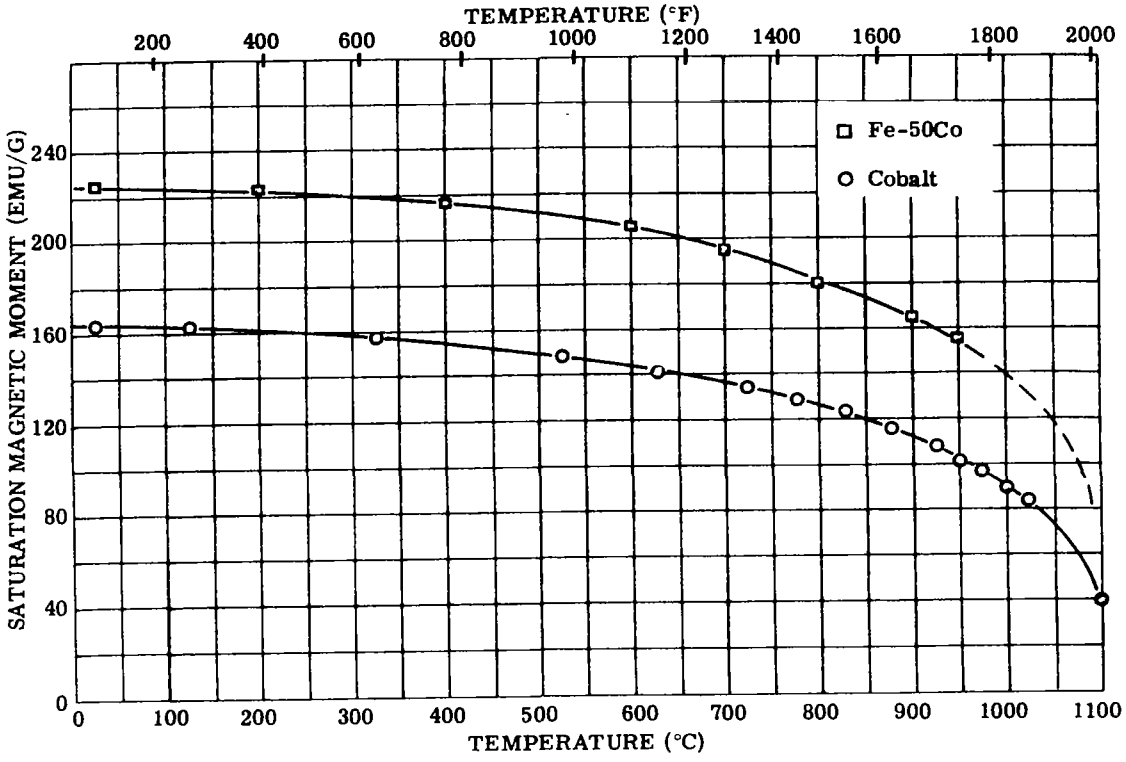

FIGURE III-3. Saturation Magnetic Moment of Cobalt and Iron-Cobalt Binary Alloys as a Function of Temperature. (Reference III-1)

B. EXPERIMENTAL PROCEDURES AND TESTING

A ratio of Fe to Co between 55:45 and 50:50 weight percent was maintained in the experimental alloys. The compositions of the alloys tested are listed in table III-1. The range of alloying additions was 0.5 to 2 weight percent. Most of the addition elements were those which are known to increase the transformation temperature of pure iron (ref. III-3). Other elements such as Mn, Cr, Au, Zn, Gd, and Dy were also included, even though they do not increase the transformation temperature of pure iron because their influence in cobalt-iron alloys could be beneficial. The electronic structure of the selected elements make them potentially useful candidates.

All of the alloys were made with high-purity, commercially available metals. The iron and cobalt used in the alloys were electrolytic grade materials which were 99.9 percent and 99.6 percent pure respectively. The latter contained 0.35 percent

TABLE III-1. Alloys for the Alpha to Gamma Transformation Study

Alloy Number	Nominal Alloy Composition (weight percent)	Alloy Composition (atomic percent)	Preparation
2-0	50Fe-50Co	51.3Fe-48.7Co	(a)
2-01	55Fe-45Co	56.3Fe-43.7Co	(a)
2-02	60Fe-40Co	61.3Fe-38.7Co	(a)
2-1	49.5Fe-49.5Co-1Al	50.3Fe-47.6Co-2.1Al	(a)
2-3	49.5Fe-49.5Co-1Be	48.2Fe-45.7Co-6.1Be	(a)
2-4	49.5Fe-49.5Co-1Ge	50.9Fe-48.3Co-0.8Ge	(a)
2-5	49.5Fe-49.5Co-1Mo	51.0Fe-48.4Co-0.6Mo	(a)
2-7	49.5Fe-49.5Co-1Sb	51.1Fe-48.4Co-0.5Sb	(a)
2-8	49.5Fe-49.5Co-1Si	50.3Fe-47.7Co-2.0Si	(a)
2-9	49.5Fe-49.5Co-1Sn	51.1Fe-48.4Co-0.5Sn	(a)
2-10	49.5Fe-49.5Co-1Ti	50.7Fe-48.1Co-1.2Ti	(a)
2-11	49.5Fe-49.5Co-1V	50.8Fe-48.1Co-1.1V	(a)
2-12	49.5Fe-49.5Co-1W	51.2Te-48.5Co-0.3W	(a)
2-13	49.75Fe-49.75Co-0.5Nb	51.2Fe-48.5Co-0.3Nb	(a)
2-14	49.75Fe-49.75Co-0.5Ta	51.2Fe-48.6Co-0.2Ta	(a)
2-15	49.5Fe-49.5Co-1Cr	50.8Fe-48.1Co-1.1Cr	(a)
2-17	49.5Fe-49.5Co-1Au[c]	51.2Fe-48.5Co-0.3Au	(a)
2-18	49.5Fe-49.5Co-1Mn	50.8Fe-48.2Co-1.0Mn	(a)
2-2m	54Fe-45Co-1As[d]	55.0Fe-44.3Co-0.7As	(b)
2-6m	53Fe-45Co-2P	53.4Fe-43.0Co-3.6P	(a)
2-16m	54.5Fe-45Co-0.5Zn[e]	54.9Fe-44.7Co-0.4Zn	(b)
2-19m	53Fe-45Co-2Dy	55.0Fe-44.3Co-0.7Dy	(a)
2-20m	53Fe-45Co-2Gd	55.0Fe-44.3Co-0.7Gd	(a)

(a) Samples were prepared by the levitation melting method described in the text.
(b) Samples were prepared by the sintering techniques described in the text; in the case of alloy 2-6m phosphorus was added in the form of a master alloy Fe-P.
(c) The gold content of the levitation-melted sample was 0.95 weight percent as determined by spectrographic analysis.
(d) One weight percent arsenic in sintered alloy 2-2m was the analyzed, retained content. The nominal composition was 2 weight percent.
(e) One-half weight percent zinc in sintered alloy 2-16m was the analyzed, retained content. The intended nominal composition was 2 weight percent.

nickel. The method of alloy preparation is indicated in table III-1. Most of the experimental alloys were prepared by levitation melting under pure (99.995%) argon at slightly less than atmospheric pressure. Melting practice was the same as that described in section II.B.1. (also see ref. III-4). Rod-shaped ingots (~25 grams) were obtained from these melts by casting into copper molds. Because of the small volume of molten material, the solidification of the ingots was similar to that obtained in chill castings; so good ingot homogeneity was achieved. The alloys containing arsenic or zinc were not prepared by melting because of their high vapor pressure. These alloys were made by sintering. After thorough mixing of the weighed metal powders, the mixture was pressed into a bar. The bar was placed in a sealed quartz tube at a pressure of 10^{-3} torr, and slowly heated in steps of 180°F from 932° to 1832°F (500° to 1000°C). The temperature was held at each step for 24 hours before proceeding to the next higher temperature. Chemical analyses were made in several cases as indicated in table III-1. The amount of addition lost during levitation melting was small; agreement between nominal and the actual amount present in the alloy was within 0.1 total weight percent. However, during sintering of samples containing the As and Zn an appreciable amount of alloy was lost as indicated in table III-1.

Samples for dilatometer measurements and saturation measurements were machined from the cast rods or sintered bars. Specimens 250 mils in diameter and one inch long were used for the dilatometer measurements. Each specimen contained a small hole for thermocouple placement. The samples were held in an argon-filled (99.99% argon) quartz tube during testing. The change in length during heating and cooling at a rate of approximately 5.4°F/min (3°C/min) was recorded as a function of temperature. The temperature measurement was accurate to $\pm$ 9°F; the sensitivity of change in length was 0.01 percent.

Magnetic saturation was measured on small cylindrical samples having a length and diameter of 0.1 inch. The samples were placed in a magnetic field gradient of 975 oersteds per centimeter at a mean applied field of 11,500 oersteds. Measurements were accurate to within 1 percent. For measuring the magnetic saturation at higher temperature, the samples were placed in a small bifilar-wound furnace placed in the gap of the magnet. During measurement, the samples were held in an argon-filled sealed quartz tube to prevent oxidation. The measured values are presented in this report as magnetic moment per gram (σ) expressed in cgs units, to obviate the measurement of density and the correction for change of density with temperature. An approximation of the induction (B) expressed in gauss may be determined from the formula

$$B = 4\pi\delta\sigma$$

where δ is the density of the alloy.

An approximate value of magnetic induction for the iron-cobalt alloys under study here may be obtained by multiplying the measured sigma values by 100.

C. RESULTS AND EVALUATION

The measured transformation temperatures of the experimental alloys are listed in table III-2 and table III-3. In some cases, duplicate tests were made and the results are listed. Table III-2 presents the data from samples which had not been annealed prior to testing. Table III-3 presents data from tests in which the samples had been heat treated for 100 hours at 1742°F (950°C) and then for 100 hours at 2012°F (1100°C). The beginning and end of transformation were defined as the temperature at which a deviation in the linear thermal expansion curve of the homogeneous phase was observed.

The arithmetic mean of these temperatures for each alloy, which is believed to be near the equilibrium temperature, is also listed in tables III-2 and III-3. However, in two cases, the shape of the thermal expansion curve indicated that the mean value did not represent the equilibrium temperature. These deviations are noted. The results show that in binary iron-cobalt alloys, the transformation temperature increased with successive determinations on one alloy sample and were considerably higher after the long annealing treatment. The results obtained on the annealed specimens are in agreement with measurements on binary alloys reported by Masumoto (ref. III-5) and by Ellis and Greiner (ref. III-6). Ellis and Greiner had annealed their samples for 100 hours at 1832°F (1000°C) before testing, while Masumoto annealed samples for 3 hours at 2012°F (1100°C) before testing. The latter treatment produced somewhat lower transformation temperatures. The values reported by these investigators and those determined on this program are shown in table III-4. It is believed that higher transformation temperatures obtained after a long annealing treatment results from improved homogeneity of the alloy.

In comparing the transformation temperature of a ternary alloy to the corresponding binary Fe-Co alloy, one notices from the data in table III-2, that alloys 2-3, 2-10, 2-12, 2-14, 2-17, 2-6m, 2-16m, 2-19m and 2-20m with Be, Ti, W, Ta, Au, P, Zn, Dy and Gd, respectively, exhibit 9° to 18°F higher transformation temperatures. However, if the results after a long annealing treatment are compared, (see table III-3), only those alloys with P, Dy and Ta indicate a rise in transformation temperature. It is interesting to note that after long anneal none of the elements cause a significant increase in transformation temperature while Si, Mo, Cr, and Mn produced a decrease of more than 38°F (20°C) in transformation temperature.

TABLE III-2. Alpha to Gamma Transformation Temperatures of Alloys as Prepared During Heating and Cooling in °C (Rate 5.4°F/min or 3°C/min)

Alloy Number	Nominal Alloy Composition (weight percent)	Transformation on Heating (°C)	Transformation on Cooling (°C)	Average Temperature (°F)	Average Temperature (°C)	Change Over 50Fe-50Co (°F)	Change Over 50Fe-50Co (°C)
2-0	50Fe-50Co	948-958	953-935	1740	949	Standard 1755	Standard 957
		960-973	964-948	1762	961		
		963-973	960-948	1762	961		
2-01	55Fe-45Co	948-953	948-940	1738	948	+5	+3
		975-980	970-963	1783	973		
2-02	60Fe-40Co	948-958	963-953	1751	955	+14	+8
		973-983	973-967	1787	975		
2-1	49.5Fe-49.5Co-1Al	958-963	950-938	1746	952	-9	-5
2-3	49.5Fe-49.5Co-1Be	973-978	965-953	1774	968	+20	+11
2-4	49.5Fe-49.5Co-1Ge	953-963	953-938	1755	957	0	0
2-5	49.5Fe-49.5Co-1Mo	925-963	933-791	1724	940[a]	-31	-17
2-7	49.5Fe-49.5Co-1Sb	955-968	953-938	1749	954	-5	-3
2-8	49.5Fe-49.5Co-1Si	948-958	938-928	1729	943	-25	-14
2-9	49.5Fe-49.5Co-1Sn	963-970	948-958	1762	961	+7	+4
2-10	49.5Fe-49.5Co-1Ti	968-980	965-950	1773	967	+18	+10
		963-974	964-955	1767	964	+13	+7
		963-970	958-943	1760	960	+5	+3
2-11	49.5Fe-49.5Co-1V	953-973	948-925	1742	950	-13	-7
2-12	49.5Fe-49.5Co-1W	965-980	958-938	1760	960	+5	+3
		960-975	948-932	1751	955	-4	-2
		971-987	967-945	1773	967	+18	+10
2-13	49.75Fe-49.75Co-0.5Nb	965-975	958-935	1756	958	+2	+1
2-14	49.75Fe-49.75Co-0.5Ta	963-970	960-953	1764	962	+9	+5
		965-970	960-945	1762	961	+7	+4
		969-982	969-961	1778	970	+22	+13
2-15	49.5Fe-49.5Co-1Cr	913-970	898-842	1670	920[b]	-67	-37
2-17	49.5Fe-49.5Co-1Au	963-975	963-945	1764	962	+9	+5
		963-978	953-938	1751	955	-4	-2
		965-978	958-943	1762	961	+7	+4
		969-982	969-954	1776	969	+20	+12
2-18	49.5Fe-49.5Co-1Mn	943-970	938-912	1724	940	-31	-17
2-2m	54Fe-45Co-1As	965-977	973-965	1778	970	+14	+8 [c]
2-6m	53Fe-45Co-2P	984-997	984-978	1807	986	+44	+24[c]
2-16m	54.5Fe-45Co-0.5Zn	978-992	992-980	1807	986	+44	+24[c]
2-19m	53Fe-45Co-2Dy	982-989	982-972	1798	981	+34	+19[c]
2-20m	53Fe-45Co-2Gd	977-987	982-972	1796	980	+32	+18[c]

(a) The actual mean value was 903°C; the 940°C value is nearer to the equilibrium temperature as indicated by the expansion curve.

(b) The actual mean value was 906°C; the 920°C value is nearer to the equilibrium temperature as indicated by the expansion curve.

(c) Change over 55Fe-45Co Composition

TABLE III-3. Alpha to Gamma Transformation Temperature of Alloys After Special Heat Treatment(a)

Alloy Number	Nominal Alloy Composition (weight percent)	Transformation on Heating (°C)	Transformation on Cooling (°C)	Average Temperature (°F)	Average Temperature (°C)
2-0	50Fe-50Co	977-987	975-964	1789	976
2-01	55Fe-45Co	982-989	979-972	1798	981
2-02	60Fe-40Co	982-988	979-961	1792	978
2-6m	53Fe-45Co-2P	987-1000	984-971	1807	986
2-19m	53Fe-45Co-2Dy	984-995	982-969	1801	983
2-3	49.5Fe-49.5Co-1Be	977-987	977-962	1789	976
2-16	49.5Fe-49.5Co-1Ti	977-987	974-962	1787	975
2-14	49.75Fe-49.75Co-0.5Ta	979-987	979-969	1794	979
2-17	49.5Fe-49.5Co-1Au	982-987	974-964	1791	977

(a) Samples were heat treated for 100 hours at 1742°F (950°C); then 100 hours at 2012°F (1100°C) before testing.

Table III-5 presents the measured magnetic saturation values for each alloy at room temperature, 1112°F (600°C) and 1202°F (650°C). The magnetic saturation intensity was lower in all of the ternary alloys studied than in the corresponding Fe-Co alloys. The elements Au, Mn, and Ta have the least influence at room temperature on a weight percent basis. At 1652°F (900°C) Ta and Ti have the least influence based on weight percent.

The influence of the addition elements on magnetic saturation based on atomic percent (derived from the nominal compositions) is shown in table III-6. It is evident that the depressing influence of Mn is very small, yet Al, Si, and Be also exhibit only a slight influence on the magnetic saturation intensity at room temperature. The depressing influence of Sb, Sn, Nb, Dy, and Gd are large; while As and Zn have the greatest effect.

TABLE III-4. Alpha to Gamma Transformation Temperature of Iron-Cobalt Alloys Determined in this Program Compared to Values from the Literature

Alloy Composition (weight percent)	Transformation Temperature (°C)			
	From Masumoto[a]	From Ellis and Greiner[b]	Value Determined on the Program	
			As Prepared No Anneal	After Long Anneal[c]
50Fe-50Co	961	979	962	976
55Fe-45Co	970	---	973	981
60Fe-40Co	968	986	975	978

(a) Reference III-5; Samples Annealed 3 hours at 1100°C Before Testing.

(b) Reference III-6; Samples Annealed for 100 hours at 1000°C Before Testing.

(c) Samples Annealed for 100 hours at 950°C; then 100 hours at 1100°C Before Testing.

At 1652°F (900°C) the effect of Al, Be, and Ti were small, yet, larger than at room temperature. Dy, Cr, Sn and Mo exhibited a large influence and the effect of W, Au, As, and Zr were the greatest. If the influence of the added elements had been such that the magnetic saturation was reduced the same fraction at all temperatures, it may have been concluded that the paramagnetic moment had been changed. However, in all of the alloys studied, the influence of the added elements increased with higher temperatures; therefore, one can conclude that the strength of the ferromagnetic coupling had been reduced. One might attempt to explain these effects in terms of the associated change and perturbation of the electronic structure of the crystal; however, one must consider that the derived values for the influence of one atomic percent of the addition element may be in error because the atomic compositions were based in most cases on the nominal compositions of the levitation-melted alloys. Furthermore, micrographic analyses of the alloys are required to verify the similarity in structure of the homogeneous phase containing the various added elements in solid solution.

TABLE III-5. Saturation Magnetic Moment of the Iron Cobalt Alloys Investigated in the Alpha to Gamma Transformation

Alloy Number	Nominal Alloy Composition (weight percent	Saturation Magnetic Moment (emu/g)[a]				
		Room Temperature	1112°F (600°C)	Percent Change Relative to Room Temperature Value	1652°F (900°C)	Percent Change Relative to Room Temperature Value
2-0	50Fe-50Co	230	214	-7.6	173	-24.9
2-01	55Fe-45Co	233	215	-7.6	169	-27.5
		233	-	-	-	-
2-02	60Fe-40Co	235	214	-8.8	167	-29.0
		236	-	-	-	-
2-1	49.5Fe-49.5Co-1Al	224	207	-7.7	163	-27.4
2-3	49.5Fe-49.5Co-1Be	218	197	-9.7	150	-31.3
2-4	49.5Fe-49.5Co-1Ge	226	207	-8.4	164	-27.7
2-5	49.5Fe-49.5Co-1Mo	225	208	-7.5	162	-27.9
2-7	49.5Fe-49.5Co-1Sb	225	210	-6.7	165	-26.8
2-8	49.5Fe-49.5Co-1Si	226	208	-8.1	159	-29.8
2-9	49.5Fe-49.5Co-1Sn	225	209	-7.4	164	-27.4
2-10	49.5Fe-49.5Co-1Ti	225	210	-6.7	167	-25.9
2-11	49.5Fe-49.5Co-1V	225	209	-6.9	165	-26.5
2-12	49.5Fe-49.5Co-1W	226	209	-7.1	166	-26.4
2-13	49.75Fe-49.75Co-0.5Nb	227	211	-6.9	168	-26.2
2-14	49.75Fe-49.75Co-0.5Ta	229	213	-6.8	170	-25.7
2-15	49.5Fe-49.5Co-1Cr	225	208	-7.6	155	-31.1
2-17	49.5Fe-49.5Co-1Au	229	211	-7.8	166	-27.4
2-18	49.5Fe-49.5Co-1Mn	229	211	-7.9	165	-28.3
2-2m	54Fe-45Co-1As	219	200	-8.7	150	-30.6
2-6m	53Fe-45Co-2P	214	190	-11.3	142	-33.2
2-16m	54.5Fe-45Co-0.5Zn	225	206	-8.4	160	-29.0
2-19m	53Fe-45Co-2Dy	225	206	-8.4	157	-30.2
2-20m	53Fe-45Co-2Gd	225	207	-8.0	157	-30.2

(a) To convert saturation magnetic moment to the approximate induction in gauss, multiply the listed value by 100.

TABLE III-6. The Influence of Alloying Elements on the Saturation Magnetic Moment of Iron-Cobalt Alloys Based on Atomic Percent Addition

Alloy Number	Alloy Composition (atomic percent)		Room Temperature		1112°F (600°C)		1652°F (900°C)	
	Base Composition	Addition Element	Change in Saturation Magnetic Moment ($\Delta\sigma$) (percent)	$\frac{\Delta\sigma}{1\ At\ \%}$ (a)	Change in Saturation Magnetic Moment ($\Delta\sigma$) (percent)	$\frac{\Delta\sigma}{1\ At\ \%}$ (a)	Change in Saturation Magnetic Moment ($\Delta\sigma$) (percent)	$\frac{\Delta\sigma}{1\ At\ \%}$ (a)
2-0	51.3Fe-48.7Co		Base value 230 emu/g		Base value 214 emu/g		Base value 173 emu/g	
2-1	50.3Fe-47.6Co	2.1Al	-6	-2.9	-7	-3.3	-9	-4.3
2-3	48.2Fe-45.7Co	6.1Be	-12	-2.0	-17	-2.8	-22	-3.6
2-4	50.9Fe-48.3Co	0.8Ge	-4	-5.0	-13	-16	-8	-10
2-5	51.0Fe-48.4Co	0.6Mo	-5	-8.3	-6	-10	-10	-17
2-7	51.1Fe-48.4Co	0.5Sb	-5	-10	-4	-8	-7	-14
2-8	50.3Fe-47.7Co	2.0Si	-4	-2.0	-6	-3.0	-13	-6.5
2-9	51.1Fe-48.4Co	0.5Sn	-5	-10	-5	-10	-8	-16
2-10	50.7Fe-48.1Co	1.2Ti	-5	-4.2	-4	-3.3	-5	-4.2
2-11	50.8Fe-48.1Co	1.1V	-5	-4.5	-5	-4.5	-7	-5.9
2-12	51.2Fe-48.5Co	0.3W	-4	-13	-5	-17	-6	-20
2-13	51.2Fe-48.5Co	0.3Nb	-3	-10	-3	-10	-4	-13
2-14	51.2Fe-48.6Co	0.2Ta	-1	-5	-1	-5	-2	-10
2-15	50.8Fe-48.1Co	1.1Cr	-5	-4.5	-6	-5.5	-17	-15.5
2-17	51.2Fe-48.5Co	0.3Au	-1	-0.3	-3	-10	-6	-20
2-18	50.8Fe-48.2Co	1.0Mn	-1	-1	-3	-3	-7	-7
2-2m	55.0Fe-44.3Co	0.7As	-14	-20	-15	-21	-19	-27
2-6m	53.4Fe-43.0Co	3.6P	-17	-4.7	-25	-7	-27	-7.5
2-16m	54.9Fe-44.7Co	0.4Zn	-8	-20	-9	-22	-9	-22
2-19m	55.0Fe-44.3Co	0.7Dy	-8	-11	-9	-13	-12	-17
2-20m	55.0Fe-44.3Co	0.7Gd	-8	-11	-8	-11	-10	-14

(a) $\frac{\Delta\sigma}{1\ At\ \%}$ is the change in saturation from the 50Fe-50Co base per unit atomic percent of the addition elements.

D. CONCLUSIONS

A few addition elements including phosphorus, dysprosium and tantalum produced a slight increase in transformation temperature compared to the binary iron-cobalt alloys.

Other elements such as silicon, molybdenum, chromium, and manganese produced a decrease in transformation temperature of more than 38°F.

The magnetic saturation of iron-cobalt alloys was reduced by all of the elements tested. Addition of manganese resulted in the smallest decrease in saturation at room temperature. At 1652°F (900°C) titanium showed a slight depressing effect on magnetic saturation.

SECTION IV

DISPERSION-STRENGTHENED MAGNETIC MATERIALS FOR APPLICATION IN THE 1200° TO 1600° F RANGE

By R. J. Towner

A. INTRODUCTION

The purpose of this project was to develop a dispersion-strengthened, magnetically soft material for use in the 1200° to 1600° F temperature range for rotor applications. As a tentative goal, the material should have the following properties at some temperature between 1200° and 1600° F, preferably at 1600° F.

Saturation magnetization, B_S - 12,000 gauss minimum

Coercive force, H_C - 25 oersteds maximum

Creep strain in 10,000 hours at 10,000 psi - 0.4 percent maximum.

In pursuit of this goal, dispersion-strengthened cobalt-base and iron+27 w/o cobalt-base extrusions were made from (1) prealloyed atomized powders containing boride compound and zirconium oxide particles, (2) internally oxidized powders containing alumina or beryllia, and (3) composite powders containing both a metal phase and a refractory oxide phase (alumina or thoria) within each powder particle. Also, dispersion-strengthened cobalt-base extrusions containing thoria were purchased from two suppliers. Cobalt and iron+27 w/o cobalt were selected for base compositions because they have higher values of saturation magnetization in the 1200° to 1600° F range.

The initial evaluation phase (phase 1) of this project included determination of saturation magnetization, coercive force, and tensile properties of extrusions at room temperature and in the 1200° to 1600° F range. It was expected that the dispersoid parameters (dispersoid type and composition, volume percent, particle size, and interparticle spacing) would have important effects on the coercive force and other soft-magnetic properties, as well as on mechanical properties. The dispersoid parameters were expected to exert strong effects on the matrix grain structure, response to secondary working treatments applied later to the hot-extruded material, and thermal stability of the dispersoid and matrix structure. Coercive force was measured because it was an important magnetic property in itself, and it could also be used as an indicator for other structure-sensitive, soft-magnetic properties. Permeability, for example, is inversely related to coercive force. The various theories of coercive

force were not in agreement and did not permit precise calculations or even reliable estimates to be made for values in the 1200° to 1600° F range. Therefore, it was necessary to employ an empirical, screening-type of approach in the initial evaluation phase of this program. Wide variations in dispersoid parameters were necessarily employed. Measurements were made on hot-worked (hot-extruded) products in order to separate and identify the effect of these variations in dispersoid parameters in the cobalt and iron+27 w/o cobalt matrices.

The intermediate evaluation (phase 2) of the program was directed towards exploiting and extending the best compositional systems developed in the first phase in regard to magnetic and mechanical properties. The dispersoids of relatively fine particle size were further investigated since it was determined in phase 1 that they did not increase coercive force prohibitively. The amount of dispersoid was held to a relatively low level in order to minimize the dilution effect on saturation magnetization and insure better ductility and lower notch sensitivity. Also, the possibility existed of reducing clustering and achieving a more uniform dispersion at the lower concentration levels which might maintain or even increase strength levels. Secondary working was initiated in order to identify those compositional systems and types of powder which showed the greatest response (improvement in tensile properties). Creep testing on selected compositions in the as-extruded and secondary worked conditions was performed.

The final evaluation (phase 3) of the program dealt with the production and investigation for thermal stability of a fibrous grain structure in selected cobalt-base and iron+27 w/o cobalt-base dispersion-strengthened compositions. Included were compositions which had relatively fine particles sizes of dispersoid as well as those containing coarser particles which would provide still lower values of coercive force in the 1200° to 1600° F range. A calibration study of the effect of cycles of secondary working and proof testing of the thermal stability of the matrix grain structure were undertaken. Creep and tensile tests were performed on the more stable compositions in the secondary-worked condition.

Conclusions were drawn and recommendations made concerning the processing and secondary working of iron+27 w/o cobalt-base and cobalt-base compositions which would meet the goals of the program and were applicable to the fabrication of solid rotor material having a product size of 8 to 28 inches diameter and 8 to 28 inches long.

B. MATERIALS

1. Powder Types and Compositions

Various powder types and compositions were selected for investigation. The powder composition numbers used for iden-

tification purposes in this report are the same as used for preliminary discussions and requests for quotation from suppliers.

a. PREALLOYED ATOMIZED POWDERS

The atomizing process provides an extremely rapid quench of molten particles to the solid state (ref. IV-1 - IV-4). This tends to insure that the constituent particles of high-melting point, which solidify first, will be uniformly dispersed within each particle and not have time to grow much above submicron size before the cobalt or iron+27 w/o cobalt matrix has solidified.

Sixteen prealloyed atomized powders which were obtained for extrusion on this program are listed in table IV-1. Powder Nos. 3 through 9 and 12 through 18 were obtained for the initial evaluation effort (phase 1) of the program. The boron additions in powder Nos. 3 through 6 and 12 through 15 were for the purpose of formation of dispersed boride particles containing titanium, zirconium, columbium, or tantalum. Boron was held at the 1 w/o level and the ratio of 2 a/o boron to 1 a/o titanium, zirconium, columbium or tantalum was maintained. Powder Nos. 7 and 16 contained cerium and provided another possible dispersion-hardening agent, the intermetallic compound $CeCo_5$. The aluminum and beryllium containing Powders Nos. 8, 9, 17, and 18 were later given internal oxidation treatments to form Al_2O_3 and BeO dispersed particles.

Powder No. 19 was obtained for the intermediate evaluation portion (phase 2) of the program to investigate ZrO_2 dispersoid. The final evaluation phase (phase 3) included in the boride-containing compositions No. 30 which was similar to No. 5 but with less dispersoid.

The -325 mesh and +325 mesh fractions of each powder were delivered to Westinghouse air-packed in plastic bags inside separate, sealed metal cans. The weights of atomized powders produced by the two suppliers and shipped to Westinghouse are given in table IV-1. Also, the supplier's lot or batch number is listed. The suppliers sufficiently defined and recorded the details of their process so that they could reproduce the production of their products at a later date, if desired. The requirements that at least 10 pounds of -325 mesh powder of each alloy be provided, was met. The powders which were ordered through Domtar Chemicals Ltd. were made by B.S.A. Metal Powders Ltd., Birmingham,

TABLE IV-1. Prealloyed Atomized Powder Compositions, Suppliers, and Weights Received

Atomized Powder No.	Nominal Composition (weight percent)	Weight of Powder Received				Supplier	Supplier's Lot No.
		-325 Mesh		+325 Mesh			
		(pounds)[a]	(weight percent of total lot)	(pounds)[a]	(weight percent of total lot)		
3	Co+1.0B+2.2Ti	24	41	34	59	Hoeganaes[c]	AN-1858
4	Co+1.0B+4.2Zr	44	52	40	48	Hoeganaes	AN-1859
5	Co+1.0B+4.2Cb	10	14	63	86	Hoeganaes	AN-1856
6	Co+1.0B+8.3Ta	22	24	70	76	Hoeganaes	AN-1857
7	Co+4.0Ce	31	39	49	61	Domtar[d]	HN-182
8	Co+2.5Al	31	36	55	64	Hoeganaes	AN-1811
9	Co+1.3Be	21	25	63	75	Domtar	HN-181
12	70.7Fe+26.1Co+1.0B+2.2Ti	28	33	58	67	Hoeganaes	AN-1810
13	69.2Fe+25.6Co+1.0B+4.2Zr	42	48	46	52	Hoeganaes	AN-1809
14	69.2Fe+25.6Co+1.0B+4.2Cb	11	24	34	76	Hoeganaes	AN-1807
15	66.2Fe+24.5Co+1.0B+8.3Ta	13	15	73	85	Hoeganaes	AN-1808
16[b]	70.1Fe+25.9Co+4.0Ce	4	17	20	83	Domtar	HN-183[b]
16[b]	70.1Fe+25.9Co+4.0Ce	16	28	42	72	Domtar	HN-185[b]
17	71.0Fe+26.3Co+2.7Al	26	46	31	54	Hoeganaes	AN-1812
18	72.0Fe+26.6Co+1.4Be	23	27	62	73	Domtar	HN-184
19	66.9Fe+24.8Co+8.3Zr	34	43	45	57	Hoeganaes	92-3130
30	Co+0.8B+3.2Cb	23	24	73	76	Hoeganaes	92-3828

(a) Yield from 100 pound melts.
(b) Two atomizing runs, HN-183 and HN-185. Metal froze in nozzle and plugged it during first run because metal temperature was too low. Cerium added and metal temperature raised for second run.
(c) Hoeganaes Sponge Iron Corp., Riverton, N. J.
(d) Domtar Chemicals Ltd., Metal Powders Division, Montreal, Canada.

England. The greatest yield of -325 mesh powder was obtained with alloy Nos. 4, 13, and 19, all of which contain zirconium.

The chemical analyses of the -325 mesh fractions of the 16 atomized powders were reported by the powder suppliers and are listed in tables IV-2 and IV-3. Also listed for comparison are the intended compositions and the target compositions for the various elements which the suppliers worked towards.

The following general trends were observed in regard to meeting the target chemical composition specifications which the suppliers worked towards for prealloyed atomized powders in table IV-2.

(1) Cobalt-Base Alloys

(a) Hoeganaes Powders

TABLE IV-2. - Chemical Analyses[a] of Prealloyed Atomized Powder

	Mn	Si	C	S	P	Ni	Cr
Westinghouse Compositional Targets	0.04 max.	0.04 max.	0.020 max.	0.006 max.	0.010 max.	0.70 max.	—
Powder No.							
3. Intended							
Actual	0.24	0.23	0.035	0.005	<0.005	0.32	0.012
4. Intended							
Actual	0.26	0.10	0.044	0.005	<0.005	0.26	<0.01
5. Intended							
Actual	0.19	0.04	0.043	0.007	<0.005	0.58	0.02
6. Intended							
Actual	0.17	0.38	0.069	0.005	<0.005	0.58	0.016
7. Intended							
Actual	<0.1	0.07	0.033	<0.002	<0.005	0.36	<0.1
8. Intended							
Actual	0.22	0.27	0.009	0.004	<0.005	0.29	0.022
9. Intended							
Actual	<0.05	0.012	0.028	<0.002	0.01	0.48	0.07
Westinghouse Compositional Targets	0.50 max.	0.25 max.	0.020 max.	0.025 max.	0.015 max.	0.70 max.	—
Powder No.							
12. Intended							
Actual	0.14	0.08	0.024	0.013	<0.005	0.14	0.050
13. Intended							
Actual	0.11	0.22	0.023	0.011	<0.005	0.12	0.064
14. Intended							
Actual	0.14	0.14	0.038	0.013	<0.005	0.16	0.038
15. Intended							
Actual	0.08	0.09	0.084	0.010	<0.005	0.16	0.030
16. Intended							
Actual [c]	<0.1	0.017	0.034	<0.002	0.011	<0.05	<0.1
Actual [d]	<0.1	0.16	0.032	<0.002	0.014	<0.05	<0.1
17. Intended							
Actual	0.43	0.26	0.010	0.010	<0.005	0.10	0.016
18. Intended							
Actual	<0.1	0.08	0.026	<0.002	<0.005	<0.05	<0.1

(a) Reported by the powder supplier
(b) Hoeganaes Sponge Iron Corporation agreed to a tolerance of ± 0.8% for B and Ti.
(c) Domtar Chemicals Ltd., Lot No. HN-183
(d) Domtar Chemicals Ltd., Lot No. HN-185

(Minus 325 Mesh Fraction) Obtained for Initial Evaluation Effort (Phase I)

Element (percent by weight)									
Co	Fe	B	Ti	Zr	Cb	Ta	Ce	Al	Be
—	—	±0.2 (b)	±0.4 (b)	±0.8	±0.8	±1.6	±0.8	±0.5	±0.3
96.8		1.0	2.2						
95.34	0.25	1.3	1.60						
94.8		1.0		4.2					
93.43	0.62	1.3		3.43					
94.8		1.0			4.2				
93.11	0.21	1.1			4.38				
90.7		1.0				8.3			
90.01	0.14	1.2				7.66			
96.0							4.0		
96.9	(e)						2.27		
97.5								2.5	
95.59	0.97							2.46	
98.7									1.3
97.7	(e)								1.94
±1.50	±2.0	±0.2 (b)	±0.4 (b)	±0.8	±0.8	±1.6	±0.8	±0.5	±0.3
26.1	70.7	1.0	2.2						
26.48	71.29	0.9	1.83						
25.6	69.2	1.0		4.2					
24.75	69.73	1.1		3.24					
25.6	69.2	1.0			4.2				
25.82	68.90	0.9			4.07				
24.5	66.2	1.0				8.3			
24.13	67.16	1.0				6.95			
25.9	70.1						4.0		
29.5	67.3						2.61		
29.8	68.4						0.7		
26.3	71.0							2.7	
26.47	69.69							2.33	
26.6	72.0								1.4
27.9	70.0								1.4

(e) Not detected.

TABLE IV-3. Chemical Analyses of Prealloyed Atomized Powders (Minus 325 Mesh Fraction) Obtained for Intermediate and Final Evaluation Efforts (Phases 2 and 3)

Final Westinghouse Compositional Targets	Element (percent by weight)											
	Mn 0.50 max.	Si 0.25 max.	C 0.020 max.	S 0.025 max.	P 0.015 max.	Ni 0.70 max.	Cr -	Co ±1.50	Fe ±2.0	B -	Zr ±0.8	Cb -
Powder No.												
19. Intended								24.8	66.9		8.3	
Actual[a]	0.23	0.033	0.018	0.021	<0.005	0.0	-	23.68	66.97	-	7.29	-
Final Westinghouse Compositional Targets	0.20 max.	0.10 max.	0.050 max.	0.006 max.	0.010 max.	0.70 max.	0.10 max.	-	-	±0.2	-	±0.4
Powder No.												
30. Intended								96.0		0.8		3.2
Actual[b]	0.09	0.07	0.018	0.003	<0.001	0.05	0.003	-	0.84	0.73	-	3.20

(a) Reported by the powder supplier.
(b) Determined by Westinghouse.

The impurities Mn, Si, and C tended to be slightly higher than the target specifications, while, S, P, and Ni tended to be within the specifications. The Co and alloying element contents were within the specifications.

(b) Domtar Powders

The impurities Mn, Si, and C tended to be slightly high, while S, P, and Ni were within the specifications. In regard to alloying elements, Ce was lower and Be slightly higher than desired.

(2) Iron+27 w/o Cobalt-Base Alloys

(a) Hoeganaes Powders

Concerning the impurities, C tended to be high while Mn, Si, S, P, and Ni were within the specifications. The Co, Fe, and alloying element contents were within the specifications.

(b) Domtar Powders

The C contents were higher than the specifications, while Mn, Si, S, P, and Ni impurities were within the specifications. The Ce alloy content was low, while Be was as intended.

In addition, the following specific comments are made in regard to chemical analyses. The manganese and silicon contents of atomized powders Nos. 3, 4, 6, and 17 were higher than average. It was necessary for Hoeganaes Sponge Iron Corporation to add intentionally manganese and silicon, usually in amounts of approximately 0.25 percent each, in order to increase fluidity and achieve proper flow of the molten metal through the atomizing nozzle. Of all the alloying elements, cerium was the most difficult to retain in the powder in the intended amount. The greatest difficulty was encountered during the atomizing of powder No. 16. The molten alloy froze in the atomizing nozzle because the metal temperature was too low during the first run (Domtar Lot No. HN-183), and atomizing ceased after only 21 pounds of powder had been produced. The remainder of the charge was

remelted, more cerium added in an attempt to compensate for melt loss, and atomization proceeded for the second time (Domtar Lot No. HN-185). However, the cerium losses in both runs of powder No. 16 were higher than anticipated and the actual cerium contents were 2.61 and 0.7 percent, respectively, compared with 4.0 percent intended.

All of the 16 prealloyed atomized powders in tables IV-2 and IV-3 had chemical analyses close enough to the intended compositions (with the exception of Domtar Lot No. HN-185 of atomized powder No. 16) so that they could be used and processed into extrusions for this project. The impurities were sufficiently low that no detrimental effect on magnetic or mechanical properties was expected. When the target chemical composition specifications in table IV-2 were written, they were intended to serve as rigorous goals for achievement. Since these powder compositions had not been atomized before, the specifications were probably unrealistic in certain aspects. Therefore, the target limits were raised for Mn, Si, and C impurities in the cobalt-base alloy obtained later in the program, table IV-3.

The average particle diameter (APD) of the -325 mesh fraction of the atomized powders ranged from 10 to 26 microns, as determined with the Fisher Sub-Sieve Sizer, ASTM Method B330-58T. The Fisher APD values for the various powders will be presented later in this report in connection with powder compacting and sintering characteristics, table IV-10.

The particle size distribution band for the -325 fraction of the atomized powders from the two suppliers, as determined with the Coulter Counter, are presented in figure IV-1. There was relatively little variation in particle size distribution between compositions and suppliers. This is indicated by the spread in particle size from 23 to 35 microns at 50 cumulative weight percent in figure IV-1.

Microscopic examination of the particle size, shape, and microstructure was conducted on samples of the -325 mesh powders mounted in plastic, polished, and etched according to standard metallographic techniques. By this method, the cross

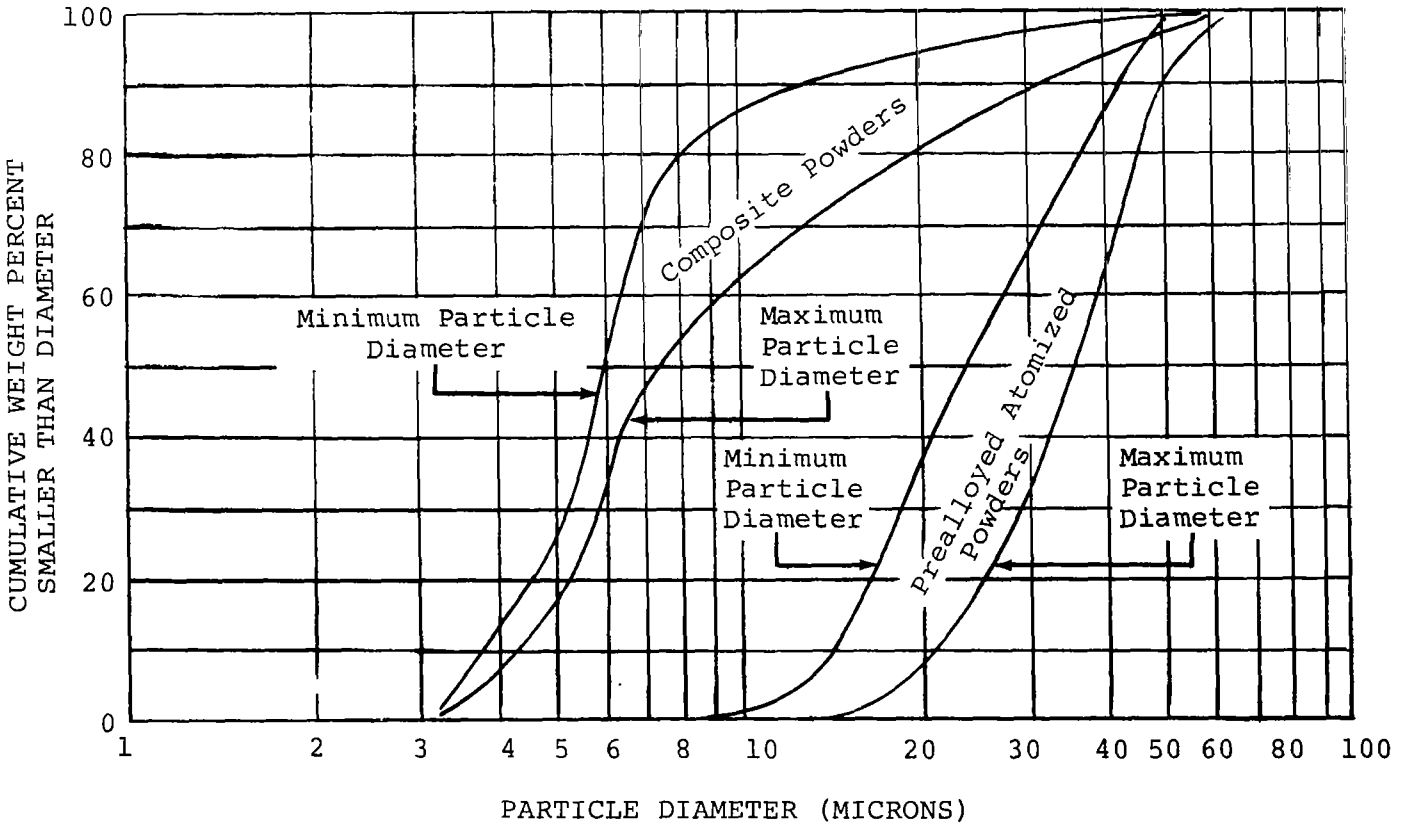

FIGURE IV-1. Particle Size Distributions of Prealloyed Atomized Powders and Composite Powders as Determined With Coulter Counter

sections of numerous powder particles were presented for viewing. The powder particle sizes seen under the microscope were in general agreement with the other particle size measurements.

The shape of the powder particles for each alloy was qualitatively described in table IV-10 as tending towards equiaxed, spherical, or irregular. The irregular shaped particles were elongated in one or more directions, while the equiaxed, had equal dimensions in three directions but were not rounded enough to be called spherical. The shape of selected powders may be seen at 1000X in figures IV-2 and IV-3. Since all powders were atomized by essentially the same process, which involved breaking up the stream of molten metal by water jets and collecting the powder in a tank filled with nitrogen, the shape of the powder particles was mainly influenced by their chemical composition. All of the powders containing boron tended to have more or less rounded shape even though they may not have reached the spherical state. Alloying additions of the strong oxide forming elements Ti, Zr, Ce, Al and Be tended to turn the particles towards an irregular shape.

The Co-base powders tended to be more spherical than the Fe +27 w/o Co-base. The microstructures of prealloyed atomized powders at 1000X magnification in figures IV-2 and IV-3 showed a fine grain structure and a fine dispersion of constituent particles.

The apparent density is the weight of powder that fills a standard volume under free-flowing conditions (without jarring) and is expressed as grams per cubic centimeter, ASTM Method B212-48, in table IV-10. The -325 mesh particles which were substantially spherical or equiaxed had the larger particle diameters and gave the higher apparent densities because of their better packing characteristics under free-flowing conditions. This can be a valuable property because a greater weight of powder can be poured into a container or die of given volume for compaction.

b. COMPOSITE POWDERS

Twelve composite powders, consisting of a refractory oxide phase distributed in a metal phase within each

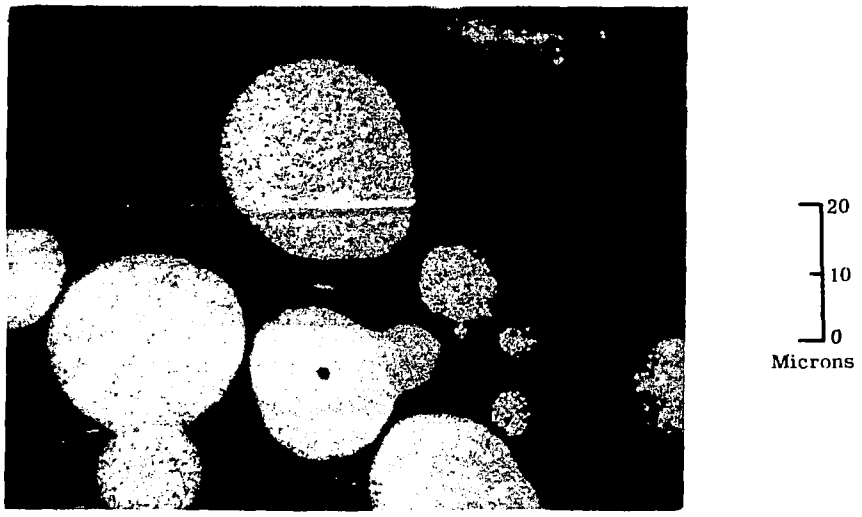

FIGURE IV-2. Atomized Powder No. 5, Co+1.0w/oB+4.2w/oCb, Showing Tendency Toward Spherical Shape and Fine Grain Structure, 1000X, Etched in Acetic-Nitric-Hydrochloric-Water (1:1:4:1 Ratio)

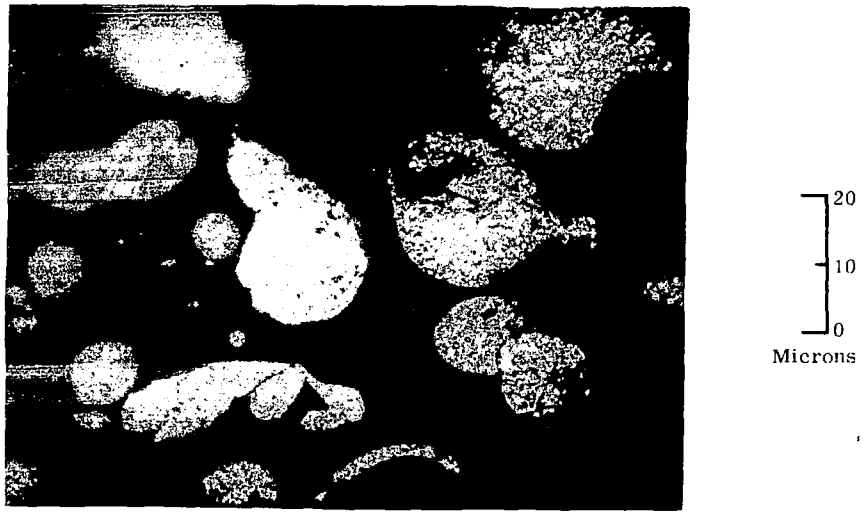

FIGURE IV-3. Atomized Powder No. 12, Fe+26.1w/oCo+1.0w/oB+2.2w/o Ti, Showing Irregular Shape and Fine Grain Structure, 1000X, Etched in Acetic-Nitric-Hydrochloric-Water (1:1:4:1 Ratio)

powder particle, were obtained according to Westinghouse specifications from the three suppliers listed in table IV-4. The Sherritt Gordon manufacturing process consisted of coating suspended oxide core particles by precipitation of metal from aqueous solution (ref. IV-5). Vitro Laboratories process was the high intensity arc covaporization of mixed oxides of iron-cobalt oxides to metal (ref. IV-6). The Chas. Pfizer proprietary semimetallic powder process was selected to provide eight compositions.

Composite powder Nos. 1, 2, 3, 4, and 11 were obtained for the initial evaluation (phase 1) of the program. Powder Nos. 13, 14, and 15 were used for the intermediate evaluation (phase 2), and the final evaluation (phase 3).

TABLE IV-4. Composite Powder Compositions, Suppliers, and Weights Received

Composite Powder No.	Nominal Composition (weight percent)	Specified Particle Size of Oxide (microns)	Amount of Oxide (volume percent)	Weight of Powder Received (pounds)	Supplier	Supplier's Lot No.
3	Co+11.2ThO_2	0.01-0.06	10.0	3.3	Sherritt Gordon[a]	951
11	64.2Fe+23.7Co+12.1ThO_2	0.01-0.06	10.0	4	Vitro Labs[b]	38, 39
1	Co+4.75Al_2O_3	0.01-0.06	10.0	5	Chas. Pfizer[c]	RX2002
2	Co+4.75Al_2O_3	0.1-0.6	10.0	5	Chas. Pfizer	RX2003
3	Co+11.2ThO_2	0.01-0.06	10.0	4	Chas. Pfizer	RX2044
4	Co+11.2ThO_2	0.1-0.6	10.0	4	Chas. Pfizer	RX2045
11	64.2Fe+23.7Co+12.1ThO_2	0.01-0.06	10.0	4	Chas. Pfizer	RX2059
13	Co+4.5ThO_2	0.01-0.06	4.0	4	Sherritt Gordon	1006
14	Co+8.4ThO_2	0.01-0.06	7.5	4	Sherritt Gordon	1007
13	Co+4.5ThO_2	0.01-0.06	4.0	4	Chas. Pfizer	RX2073-A
14	Co+8.4ThO_2	0.01-0.06	7.5	4	Chas. Pfizer	RX2073-B
15	66.2Fe+24.5Co+9.3ThO_2	0.01-0.06	7.5	4	Chas. Pfizer	RX2090

(a) Sherritt Gordon Mines Ltd., Fort Saskatchewan, Alberta, Canada
(b) Vitro Laboratories, West Orange, New Jersey
(c) Chas. Pfizer and Company, Inc., Easton, Pennsylvania

Information concerning chemical analyses of six composite powders were provided by the powder suppliers and are listed in table IV-5 and IV-6. It should be pointed out that the Westinghouse Specifications for composite powders which accompanied the Purchase Orders stated that the purity of the cobalt and thoria shall be 99.5 percent or greater, and that the supplier shall report the major impurities anticipated in the composite powder. The target limits for the various elements in tables IV-5 and IV-6 were what the supplier worked toward in his processing, and were considered to be goals rather than rigid limits for acceptance or rejection. Extrusions of four of these powders were selected for chemical analysis by Westinghouse during the course of the program.

Thorium oxide powder was supplied by Westinghouse to Sherritt Gordon and Chas. Pfizer for making their thoriated composite powders. The thorium oxide in two particle size ranges, 100 to 300 angstrom and 400 to 800 angstrom, was purchased from Thorium Limited, London, England. The impurity content is given in table IV-7.

The composite powders were delivered to Westinghouse air-packed (with the exception of composite powder No. 11 from Vitro Labs which was sealed under argon) in plastic bags inside sealed metal cans.

The average particle diameter (APD) of the composite powders, as determined with the Fisher Sub-Sieve Sizer, ranged from about 2 to 4 microns. The powder particle size of all composite powders was much smaller than that of the prealloyed atomized powders. The Fisher APD values are presented later in this report in connection with powder compacting and sintering characteristics, table IV-11.

The particle size distribution band for the Sherritt Gordon and Chas. Pfizer composite powders as determined with the Coulter Counter are presented in figure IV-1. The particle size distribution of the Vitro Labs powder No. 11 was not determined, since it was reported to be submicron in size and pyrophorric. Figure IV-1 shows that the composite powders were finer than the prealloyed atomized powders. The particle size distributions were largely independent of composition and supplier.

The powder particle size, shape, and microstructure were examined under the microscope after mounting in plastic and polishing to reveal cross-sections. Photomicrographs of two typical composite powder samples

TABLE IV-5. Chemical Analyses of Composite Powders Obtained for Initial Evaluation Effort (Phase 1)

Element	Sherritt Gordon Composite Powder No. 3 [a] (weight percent)		Vitro Labs Composite Powder No. 11 [a] (weight percent)	
	Westinghouse Specification Target Limits	Analysis [b]	Westinghouse Specification Target Limits	Analysis
Mn	0.04 max.	0.001	0.50 max.	0.3 [c]
Si	0.04 max.	0.01	0.25 max.	0.2 [c]
C	0.020 max.	0.04	0.020 max.	0.02 [c]
S	0.006 max.	0.02	0.025 max.	0.025 [c]
P	0.010 max.	Not Detected	0.015 max.	0.003 [c]
Ni	0.70 max	0.076	0.70 max.	0.6 [c]
Cr	0.10 max.	0.001	0.10 max.	0.06 [c]
Co	Remainder	88.0	22.5-25.2	23.5
Fe	--	--	62.2-66.2	63.0
ThO_2	9.7-12.7	11.8	9.7-12.7	10.8
O_2 (other than as ThO_2)	--	--	--	1.0

(a) Reported by the powder supplier.
(b) Analysis of composite powder after heating 2 hours at 1800°F in H_2 atmosphere.
(c) Not analyzed for. Estimated order of magnitude of anticipated elements.

TABLE IV-6. Chemical Analyses of Composite Powders [a] Obtained for Intermediate and Final Evaluation Efforts (Phases 2 and 3)

Element	Composite Powder No. 13			Composite Powder No. 14		
	Westinghouse Spec. Target Limits (weight percent)	Chas. Pfizer Lot No. RX2073-A Analysis (weight percent)	Sherritt Gordon Lot No. 1006 Analysis (weight percent)	Westinghouse Spec. Target Limits (weight percent)	Chas. Pfizer Lot No. RX2073-B Analysis (weight percent)	Sherritt Gordon Lot No. 1007 Analysis (weight percent)
Mn	0.04 max.	--	--	0.04 max.	--	--
Si	0.04 max.	--	--	0.04 max.	--	--
C	0.020 max.	--	0.035	0.020 max.	--	0.040
S	0.006 max.	0.010 [b]	0.032	0.006 max.	0.010 [b]	0.032
P	0.010 max.	--	--	0.010 max.	--	--
Ni	0.70 max.	0.030 [b]	0.09	0.70 max.	0.030 [b]	0.08
Cr	0.10 max.	--	--	0.10 max.	--	--
Fe	--	0.050 [b]	--	--	0.050 [b]	--
ThO_2	4.52±0.50	--	4.2	8.41±0.50	--	8.6
Co	Remainder	96.1	95.5	Remainder	91.9	91.1

(a) Reported by the powder supplier.
(b) Analysis of cobalt used in making composite powder.

TABLE IV-7. Analysis of Impurities[a] in the ThO_2 Used in Making Composite Powders

Impurity	ThO_2 for Composite Powders		
	No. 3 & 11 (100-300Å ThO_2)	No. 4 (400-800Å ThO2)	No. 13, 14, & 15 (100-300Å ThO_2)
Cerium Oxide, CeO_2	8 ppm	9 ppm	3 ppm
Other Rare Earth Oxides	14	14	5
Sodium Oxide, Na_2O	10	10	50
Calcium Oxide, CaO	80	30	250
Silica, SiO_2	<50	<50	-
Iron Oxide, Fe_2O_3	-	-	13
Heavy Metal Oxides, PbO	-	-	10

(a) Reported by Thorium Limited.

are presented in figures IV-4 and IV-5. The composite powder from Sherritt Gordon had an irregular particle shape and, judging from the fine black specks in the cobalt matrix, the thoria particles were well dispersed. The composite powders from Chas. Pfizer were equiaxed and contained numerous pores or holes which appeared as relatively large dark areas within each powder particle. The alumina particles dispersed in the cobalt matrix were not nearly as prominent. Etching was used to reveal the grain structure within the Pfizer powder particles.

The composite powders tended to have lower apparent densities than the minus 325 mesh atomized powders, tables IV-10 and IV-11.

2. Supplier Extrusions of Dispersion-Strengthened Cobalt

The two extruded compositions listed in table IV-8 were obtained for the initial evaluation phase of this program. The cobalt +10 v/o thoria composition (No. 3) from the New England Materials Laboratory (ref. IV-7) was received in the hot-extruded condition. The Metals Processing Division of Curtiss-Wright Corporation (ref. IV-8) supplied the cobalt +2 v/o thoria composition (No. 9) in two conditions: hot-extruded and 85 percent cold worked by swaging (after hot-

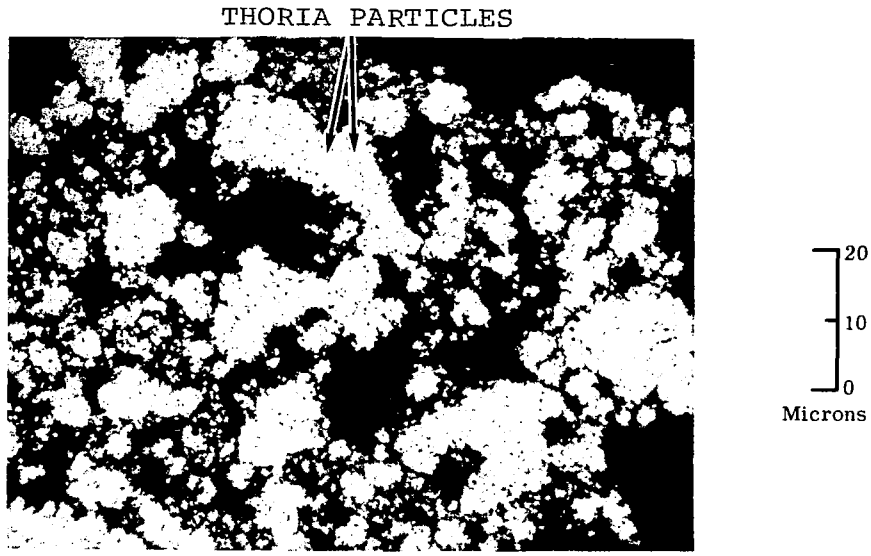

FIGURE IV-4. Composite Powder No. 3, Co+10v/oThO_2 (0.01-0.06 micron thoria), from Sherritt Gordon, Showing Irregular Particle Shape and Dispersion of Thoria Particles in Cobalt Matrix, 1000X, Unetched

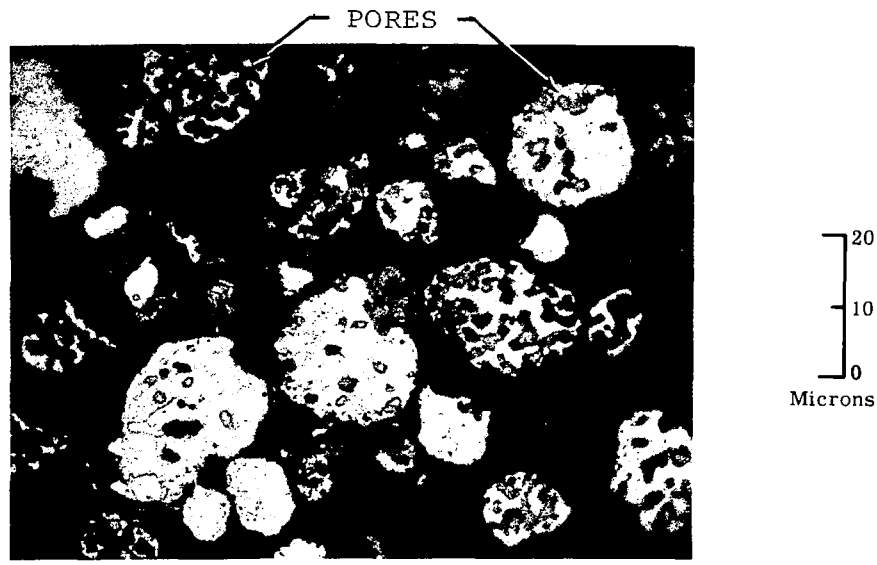

FIGURE IV-5. Composite Powder No. 2, Co+10v/oAl_2O_3 (0.1-0.6 micron alumina), from Chas. Pfizer, Showing Numerous Pores in Particles of Equiaxed to Irregular Shape and Outline of Grain Boundaries, 1000X, Etched in Acetic-Nitric-Hydrochloric-Water (1:1:4:1 Ratio)

extrusion). According to the specifications that the suppliers worked toward, the purity of the cobalt and ThO_2 was 99.5 percent or greater.

The New England Materials Laboratory supplied two 42-inch long pieces of extrusion designated CR-68-1 and CR-68-2 with an alloy core and mild steel cladding on the surface. The core diameter was 0.375 to 0.400 inches and the overall diameter was 0.562 inches. The material was reported to have been extruded at 1850° F with a 25 to 1 reduction ratio. The chemical analysis of the extruded alloy core reported by the supplier is indicated in table IV-9. The carbon content was slightly higher than the desired target limit, while sulphur content exceeded the target limit by a considerable amount. Also, the oxygen content (other than ThO_2) was very high, 0.21 percent.

Curtiss-Wright Corporation sent three pieces of hot-extruded rod (24-1/8, 28-15/16, and 31-1/16 inches long) having a total length of 84-1/8 inches. Four pieces of cold swaged rod (16-1/16, 23-3/16, 20-1/4, and 24 inches long) with a length totaling 83-1/2 inches were supplied from their lot No. PP1-18A-1. Table IV-9 shows that the ThO_2 content was slightly lower than the target limit.

TABLE IV-8. Supplier Extrusions of Dispersion-Strengthened Cobalt

Extrusion Number	Nominal Composition (weight percent)	Particle Size of Oxide (microns)	Supplier's Process of Manufacture	Supplier	Supplier's Lot Number
3	$88.8Co+11.2ThO_2$	0.01-0.06	The ThO_2 is introduced by the thermal decomposition of a thorium salt onto the cobalt powder, followed by hydrogen reduction, pressing, sintering, and extrusion.	New England Materials Laboratory	CR-68-1 and CR-68-2
9	$97.7Co+2.3ThO_2$	0.01-0.06	Prepared by co-dissolving the desired elements in a volatile solvent, flash-drying, heating, grinding, and reduction of cobalt oxide. Compacting, sintering, and extrusion are then performed.	Curtiss-Wright, Metals Processing Division	PP1-18A-1
9(a)	$97.7Co+2.3ThO_2$	0.01-0.06	Same as above plus cold working.	Same as above	Same as above

(a) Supplied in cold worked condition. Cold reduction of 85 percent by swaging given to hot extruded rod. All other material supplied in hot extruded condition.

TABLE IV-9. Chemical Analysis of Supplier Extrusions[a]

Element	New England Materials Lab. Supplier Extrusion No. 3, Co+11.2ThO_2 (weight percent)		Curtiss-Wright Supplier Extrusion No. 9, Co+2.26ThO_2 (weight percent)		
	Westinghouse Specification Target Limits	Analysis	Westinghouse Specification Target Limits	Hot Extruded Analysis[d]	85% Cold Reduction Analysis[e]
Mn	0.04 max.	<0.01[b]	0.04 max.	0.002	0.001
Si	0.04 max.	<0.03[b]	0.04 max.	0.001	0.002
C	0.020 max.	0.023	0.020 max.	0.0085	0.0092
S	0.006 max.	0.028	0.006 max.	<0.001	<0.001
P	0.010 max.	<0.001	0.010 max.	0.0003	0.0004
Ni	0.70 max.	<0.01[b]	0.70 max.	0.49	0.46
Cr	0.10 max.	<0.01[b]	0.10 max.	0.079	0.070
Co	Remainder	---	Remainder	---	---
Fe	---	0.06	---	0.10[e]	0.01[b]
ThO_2	9.7-12.7	10.4	2.11-2.41	1.96	2.05
O (other than as ThO_2)	---	0.21	---	0.00	0.00
O (total)	---	1.47[c]	---	---	---
N	---	0.004[c]	---	0.0010	0.0028
H	---	0.0182[c]		0.0019	0.0011

(a) Reported by the extrusion supplier.
(b) Spectrographic analysis.
(c) Vacuum fusion at 1700°C.
(d) Designated by supplier as Lot No. PP1-18A-1, Ext. #15.
(e) Designated by supplier as Lot No. PP1-18A-1, Ext. #5.

C. PROCESSING AND TESTING PROCEDURES

1. Powder Processing

The processing of the prealloyed atomized powders and composite powders into extrusions was conducted according to the flow diagram in figure IV-6.

a. MIXING OF POWDERS

Upon receipt, the entire -325 mesh portion of each prealloyed atomized powder and the entire lot of each composite powder (-100 mesh) was mixed in air for 15

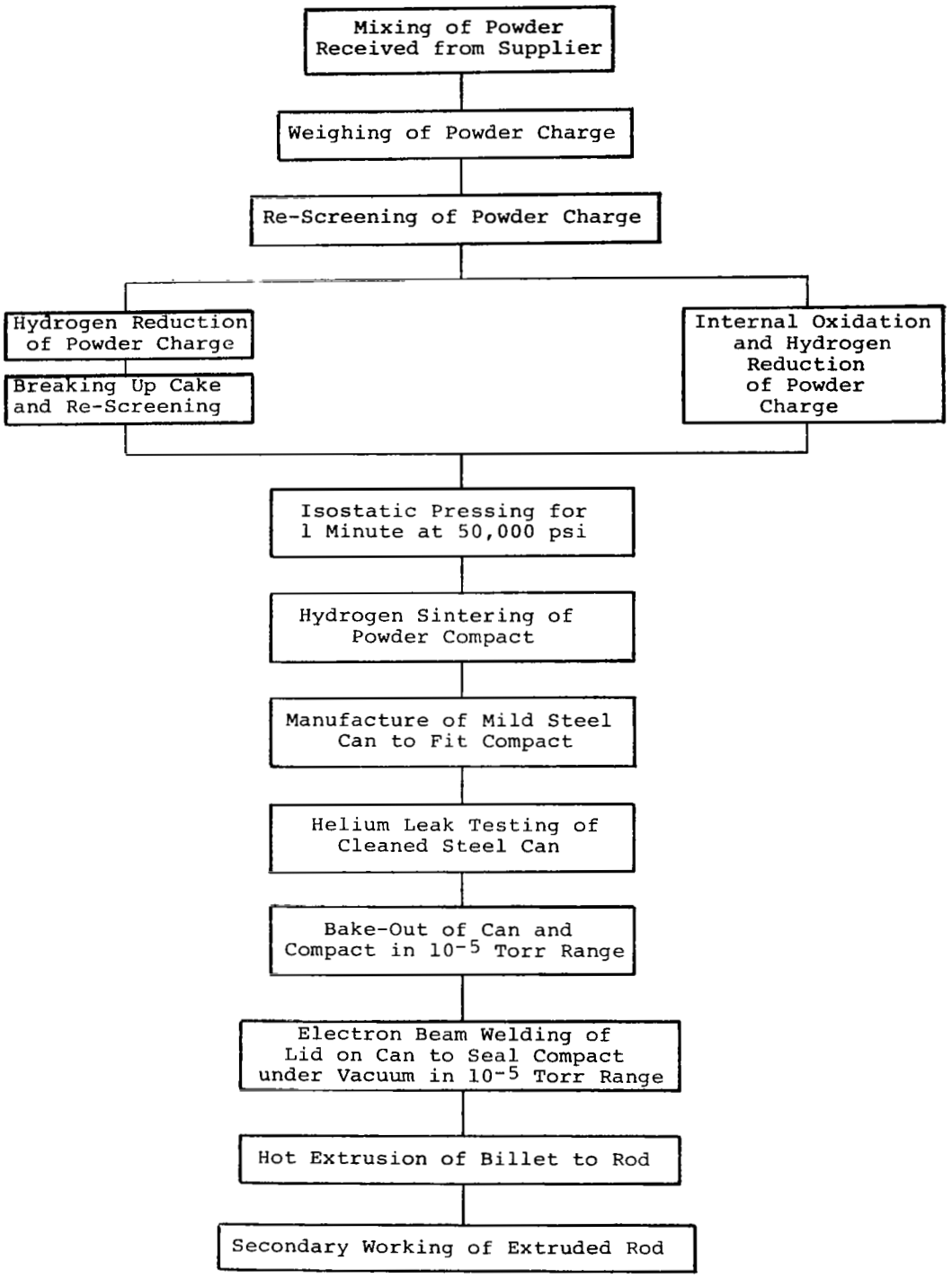

FIGURE IV-6. Flow Diagram for Processing of Powders

minutes in a 0.25 cubic foot double cone blender made of type 304 stainless steel (U.S. Stoneware Universal Laboratory Mixer). The exception was composite powder No. 11 from Vitro Labs which was reported to be pyrophoric (estimated 0.5 micron particle size). This powder was not mixed, but unpacked and carried directly into hydrogen reduction under a cover gas of argon.

b. WEIGHING OF POWDER CHARGE

A 1050-gram (2.3 lb.) charge of each cobalt-base powder and a 950-gram (2.1 lb.) charge of each iron+27 w/o cobalt-base powder were used for subsequent processing into an extrusion.

TABLE IV-10. Particle Size, Shape, and Apparent Densities of Prealloyed Atomized Powders and Density of Compacts (Minus 325 Mesh Powders)

Atomized Powder No.	Atomized Powder Type	Powder Particle Size Fisher APD (microns)	Powder Particle Shape	Apparent Density of Powder (g/cc)	Apparent Density of Powder (percent)	Density of Green[a] Compact (percent) Pressed at 50,000 psi	Density of Green[a] Compact (percent) Pressed at 100,000 psi	Density of Sintered Compact (percent)[a] 2 hrs. 1800°F in H_2
3	Co+B+Ti	14.5	Irregular	3.16	35.7	59[b]	--	59[b]
4	Co+B+Zr	12.3	Irregular	2.86	32.3	61	69[c]	66[c]
5	Co+B+Cb	25.6	Moderately Spherical	4.34	49.1	--	73	71
6	Co+B+Ta	18.2	Moderately Spherical	4.33	48.9	66	--	66
7	Co+Ce	15.6	Irregular to Equiaxed	3.55	40.1	60	--	61
8	Co+Al	13.7	Irregular	2.63	29.7	65[f]	--	65
9	Co+Be	16.8	Irregular to Equiaxed	3.54	40.0	66[f]	--	67
12	Fe+Co+B+Ti	15.7	Irregular	2.90	36.5	65	--	65
13	Fe+Co+B+Zr	11.2	Irregular	2.63	33.1	69	--	67
14	Fe+Co+B+Cb	21.0	Moderately Spherical	3.32	41.8	66	--	66
15	Fe+Co+B+Ta	17.5	Irregular to Spherical	3.08	38.8	65	--	65
16[d]	Fe+Co+Ce	9.7	Irregular	1.90	23.9	--	--	--
16[e]	Fe+Co+Ce	19.4	Irregular to Equiaxed	3.39	42.6	78	--	78
17	Fe+Co+Al	14.6	Irregular	2.57	32.3	67[f]	--	67
18	Fe+Co+Be	14.5	Irregular	2.71	34.1	69[f]	--	69
19	Fe+Co+Zr	10.2	Irregular	1.90	23.9	66	--	66
30	Co+B+Cb	20.1	Moderately Spherical	3.41	38.5	76	--	76

(a) Estimated accuracy approximately ± 1% because densities were measured on unmachined compacts.
(b) Difficult to measure accurately because cracks developed at top of compact during storage.
(c) Green compact was repressed at 100,000 after first pressing at 50,000 psi.
(d) Domtar Chemicals Ltd., Lot No. HN-183.
(e) Domtar Chemicals Ltd., Lot No. HN-185.
(f) Powder given internal oxidation treatment before pressing.

c. RE-SCREENING OF POWDER CHARGE

In the case of the prealloyed atomized powders, all powder samples taken for subsequent testing or processing were screened again through 325 mesh at Westinghouse. On the average, six percent by weight of the powder designated -325 mesh by the supplier was too coarse to pass through the 325 mesh sieve in our laboratory. No treatment was applied to this oversize portion to try to make it pass through 325 mesh.

d. HYDROGEN REDUCTION TREATMENTS FOR POWDERS

An electron diffraction study of the oxide films formed on cobalt at 0.1 atmosphere of oxygen over the temperature range of 392° to 932° F (200° to 500° C) has been reported in the literature (ref. IV-9). After 50 minutes at 392° F (200° C), both CoO and Co_3O_4 were detected. The oxidation of cobalt was later investigated at temperatures of 392° to 1292° F (200° to 700° C) for oxygen pressures of 0.1 to 0.005 atmospheres (ref. IV-10).

Oxidation of cobalt at higher temperatures, 1472° to 2192° F (800° to 1200° C) and 1112° to 2192° F (600° to 1200° C), has also been explored (refs. IV-11 and IV-12). Co_3O_4 has been variously reported to be unstable above 1742° F (950° C) in air (ref. IV-11), above 1688° F (920° C) in air (ref. IV-12), above 1652° F (900°C) in 0.013 to 27.2 atmospheres oxygen pressure (ref. IV-13), and above 1688° F (920° C) in oxygen pressure of less than one atmosphere (ref. IV-14). Summaries of oxidation studies are readily available (refs. IV-15 and IV-16).

An Fe+30 w/o Co alloy oxidized at 572° F (300° C) for 30 minutes in 0.1 atmosphere of oxygen showed the presence of Fe_3O_4 on the surface and a spinel, which may have been either Fe_3O_4, $CoO \cdot Fe_2O_3$ spinels or a mixture of the two (ref. IV-17). CoO was not observed on the surface or in the body of the oxide even though the weight percentage of cobalt was as high as 30. There may have been a solid phase reaction between CoO and Fe_2O_3 to form the spinel, $CoO \cdot Fe_2O_3$. Also it was reported that oxide films formed at 1112° F (600° C) and one millimeter oxygen pressure on 5, 30, and 40 percent Co-Fe all gave Fe_3O_4 type patterns (ref. IV-18). The standard free energy of formation of the spinel cobalt ferrite, $CoFe_2O_4$, from the oxide components CoO and Fe_2O_3 has been calculated (ref. IV-19). Also, the stabilities of Co and CoO as a function of oxygen activity and temperature, and the activity of CoO in con-

TABLE IV-11. Particle Size, Shape, and Apparent Densities of Composite Powders and Density of Compacts

Composite Powder No.	Supplier	Supplier's Lot No.	Nominal Composition (weight percent)	Specified Particle Size of Oxide (microns)	Powder Particle Size-Fisher APD (microns)	Powder Particle Shape	Apparent Density of Powder		Density of Compact	
							(g/cc)	(percent)[a]	Green-pressed at 50,000 psi (percent)[a]	Sintered - 2 hrs. 1800°F in H_2 (percent)[a]
3	Sherritt Gordon	951	Co+11.2ThO_2	0.01-0.06	2.6	Irregular	2.40	26.8	69	67
11	Vitro Labs	38, 39	64.2Fe+23.7Co+12.1ThO_2	0.01-0.06	1.3[b][c]	Irregular[c]	1.58[c]	19.4[b]	57	79
1	Chas. Pfizer	RX2002	Co+4.75Al_2O_3	0.01-0.06	2.6	Equiaxed	2.53	30.3	70	71
2	Chas. Pfizer	RX2003	Co+4.75Al_2O_3	0.1-0.6	3.9	Equiaxed	2.60	31.1	66	69
3	Chas. Pfizer	RX2044	Co+11.2ThO_2	0.01-0.06	3.6	Equiaxed	2.69	30.0	71	73
4	Chas. Pfizer	RX2045	Co+11.2ThO_2	0.1-0.6	3.6	Equiaxed	2.63	29.4	73	73
11	Chas. Pfizer	RX2059	64.2Fe+23.7Co+12.1ThO_2	0.01-0.06	1.6	Equiaxed	1.35	16.5	75	75
13	Sherritt Gordon	1006	Co+4.5ThO_2	0.01-0.06	4.0	Irregular	2.44	27.4	68	68[d]
14	Sherritt Gordon	1007	Co+8.4ThO_2	0.01-0.06	2.6	Irregular	2.23	25.0	71	71[d]
13	Chas. Pfizer	RX2073-A	Co+4.5ThO_2	0.01-0.06	3.9	Equiaxed	2.88	32.4	74	74[d]
14	Chas. Pfizer	RX2073-B	Co+8.4ThO_2	0.01-0.06	1.5	Equiaxed	1.86	20.8	73	73[d]
15	Chas. Pfizer	RX2090	66.2Fe+24.5Co+9.3ThO_2	0.01-0.06	2.5	Equiaxed	1.40	17.3	74	74[d]

(a) Percent of theoretical density.
(b) After hydrogen reduction of 6 hours at 1220°F.
(c) Estimated by supplier to be 0.5 micron before hydrogen reduction.
(d) Sintered 2 hrs. 2000°F in hydrogen.

tact with a Co-Fe alloy as a function of oxide composition in the system CoO-FeO at 2192° F (1200° C) have been determined (ref. IV-20).

Thermodynamic calculations have shown that the oxides of cobalt (CoO and Co_3O_4) are reduced by hydrogen even in atmospheres containing large amounts of water vapor (ref. IV-10). Furthermore, a graphical presentation of the thermodynamic requirements in regard to temperature and dew point on the oxidation of metals and reduction of their oxides in hydrogen indicated that a dew point of well above +65° F at 1220° F was sufficient for reduction of CoO to Co, and FeO and Fe_3O_4 to Fe (ref. IV-21). However, it should be mentioned that spinels might respond to a given hydrogen atmosphere in a manner unlike that shown by the individual oxides (refs. IV-21 and IV-22).

Hydrogen reduction treatments were applied to all powders on this program for the purpose of reducing oxides of cobalt and iron before compaction. The powders, with the exception of those given internal oxidation treatments which will be discussed later, were hydrogen reduced for six hours at 1220° F.

An Inconel 600 retort inside an electrical resistance heated box furnace (Pereco Model FGO-7800 furnace 18 inches wide by 18 inches high by 24 inches deep) was employed for hydrogen reduction treatments. The retort was constructed from 1/8-inch-thick sheet and had inside dimensions of 14-3/4 inches wide by 7-3/4 inches high by 21-1/4 inches long. For the initial evaluation phase (phase 1) of the program, a mechanical seal was used between the retort lid and pan. This consisted of machine screws and nuts of 18-8 stainless steel spaced at approximately 2-inch intervals along the one inch wide top flange to draw the lid down against the soft copper gasket (1/16-inch-thick by 1-inch wide) interposed between retort pan and lid. The gasket was dispensed with and the lid was TIG welded to the flange on the retort pan for the intermediate and final evaluation phases of the program. This further insured against leakage and promoted the attainment of the lowest dew point possible under the conditions used. A maximum of four powder charges could be hydrogen reduced at the same time in the retort by spreading out each powder to a depth of 1/4-inch in shallow, rectangular trays (150-mm long by 65-mm wide by 19-mm high) of impervious, recrystallized 99% alumina (Coors AD-99). A 1050-gram (2.3 lb.) powder charge was used with the

cobalt-base alloys and a 950-gram (2.1 lb.) powder charge with the Fe+27 w/o Co-base alloys.

These weights would yield about 120 cc (7.2 cubic inches) of 100 percent dense metal, after extrusion, allowing for the difference in density between cobalt and Fe+27 w/o Co, but without allowance for metal loss during handling, compacting, and extrusion.

Six trays of powder charges were placed inside each of two Alundum D-shaped muffles of 3 inches inside height by 6 inches inside width by 20 inches length by 3/8-inch wall thickness (Norton Co. No. 46230, Mixture RA-4139, fused 98.8% alumina, 36 percent apparent porosity). The muffles acted to channel the hydrogen from the two inlet ports at the back of the retort over the powder and also prevented loose material from falling into the powder.

Since composite powder No. 11 from Vitro Labs was reported by them to be submicron (estimated 0.5 micron) size and pyrophoric, the entire four pound quantity received was removed under argon from two hermetically sealed cans in which it was shipped and spread out to a depth of 0.5 inches in 15 shallow, rectangular trays (150-mm long by 65-mm wide by 19-mm high) of impervious, recrystallized 99 percent alumina (Coors AD99) placed inside the Inconel 600 retort. This work was performed inside a 30-inch I.D. by 48-inch long Vacuum Industries glove box which had been evacuated to less than one micron of mercury before back-filling with argon. After bolting on the retort lid and sealing off inlet and outlet tubes, the retort and powder were removed from the glove box and placed in an electrical resistance furnace where a hydrogen reduction treatment was applied in the normal manner. The powder was not pyrophoric after hydrogen reduction because of a sintering together of individual powder particles, thus effectively increasing their size.

The hydrogen used for reduction and the argon used for pre-purge and post-purge of the retort flowed from their respective cylinders through an attached Deoxo Hydrogen Catalytic Purifier (Model 10-50) and then through a Drierite Drying Apparatus. The gas inlet line was 1/4-inch O.D. by 0.035-inch wall Inconel 600 tubing running outside the retort to the back where the gas entered through two inlet ports. The outlet line on the front of the retort was 3/8-inch O.D. by 0.035-inch wall tubing of the same material which ran to a Lectrodryer Dew Point Indicator containing dry ice in acetone in

the cup with mirror finish. Copper tubing from the outlet of the dew point cup carried the hydrogen to burn-off.

The hydrogen cylinder gas was purchased with a guaranteed purity of 99.95 percent and contained less than 10 ppm O_2, less than 100 ppm N_2, less than 40 ppm carbon bearing gases, and less than 30 ppm moisture. The argon was guaranteed 99.996 percent pure with less than the following amounts of impurities: 7 ppm O_2, 15 ppm N_2, 5 ppm carbon bearing gases, 1 ppm H_2, and 15 ppm moisture. After passing through the Deoxo Purifier and Drierite, the dew point of the hydrogen was measured to be lower than -90° F. The gas flow rates were adjusted by means of cylinder flow meters to give a minimum of five volume changes per hour in the retort. After pre-purging the retort with argon, the hydrogen was turned on and the temperature raised to 1220° F. During the first four hours at 1220° F the dew point steadily improved as moisture was removed. During the last two hours at 1220° F, the dew point measured at the outlet averaged -64° F for all reduction treatments. The argon was turned on and the hydrogen off when the retort had cooled to about 400° F. Upon further cooling to about 100° F, the dew point of the argon at the outlet averaged -83° F.

e. BREAKING UP CAKE AND RE-SCREENING

The hydrogen reduced powders were dumped from the alumina trays into a high-speed blender for purposes of breaking up the soft cake which formed in some alloys. This operation was performed dry. The powder was then screened and loaded into rubber bags for isostatic pressing. The prealloyed atomized powders were screened through 325 mesh to remove the few remaining agglomerated particles. The composite powders, which had a much finer original particle size that the atomized powders, tended to form a stronger cake. Rather than employ extended periods in the blender, the composite powders were screened through 28 mesh.

At this point before pressing, a 0.25 w/o Zr addition in the form of ZrH_2 powder from Ventron Corporation, Metal Hydrides Division having a purity greater than 99 percent and a particle size of less than 2 microns was made to one charge of composite powder No. 14, Co + 8.4 w/o ThO_2 from Sherritt Gordon. The ZrH_2 was mixed with the composite powder using a high-speed stainless steel blender under argon inside a glove box which was first evacuated to $1x10^{-3}$ torr and then

back-filled with argon. A master blend was first made from the ZrH_2 addition and 200 grams of composite powder. This was split into three equal weights and mixed separately with three charges of composite powder weighing 233 grams each. Finally the three charges were placed in a double cone blender, sealed under argon, and blended together for 30 minutes. The mixture was isostatically pressed, hydrogen sintered, and extruded in the usual manner to be described later.

f. INTERNAL OXIDATION TREATMENTS AND SUBSEQUENT HYDROGEN REDUCTION

It was reported in the literature (ref. IV-23) that internal oxidation began at 1652° F (900° C) and became more intense at higher temperature in a Co + 5 w/o Al alloy specimen cut from a vacuum-melted ingot and exposed to air for 50 hours. The 5 w/o Al present had little effect on the scaling rate of cobalt above 1652° F (900° C). Also, Co+32w/oCr+0.41w/oAl and Co+32 w/oCr+0.39w/o Be alloys were oxidized for 50 hours. In both alloys internal oxidation was evident at 1652° F (900° C) and became deeper with increasing temperature. The oxidation of cobalt-aluminum alloys at 1112° to 2462° F (600° to 1350° C) in low-pressure oxygen was reported to result in the formation of gamma alumina on the surface below about 1652° F (900° C) which permitted the passage of cobalt ions through the layer, becoming oxidized to Co_3O_4. The transformation from gamma alumina to alpha alumina occurs between 1652° to 2012° F (900° to 1100° C) and is accompanied by volume changes which can cause fissuring of the scale (refs. IV-24 and IV-25).

The internal oxidation of Ni+Al alloy specimens from castings at 1830° F for times of 6.25, 25, and 100 hours has been studied at four levels of oxygen pressure ranging from 10^{-4} to 10 atmospheres. The extent of the subscale formation was generally independent of oxygen pressure, as were subscale particle characteristics and hardnesses (ref. IV-26). Powders of dilute Cu+Si, Cu+Al, Ni+Al, and Ni+Cr alloys were internally oxidized, hydrogen reduced, compacted, sintered and extruded. A substantial strengthening effect was achieved with the Al_2O_3 dispersions (ref. IV-27). The internal oxidation of dilute alloys of Cu+Si and Cu+Al in the form of -20 mesh powder has been reported (ref. IV-28). Powder compacts of Cu+0.38w/o Be, Cu+0.19w/o Al, Ni+1.9w/o Al and Ni+1.0w/o Cr alloys have been internally oxidized (ref. IV-29). Furthermore, Al_2O_3 dispersions in Fe+Al alloy powders (-100 mesh) have been produced by internal oxidation treatments (ref. IV-30).

Internal oxidation treatments were applied to the following four prealloyed atomized powders to produce nominally 10 v/o dispersed alumina or beryllia in the matrix.

Atomized Powder No.	Nominal Composition (weight percent)
8	Co+2.5Al
9	Co+1.3Be
17	Fe+26.3Co+2.7Al
18	Fe+26.6Co+1.4Be

The Inconel 600 retort and furnace used for internal oxidation treatment of the powders, and the subsequent hydrogen reduction of cobalt and iron oxides back to metal were described previously. The flange on the retort pan was machined flat by milling and then polished. A 1/16-inch-thick nickel gasket was interposed between the retort pan and lid, which was drawn tight by bolts at two inch intervals.

The 99.5 percent purity oxygen (water-pumped) used for internal oxidation was dried by passing through a Drierite drying apparatus. The hydrogen used for reduction and the argon used for pre-purge and post-purge of the retort flowed from their cylinders through two Deoxo Hydrogen Catalytic Purifiers (Model 10-50) attached in parallel and thence through a Drierite drying apparatus, as described earlier.

The treatment used in the preliminary internal oxidation trials involved first heating the -325 mesh powders to 1830° F and holding for two hours in purified and dried hydrogen flowing at 7 SCFH (5 retort volume changes per hour) in order to reduce cobalt and iron oxides, that might be present, back to metal, and to put the aluminum and beryllium additions in solid solution. After holding an additional 1/2-hour at 1830° F while the hydrogen atmosphere was replaced by purified and dried argon, dried oxygen was slowly introduced over a 1/2-hour period until a complete oxygen atmosphere flowing at 5 SCFH was obtained. The powder was exposed for an additional six hours at 1830° F to the flowing oxygen while spread out to a depth varying from 5/8 to 1/16-inch in flat, 99 percent alumina trays (Coors AD99) 150-mm long by 65-mm wide by 19-mm high. The trays were located inside two Alundum D-shaped muffles

of 3-inch inside height by 6-inch inside width by 20-inch length by 3/8-inch wall thickness (Norton Co. No. 46230, Mixture RA-4139, fused 98.8% alumina, 36% apparent porosity). The powder was cooled to room temperature under argon flowing at 5 SCFH.

Cross sections of both oxidized powder cake, and the cake after hydrogen reduction at 1220° F for 38 hours were examined under the microscope. The alumina and beryllia particles resulting from this treatment varied from coarse (micron size range) at the top of the 5/8-inch-thick cake to fine (submicron size range) at the bottom of the cross section.

On the basis of these preliminary tests, it was decided to internally oxidize new samples of the same -325 mesh powders spread out in trays to a uniform depth of 1/8 inch using a two hour instead of the previous six hour holding time at 1830° F in oxygen flowing at 7 SCFH. Otherwise, the internal oxidation procedure and equipment were the same as in the preliminary trials. Each powder sample was oxidized separately while spread out in 12 alumina trays to a depth of 1/8-inch. The powder charge weights were 1050 grams each of the Co-base powders (Nos. 8 and 9), and 950 grams each of the Fe+27w/oCo powders (Nos. 17 and 18). This procedure resulted in the formation of a relatively uniform size of dispersed alumina and beryllia particles (mainly submicron) from top to bottom of the cross section of the cake. Therefore, the powders oxidized in this manner appeared to be satisfactory for processing into extrusions.

The oxidized cake was broken up into powder in a stainless steel tray, high speed blender, and, where necessary, Pitchford Pica Blender-Mill Model No. 3800, (Pitchford Manufacturing Co., Pittsburgh, Pa.) using stainless steel containers and hardened steel balls. The oxidized powder was screened through 65 mesh before hydrogen reduction.

Six Alundum tubes 2-inch inside diameter by 3/8-inch-thick wall by 2-1/2 inches long of 99.8 percent alumina with 36 percent apparent porosity (Norton Co. RA-4139) were fitted inside six 99 percent alumina trays and filled with oxidized powder to a height of approximately 1-1/2 inches. The trays were placed inside two Alundum D-shaped muffles described previously to keep solid contaminants from falling into the powder, and loaded into an Inconel 600 retort. Each oxidized powder composition was given hydrogen reduction treatments separately. The purpose of containing the powder in 2-inch

inside diameter tubes was to provide a cylindrical shape of the proper diameter suitable for an extrusion billet in case the powder particles strongly bonded together and formed a dense, ductile, metallic cake during hydrogen reduction which would not lend itself to compaction to size by the normal isostatic pressing procedure.

Hydrogen reduction of the cobalt and iron oxides consisted of heating to 1200° F and holding for approximately 18 hours with a 6 to 1 ratio of argon and hydrogen mixture flowing at 7 SCFH through the retort. Then the temperature was raised to 1800° F and held for approximately 11 hours. The 6 to 1 argon-hydrogen mixture flowing at a minimum of 7 SCFH was maintained during heating from 1220° to 1800° F, and during the first 3 hours (approximately) at 1800° F. For the remaining 8 hours at 1800° F, purified and dried hydrogen was used, and flowed through the retort at a minimum of 7 SCFH. Furnace cooling to room temperature was performed under hydrogen. The argon-hydrogen mixture was used initially, rather than pure hydrogen, because substantial amounts of moisture were being carried from the retort.

Upon removal from the retort, the reduced powders were in the form of soft cakes approximately 1-3/4-inch diameter. The six cakes of each composition were stacked on top of each other in a rubber bag for isostatic pressing.

During the intermediate evaluation phase (phase 2) of the program another charge of atomized powder No. 9, Co+1.3w/oBe, was given a shorter internal oxidation treatment (1/2 hour instead of 2 hours at 1830° F) in an attempt to achieve a still finer dispersoid of BeO in cobalt. The equipment and procedure used for internal oxidation and subsequent hydrogen reduction were similar to that used before except that the retort lid was TIG welded to the pan instead of using a mechanical seal. As an extra last step in hydrogen reduction, the temperature was raised to 2000° F and held for 3 hours with hydrogen flowing at 7 SCFH.

g. ISOSTATIC PRESSING OF POWDERS

The hydrogen reduced powders (dry and without binders) were loaded into cylindrical 7-1/4-inch long rubber bags having a 1/8-inch wall thickness. The rubber bag diameter used for the prealloyed atomized powders was 2.15-inch I.D. and for the composite powders 2.52-inch I.D., adjusting for the lower apparent densities of the

latter powders. A 1/32-inch diameter stainless steel wire was placed vertically along the inside wall of the bag and then slowly withdrawn to allow air to escape as the rubber end closure (with an aluminum sealing ring for support on the inside) was pressed down against the top of the powder charge. A metal band clamp with worm screw was placed around the outside of the bag, and tightened against the end closure on the inside, thus insuring that the water-glycerine mixture used as the working fluid in the isostatic press could not leak into the powder. The press used for this work had a 7-inch I.D. by 24-inch long working chamber and was made by National Forge Company.

Isostatic pressing was conducted at 50,000 psi and that pressure held for one minute. The selection of 50,000 psi was made because it provided densities in the green compacts which enabled them to be handled satisfactorily, and it was also a pressure which was readily available in large isostatic presses which would be required if the process was scaled up at a later date. However, 100,000 psi pressure was used with two atomized powders in order to see what the effect would be, as indicated in Table IV-10. The higher pressure increased the green compact density by eight percent. Green compact densities were calculated first in terms of grams per cubic centimeter from measurements on the weights and sizes of the compacts, which were approximately 2 inches in diameter by 3 inches long. Then the density was converted to percent of theoretical density for purposes of comparison, tables IV-10 and IV-11.

h. HYDROGEN SINTERING OF COMPACTS

The same type of retort and other equipment, the purified and dried hydrogen and argon gases, and general operating procedure used for hydrogen reduction of powders were also employed for the sintering of compacts in hydrogen. However, the alundum muffles were not used, but the compacts were placed on the 99% alumina trays inside the retort. Sintering in hydrogen was carried out at 1800° F for two hours on all compacts of prealloyed atomized and internally oxidized powders. The compacts of composite powder Nos. 1 to 11 were also sintered at 1800° F for two hours. However, composite powder Nos. 13 thru 15 containing ThO_2 obtained for the intermediate and final evaluations (phases 2 and 3) were given an additional sintering treatment of two hours at 2000° F in order to reduce oxygen (not combined as ThO_2) to the lowest possible level.

The 1800° F temperature used exclusively during the initial evaluation (phase 1) was high enough to produce compacts which were sufficiently strong and could be easily machined dry for fitting inside low carbon steel cans prior to extrusion. This temperature was believed to be low enough to avoid agglomeration of the dispersed constituent resulting from diffusion of the elements present in some of the compositions under study. Also, it was below the extrusion temperature, 2000° F, but above the 1200° to 1600° F service temperature range for these products. A study of the microstructures of the sintered compacts was conducted to determine which compositions were the most stable in regard to agglomeration of dispersed constituent particles. At this stage the cerium-containing atomized powder compositions No. 7 and 16 were found to contain constituent particles too coarse for dispersion-strengthening purposes and were dropped from further study.

The sintered compact densities obtained are listed in tables IV-10 and IV-11. Little, if any densification occurred as a result of sintering at 1800° F with the exception of composite powder No. 11 from Vitro Labs. That powder had the smallest particle size and the lowest green compact density of any powder.

i. MACHINING OF SINTERED COMPACTS AND CANS

The compacts, which were approximately 2 inches in diameter by 3 inches long after sintering, were machined to a 1.95-inch diameter so that they would fit inside 2-inch I.D. by 0.125-inch thick wall mild-steel cans. Care was taken to insure that the compacts remained dry and clean during the machining operation. The mild-steel can (SAE 1020) had a 1.5-inch thick nose plug on the front end which was machined on the outside to a 90 degree truncated cone with a 0.75-inch diameter flat section on the nose. This matched the entrance angle on the die and the die opening of 0.75 inch diameter. During the intermediate and final evaluation efforts (phases 2 and 3) of the program, this dimension was increased from 0.75 to 0.875 inch to provide larger diameter rod in order to accomodate a larger number of cyclic secondary working treatments.

The can was made with the back-end open to receive the compact and the 2-inch diameter by 0.25-inch-thick end plug of mild steel which later was electron-beam welded flush with the end of the can. The inside length of the can matched the length of each compact plus the 0.25-

inch thickness of the end plug. All outside surfaces of the can were sand blasted to promote adherence of the glass lubricant. The total weight of compact, can, and end plug was about four pounds. The compacts themselves weighed approximately two pounds each.

j. HERMETICALLY SEALING COMPACTS IN CANS

The cans were evacuated to less than $1x10^{-5}$ torr and tested for helium leak tightness before the compact was inserted and the end sealed.

Each can with the compact inside and end plug was baked out for two hours at 1220° F in the 10^{-5} torr range. This temperature was raised to 1500° F for the intermediate and final evaluation phases. After cooling to room temperature and back-filling with 99.996 percent purity argon, the cans, compacts, and end plugs were removed from the furnace and carried in a covered container to a Sciaky electron-beam welder (30 kW, Type VX-50x30x42 with 16-inch diffusion pump), where they were immediately evacuated to the 10^{-5} torr range. Each end plug had eight longitudinal slots 0.063 inches wide by 0.032 inches deep equally spaced around the periphery to facilitate evacuation of the can. The welding conditions were fixed from trial runs so as to give 30 to 50 percent penetration through the 0.25-inch thick end plug. The method had been found by previous experience to give leak tight joints.

k. HYDRAULIC EXTRUSION OF BILLET TO ROD

Before preheating the canned compacts for extrusion, the outside of the can, except for the back-end, was coated with a 0.125-inch thickness of glass slurry consisting of a water soluble, borate-type glass (Code No. 9773, Corning Glass Works, Corning, New York) with collodion and amyl acetate binder, and air dried.

The extrusion tools were made of AISI H-12 hot-work tool steel hardened to Rockwell C 45 to 50 and consisted of an extrusion container 12 inches long with a 2.360-inch diameter bore, a die with a 0.750-inch diameter hole and a conical entrance of 90 degrees included angle, and a ram with a 2.350-inch diameter dummy block attached. The tools were mounted on the horizontal bed of a down acting, 200-ton hydraulic press. The extrusion direction was downward.

Preparations for extrusion involved brushing the die, bore of the container, and dummy block while cold with

either Sicon Lubricant (colloidal suspension of silicone resin and graphite in water, Lot 11X915, Midland Industrial Finishes Co., Inc., Waukegan, Illinois) or Dag Dispersion No. 99 (colloidal suspension of graphite in organic solvent, Acheson Colloids Co., Port Huron, Michigan). In addition, two glass disks of the borate-type glass weighing 30 grams each and measuring 2.25 inches in diameter by 0.5-inch thick were placed inside the bore of the extrusion container on top of the die. Next 50 grams of loose borate glass powder were poured into the bore of the container on top of the disks. Before the glass was added to the bore, a 0.75-inch diameter by 0.5-inch thick plug of mild steel with a slightly oversize diameter on the top end was placed in the hole of the extrusion die to insure glass was retained until extrusion started. This lubrication practice for extrusion was generally in line with the recent literature on the subject (refs. IV-31 to IV-35). The borate-type glass (Corning Code No. 9773) was selected for use because it has a viscosity of between 100 and 300 Poises at 2000° F (the billet extrusion temperature), and could easily be removed from the extrusion, die and other tools since it was soluble in water.

The extrusion container and die were preheated to approximately 900° F for extrusion. The canned compact previously coated with glass was placed in a Type 304 stainless steel retort 3.75 inches I.D. by 7.5 inches inside length with the uncoated back end of the billet resting on the bottom of the retort. A matching cover plate was placed over the top of the retort. Argon of 99.996 percent purity flowed through the retort at five SCFH by means of an inlet tube at the bottom and an outlet tube at the top during preheat. A thermocouple placed inside the retort alongside the canned billet gave temperature readings which corresponded very closely with the indicated furnace temperature. The billet temperature was raised from room temperature to 2000° F and held at 2000° F for one hour.

The billet was removed from the furnace and retort, and immediately extruded to 0.75-inch diameter rod with an extrusion speed of 43 feet per minute (8.6 inches per second). The material from the sintered compact was present in the 0.75-inch diameter extrusion as a central core, whose diameter varied from 0.38 to 0.63 inches, surrounded by mild-steel cladding. The minimum extrusion ratio for the alloy core was 11 to 1. Later in the program, 0.875-inch diameter extrusions were made for subsequent secondary working purposes with an

8 to 1 extrusion ratio for the alloy core. The extrusion starting pressures for the compacts varied from 53,000 psi to 91,000 psi. The maximum length of 0.75-inch diameter rod obtained was 33 inches. After scrapping a 9-inch length from the front and a 4-inch length from the back (because of rear-end extrusion defect) the maximum length of core material available for subsequent testing purposes was 20 inches.

1. DYNAPAK EXTRUSION OF BILLET TO ROD

Sintered compacts of the atomized powders listed in the following table (-325 mesh) were extruded to rod in a Dynapak 1220C Machine at the Westinghouse Astronuclear Laboratory.

Atomized Powder Number	Nominal Composition (weight percent)	Sintered Compact Density (percent of theoretical)	Billet Size Diameter (inches)	Billet Size Length (inches)
4	Co+1.0B+4.2Zr	60	1.6	3-15/16
13	Fe+25.6Co+1.0B+4.2Zr	66	1.6	3-11/16
14	Fe+25.6Co+1.0B+4.2Cb	68	1.6	3-5/6

The purpose of this work was to investigate the effect of lower processing temperatures, 1600° F maximum, on the magnetic and tensile properties. The Dynapak extrusions (1600° F billet) were made below the transformation temperature of the iron-cobalt matrix (approximately 1770° F from face centered cubic to body centered cubic on cooling) whereas the hydraulic extrusions (2000° F billet) of the iron-cobalt compositions were made above the transformation temperature and underwent a phase change on cooling. The extrusion ratios were 11 to 1 for conventional extrusion and 6 to 1 for the Dynapak.

The powders for the billet extruded in the Dynapak Machine were processed into compacts in the same manner as described earlier, except that the compact sintering temperature was 1600° F (for two hours) instead of 1800° F. The compacts were canned in mild steel and hermetically sealed by electron beam welding prior to extrusion. The billet was preheated to 1600° F in an induction coil under argon and held at temperature approximately 15 minutes. (The billet preheat for hy-

draulic extrusion was one hour at 2000° F.) Rod with an overall diameter of 0.763-inch and an alloy core diameter of 0.656-inch was produced.

m. SECONDARY WORKING OF HOT-EXTRUDED ROD

Secondary working and thermo-mechanical treatments have been reported to have a substantial effect on the strength of dispersion-strengthened copper (ref. IV-36), nickel (refs. IV-37 to IV-43), cobalt (ref. IV-44), and iron (ref. IV-45) having oxide contents in the range from 0.4 to 3 percent by volume. The mechanical properties of TD Nickel are reported to depend on the cold work-stress relief cycle (ref. IV-37). The best high-temperature strength of nickel-thoria strip was obtained by working with a maximum number (21) of cold reduction-annealing cycles with a minimum reduction in thickness (less than 10 percent) in each working cycle (ref. IV-39).

The literature on the effect of secondary working and thermo-mechanical treatments of dispersion-strengthened metals revealed that these methods of improving elevated temperature strength have been applied successfully to wire, small diameter bar, sheet, and tubing where the product size is small or at least the thickness of the material is small in one direction (sheet and tubing). Small cross-sections permit dispersion-strengthened products to be worked thoroughly and uniformly. However, the eventual application for the material being developed on this program will be a solid, high-speed rotor whose size may be 8 to 28 inches in diameter by 8 to 28 inches long. One method of fabrication would be to make the rotor as one piece. Another method would be to fabricate it from laminated and bonded sections with a minimum of reluctance added to the magnetic circuit. Therefore, secondary working treatments which are selected and applied to small diameter extrusions in this program were designed with consideration for methods which could be applied later on to the fabrication of much larger products.

Secondary working treatments were applied to selected compositions in the form of 7/8-inch diameter hot-extruded rod stock made in a conventional hydraulic press. The extrusion ratio for the alloy core material was 8 to 1. Each cycle of secondary working consisted of approximately a 10 percent reduction in area per pass in a swaging machine followed by a 10 minute stress-relief anneal after each pass at the secondary working temperature. The intermediate anneals between passes

and the final anneal were performed in flowing argon atmospheres in electrically resistance heated box furnaces. Various temperatures of secondary working in the 1500° to 800° F range were employed during the course of the program. The 1500° F temperature was used first because it was anticipated that all compositions could be swaged successfully at that temperature without breaking up, and this would permit comparison of properties of compositions having a common fabrication history. Later in the program, lower secondary working temperatures were applied which were related to the specific working characteristics of each composition. In the final evaluation effort (phase 3) a calibration study of the effect of secondary working at 1000° and/or 1250° F was conducted on four iron+27 w/o cobalt-base and four cobalt-base compositions given 0, 4, 8, 16 and 28 to 36 cycles (or the maximum number of cycles achieved before the rod broke up). In addition, a length of the Dynapak extruded 0.763-inch diameter rod of prealloyed atomized powder composition No. 13, Fe+25.6w/o Co+1.0w/oB+4.2w/oZr, was swaged at room temperature.

Swaging of rod in the size range of 7/8-inch to 3/8-inch diameter was performed in a four-die Fenn #4-F machine at the Westinghouse Astronuclear Laboratory. Two-die swaging machines, a Fenn #4-SA for 3/8 to 1/4-inch diameter rod and a Torrington #3 for rod sizes under 1/4-inch were employed at Battelle Memorial Institute. The die sizes used and the reduction per pass are indicated in table IV-12.

The mild steel cladding approximately 1/16-inch-thick resulting from the extrusion operation was left on the core material for the secondary working process.

2. Testing Procedures for Extruded and Secondary Worked Rod

a. INSPECTION FOR DEFECTS AND MACROSTRUCTURE

Transverse sections from the front and back of each rod were cut with an abrasive cut-off wheel using coolant for macroscopic examination in order to locate sound core material before test specimens were taken. Macroetching was performed with the following solutions: 5 percent nital, 50 percent nitric acid in water, and 50 percent hydrochloric acid in water.

No gross defects were found in the core material near the front of the extrusions. As a further precaution,

TABLE IV-12. Swaging Die Sizes Employed During Secondary Working

Secondary Working Cycle (No.)	Swaging Die Diameter (inches)	Reduction in Area per Die (percent)	Cumulative Reduction in Area in Die Series (percent)
0	0.875	0	0
1	0.830	10.2	-
2	0.795	8.1	-
3	0.750	10.9	-
4	0.720	8.0	32.3
5	0.680	10.9	-
6	0.645	10.0	-
7	0.610	10.6	-
8	0.580	9.7	56.1
9	0.550	10.1	-
10	0.520	10.8	-
11	0.500	7.4	-
12	0.470	11.6	71.2
13	0.445	10.4	-
14	0.420	10.9	-
15	0.400	9.4	-
16	0.375	12.1	81.6
17	0.362	6.8	-
18	0.341	11.2	-
19	0.320	12.0	-
20	0.302	10.9	88.1
21	0.279	14.7	-
22	0.266	9.1	-
23	0.250	11.7	-
24	0.244	4.7	92.2
25	0.229	11.9	-
26	0.216	11.0	-
27	0.204	10.8	-
28	0.192	11.4	95.2
29	0.182	10.2	-
30	0.171	11.7	-
31	0.162	10.3	-
32	0.153	10.8	96.9
33	0.144	11.5	-
34	0.136	10.8	-
35	0.128	11.5	-
36	0.121	10.6	98.1

transverse and longitudinal sections from the front and back were examined under the microscope in the as-polished condition and after etching.

b. MICROSTRUCTURE OF SOUND MATERIAL

The microstructure was revealed by etching in the acetic-nitric-hydrochloric-water solution or Carapella's reagent. Longitudinal and transverse sections were examined with a metallograph at magnifications up to 1500X. The size of secondary-phase particles (average particle-intercept length) dispersed in the cobalt and iron+27w/o cobalt matrix, their interparticle spacing (average matrix-intercept length), and the percent by volume of dispersed phase were determined in representative areas using a filar micrometer eyepiece. Also, measurements were made on photomicrographs using a Norelco Type 52022 film illuminator and measuring device (with millimeter scale and vernier). Lineal analysis and point counting techniques were applied (refs. IV-46, IV-47 and IV-48). Electron micrographs were obtained on seven compositions to better reveal the dispersoid for measurement. Identification or confirmation of the dispersed phase in the matrix was performed by x-ray diffraction on both powder and rod material.

The uniformity of the dispersion, the amount of porosity, and possible indications of lack of bonding between the dispersoid and the matrix were noted. X-ray diffraction back reflection Laue patterns were obtained from various regions on the metallographic specimens of rod to indicate the degree of recrystallization and grain size (refs. IV-49 and IV-50).

c. LOCATION AND PREPARATION OF TEST SPECIMENS

After the macroscopic and microscopic examinations of sections from the front and back of the rod had confirmed the intermediate core material was sound, samples were taken for testing starting near the front of the extrusion. The d-c magnetic test specimens were taken first. The magnetic saturation specimen was machined to 0.1-inch diameter by 0.1-inch long, and the coercive force specimens to 0.25-inch diameter by 1.0-inch long. In the case of rod secondary worked for 28 to 32 cycles, the coercive force specimen diameter was 0.12 to 0.15-inch.

The dimensions of the tensile and creep specimens are shown in figures IV-7, IV-8, and IV-9. These speci-

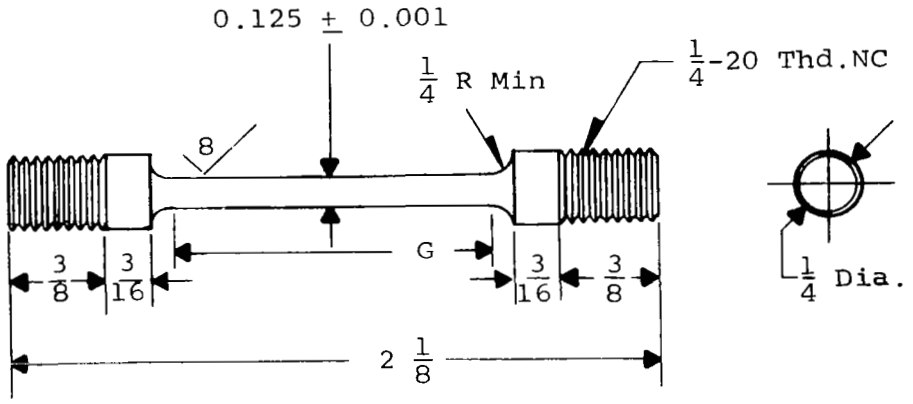

NOTE: Taper gauge length "G" to center so that the dia. at the ends of the gauge length exceeds the dia. at the center of the gauge length by not less than 0.0005 inch nor more than 0.001 inch. "G" and total length are nominal.

Westinghouse Dwg. No. Ref. EDSK 326749

FIGURE IV-7. Vacuum Tensile Specimen for Hot-Extruded Rod, and Tensile and Creep Specimen for Rod Secondary Worked 16 Cycles or Less

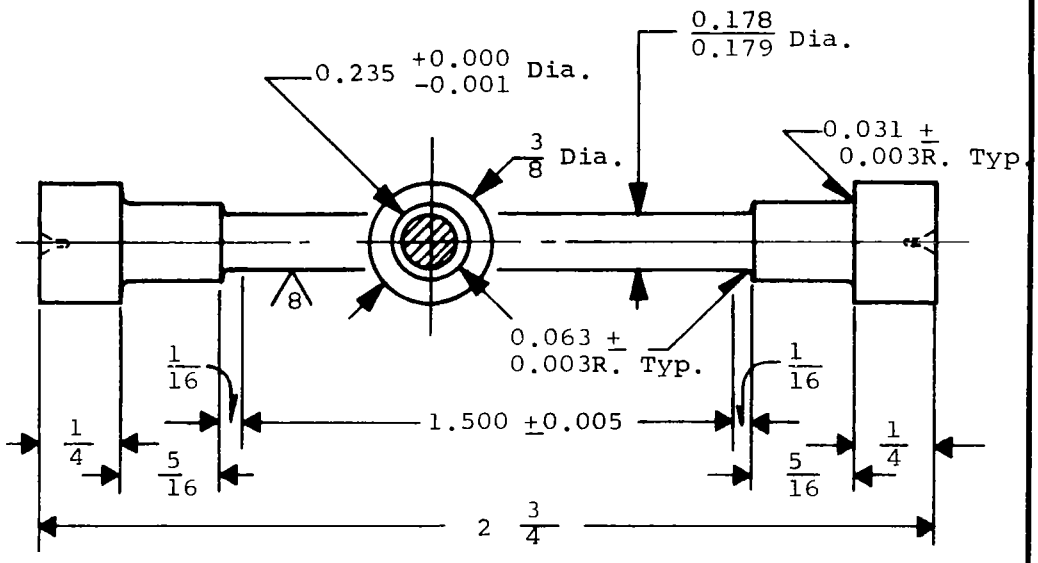

NOTE: Eccentricity on end centers must not exceed 0.0005 inch.

Westinghouse Dwg. Ref. No. 627A084

FIGURE IV-8. Vacuum Creep Specimen for Hot-Extruded Rod

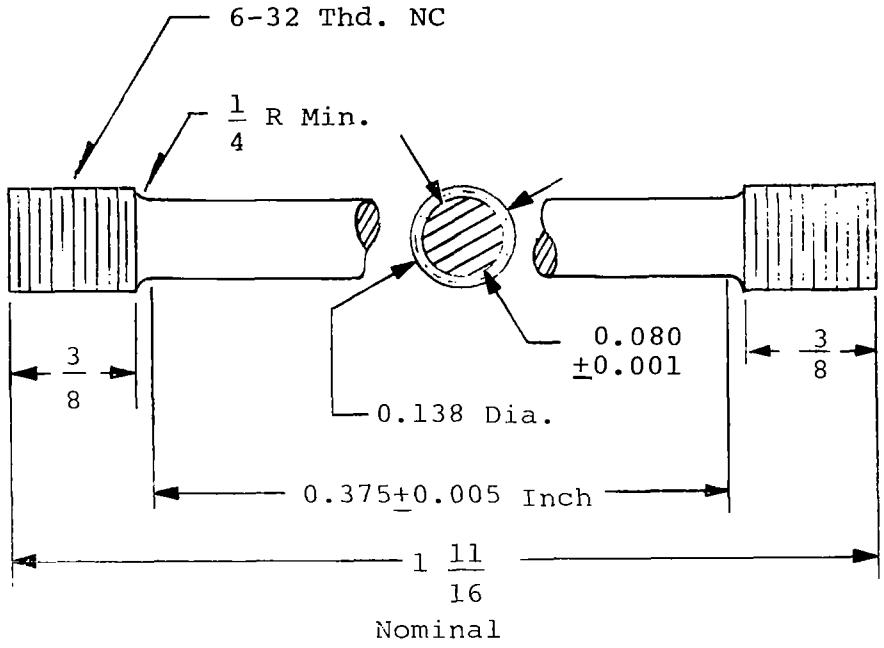

NOTE: Taper gauge length 0.375 inch to center so that the diameter at the ends exceeds the diameter at the center by not less than 0.0005 inch nor more than 0.001 inch. Locate gauge length 0.375 inch in center of area between the threaded ends.

Westinghouse Dwg. No. Ref. EDSK 343243

FIGURE IV-9. Vacuum Tensile and Creep Specimen for Rod Secondary Worked 28 Cycles

mens were rough machined in a lathe and left with an 0.020 inch minimum oversize diameter on the reduced section. Specimens aged 100 hours at elevated temperatures in a vacuum of $1x10^{-5}$ torr before testing were given their aging treatments before machining or grinding the diameter of the reduced section to final size. Coolant was used in all machining and grinding operations.

d. MAGNETIC TESTING

In general, magnetic properties of materials may be divided into two classes: structure insensitive and structure sensitive. The primary or structure insensitive properties include saturation magnetization, Curie temperature, crystalline anisotropy and magnetostriction. These are dependent on atomic structure and chemical composition of the material. The properties which are considered to be secondary and influenced by the microstructure and internal condition of the material are coercive force, permeability, residual magnetization, and hysteresis loss.

A "soft" magnetic material can be magnetized to saturation and then demagnetized by the application of rather weak magnetic fields. The ideal soft magnetic material for a power application would have high permeability, high saturation and residual magnetizations, low coercive force, high electrical resistivity, low losses, high degree of preferred grain orientation, and low crystal anisotropy and magnetostrictive constants.

Since the coercive force is the strength of reverse field which has to be applied to demagnetize a previously magnetized sample, it is an excellent indicator of the "softness" of a magnetic material.

The saturation magnetization of dispersion-strengthened alloys might be expected to decrease in proportion to the amount of non-magnetic, insoluble dispersed phase added.

The coercive force, H_c, was measured directly on this program using a Precision Coercive Force Meter, Manufactured by Institute Förster Reutlingen, West Germany (ref. IV-51). The specimen was magnetized in a field of 1300 oersteds in a large field coil. After switching off the field, the remanent field of the specimen was picked up by a sensitive field probe and a reverse field gradually applied until the field probe measured no remanent field coming from the specimen. For tests

at 1200° to 1600° F, a tube furnace with electrical resistance heating coil of platinum - 10 percent rhodium wire, bifilar wound, was placed inside the field coil of the coercive force meter. A flow of 99.996 percent purity argon was maintained through the tube to protect the specimen against oxidation. The specimen was held at temperature for five minutes before its coercive force was measured. Alternating current was supplied to the furnace during measurements. The accuracy of the coercive force values at all temperatures was plus or minus two percent or better, while the temperature was held within plus or minus 10° F of that intended, as indicated by a thermocouple. Measurements were made on standard specimens at the start and end of each series of tests for verification of test procedure.

The specific saturation was measured on a 0.1-inch diameter by 0.1-inch long specimen weighing approximately 0.1 gram. The length was short in order to avoid too high demagnetizing forces. The saturation was measured by means of a magnetic balance in a field gradient of 975 oersteds per centimeter with a mean applied magnetizing field of 11,500 oersteds (ref. IV-52). Actually, even this high a field is not enough to reach saturation in cobalt alloys at room temperature. It has been reported that 17,000 oersteds are required for pure cobalt (ref. IV-53). The magnet was supplied by Varian Associates, Model V-4007. The specimen was sealed in a quartz tube which was evacuated and back-filled with 99.996 percent purity argon to a pressure of 100 mm of mercury. The quartz tube was attached to a transducer gauge supplied by Statham Transducer Inc. The force acting on the specimen due to the applied magnetic field was determined. For measurements above room temperature, a small furnace slightly under 1-inch outside diameter by 0.25-inch inside diameter by 3 inches long, bifilar wound with platinum - 10 percent rhodium wire was used. During saturation measurement, alternating current was supplied to the furnace. The temperature was checked by placing a separate thermocouple inside the furnace at the position of the specimen to be measured. The temperature was controlled to better than plus or minus 10° F. The accuracy of the saturation values was plus or minus one percent. The holding time at elevated temperature before testing was five minutes. A standard iron or cobalt specimen was measured at the start and end of each series of experimental compositions for calibration purposes. The saturation magnetization, B_S, in guass was calculated from the specific saturation, (saturation magnetic moment), σ_S, from the equation:

$$B_S = 4\pi\delta\sigma_S$$

where:

δ = density in g/cm^3

σ_S = saturation magnetic moment, emu/g

e. TENSILE TESTING

The tensile specimens were tested in an Instron Universal Testing Instrument, Model TTC. For the elevated temperature tests, a Satec Power Positioning Furnace, Model RA-1800 with a Kanthal-Al heating element was used to heat the specimen under vacuum to temperature. The specimens were tested in a vacuum of 0.9 to 2.6×10^{-5} torr using a liquid nitrogen trap after stabilizing at the test temperature for half an hour. A strain rate of 0.005 inch per inch per minute was used up to the yield stress (0.2 percent offset) and 0.05 inch per inch per minute beyond that to fracture. Prior to tensile testing, elevated temperature test specimens were rough machined and aged 100 hours at the test temperature to stabilize the dispersoid and matrix structure in a vacuum of 1×10^{-5} torr or better (mainly 1×10^{-6} torr). It was decided to age at the test temperature, rather than at some higher temperature, before testing because the thermal stability of some compositional systems were largely unknown. The iron+27w/o cobalt-base systems had a phase transformation at 1770° F, and might be expected to be prone towards recrystallization and grain growth at temperatures approaching this. Therefore, it was necessary to restrict the aging temperature to something below 1770° F in the early part of the investigation in order to have a valid comparison between cobalt-base and iron+27w/o cobalt-base compositions.

f. VACUUM CREEP TESTING

Vacuum creep testing was performed at the Westinghouse Research and Development Center in a spring-loaded machine developed by M. J. Manjoine. The specimen and holders were enclosed in an Inconel capsule with bellows at one end and heated by an external electrical resistance furnace. Thermocouples were located at the radius of the shoulders and in the center of the gage length of the specimen. Temperature distribution over the length of the specimen was maintained within 5° F.

The temperature fluctuation during the course of testing was ±3° F. A vacuum of less than $1x10^{-6}$ torr (10^{-7} torr range) was held during heating to temperature and testing using a diffusion pumped system with a liquid nitrogen trap. The capsule was pumped out overnight to less than $1x10^{-6}$ torr and the specimen was brought up to temperature and stabilized over approximately a four hour period before the load was applied. The creep strain was computed over the gage length of the specimen from measurements made at room temperature between punch marks on the shoulders using a toolmakers traveling microscope.

D. RESULTS AND EVALUATION

1. Comparison of Chemical Analyses of Extrusions and Powders (Phases 1, 2, and 3)

Chemical analyses were determined on a total of 10 extrusions made from powder during the course of the program. There was generally good agreement between the chemical analyses of the extrusions (as determined by Westinghouse), the chemical analyses of the powders (as reported by the powder suppliers), and the intended compositions (as defined by the Westinghouse compositional target limits). The results are presented in table IV-13.

In regard to the prealloyed atomized powder target specifications, it was stated earlier that the chemical analyses reported by the two suppliers, Hoeganaes Sponge Iron Corporation and Domtar Chemicals Limited, indicated that the impurities Mn and Si were high in the cobalt-base powders. It was necessary in some instances for the supplier to add intentionally Mn and Si, usually in amounts of approximately 0.25 percent each, in order to increase fluidity and achieve proper flow of the molten metal through the atomizing nozzle.

The Mn content of the extrusion of cobalt-base internally oxidized atomized powder No. 8 exceeded the target specification limit. The Si contents of the extrusions of cobalt-base atomized powder No. 5, and internally oxidized powders Nos. 8 and 9 were also high. Extrusions of atomized powder Nos. 5 and 13, internally oxidized powder Nos. 9 and 18, and composite powder No. 11 from Chas. Pfizer were somewhat in excess of the target limits for C. The extrusions of cobalt-base composite powder Nos. 3 from Chas. Pfizer, and 13 and 14 from Sherritt Gordon were high in S. No detrimental effects on magnetic or mechanical properties were identified with the fact that the impurity contents of some of the extrusions in table IV-13 were slightly higher than the original goals.

The concentrations of the alloying elements and dispersed thoria in the extrusions in table IV-13 were generally close to the intended values. However, the beryllium content of the extrusion made from the internally oxidized powder No. 9 was analyzed by Westinghouse to be 0.69 w/o compared with 1.94 w/o for the original powder before oxidation, as reported by Domtar Chemicals Limited. No reason was found to explain this anomaly. Small amounts of free Th(not combined as ThO_2) were detected in all extrusions of the composite powders.

The presence of 0.05 w/o to 0.15 w/o (500 to 1500 ppm) of oxygen in the original prealloyed atomized powders might be anticipated from oxygen analyses reported for nickel-base and iron-base prealloyed atomized powders (ref. IV-54 to IV-57). Furthermore, only the -325 mesh fraction, which would have a high specific surface area, was used on this program. Thus, rather substantial amounts of oxygen were present in the original atomized powders. This oxygen had to be removed during subsequent hydrogen reduction and sintering before extrusion if internal oxidation of the more reactive alloying elements (beyond that which might have occurred in making of the atomized powders) was to be avoided. The substitution of completely welded Inconel 600 retorts for the mechanical-seal arrangement used during the preliminary evaluation (phase 1) was employed as a method of further insuring minimum dew points during hydrogen reduction of the powders and sintering of the powder compacts.

The oxygen contents of prealloyed atomized powder extrusions Nos. 5 (Co+1.0w/oB+4.2w/oCb) and 13 (Fe+25.6w/oCo+1.0w/oB+4.2w/oZr) in table IV-13 were analyzed during the first phase of the program, and found to be 1300 and 1850 ppm, respectively. The oxygen content of the latter extrusion was especially high. Also, its nitrogen content (660 ppm) was higher by an order of magnitude than that of any other extruded composition analyzed on this program. An x-ray powder diffraction investigation conducted on the original -325 mesh fraction of powder No. 13 as received from the supplier showed that some of the zirconium alloying element was already present as ZrO_2, while the rest was in a complex boride compound (containing boron, zirconium, cobalt, and probably iron) having the $Cr_{23}C_6$ type of crystal structure (refs. IV-58 to IV-60). Diffraction patterns of the extrusion made from the powder revealed that the complex boride compound was no longer present, but that $(Fe, Co)_2B$ and ZrO_2 were the final dispersed phases. No nitrides were detected.

In view of the oxidation of zirconium, it was decided to investigate additional prealloyed atomized powders (-325 mesh) in the following list by x-ray diffraction in order to determine if other reactive alloying elements were present as oxides (or nitrides) in the original powders.

Atomized Powder No.	Nominal Composition (weight percent)	Powder Supplier
5	Co+1.0B+4.2Cb	Hoeganaes Sponge Iron Corp.
9(a)	Co+1.3Be	Domtar Chemicals Ltd.
16	Fe+25.9Co+4.0Ce	Domtar Chemicals Ltd.
17(a)	Fe+26.3Co+2.7Al	Hoeganaes Sponge Iron Corp.
18(a)	Fe+26.6Co+1.4Be	Domtar Chemicals Ltd.
19(b)	Fe+24.8Co+8.3Zr	Hoeganaes Sponge Iron Corp.

(a) Used later for internal oxidation treatment.

(b) Powder obtained for the intermediate evaluation portion (phase 2) of the program. All other powders obtained for phase 1.

The diffraction patterns of the preceding atomized powders without Zr did not reveal the presence of any oxides (or nitrides), and it was concluded that the alloying elements were either in solid solution or in the form of intermetallic compounds. However, atomized powder No. 19 containing Zr was indicated to contain a substantial amount of ZrO_2, but no nitrides.

Zirconium was found to be the most reactive element with oxygen during atomized powder-making and processing in this program--more reactive than cerium, aluminum, or beryllium. This was contrary to expectations based on the thermodynamic free energy of formation (ref. IV-61).

The presence of ZrO_2 in atomized powder No. 13 and the extruded form indicated that such a composition, probably with higher zirconium content, should be considered for a ZrO_2 dispersion-strengthened product. This was done on the intermediate evaluation portion (phase 2) of the program with prealloyed atomized powder No. 19.

It should be noted that all prealloyed atomized powders obtained for this program from both suppliers were made by essentially the same process. The metal charge was melted under argon and the molten metal stream was broken up into discrete particles which were cooled and solidified very rapidly by water jets in a large tank filled with nitrogen.

TABLE IV-13. - Chemical Analyses of Extrusions

Powder or Extrusion No.	Powder Supplier	Intended Composition or Analysis	Mn	Si	C	S	P
a. Prealloyed Atomized Powders							
5.	Hoeganaes	Intended Composition[a]	0.04 max.	0.04 max.	0.020 max.	0.006 max.	0.010 m
		Powder Analysis[b]	0.19	0.04	0.043	0.007	<0.005
		Extrusion Analysis[c]	0.02[d]	0.10	0.048	0.006	<0.001
13.	Hoeganaes	Intended Composition[a]	0.50 max.	0.25 max.	0.020 max.	0.025 max.	0.015 m
		Powder Analysis[b]	0.11	0.22	0.023	0.011	<0.005
		Extrusion Analysis[c]	0.30	0.23	0.048	0.007	0.005
19.	Hoeganaes	Intended Composition[a]	0.50 max.	0.25 max.	0.020 max.	0.025 max.	0.015 m
		Powder Analysis[b]	0.23	0.033	0.018	0.021	<0.005
		Extrusion Analysis[c]	0.25	<0.03	0.010	0.021	0.003
b. Internally Oxidized Prealloyed Atomized Powders							
8.	Hoeganaes	Intended Composition[a][e]	0.04 max.	0.04 max.	0.020 max.	0.006 max.	0.010 m
		Powder Analysis[b][e]	0.22	0.27	0.009	0.004	<0.005
		Extrusion Analysis[c][f]	0.5[d]	0.18	0.013	0.005	<0.001
9.	Domtar	Intended Composition[a][e]	0.04 max.	0.04 max.	0.020 max.	0.006 max.	0.010 m
		Powder Analysis[b][e]	<0.05	0.012	0.028	<0.002	0.010
		Extrusion Analysis[c][f]	0.02[d]	0.10	0.047	0.002	0.004
18.	Domtar	Intended Composition[a][e]	0.50 max.	0.25 max.	0.020 max.	0.025 max.	0.015 m
		Powder Analysis[b][e]	<0.1	0.08	0.026	<0.002	<0.005
		Extrusion Analysis[c][f]	0.04	0.14	0.026	0.008	0.006
c. Composite Powders							
3.	Pfizer	Intended Composition[a]	0.04 max.	0.04 max.	0.020 max.	0.006 max.	0.010 m
		Powder Analysis[b]	--	--	--	--	--
		Extrusion Analysis[c]	0.02[d]	<0.02	0.019	0.011	<0.001
11.	Pfizer	Intended Composition[a]	0.50 max.	0.25 max.	0.020 max.	0.025 max.	0.015 m
		Powder Analysis[b]	--	--	--	--	--
		Extrusion Analysis[c]	0.21	<0.02	0.044	0.017	<0.001
13.	Sherritt Gordon	Intended Composition[a]	0.04 max.	0.04 max.	0.020 max.	0.006 max.	0.010 m
		Powder Analysis[b]	--	--	0.035	0.032	--
		Extrusion Analysis[c]	<0.005	<0.03	0.008	0.025	0.003
14.	Sherritt Gordon	Intended Composition[a]	0.04 max.	0.04 max.	0.020 max.	0.006 max.	0.010 ma
		Powder Analysis[b]	--	--	0.040	0.032	--
		Extrusion Analysis[c]	<0.005	<0.03	0.010	0.025	0.001

(a) Westinghouse target limits.
(b) Analysis reported by powder supplier.
(c) Analysis made by Westinghouse.
(d) Emission spectrographic semi-quantitative analysis.
(e) Before internal oxidation treatment.
(f) After internal oxidation treatment.

ompared with Analyses of Original Powders

ient (weight percent)

Ni	Cr	Co	Fe	B	Ti	Zr	ZrO_2
). 70 max.	--	94. 8	--	1. 0±0. 2	--	--	--
). 58	0. 02	93. 11	0. 21	1. 1	--	--	--
). 8(d)	0. 2(d)	Remainder	0. 4(d)	1. 14	< 0. 01(d)	< 0. 02(d)	--
). 70 max.	--	25. 6±1. 5	69. 2±2. 0	1. 0±0. 2	--	4. 2±0. 8	--
). 12	0. 064	24. 75	69. 73	1. 1	--	3. 24(j)	--
). 09	0. 026	24. 4	69. 5	1. 33	0. 03(d)	3. 40(j)	--
). 70 max.	--	24. 8±1. 5	66. 9±2. 0	--	--	8. 3±0. 8	--
). 0	--	23. 68	66. 97	--	--	7. 29(j)	--
0. 74	0. 001	24. 1	Remainder	< 0. 1(d)	0. 1(d)	7. 10(j)	4. 65(k)
0. 70 max.	--	97. 5	--	--	--	--	--
0. 29	0. 022	95. 59	0. 97	--	--	--	--
0. 7(d)	0. 1(d)	Remainder	1(d)	0. 01(d)	0. 4(d)	0. 5(d)	--
0. 70 max.	--	98. 7	--	--	--	--	--
0. 48	0. 07	97. 7	Not detected	--	--	--	--
1(d)	0. 2(d)	Remainder	0. 6(d)	0. 01(d)	< 0. 01(d)	< 0. 02(d)	--
0. 70 max.	--	26. 6±1. 5	72. 0±2. 0	--	--	--	--
0. 05	< 0. 1	27. 9	70. 0	--	--	--	--
0. 8(d)	0. 1(d)	27. 3	Remainder	0. 02(d)	< 0. 01(d)	0. 3(d)	--
0. 70 max.	0. 10 max.	Remainder	--	--	--	--	--
--	--	--	--	--	--	--	--
0. 3(d)	< 0. 05(d)	Remainder	0. 06(d)	0. 02(d)	< 0. 01(d)	< 0. 02(d)	--
0. 70 max.	0. 10 max.	23. 7±1. 5	64. 2±2. 0	--	--	--	--
--	--	--	--	--	--	--	--
0. 2(d)	< 0. 05(d)	23. 5	Remainder	0. 01(d)	< 0. 01(d)	< 0. 02(d)	--
0. 70 max.	0. 10 max.	Remainder	--	--	--	--	--
0. 09	--	95. 5	--	--	--	--	--
0. 023	0. 002	Remainder	0. 037	< 0. 1(d)	< 0. 1(d)	--	--
0. 70 max.	0. 10 max.	Remainder	--	--	--	--	--
0. 08	--	91. 1	--	--	--	--	--
0. 020	0. 001	Remainder	0. 051	< 0. 1(d)	< 0. 1(d)	--	--

r) Includes 0. 04 percent soluble aluminum and 2. 74 percent insoluble aluminum.
i) Determined by vacuum fusion using platinum bath at 3542°F (1950°C).
) Both Th and ThO_2 were determined by an X-ray fluorescence method. Th is that found by dissolving sample in 1 water: $3HNO_3$ solution.
i) Determined by wet analysis.
:) Calculated from 3. 44 percent insoluble Zr content which was determined.

TABLE IV-13. - Continued. Chemical Analyses of

Powder or Extrusion No.	Powder Supplier	Intended Composition or Analysis	Cb	Al	Al_2O_3	Be
a. Prealloyed Atomized Powders						
5.	Hoeganaes	Intended Composition[a]	4.2±0.8	--	--	--
		Powder Analysis[b]	4.38	--	--	--
		Extrusion Analysis[c]	4.03	0.01[d]	--	--
13.	Hoeganaes	Intended Composition[a]	--	--	--	--
		Powder Analysis[b]	--	--	--	--
		Extrusion Analysis[c]	--	0.2[d]	--	<0.001[d]
19	Hoeganaes	Intended Composition[a]	--	--	--	--
		Powder Analysis[b]	--	--	--	--
		Extrusion Analysis[c]	--	<0.1[d]	--	--
b. Internally Oxidized Powders						
8.	Hoeganaes	Intended Composition[a][e]	--	2.5±0.5	--	--
		Powder Analysis[b][e]	--	2.46[j]	4.64[l]	--
		Extrusion Analysis[c][f]	--	2.78[g][j]	5.18[m]	--
9.	Domtar	Intended Composition[a][e]	--	--	--	1.3±0.3
		Powder Analysis[b][e]	--	--	--	1.94[j]
		Extrusion Analysis[c][f]	--	0.2[d]	--	0.69[j]
18.	Domtar	Intended Composition[a][e]	--	--	--	1.4±0.3
		Powder Analysis[b][e]	--	--	--	1.4[j]
		Extrusion Analysis[c][f]	--	0.05[d]	--	1.14[j]
c. Composite Powders						
3.	Pfizer	Intended Composition[a]	--	--	--	--
		Powder Analysis[b]	--	--	--	--
		Extrusion Analysis[c]	--	0.3[d]	--	--
11.	Pfizer	Intended Composition[a]	--	--	--	--
		Powder Analysis[b]	--	--	--	--
		Extrusion Analysis[c]	--	0.3[d]	--	--
13.	Sherritt Gordon	Intended Composition[a]	--	--	--	--
		Powder Analysis[b]	--	--	--	--
		Extrusion Analysis[c]	--	<0.1[d]	--	--
14.	Sherritt Gordon	Intended Composition[a]	--	--	--	--
		Powder Analysis[b]	--	--	--	--
		Extrusion Analysis[c]	--	<0.1[d]	--	--

(a) Westinghouse target limits.
(b) Analysis reported by powder supplier.
(c) Analysis made by Westinghouse.
(d) Emission spectrographic semi-quantitative analysis.
(e) Before internal oxidation treatment.
(f) After internal oxidation treatment.
(g) Includes 0.04 percent soluble aluminum and 2.74 percent insoluble aluminum.

Extrusions Compared with Analyses of Original Powders

Element (weight percent)							
BeO	Th[i]	ThO_2[i]	O[h]	N	Cu	Ca	Mg
--	--	--	--	--	--	--	--
--	--	--	--	--	--	--	--
--	--	--	0.13	0.0008	0.3[d]	<0.01[d]	0.01[d]
--	--	--	--	--	--	--	--
--	--	--	--	--	--	--	--
--	--	--	0.185	0.066	0.2[d]	<0.01[d]	<0.01[d]
--	--	--	--	--	--	--	--
--	--	--	--	--	--	--	--
--	--	--	1.23	0.0057	<0.1[d]	<0.1[d]	<0.1[d]
--	--	--	--	--	--	--	--
--	--	--	--	--	--	--	--
--	--	--	2.24	0.0006	0.2[d]	<0.01[d]	0.01[d]
--	--	--	--	--	--	--	--
--	--	--	--	--	--	--	--
5.38[n]	--	--	--	--	--	--	--
1.81[n]	--	--	0.85	0.0012	0.2[d]	<0.01[d]	<0.01[d]
--	--	--	--	--	--	--	--
3.9[n]	--	--	--	--	--	--	--
3.16[n]	--	--	1.55	<0.0005	0.2[d]	0.2[d]	<0.01[d]
--	--	11.2±1.5	--	--	--	--	--
--	--	--	--	--	--	--	--
--	0.25	11.2	1.31	<0.0005	0.2[d]	0.5[d]	0.01[d]
--	--	12.1±1.5	--	--	--	--	--
--	--	--	--	--	--	--	--
--	0.07	12.5	1.52	0.0032	0.1[d]	0.5[d]	0.08[d]
--	--	4.52±0.50	--	--	--	--	--
--	--	4.2	--	--	--	--	--
--	0.02	4.00	0.49	<0.0005	<0.1[d]	<0.1[d]	<0.1[d]
--	--	8.41±0.50	--	--	--	--	--
--	--	8.6	--	--	--	--	--
--	0.08	8.29	0.98	0.0007	<0.1[d]	<0.1[d]	<0.1[d]

(h) Determined by vacuum fusion using platinum bath at 3542°F (1950°C).
(i) Both Th and ThO_2 were determined by an X-ray fluorescence method. Th is that found by dissolving sample in 1 water: $3HNO_3$ solution.
(j) Determined by wet analysis.
(k) Calculated from 3.44 percent insoluble Zr content which was determined.
(l) Calculated from 2.46 percent total Al content which was determined.
(m) Calculated from 2.74 percent insoluble Al content which was determined.
(n) Calculated from total Be contents, as given in preceding column, which were determined.

Table IV-14 gives the oxide and oxygen contents of eight oxide dispersion-strengthened extrusions made from prealloyed atomized, internally oxidized, and composite powders. The total oxygen contents measured by vacuum fusion were in quite good agreement with the combined oxygen values calculated from the ZrO_2, Al_2O_3, BeO, and ThO_2 contents. In the case of the internally oxidized powder Nos. 8, 9, and 18, the difference between the measured and calculated oxygen contents was greater (and indicated a deficiency of oxygen) than for the composite powder Nos. 3, 11, 13, and 14. However, the good agreement between the measured and calculated oxygen values for the internally oxidized materials provided evidence that, where internal oxidation and subsequent hydrogen reduction treatments had been applied to powders, the oxidation of the aluminum and beryllium alloy additions was substantially complete, and oxides of cobalt and iron had been reduced.

The residual nitrogen contents of these extrusions were low, table IV-13.

2. Microstructure of Hot-Extruded and Secondary Worked Compositions (Phases 1, 2, and 3)

As mentioned earlier, the dispersoid types and compositions, volume percentages, particle sizes, and interparticle spacings were varied over a wide range in cobalt-base and iron +27w/o cobalt-base matrices in this program in order to evaluate their effect on soft magnetic properties, as indicated by changes in coercive force, and to a lesser extent on mechanical properties. The dispersoid parameters were expected to have important effects on the matrix grain structure, response to secondary working treatments applied to hot-extruded material, and thermal stability of the dispersoid and matrix structure.

A summary of the microstructural parameters measured or carefully estimated through comparative photomicrographs at 1000 to 1500X on compositions extruded with a conventional hydraulic press are given in tables IV-15 and IV-16. Some of the microstructural parameters were re-measured more precisely on electron micrographs of seven of the more important compositions and powder types. Although these parametric values are mainly only approximate, they were regarded as satisfactory and useful for purposes of semi-quantitative correlation with magnetic and mechanical properties. Secondary working of the hot-extruded compositions caused no significant change in average effective particle size and average interparticle spacing of the dispersoid.

TABLE IV-14. Oxygen Contents of Oxide Dispersion-Strengthened Extrusions

Powder or Extrusion No.	Intended Composition (weight percent)	Oxide Forming Element (weight percent)	Oxide (weight percent)	Calculated Oxygen (O) Combined as Oxide (weight percent)	Measured Total Oxygen (O) (weight percent)	Difference Between Measured and Calculated Oxygen (O) (weight percent)
a. Prealloyed Atomized Powders (Extruded)						
19.	Fe+24.8Co+8.3Zr	3.44Zr[g]	4.65ZrO_2[h]	1.21	1.23	+0.02 (excess)
b. Internally Oxidized Powders (Extruded)						
8.	Co+4.7Al_2O_3	2.74Al[a]	5.18Al_2O_3[b]	2.44	2.24	-0.20 (deficiency)
9.	Co+3.6BeO	0.69Be[c]	1.91BeO[d]	1.22	0.85	-0.37 (deficiency)
18.	Fe+26.0Co+3.9BeO	1.14Be[c]	3.16BeO[e]	2.02	1.55	-0.47 (deficiency)
c. Composite Powders (Extruded)						
3.	Co+11.2ThO_2 (Pfizer)	--	11.2ThO_2[f]	1.36	1.31	-0.05 (deficiency)
11.	Fe+23.7Co+12.1ThO_2 (Pfizer)	--	12.5ThO_2[f]	1.51	1.52	+0.01 (excess)
13.	Co+4.5ThO_2 (Sherritt Gordon)	--	4.00ThO_2[f]	0.48	0.49	+0.01 (excess)
14.	Co+8.4ThO_2 (Sherritt Gordon)	--	8.29ThO_2[f]	1.00	0.98	-0.02 (deficiency)

(a) Determined as insoluble Al. The soluble Al was 0.04 percent.
(b) Equivalent to 2.74 percent insoluble Al.
(c) Determined as total Be.
(d) Equivalent to 0.69 percent total Be.
(e) Equivalent to 1.14 percent total Be.
(f) Determined as ThO_2 by X-ray flourescence.
(g) Determined as insoluble Zr.
(h) Equivalent to 3.44 percent insoluble Zr.

TABLE IV-15. Approximate Values of Microstructural Parameters for Hydraulic Extrusions Obtained for Initial Evaluation Effort (Phase 1)

Powder or Extrusion No.	Nominal Composition (weight percent)	Amount of Dispersed Phase (percent by volume)	Average Effective Size of Dispersed Particles[g] (microns)	Average Interparticle Spacing (microns)	Degree of Recrystallization (percent)	Average Grain Size (Approx.) (microns)	Amount of Porosity (percent)
a. Prealloyed Atomized Powders (Extruded)							
3	Co+1.0B+2.2Ti	32	1.5	3.2	(d)	5	2
4	Co+1.0B+4.2Zr	26	0.95	2.7	(d)	5	2
5	Co+1.0B+4.2Cb	27	0.75	2.0	(d)	5	2
6	Co+1.0B+8.3Ta	27	0.73	2.0	(d)	5	2
12	Fe+26.1Co+1.0B+2.2Ti	20	1.6	6.4	Complete[e]	20	2
13	Fe+25.6Co+1.0B+4.2Zr	20	0.90	3.6	Complete[e]	20	2
14	Fe+25.6Co+1.0B+4.2Cb	20	0.77	3.1	Complete[e]	20	2
15	Fe+24.5Co+1.0B+8.3Ta	21	0.74	2.8	Complete[e]	20	2
b. Internally Oxidized Powders (Extruded)							
8	Co+4.7Al_2O_3	9.8	0.3[f]	2.8	(d)	4	2
9 and 9A	Co+3.6BeO	8.3	0.3[f]	3.3	(d)	4	2
17	Fe+25.6Co+5.1Al_2O_3	8.4	1.0	10.9	Complete[e]	25	2
18	Fe+26.0Co+3.9BeO	9.6	0.3[f]	2.8	Complete[e]	10	2
c. Composite Powders (Extruded)							
3	Co+11.2ThO_2(0.01-0.06μ), Sherritt Gordon	10	0.1[f]	0.9	(d)	4	2
11	Fe+23.7Co+12.1ThO_2(0.01-0.06μ), Vitro Labs	10	1.1	9.9	Complete[e]	30	2
1	Co+4.75Al_2O_3(0.01-0.06μ), Chas. Pfizer	10	0.2[f]	1.8	(d)	5	2
2	Co+4.75Al_2O_3(0.1-0.6μ), Chas. Pfizer	10	0.6[f]	5.4	(d)	12	2
3	Co+11.2ThO_2(0.01-0.06μ), Chas. Pfizer	10	0.2[f]	1.8	(d)	5	2
4	Co+11.2ThO_2(0.1-0.6μ), Chas. Pfizer	10	0.3[f]	2.7	(d)	7	2
11	Fe+23.7Co+12.1ThO_2(0.01-0.06μ), Chas. Pfizer	10	0.3[f]	2.7	Complete[e]	10	2
d. Supplier Extrusions of Dispersion-Strengthened Cobalt							
3(b)	Co+11.2ThO_2(0.01-0.06μ ThO_2)	9.3	0.1[f]	1.0	(d)	2	2
9(c)	Co+2.3ThO_2(0.01-0.06μ ThO_2)	1.8	0.1[f]	5.5	(d)	5	0-1
9(a)(c)	Co+2.3ThO_2(0.01-0.06μ ThO_2)	1.8	0.1[f]	5.5	(d)	-	0-1

(a) Given 85 percent cold reduction by swaging after hot extrusion. All other material in hot extruded condition.
(b) Extrusion supplied by New England Materials Laboratory, Inc., Medford, Massachusetts.
(c) Extrusion supplied by Curtiss-Wright Corp., Metals Processing Division, Buffalo, New York.
(d) Cobalt undergoes phase transformation at 783°F from cubic to hexagonal structure on cooling. These materials were partially transformed and contained a mixture of hexagonal and cubic cobalt at room temperature.
(e) Iron-cobalt matrix undergoes phase transformation at approximately 1770°F from face centered cubic to body centered cubic on cooling.
(f) Estimated value from observations under light microscope and on photomicrographs. Could not be measured with light microscope.
(g) No evidence of lack of bonding between the dispersed phase and the matrix was found.

TABLE IV-16. Approximate Values of Microstructural Parameters for Hydraulic Extrusions Obtained for Intermediate and Final Evaluation Efforts (Phases 2 and 3)

Powder or Extrusion No.	Nominal Composition (weight percent)	Amount of Dispersed Phase (percent by volume)	Average Effective Size of Dispersed Particles (microns)	Average Interparticle Spacing (microns)	Degree of Recrystallization (percent)	Average Grain Size (approx.) (microns)	Amount of Porosity (percent)
a. Prealloyed Atomized Powders (Extruded)							
19	Fe+24.8Co+8.3Zr	(d)	0.3(c)	3.0	Complete(b)	18	0
30	Co+0.8B+3.2Cb	20	0.77	3.1	(a)	8	2
b. Composite Powders (Extruded)							
13	$Co+4.5ThO_2$(0.01-0.06μ), Sherritt Gordon	4	0.1(c)	2.4	(a)	6	2
14	$Co+8.4ThO_2$(0.01-0.06μ), Sherritt Gordon	7.5	0.1(c)	1.2	(a)	4	2
13	$Co+4.5ThO_2$(0.01-0.06μ), Chas. Pfizer	4	0.2(c)	4.8	(a)	6	2
14	$Co+8.4ThO_2$(0.01-0.06μ), Chas. Pfizer	7.5	0.2(c)	2.5	(a)	4	2
15	$Fe+24.5Co+9.3ThO_2$(0.01-0.06μ), Chas. Pfizer	7.5	0.3(c)	3.7	Complete(b)	12	2

(a) Cobalt undergoes phase transformation at 783°F from cubic to hexagonal structure on cooling. These materials were partially transformed and contained a mixture of hexagonal and cubic cobalt at room temperature.
(b) Iron-cobalt matrix undergoes phase transformation at approximately 1770°F from face centered cubic to body centered cubic on cooling.
(c) Estimated value from observations under light microscope and on photomicrographs. Could not be measured with light microscope.
(d) 6.4 v/o ZrO_2 + 14 v/o coarse, elongated Fe-Co-Zr constituent.

In regard to the three prealloyed atomized powder compositions extruded by Dynapak (Nos. 4, 13, and 14), the size of the dispersed particles and the interparticle spacing were approximately 30 percent less than in the hydraulic extrusions.

All of the Fe+Co-base extrusions made on this program from prealloyed atomized, internally oxidized, and composite powders had a recrystallized grain structure and a coarser grain size than the Co-base extrusions. This was also true for the Dynapak extrusions of the three prealloyed atomized powders. These were extruded at 1600° F which is below the 1770° F transformation temperature of the Fe+27w/o Co matrix.

The matrix of cobalt-base extrusions at room temperature consisted of a mixture of hexagonal and face centered cubic cobalt of fine grain size.

Complete densification of the powders by hydraulic extrusion was essentially accomplished, since only about two percent maximum of internal porosity was noted.

a. IDENTIFICATION OF DISPERSOIDS BY X-RAY DIFFRACTION

X-ray diffraction studies performed on hydraulic extrusions of the compositions listed in table IV-17 identified and confirmed the secondary phases present in the matrix. In the cobalt-base alloys made from prealloyed atomized powders, some of these constituent particles belonged to the family of ternary borides called tau which have the $Cr_{23}C_6$ structure ($D8_4$ structure type) and are represented by $T_{23-m}M_mB_n$, where T is Co, and M is one of the following: Ti, Zr, Cb or Ta, (refs. IV-58 to IV-60). Roughly, m ranges from 2 to 3.5 and n from 5 to 12. The composition of the cobalt-columbium boride is $Co_{21}Cb_2B_6$ and that of the cobalt-tantalum boride is $Co_{21}Ta_2B_6$ at 800° C (1472° F). In the isothermal sections of the ternary diagrams no tie lines run in the direction from Co to the diborides CbB_2 and TaB_2. The tau ternary borides crystallize congruently from the melt and are reported to have microhardness values somewhat above hardened steel (ref. IV-58). Table IV-17 shows that in addition to the tau ternary boride, a relatively small amount of ZrO_2 (monoclinic) was present in the extrusion of cobalt-base atomized powder No. 4, while a small amount of an unidentified phase was in No. 5.

Unlike cobalt-base alloys, no $D8_4$ type borides (tau) have been reported with iron, although ternary iron carbides and an iron carbo-boride with this structure have been reported in the literature. In the case of the extrusion of prealloyed atomized powder No. 13, Fe+25.6w/oCo+1.0w/oB+4.2w/oZr, the ZrO_2 and $(Fe, Co)_2B$ secondary phases were present. The original atomized powder No. 13 did contain ZrO_2 and the tau boride. In this case the tau boride may have appeared as a non-equilibrium phase in the powder, which underwent very rapid cooling from the liquid state during manufacture. Another explanation might be that the zirconium in the tau boride reacted with oxygen during powder processing into an extrusion until it was completely tied up as ZrO_2, leading to the disappearance of the tau boride and the formation of $(Fe, Co)_2B$.

The extrusion of atomized powder No. 19 contained ZrO_2 (monoclinic) and another secondary phase(s). Although the latter could not be identified by the ASTM file system, it undoubtedly was an intermetallic compound or compounds of Fe, Co, and Zr.

TABLE IV-17. X-Ray Diffraction Identification of Dispersed Constituent Particles in Extrusions

Powder Type	Powder Supplier	Nominal Composition (weight percent)	Dispersed Phases Identified In Extrusions
Atomized No. 4	Hoeganaes	Co+1.0B+4.2Zr	Tau Ternary Boride and ZrO_2
Atomized No. 5	Hoeganaes	Co+1.0B+4.2Cb	Tau Ternary Boride(c)
Atomized No. 13	Hoeganaes	Fe+25.6Co+1.0B+4.2Zr	$(Fe, Co)_2B$ and ZrO_2
Atomized No. 19	Hoeganaes	Fe+24.8Co+8.3Zr	ZrO_2(c)
Internally Oxidized No. 8(a)	Hoeganaes	Co+4.7Al_2O_3	Alpha-Al_2O_3
Internally Oxidized No. 9(b)	Domtar	Co+3.6BeO	BeO
Internally Oxidized No. 17(a)	Hoeganaes	Fe+25.6Co+5.1 Al_2O_3	Alpha-Al_2O_3
Internally Oxidized No. 18(b)	Domtar	Fe+26.0Co+3.9BeO	BeO
Composite No. 11	Chas. Pfizer	Fe+23.7Co+12.1 ThO_2	ThO_2

(a) Prealloyed atomized powder obtained from Hoeganaes and internally oxidized by Westinghouse.
(b) Prealloyed atomized powder obtained from Domtar Chemicals Ltd. and internally ozidized by Westinghouse.
(c) Contained small amount of unidentified phase or phases also.

The dispersed phases in the extrusions of internally oxidized and composite powders in table IV-17 were those expected. In the case of the internally oxidized powders, the x-ray study provided additional evidence beyond the oxygen and oxide values determined by chemical analysis on extrusions that the internal oxidation and subsequent hydrogen reduction treatments had accomplished their purpose. Oxidation of the aluminum and beryllium alloying elements was achieved, and the cobalt and iron oxides were reduced back to metal prior to extrusion.

b. MICROSTRUCTURE OF PREALLOYED ATOMIZED POWDER COMPOSITIONS

The cobalt-base and iron+27w/o cobalt-base prealloyed atomized powders containing boron, titanium, zirconium, columbium, and tantalum contained the greatest amount of dispersed phase, up to 32 percent by volume. The average dispersoid particle size ranged around one micron. The particles were evenly distributed throughout the matrix.

Figure IV-10 shows a photomicrograph and figure IV-11 an electron micrograph of the Co+1.0w/oB+4.2w/oCb hydraulic extrusion containing 27v/o dispersoid. The larger, clear constituent particles were identified by diffraction studies to be the tau ternary boride, while the small amount of finer constituent particles remained unidentified.

The larger, clear particles in figures IV-12 and IV-13 of the Fe+25.6w/oCo+1.0w/oB+4.2w/oZr hydraulic extrusion containing 20v/o dispersoid were $(Fe, Co)_2B$ with a tetragonal structure, while the smaller, dark particles were ZrO_2 having a monoclinic structure.

The three Dynapak extrusions contained a finer dispersion of constituent particles (smaller size and smaller interparticle spacing) and finer grain size, figure IV-14, than extrusions of the same prealloyed powder compositions made with a conventional hydraulic press, figure IV-12. Holding the processing temperatures to 1600° F maximum in the former, compared with 2000° F maximum in the latter, minimized the coarsening of the dispersoid in these particular compositions.

The Fe+24.8w/oCo+8.3w/oZr composition obtained for the intermediate evaluation effort (phase 2) contained a dispersion of 6.4v/oZrO_2 of approximately 0.3 micron

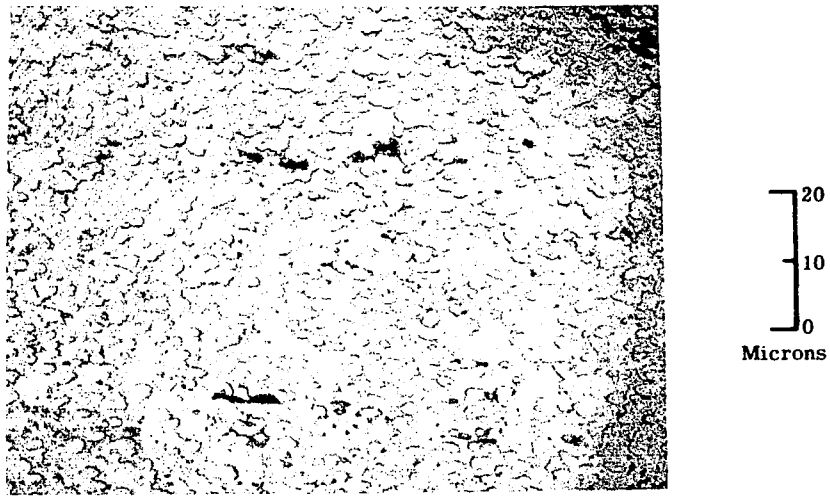

FIGURE IV-10. Photomicrograph of Hydraulic As-Extruded Atomized Powder No. 5, Co+1.0w/oB+4.2w/o Cb (27v/o Dispersoid), Showing Larger Particles of Tau Ternary Boride (Light) and Other Finer Particles (Dark) Dispersed in Cobalt Matrix, Longitudinal Section Near Front of Extrusion, 1000X, Etched in Acetic-Nitric-Hydrochloric-Water (1:1:4:1 Ratio)

FIGURE IV-11. Electron Micrograph of Replica of Hydraulic As-Extruded Atomized Powder No. 5, Co+1.0w/oB+4.2 w/oCb (27v/o Dispersoid), Showing Larger Particles of Tau Ternary Boride (A) and Finer Particles of Another Phase (B), Longitudinal Section, 7500X, Rod Etched in Carapella's Reagent

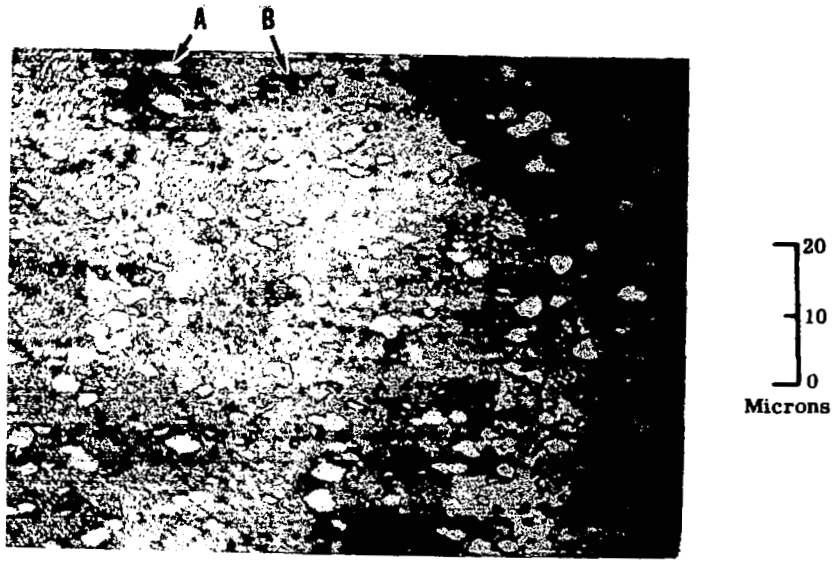

FIGURE IV-12. Photomicrograph of Hydraulic As-Extruded Atomized Powder No. 13, Fe+25.6w/oCo+1.0w/oB+4.2w/o Zr(20v/o Dispersoid), Showing Larger Particles of $(Fe, Co)_2B$, (A-light), and Finer Particles (B-dark) of ZrO_2 Dispersed in Recrystallized Matrix, Longitudinal Section Near Front of Extrusion, 1000X, Etched in Acetic-Nitric-Hydrochloric-Water (1:1:4:1 Ratio)

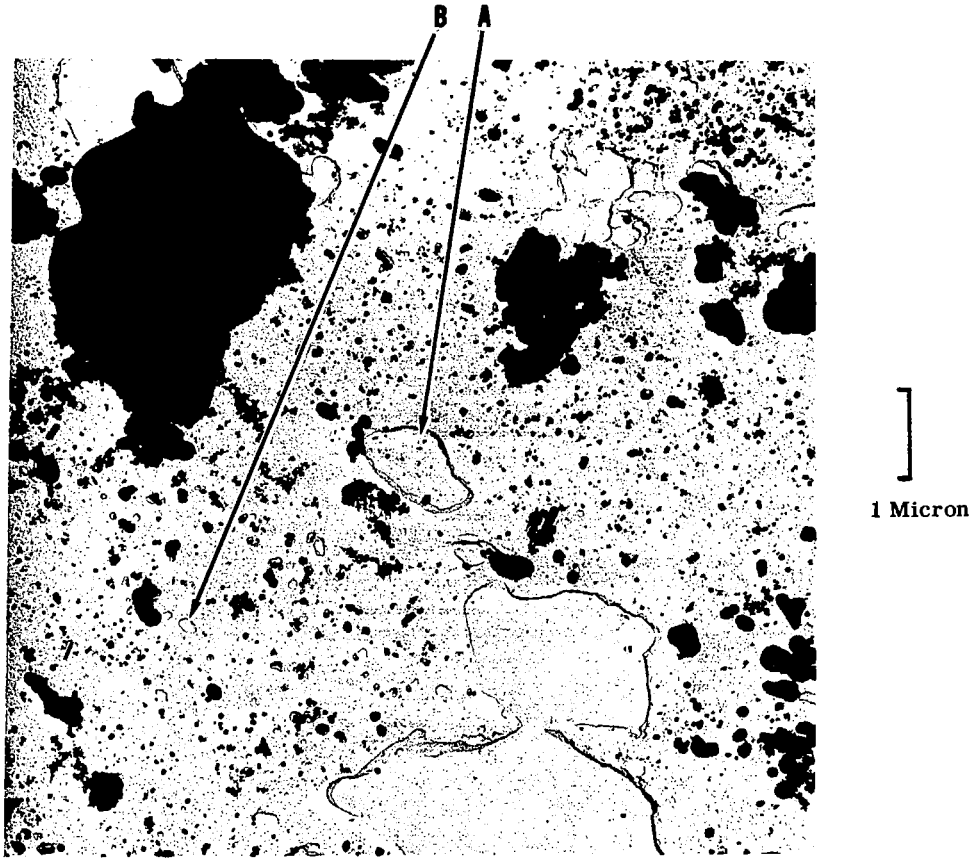

FIGURE IV-13. Electron Micrograph of Extraction Replica of Hydraulic As-Extruded Rod, Atomized Powder No. 13, Fe+25.6w/oCo+1.0w/oB+4.2w/oZr (20v/o Dispersoid), Showing Larger Particles (A) of $(Fe, Co)_2B$ and Finer Particles (B) of ZrO_2, Longitudinal Section, 12,000X, Rod Etched in Carapella's Reagent

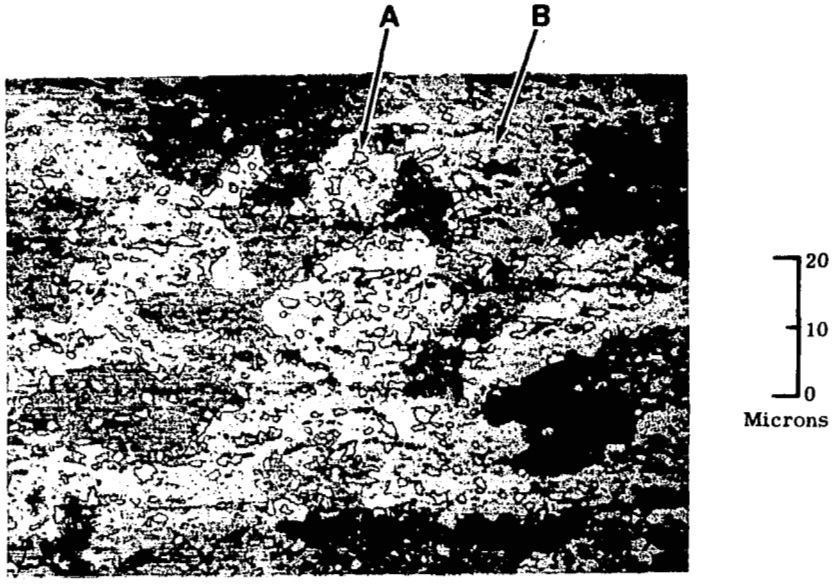

FIGURE IV-14. Photomicrograph of Dynapak As-Extruded Rod of Atomized Powder No. 13, Fe+25.6w/oCo+1.0w/oB+ 4.2w/oZr (20v/o Dispersoid), Showing $(Fe, Co)_2B$ Particles (A-light) and ZrO_2 Particles (B-dark) Dispersed in Fe-Co Recrystallized Matrix, Longitudinal Section, 1000X, Etched in Carapella's Reagent

average particle size and 14v/o of coarse, elongated particles of Fe-Co-Zr constituent. The structure of this alloy after 32 cycles of secondary working is shown in an electron micrograph, figure IV-15.

c. MICROSTRUCTURE OF INTERNALLY OXIDIZED POWDER COMPOSITIONS

Figure IV-16 shows the BeO dispersoid in the cobalt matrix (hexagonal + face centered cubic forms) of the hydraulic extrusion of internally oxidized (two hours at 1830°F) atomized powder No. 9. The secondary phase particles in the internally oxidized compositions tended to be finer, but not as uniformly dispersed as in the extrusions of prealloyed atomized powders.

d. MICROSTRUCTURE OF COMPOSITE POWDER COMPOSITIONS

The microstructures of the hot-extruded and secondary worked conditions for the Co+8.4w/oThO_2 (7.5v/oThO_2, 0.01-0.06 micron) composite powder No. 14 from Sherritt Gordon are shown in figures IV-17 and IV-18. No marked change in the uniformity of distribution of ThO_2 particles was observed with secondary working. The ThO_2 particles had an effective particle size of approximately 0.1 micron. The equiaxed matrix grain structure of the hot-extruded condition, figure IV-17, was changed to an elongated grain and subgrain structure by secondary working, figure IV-18. The subgrain boundaries appeared to be associated with the thoria particles.

The microstructure of rod secondary worked for 16 cycles at 1250° F of the Co+11.2w/oThO_2 (10v/oThO_2, 0.01-0.06 micron) composite powder No. 3 from Chas. Pfizer is shown in figure IV-19. The dispersion of the thoria was fairly uniform, but there was a definite tendency for the ThO_2 particles to be present as clusters and stringers. As a result, the effective particle size of the thoria was approximately 0.2 micron. An elongated grain structure was produced by secondary working.

The Fe+24.5w/oCo+9.3w/oThO_2 (7.5v/oThO_2, 0.01-0.06 micron) composite powder No. 15 from Chas. Pfizer was extruded and secondary worked for 28 cycles (the first 16 at 1000° F plus 12 at 1250° F). A fine, elongated grain structure was produced. The effective size of the thoria was rather large, 0.3 micron, because of the tendency to be present in clusters. As a result the interparticle spacing was larger than desired, 3.7 microns, as shown in figure IV-20.

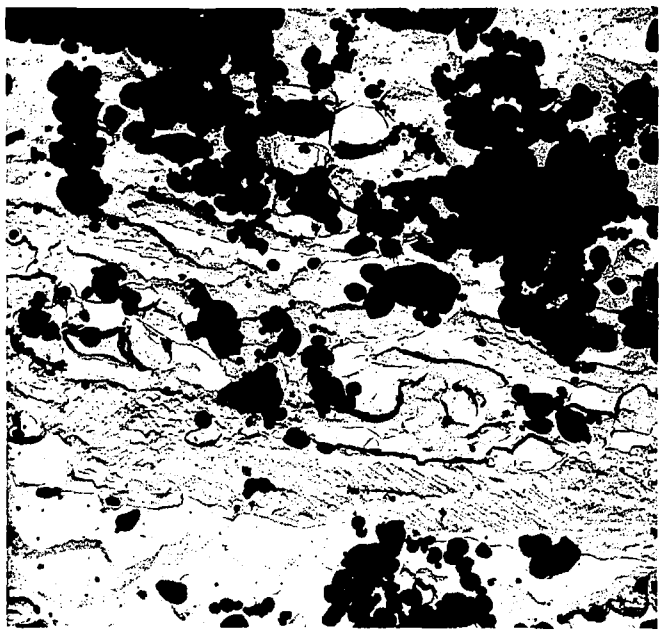

FIGURE IV-15. Electron Micrograph of Extraction Replica of Rod Secondary Worked for 32 Cycles (first 16 at 1000°F plus 16 at 1250°F) of Atomized Powder No. 19, Fe+ 24.8w/oCo+8.3w/oZr (6.4v/oZrO_2+14v/o Coarse, Elongated Fe-Co-Zr Constituent), Showing ZrO_2 Dispersoid and Elongated Grain Structure of Matrix, Longitudinal Section, 18,000X, Rod Etched in Carapella's Reagent and then in 10 Percent Solution of Bromine in Methanol

FIGURE IV-16. Electron Micrograph of Extraction Replica of Hydraulic As-Extruded Rod, Internally Oxidized Powder No. 9, Co+1.3w/oBe (8.3v/oBeO), Showing Stringers of BeO Particles, Longitudinal Section, 9000X, Rod Electrolytically Etched in 20% Perchloric Acid in Ethyl Alcohol at 10 Volts

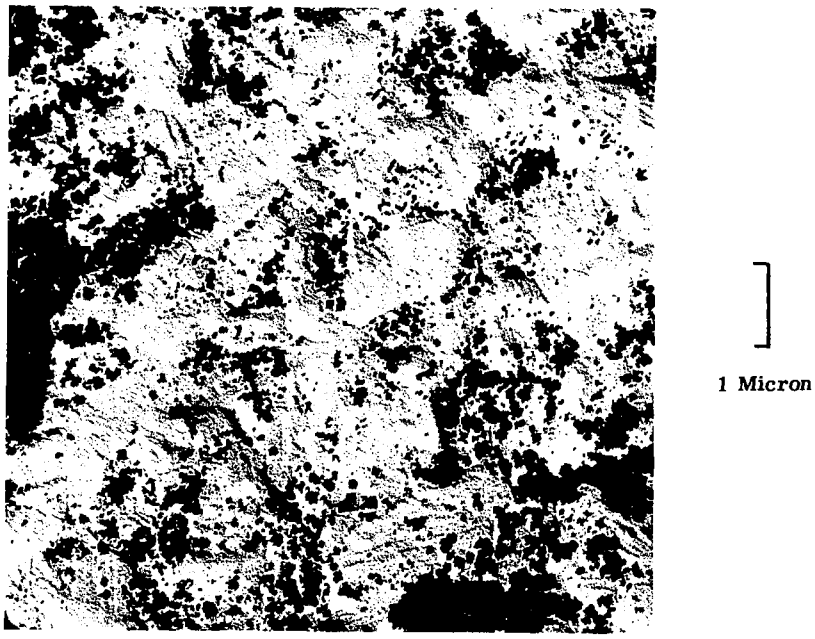

FIGURE IV-17. Electron Micrograph of Extraction Replica of Hydraulic As-Extruded Rod of Composite Powder No. 14 from Sherritt Gordon, Co+8.4w/oThO_2 (7.5 v/oThO_2, 0.01-0.06 micron). Showing ThO_2 Particles (Dark) and Equiaxed Grain Structure of Matrix containing Hexagonal and Cubic Forms, Longitudinal Section, 12,000X, Rod Etched in Carapella's Reagent and then in 10 Percent Solution of Bromine in Methanol.

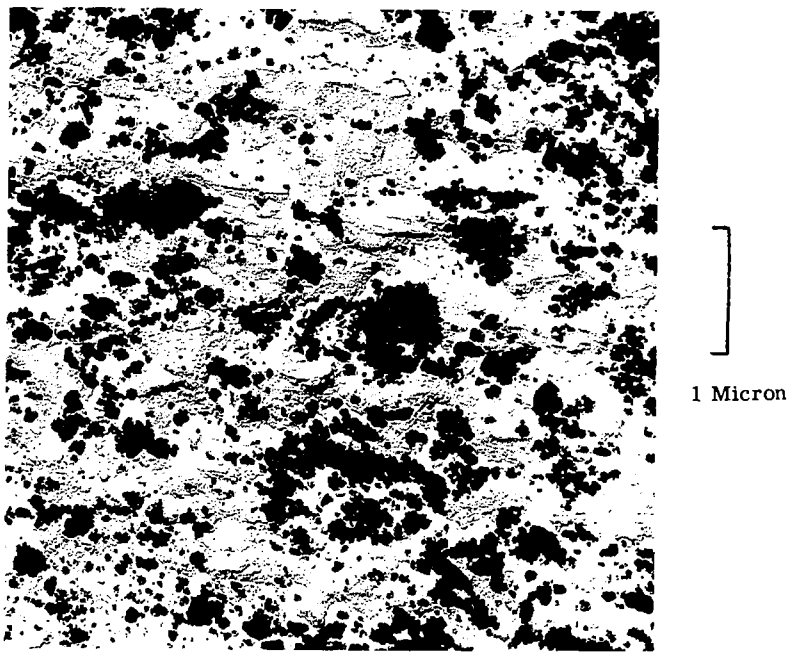

FIGURE IV-18. Electron Micrograph of Extraction Replica of Rod Secondary Worked for 28 Cycles at 1250°F of Composite Powder No. 14 from Sherritt Gordon, Co+8.4 w/oThO_2 (7.5v/oThO_2, 0.01-0.06 micron), Showing ThO_2 Particles (Dark) and Fibrous Grain Structure of Co Matrix Containing Almost Entirely Cubic Form, Longitudinal Section, 18,000X, Rod Etched in Carapella's Reagent and then in 10 Percent Solution of Bromine in Methanol

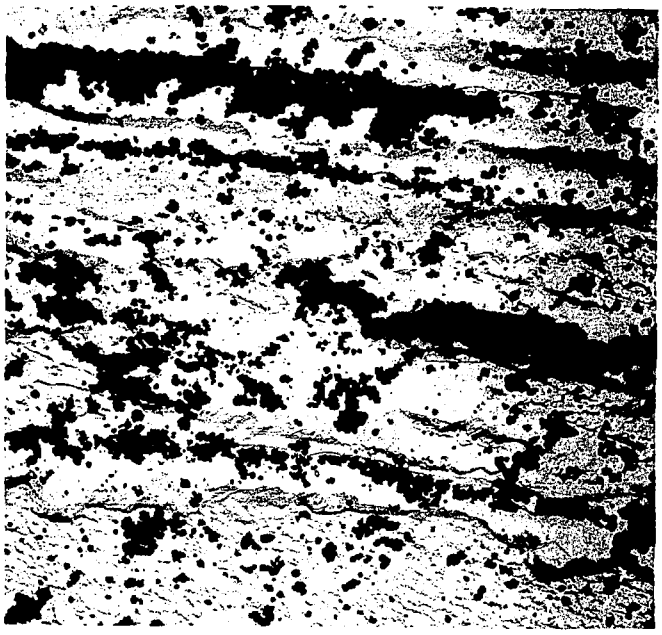

FIGURE IV-19. Electron Micrograph of Extraction Replica of Rod Secondary Worked for 16 Cycles at 1250°F of Composite Powder No. 3 from Chas. Pfizer, Co+11.2 w/oThO_2 (10v/oThO_2, 0.01-0.06 micron), Showing ThO_2 Particles (Dark) and Elongated Grain Structure of Co Matrix, Longitudinal Section, 9000X, Rod Etched in Carapella's Reagent and then in 10 Percent Solution of Bromine in Methanol

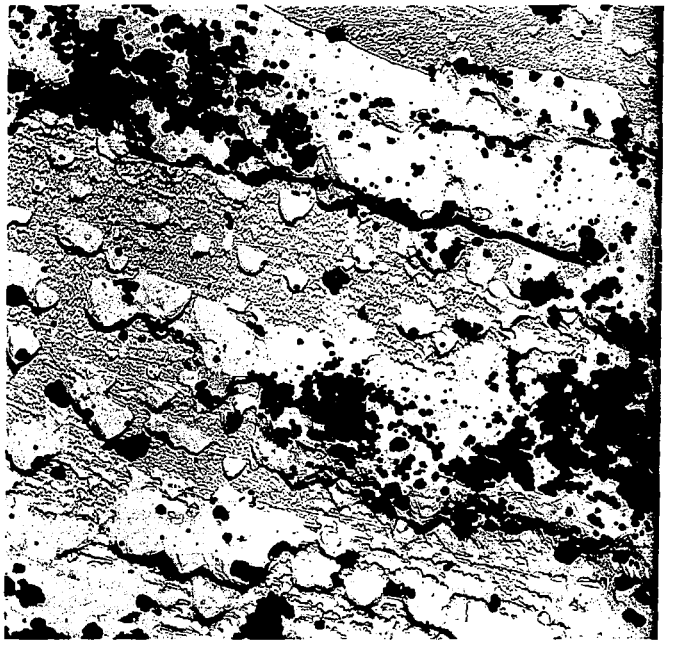

FIGURE IV-20. Electron Micrograph of Extraction Replica of Rod Secondary Worked for 28 Cycles (first 16 at 1000°F plus 12 at 1250°F) of Composite Powder No. 15 from Chas. Pfizer, Fe+24.5w/oCo+9.3w/oThO_2 (7.5v/oThO_2 0.01-0.06 micron), Showing ThO_2 Particles (Dark) and Elongated Structure of Matrix, Longitudinal Section, 9000X, Rod Etched in Carapella's Reagent and then in 10 Percent Solution of Bromine in Methanol

The ThO_2 particles in the extrusion of composite powder No. 11 from Vitro Labs, Fe+23.7w/oCo+12.1w/oThO_2 (10v/oThO_2, 0.01-0.06 micron), exhibited a greater degree of clustering and stringering than the other materials. Therefore, the effective particle size of the dispersoid was large (approximtely 1.1 microns) and so was the average interparticle spacing (approximately 9.9 microns).

e. MICROSTRUCTURE OF SUPPLIER EXTRUSIONS OF DISPERSION-STRENGTHENED COBALT

The supplier extrusion No. 3 of nominally Co+11.2w/o ThO_2 (10v/oThO_2, 0.01-0.06 micron) from New England Materials Laboratory contained a relatively uniform dispersion of ThO_2, figure IV-21, although some clusters and stringers were present.

The Curtiss-Wright rod, supplier extrusion No. 9 of nominally Co+2.3w/oThO_2 (2v/oThO_2, 0.01-0.06 micron), had a few fine stringers of non-metallic material, figure IV-22. These were stated to be ThO_2 by Curtiss-Wright. The secondary worked rod (85% total reduction at room temperature by swaging) contained similar stringers of ThO_2, although these are not shown in figure IV-23. Secondary working did not change significantly the distribution of the ThO_2 particles in the matrix.

Large stringers may result in notch sensitivity and possible erractic creep results.

3. DC Magnetic Properties of Hot-Extruded (Phases 1, 2, and 3) and Preliminary Secondary Worked (Phase 2) Compositions

The results of the coercive force and saturation measurements on hydraulic extrusions in the initial evaluation effort (phase 1) are presented in table IV-18. For purposes of discussion, these data along with that obtained on extrusions in phases 2 and 3 of the program, table IV-19, will be presented together. The compositions investigated in the later phases of the program tended to contain lesser amounts (v/o) of dispersoid, providing higher values of magnetic saturation. The effect of secondary working for 14 to 16 cycles at 800° to 1500° F (phase 2) on the coercive force of selected compositions are presented later in this section.

a. SATURATION MAGNETIZATION MEASUREMENTS ON HYDRAULIC EXTRUSIONS (PHASES 1, 2, AND 3)

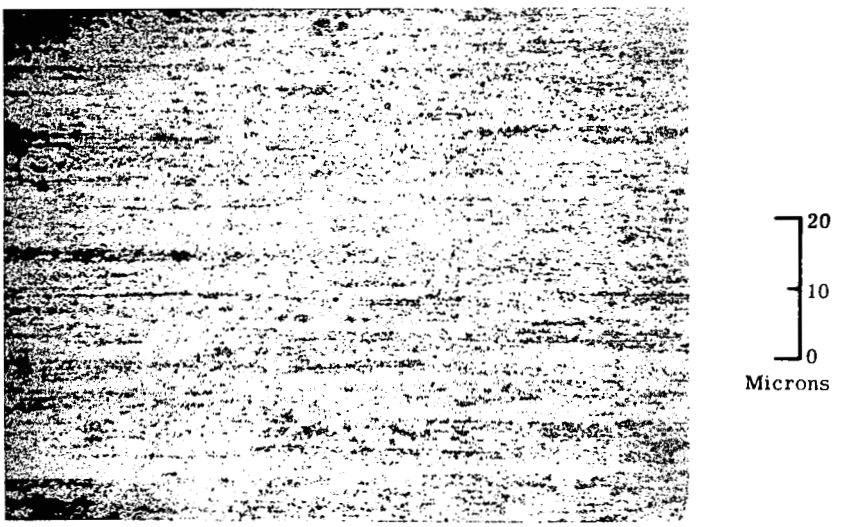

FIGURE IV-21. Photomicrograph of Hydraulic As-Extruded Rod from New England Materials Laboratory, Supplier Extrusion No. 3, Co+11.2w/oThO_2 (10v/oThO_2, 0.01-0.06 micron), Showing Distribution of Thoria Particles in Cobalt Matrix. Some of the Thoria Particles are Present as Clusters and Stringers, Longitudinal Section Near Front of Extrusions, 1000X, Lightly Etched in Acetic-Nitric-Hydrochloric-Water (1:1:4:1 Ratio)

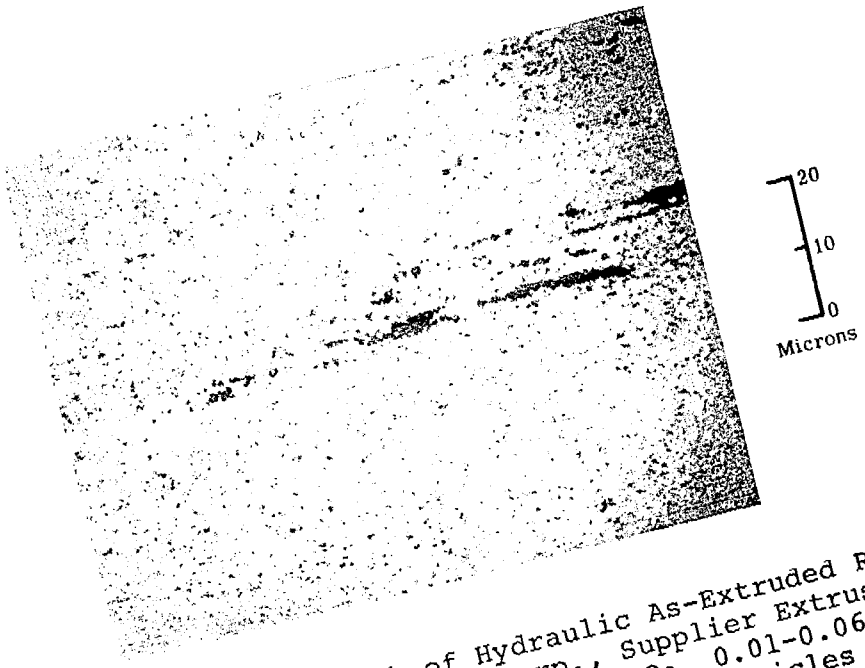

FIGURE IV-22. Photomicrograph of Hydraulic As-Extruded Rod from Curtiss-Wright Corp., Supplier Extrusion No. 9, Co+2.3w/oThO_2 (2v/oThO_2, 0.01-0.06 micron), Showing Distribution of Thoria Particles in Cobalt Matrix. Some Thoria Particles are Present as Clusters and Stringers, Longitudinal Section Near Front of Extrusion, 1000X, Lightly Etched in Acetic-Nitric-Hydrochloric-Water (1:1:4:1 Ratio)

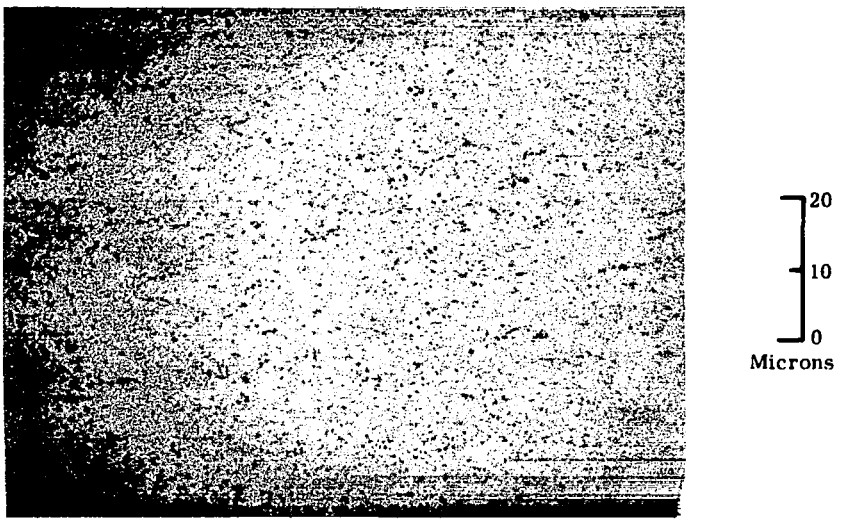

FIGURE IV-23. Photomicrograph of Rod Secondary Worked at Room Temperature (85% Total Reduction) After Extrusion by Curtiss-Wright Corp., Supplier Extrusion No. 9, Co+2.3w/oThO_2 (2v/oThO_2, 0.01-0.06 micron), Showing Distribution of Thoria Particles in Cobalt Matrix. Longitudinal Section Near Front of Extrusion, 1000X. Lightly Etched in Acetic-Nitric-Hydrochloric-Water (1:1:4:1 Ratio)

The values of saturation magnetic moment, σ_s, in emu per gram and saturation magnetization, B_s, in gauss for the various compositions are listed in table IV-18 and table IV-19. The B_s values were calculated from the equation: $B_s = 4\pi\delta\sigma$, where δ is the density of the material in grams per cubic cm. The values for B_s should be considered approximate, because the density at room temperature was used to calculate elevated temperature values of B_s as well. In the case of the cobalt-base alloys, the saturation values measured at room temperature were approximately five percent low because it was not possible to completely saturate the specimens containing hexagonal cobalt with the mean applied field of 11,500 oersteds.

The dilution effect on saturation magnetization by the amount of dispersoid present in the matrix is illustrated for cobalt-base alloys in figure IV-24. The decrease in B_s with increasing volume fraction of dispersed phase was linear at all temperatures, but the absolute values of B_s for the dispersion-strengthened materials tended to be slightly lower than predicted from a straight dilution basis. Some of this may be due to slight inaccuracies in the density values used. The relationship between B_s and volume precent dispersoid was similar for dispersion-strengthened iron+cobalt alloys. These data show that the B_s values at any temperature for dispersion-strengthened compositions could be predicted quite accurately from a knowledge of the volume percent dispersoid present.

The magnetic saturation of the cobalt-base extrusions of internally oxidized powders and composite powders, and supplier extrusions at all temperatures, was higher than that of the cobalt-base extrusions of atomized powders due to the dilution effect of the greater amount of non-magnetic dispersed phase in the latter class of materials, table IV-18. It may be seen that the cobalt-base extrusions of prealloyed atomized powders in table IV-18 which contained a minimum of 26v/o dispersoid (table IV-15) did not quite meet the saturation goal, even at 1200° F. On the other hand, the cobalt-base extrusions of internally oxidized powders, composite powders, and the supplier extrusion No. 3 containing 10v/o thoria did meet this goal at all temperatures except 1600° F. The supplier extrusion No. 9 with 2v/o thoria met the goal at all temperatures.

TABLE IV-18. - DC Magnetic Properties of Hydraulic

Powder or Extrusion No.	Nominal Composition (weight percent)	Coercive Force, H_c (oersteds)					
		At Room Temperature					
		As Recvd.	After Testing at 1600°F	At 1200°F	At 1400°F	At 1500°F	At 1600°F
a. Prealloyed Atomized Powders (Extruded)							
3	Co+1.0B+2.2Ti	25.0	27.0	6.3	4.8	4.0	3.3
4	Co+1.0B+4.2Zr	48.0	53.0	9.2	7.1	5.8	4.7
5	Co+1.0B+4.2Cb	47.0	45.5	10.3	8.0	5.9	4.6
6	Co+1.0B+8.3Ta	41.0	45.0	11.6	9.4	8.4	6.3
12	Fe+26.1Co+1.0B+2.2Ti	12.8	12.1	5.5	4.1	3.4	2.3
13	Fe+25.6Co+1.0B+4.2Zr	18.8	17.6	8.4	6.4	4.9	3.6
14	Fe+25.6Co+1.0B+4.2Cb	19.6	19.0	8.7	6.8	5.3	3.7
15	Fe+24.5Co+1.0B+8.3Ta	21.0	19.0	10.4	8.6	6.2	4.4
b. Internally Oxidized Powders (Extruded)							
8	Co+4.7Al_2O_3	44.5	42.4	9.7	8.0	7.1	6.1
9	Co+3.6BeO	56.0	52.2	9.0	6.4	5.2	4.4
17	Fe+25.6Co+5.1Al_2O_3	19.6	12.4	3.6	1.9	1.3	0.9
18	Fe+26.0Co+3.9BeO	21.0	15.3	9.3	4.9	3.7	2.7
c. Composite Powders (Extruded)							
3	Co+11.2ThO_2 (0.01-0.06μ), Sherritt Gordon	60.0	58.5	21.5	16.8	15.1	13.0
11	Fe+23.7Co+12.1ThO_2 (0.01-0.06μ), Vitro Labs	13.9	9.4	5.3	2.6	1.8	1.1
1	Co+4.75 Al_2O_3 (0.01-0.06μ), Chas. Pfizer	85.0	82.0	10.0	7.9	6.8	5.9
2	Co+4.75Al_2O_3 (0.1-0.6μ), Chas. Pfizer	79.0	78.0	9.0	7.7	6.8	5.5
3	Co+11.2ThO_2 (0.01-0.06μ), Chas. Pfizer	76.5	76.0	12.4	10.3	9.0	8.2
4	Co+11.2ThO_2 (0.1-0.6μ), Chas. Pfizer	76.9	73.0	10.5	8.8	7.8	6.4
11	Fe+23.7Co+12.1ThO_2 (0.01-0.06μ) Chas. Pfizer	19.6	19.2	9.0	6.5	5.3	4.4
d. Supplier Extrusions of Dispersion-Strengthened Cobalt							
3(d)	Co+11.2ThO_2 (0.01-0.06μ ThO_2)	49.0	49.0	19.4	16.7	14.8	13.4
9(e)	Co+2.3ThO_2 (0.01-0.06μThO_2)	68.0	62.0	8.4	7.3	6.1	5.3
9(a)(e)	Co+2.3ThO_2 (0.01-0.06μThO_2)	114.0	71.0	9.3	7.1	5.7	4.8
e. Comparison Alloy							
	Nivco[f]	11.9	9.3	6.8	5.5	3.9	2.3

(a) Given 85 percent cold reduction by swaging after hot extrusion. All other material in hot extruded condition.

(b) Based on measurements of weight in air and water (ASTM Method B 311-58) and measurements of weight and dimensions of machined rod specimens.

(c) Measured values are presumably 5 percent too low because it was not possible to saturate the specimens at room temperature.

Extrusions Obtained for Initial Evaluation Effort (Phase 1)

Magnetic Saturation										Room Temp. Density of Material [b] (g./cc)
Saturation Magnetic Moment, σ (emu/gram)					Approximate Saturation Magnetization, B_s (kilogauss)					
At Room Temp.	At 1200°F	At 1400°F	At 1500°F	At 1600°F	At Room Temp.	At 1200°F	At 1400°F	At 1500°F	At 1600°F	
132[c]	95.7	89.2	83.5	77.4	13.7[c]	9.9	9.3	8.7	8.0	8.26
132[c]	99.9	92.6	86.9	80.6	14.0[c]	10.6	9.8	9.2	8.5	8.43
127[c]	101.2	93.6	87.7	79.8	13.7[c]	10.9	10.1	9.5	8.6	8.58
134[c]	95.3	87.5	82.8	78.8	14.8[c]	10.6	9.7	9.2	8.7	8.81
216	179	156	144	129	20.9	17.3	15.1	13.9	12.5	7.70
212	175	152	142	127	20.9	17.2	15.0	14.0	12.5	7.84
211	165	152	140	127	20.8	16.3	15.0	13.8	12.5	7.86
200	159	145	135	121	20.5	16.2	14.9	13.8	12.4	8.15
152[c]	133	122	118	108	15.6[c]	13.7	12.6	12.1	11.1	8.19
153[c]	137	127	121	112	15.5[c]	13.9	12.9	12.3	11.4	8.10
219	191	179	163	153	20.4	17.7	16.7	15.2	14.3	7.40
222	191	179	172	152	20.4	17.5	16.4	15.8	14.0	7.31
144[c]	124	116	109	102	15.9[c]	13.7	12.8	12.1	11.2	8.79
204	170	160	145	126	20.5	17.0	16.1	14.6	12.6	7.99
149[c]	134	125	118	111	15.3[c]	13.8	12.9	12.1	11.4	8.19
152[c]	134	124	118	112	15.7[c]	13.8	12.8	12.1	11.5	8.18
142[c]	126	117	110	102	15.7[c]	13.9	12.9	12.1	11.2	8.78
142[c]	125	116	109	102	15.7[c]	13.8	12.8	12.0	11.2	8.79
201	172	161	152	137	20.2	17.3	16.2	15.3	13.7	7.99
144[c]	125	116	110	103	15.7[c]	13.6	12.6	12.0	11.2	8.66
155[c]	137	127	119	112	17.2[c]	15.2	14.1	13.2	12.4	8.82
155[c]	138	128	121	112	17.2[c]	15.3	14.2	13.5	12.5	8.85
124	100	75.0	61.7	40.0	13.4	10.8	8.1	6.7	4.3	8.61

(d) Extrusion supplied by New England Materials Laboratory, Inc., Medford, Massachusetts.
(e) Extrusion supplied by Curtiss-Wright Corp., Metals Processing Division, Buffalo, New York.
(f) Forged and heat treated 5/8 inch diameter rod. Heat treated 1725±25°F for 1 hour, water quenched, then air aged at 1225±5°F for 50 hours.

TABLE IV-19. - DC Magnetic Properties of Hydraulic Extrusions

Powder or Extrusion No.	Nominal Composition (weight percent)	Coercive Force, H_c (oersteds)					
		At Room Temperature					
		As Received	After Testing at 1600°F	At 1200°F	At 1400°F	At 1500°F	At 1600°F
a. Prealloyed Atomized Powders (Extruded)							
30	Co+0.8B+3.2Cb	19.7	18.2	4.1	2.9	2.3	1.5
5(a)	Co+1.0B+4.2Cb	47.0	45.5	10.3	8.0	5.9	4.6
13(a)	Fe+25.6Co+1.0B+4.2Zr	18.8	17.6	8.4	6.4	4.9	3.6
19	Fe+24.8Co+8.3Zr	15.9	13.9	7.1	4.5	2.9	1.9
b. Internally Oxidized Powders (Extruded)							
9A	Co+3.6BeO	65.8	59.5	8.7	7.0	6.3	5.4
c. Composite Powders (Extruded)							
13	Co+4.5ThO_2 (0.01-0.06μ), Sherritt Gordon	50.5	45.8	13.3	11.0	9.5	8.2
14	Co+8.4ThO_2 (0.01-0.06μ), Sherritt Gordon	48.0	43.8	20.0	16.3	15.2	13.0
3(a)	Co+11.2ThO_2 (0.01-0.06μ), Sherritt Gordon	60.0	58.5	21.5	16.8	15.1	13.0
13	Co+4.5ThO_2 (0.01-0.06μ), Chas. Pfizer	95.0	73.0	9.3	8.0	7.1	6.1
14	Co+8.4ThO_2 (0.01-0.06μ), Chas. Pfizer	84.0	73.0	13.8	11.5	10.4	9.1
3(a)	Co+11.2ThO_2 (0.01-0.06μ), Chas. Pfizer	76.5	76.0	12.4	10.3	9.0	8.2
15	Fe+24.5Co+9.3ThO_2 (0.01-0.06μ), Chas Pfizer	15.5	15.1	7.4	5.8	4.6	4.1
11(a)	Fe+23.7Co+12.1ThO_2 (0.01-0.06μ) Chas. Pfizer	19.6	19.2	9.0	6.5	5.3	4.4
d. Comparison Alloy							
	Nivco(d)	11.9	9.3	6.8	5.5	3.9	2.3

(a) Obtained for initial evaluation effort (phase 1). Included for comparison purposes only.
(b) Based on measurements of weight in air and water (ASTM Method B311-58) and measurements of weight and dimensions of machined rod specimens.

Obtained for Intermediate and Final Evaluation Efforts (Phases 2 and 3)

Magnetic Saturation										Room Temp. Density of Material[b] (g/cc)
Saturation Magnetic Moment, (emu/gram)					Approximate Saturation Magnetization, B_S (kilogauss)					
At Room Temp.	At 1200°F	At 1400°F	At 1500°F	At 1600°F	At Room Temp.	At 1200°F	At 1400°F	At 1500°F	At 1600°F	
136[c]	111	102	96.2	89.5	14.6[c]	12.0	11.0	10.4	9.7	8.58
127[c]	101.2	93.6	87.7	79.8	13.7[c]	10.9	10.1	9.5	8.3	8.58
212	175	152	142	127	20.9	17.2	15.0	14.0	12.5	7.84
204	170	152	141	128	20.1	16.7	15.0	13.9	12.5	7.82
153[c]	137	127	121	112	15.5[c]	13.9	12.9	12.3	11.4	8.10
158[c]	128	124	120	111	17.3[c]	14.0	13.6	13.1	12.1	8.73
150	128	121	114	106	16.5[c]	14.1	13.3	12.5	11.6	8.76
144[c]	124	116	109	102	15.9[c]	13.7	12.8	12.1	11.2	8.79
149[c]	134	123	120	111	16.4[c]	14.7	13.5	13.1	12.2	8.73
144[c]	128	119	113	107	15.9[c]	14.1	13.0	12.4	11.8	8.76
142[c]	126	117	110	102	15.7[c]	13.9	12.9	12.1	11.2	8.78
210	182	166	154	143	21.0	18.1	16.6	15.4	14.2	7.94
201	172	161	152	137	20.2	17.3	16.2	15.3	13.7	7.99
124	100	75	61.7	40	13.4	10.8	8.1	6.7	4.3	8.61

(c) Measured values are presumably 5 percent too low because it was not possible to saturate the specimens at room temperature.

(d) Forged and heat treated 5/8-inch diameter rod. Heat treated 1725±25°F for 1 hour, water quenched, then air aged at 1225±5°F for 50 hours.

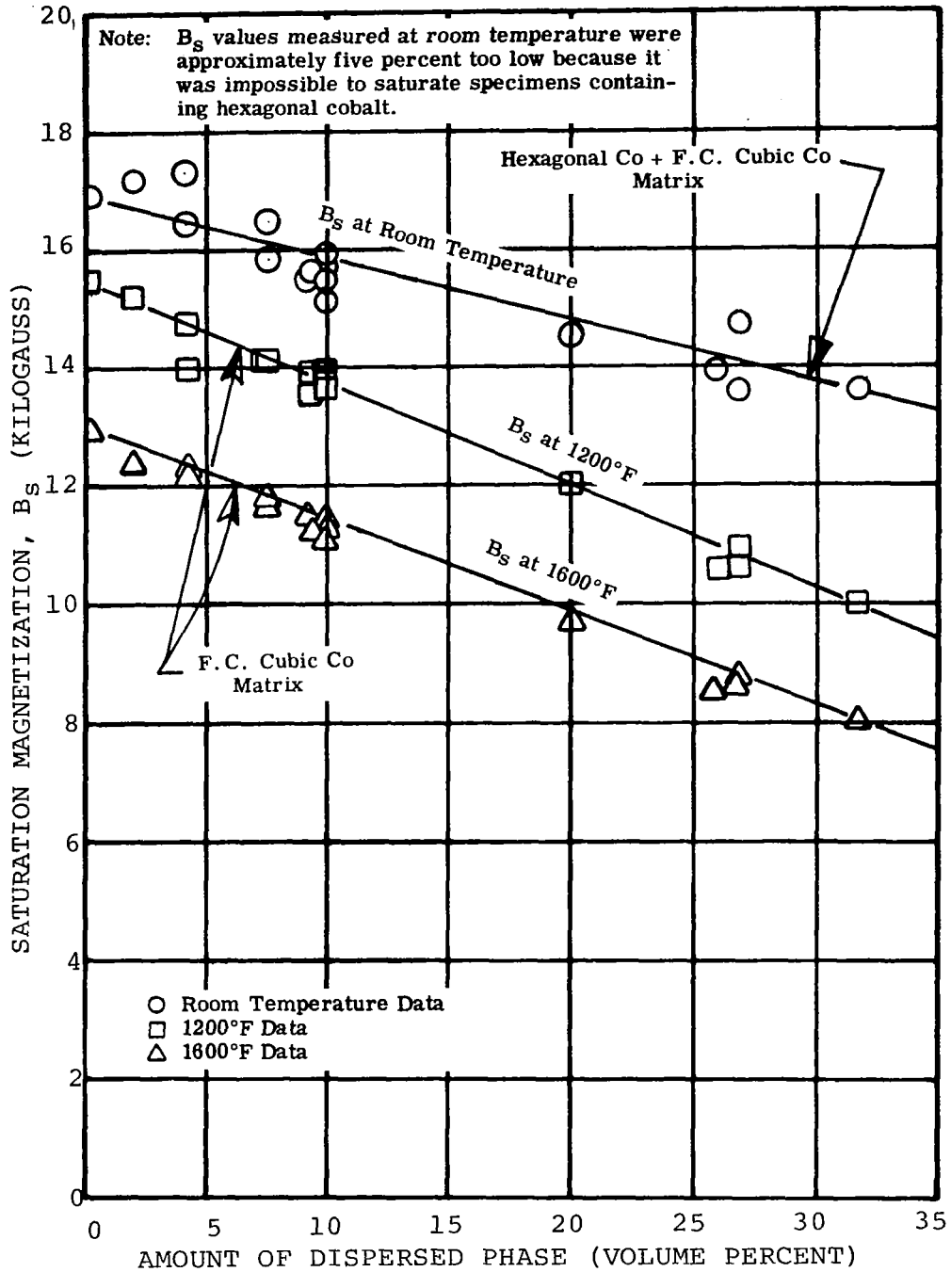

FIGURE IV-24. Effect of Amount of Dispersed Phase in Cobalt As-Extruded Rod on the Saturation Magnetization at Room Temperature, 1200°F, and 1600°F

For reaching higher levels of saturation magnetization, the Fe+Co base materials appeared more attractive than the Co-base for future development. All of the Fe+Co-base materials in table IV-18 met the current program goal of B_S = 12 kilogauss minimum at 1200° to 1600° F, while some of the cobalt-base alloys did not.

Since saturation is a structure insensitive property, the values of B_S were not influenced by the particle size of the dispersed phase or secondary working treatments.

b. COERCIVE FORCE MEASUREMENTS ON HYDRAULIC EXTRUSIONS (PHASES 1, 2, AND 3)

The coercive force values of all compositions tested were less than 25 oersteds at 1200° to 1600°F and, therefore, met the tentative program goal in that respect. For each composition, whether cobalt-base or iron+cobalt-base, the coercive force decreased as the temperature increased. This was more striking for the cobalt-base extrusions, which contained a mixture of hexagonal and face centered cubic forms of cobalt in the matrix at room temperature. Hexagonal cobalt has high crystal anisotropy and magnetostriction constants relative to the cubic form, and this in itself would contribute to a higher coercive force in dispersion-strengthened materials. Furthermore, the transformation of cubic cobalt to hexagonal as the extrusion cooled to room temperature would be expected to induce residual, internal stresses in the matrix. This would promote a still higher coercive force, considering the interaction with the magnetostriction constant of the hexagonal phase. At 1200° to 1600° F the hexagonal phase was gone and only the cubic form remained. Both anisotropy and magnetostriction constants would be expected to be much lower at 1200° to 1600° F, and the coercive force of the cobalt-base materials would be sharply reduced relative to room temperature.

The coercive force values at room temperature for the cobalt-base extrusions of internally oxidized powder No. 9, the composite powders, and the supplier extrusions were higher than for the extrusions of cobalt-base atomized powders and the Co+4.7w/oAl_2O_3 internally oxidized powder, table IV-18. This was related to the greater proportion of hexagonal cobalt and smaller proportion of cubic cobalt in the former. Cold working of supplier extrusion No. 9 further increased the amount of hexagonal cobalt at the expense of cubic cobalt and, therefore, increased the coercive force at room temperature.

The measured effect of the amount of dispersed phase on the coercive force of cobalt-base extrusions at room temperature and 1200° F is illustrated in figure IV-25. At 1200° to 1600° F, where cobalt has the cubic form, the coercive force increased as the amount of dispersoid increased. However, it should be pointed out that the rate of increase was less for dispersoids of coarser particle size. At room temperature hexagonal cobalt is the stable form, but a mixture of hexagonal and face centered cubic existed because the transformation was incomplete. The coercive force at room temperature tended to decrease with increasing amounts of dispersed phase due to a simultaneous decrease in the relative amount of hexagonal cobalt.

The iron+27w/o cobalt-base extrusions tended to have a lower coercive force at room and elevated temperatures than the cobalt-base. The iron + cobalt-base materials had a body centered cubic matrix at all testing temperatures. The crystal anisotropy constant of iron+27w/o cobalt, although less than that of cobalt, was the major factor to interact with the dispersoid and influence coercive force near room temperature. At 1200° to 1600° F the anisotropy constant would be expected to be much lower and its interaction with the dispersoid would contribute less to coercive force. The magnetostriction of iron+27w/o cobalt was expected to be relatively high at room temperature and decreased at 1200° to 1600° F. However, internal stress-magnetostriction interaction could have a significant effect on coercive force at 1200° to 1600° F. Later in this report, section 6.b., an illustration is given of the significance of the relative contributions to coercive force at temperatures in the range from room temperature to 1600° F from the dispersoid--crystal anisotropy constant interaction and from the internal stress--magnetostriction constant interaction. This is done using one cobalt-base and one iron +27w/o cobalt-base composition as examples, and calculating coercive force values from theoretical equations and comparing with measured values. For the iron+cobalt-base materials the coercive force at all temperatures increased with increasing volume percent of dispersed phase and decreasing particle size, figure IV-26.

The coercive force was measured at room temperature before and after heating specimens to 1600° F where they were held approximately 10 minutes. Changes in coercive force were indicative of changes in the grain structure of the matrix at room temperature as a result of heating. The hot-extruded compositions containing

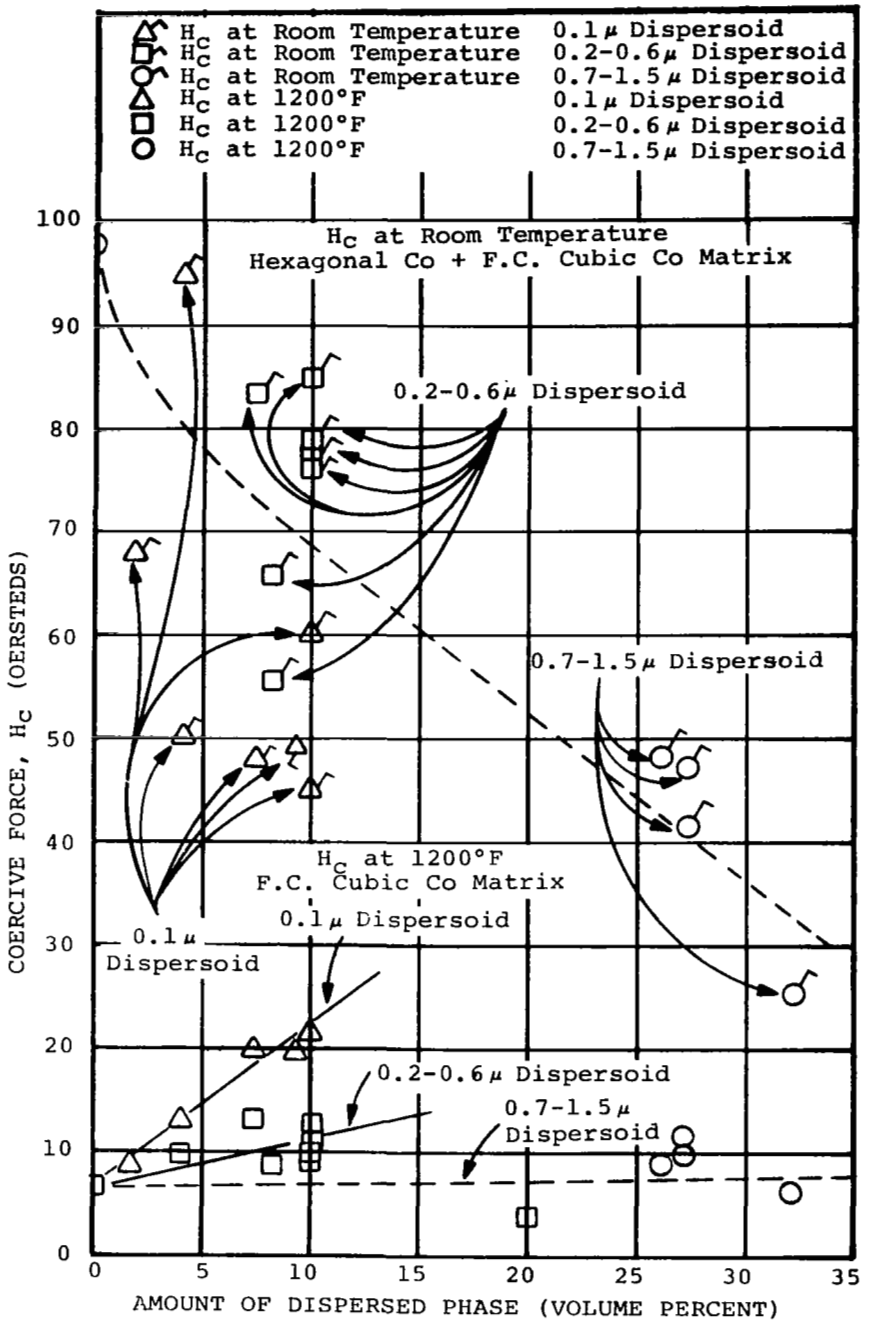

FIGURE IV-25. Effect of Amount of Dispersed Phase of Three Different Particle Sizes (Approximate Values) in Cobalt As-Extruded Rod on the Coercive Force at Room Temperature and 1200°F

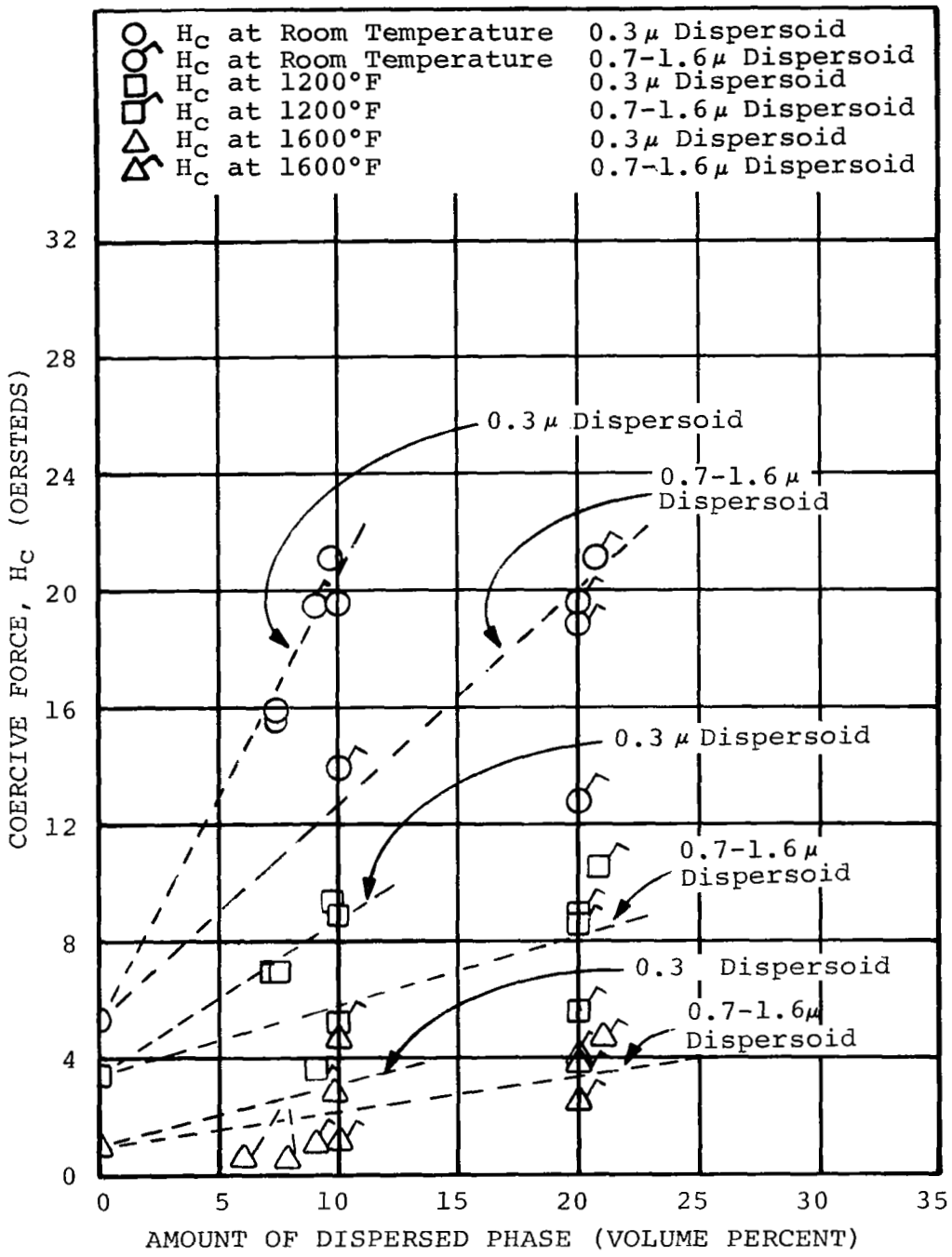

FIGURE IV-26. Effect of Amount of Dispersed Phase of Two Different Particle Sizes (Approximate Values) in Iron + 27w/o Cobalt As-Extruded Rod on the Coercive Force at Room Temperature, 1200°F, and 1600°F

the larger amounts (v/o) of dispersoid in tables IV-18 and table IV-19 tended to have the same grain structure after heating as before. In the case of the cobalt-base hot-extruded compositions, many of these originally contained substantial amounts of hexagonal cobalt as a result of cooling from the extrusion temperature. After heating through the transformation range to 1600° F in the coercive force test and cooling back to room temperature, approximately the same relative amount of hexagonal cobalt was present as originally. The supplier extrusion No. 9 in the cold-swaged condition contained substantially all hexagonal cobalt. After cooling from 1600° F to room temperature, the amount of hexagonal cobalt was reduced, as indicated by the decrease in coercive force from 114 to 71 oersteds.

c. COERCIVE FORCE MEASUREMENTS ON DYNAPAK EXTRUSIONS (PHASE 1)

The coercive force values determined at room temperature on the Dynapak extrusions are presented in table IV-20 and may be compared with those for the hydraulic extrusions. The Co+1.0w/oB+4.2w/oZr Dynapak extrusion had a much lower coercive force than the hydraulic extrusion, probably because the Dynapak extrusion contained a much lower ratio of hexagonal to cubic cobalt than did the hydraulic extrusion. This resulted from the fact that in the Dynapak process the extrusion was cooled through the transformation temperature (783° F from face centered cubic to hexagonal on cooling) to room temperature more rapidly than in the hydraulic process. Also, the finer dispersoid in the Dynapak extrusions would tend to retard the transformation. The two iron+cobalt-base Dynapak extrusions had slightly higher values of coercive force than their hydraulic extrusion counterparts. The dispersoid and recrystallized grain size was finer in the Dynapak extrusions, accounting for their higher coercive force. The one iron+cobalt-base Dynapak extrusion given a 65 percent cold reduction by swaging exhibited a large increase in coercive force due to internal stress.

Coercive force values of the Dynapak extrusions were not determined at 1200° to 1600° F. It would be expected that the coercive force in the 1200° to 1600° F range would be substantially lower than at room temperature in accordance with the trend reported previously for the hydraulic extrusions.

TABLE IV-20. Comparison of Room Temperature Coercive Force Values of Extrusions Made with a Conventional Hydraulic Press and Dynapak

Powder or Extrusion No.	Nominal Composition (weight percent)	Extrusion		Amount of Dispersed Phase (percent by volume)	Average Effective Size of Dispersed Particle (microns)	Average Inter-particle Spacing (microns)	Coercive Force, H_c at Room Temperature (oersteds)
		Method	Billet Preheat (°F)				
a. Prealloyed	Atomized Powders						
4	Co+1.0B+4.2Zr	Hydraulic	1 hr. at 2000	26	1.0	2.7	48.0
4	Co+1.0B+4.2Zr	Dynapak	15 min. at 1600	26	0.7	2.0	25.7
13	Fe+25.6Co+1.0B+4.2Zr	Hydraulic	1 hr. at 2000	20	0.9	3.6	18.8
13	Fe+25.6Co+1.0B+4.2Zr	Dynapak	15 min. at 1600	20	0.5	2.0	24.5
13	Fe+25.6Co+1.0B+4.2Zr	C.W. 65%[a]	--	20	0.5	2.0	57.3
14	Fe+25.6Co+1.0B+4.2Cb	Hydraulic	1 hr. at 2000	20	0.8	3.1	19.6
14	Fe+25.6Co+1.0B+4.2Cb	Dynapak	15 min. at 1600	20	0.6	2.4	23.3

(a) Dynapak extrusion was given a 65% reduction in area by swaging at room temperature after extrusion.

d. CORRELATION OF COERCIVE FORCE WITH DISPERSOID PARAMETERS FOR EXTRUSIONS (PHASES 1, 2, AND 3)

The coercive force at 1200° F and 1600° F for cobalt-base alloys containing a constant amount of dispersoid (10 v/o as an example) is plotted against the effective particle size of the dispersed phase in figure IV-27. (The compositions in figure IV-27 are identified by letters and numbers designating powder or extrusion types listed in table IV-21 and preceding tables.) Figure IV-27 shows the coercive force increased with decreasing particle size, reaching a maximum at 0.1 microns, the smallest effective average particle size obtained in this program. This may be tentatively explained on the basis that the 0.1 micron particles were approximately the same size as the thickness of the magnetic domain walls. Thus they were more effective in promoting sticking and retarding domain wall movement (ref. IV-62 to IV-65). The coercive force would be expected to reach a maximum when the particle size of the dispersoid was the same as the thickness of the

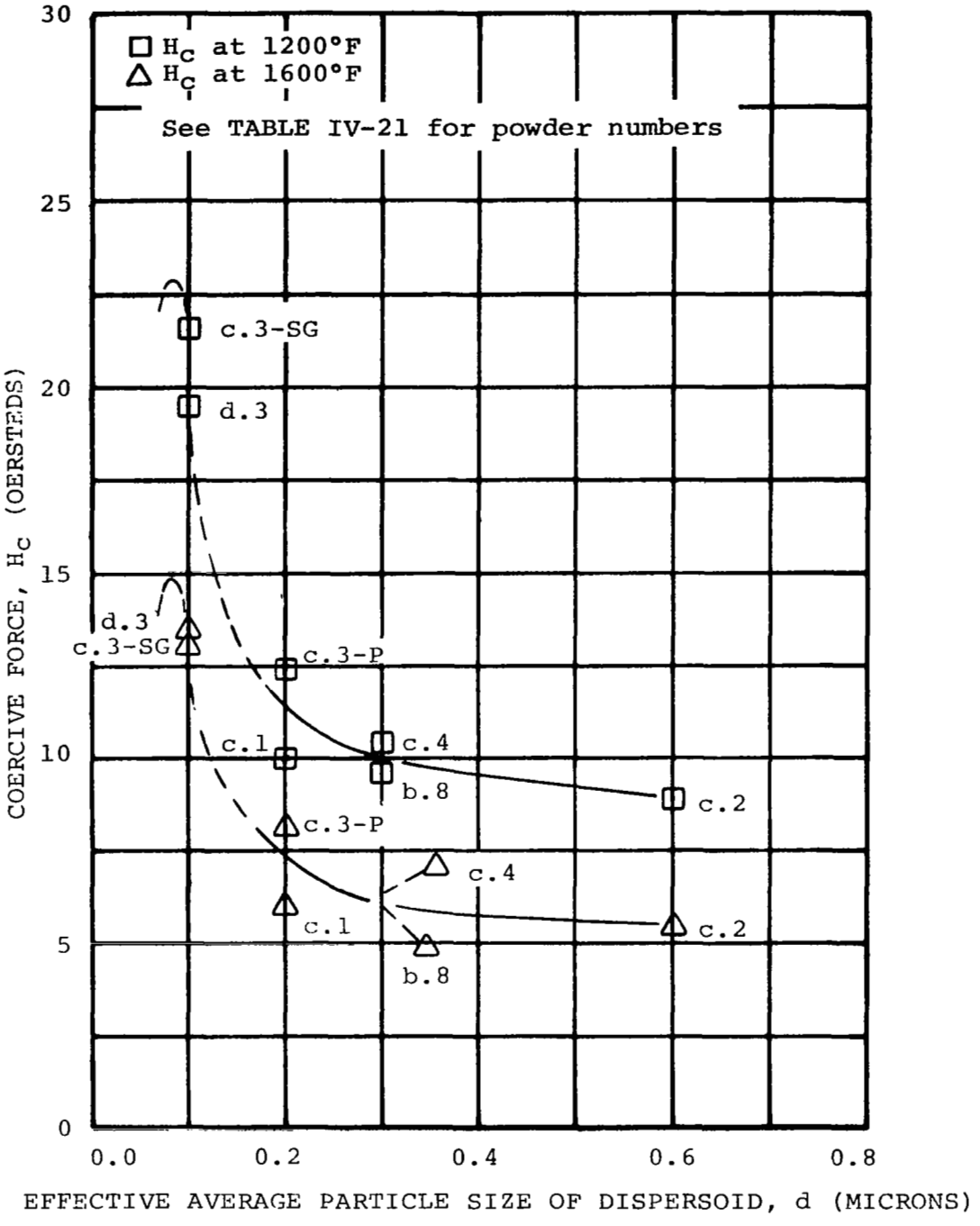

FIGURE IV-27. Effect of Particle Size of Dispersoid in Cobalt + 10 v/o Dispersoid (nominal) Extrusions on the Coercive Force at 1200°F and 1600°F

TABLE IV-21. Legend of Powder or Extrusion Composition Number for Figures IV-27, IV-28, IV-29, and IV-32

Symbol	Prealloyed Atomized Powders	Volume Percent Dispersoid
a. 3	Co+1. 0B+2. 2Ti	32
a. 4	Co+1. 0B+4. 2Zr	26
a. 5	Co+1. 0B+4. 2Cb	27
a. 6	Co+1. 0B+8. 3Ta	27
a. 12	Fe+26. 1Co+1. 0B+2. 2Ti	20
a. 13	Fe+25. 6Co+1. 0B+4. 2Zr	20
a. 14	Fe+25. 6Co+1. 0B+4. 2Cb	20
a. 15	Fe+24. 5Co+1. 0B+8. 3Ta	21
a. 19	Fe+24. 8Co+8. 3Zr	6. 4
a. 30	Co+0. 8B+3. 2Cb	20

Symbol	Composite Powders	Volume Percent Dispersoid
c. 3-SG	Co+11. 2ThO_2 (0. 01-0. 06 μ), Sherritt Gordon	10
c. 1	Co+4. 75Al_2O_3 (0. 01-0. 06 μ), Chas. Pfizer	10
c. 2	Co+4. 75Al_2O_3 (0. 1-0. 6 μ), Chas. Pfizer	10
c. 3-P	Co+11. 2ThO_2 (0. 01-0. 06 μ), Chas. Pfizer	10
c. 4	Co+11. 2ThO_2 (0. 1-0. 6 μ), Chas. Pfizer	10
c. 11-P	Fe+23. 7Co+12. 1ThO_2 (0. 01-0. 06 μ), Chas. Pfizer	10
c. 11-V	Fe+23. 7Co+12. 1ThO_2 (0. 01-0. 06 μ), Vitro Labs	10
c. 13-SG	Co+4. 5ThO_2 (0. 01-0. 06 μ), Sherritt Gordon	4
c. 14-SG	Co+8. 4ThO_2 (0. 01-0. 06 μ), Sherritt Gordon	7. 5
c. 13-P	Co+4. 5ThO_2 (0. 01-0. 06 μ), Chas. Pfizer	4
c. 14-P	Co+8. 4ThO_2 (0. 01-0. 06 μ), Chas. Pfizer	7. 5
c. 15	Fe+24. 5Co+9. 3ThO_2 (0. 01-0. 06 μ), Chas. Pfizer	7. 5

Symbol	Internally Oxidized Powders	Volume Percent Dispersoid
b. 8	Co+4. 7Al_2O_3	9. 8
b. 9	Co+3. 6BeO	8. 3
b. 17	Fe+25. 6Co+5. 1Al_2O_3	8. 4
b. 18	Fe+26. 0Co+3. 9BeO	9. 6

Symbol	Supplier Extrusions	Volume Percent Dispersoid
d. 3	Co+11. 2ThO_2 (0. 01-0. 06 μ), Nem - Lab	9. 3
d. 9	Co+2. 3ThO_2 (0. 01-0. 06 μ), Curtiss Wright	1. 8

domain walls. With particles either coarser or finer than the critical size, the coercive force would decrease.

The dispersed particles in the iron+27w/o cobalt-base alloys were not as fine (0.3 microns minimum) as in the cobalt-base (0.1 microns minimum). However, in the particle size range obtained in the iron+cobalt alloys there was also a general increase in coercive force as the dispersoid became finer, when compared on the basis of a constant volume percent of dispersoid.

For the dispersed particle sizes investigated in this program, there was good correlation between coercive force at a constant loading (constant v/o) and the inverse of the effective average particle size (1/d) for cobalt-base alloys at 1200° to 1600° F where the cubic form existed (no hexagonal cobalt), and for iron+cobalt-base alloys at room temperature and 1200° to 1600° F. Examples of this are shown in figure IV-28 for cobalt+ 10v/o dispersoid extrusions, and in figure IV-29 for (iron+27w/ocobalt)+20v/o dispersoid extrusions.

The volume percent dispersoid (V), as well as the particle size (d), was next considered as a variable and incorporated into a dispersoid parameter (V/d). All coercive force values measured at 1200° and 1600° F for the cobalt-base extrusions, and those measured at room temperature, 1200° F, and 1600° F for the iron+cobalt-base extrusions are plotted in figures IV-30 and IV-31. There was good correlation between coercive force and the dispersoid parameter at these temperature levels and at others in the 1200° to 1600° F range.

According to the theory of Kersten (ref. IV-66), the coercive force should be proportional to $\frac{V^{2/3}}{d}$ for spherical particles, where d is much greater than the domain wall thickness. On the other hand, Néel (ref. IV-66) predicted that coercive force should be directly proportional to the volume percent dispersoid (V). For the dispersoid particle size range investigated in this program, which tended to be greater than the expected domain wall thickness, the coercive force was found to be directly proportional to V, and more closely related to $\frac{V}{d}$ than to $\frac{V^{2/3}}{d}$.

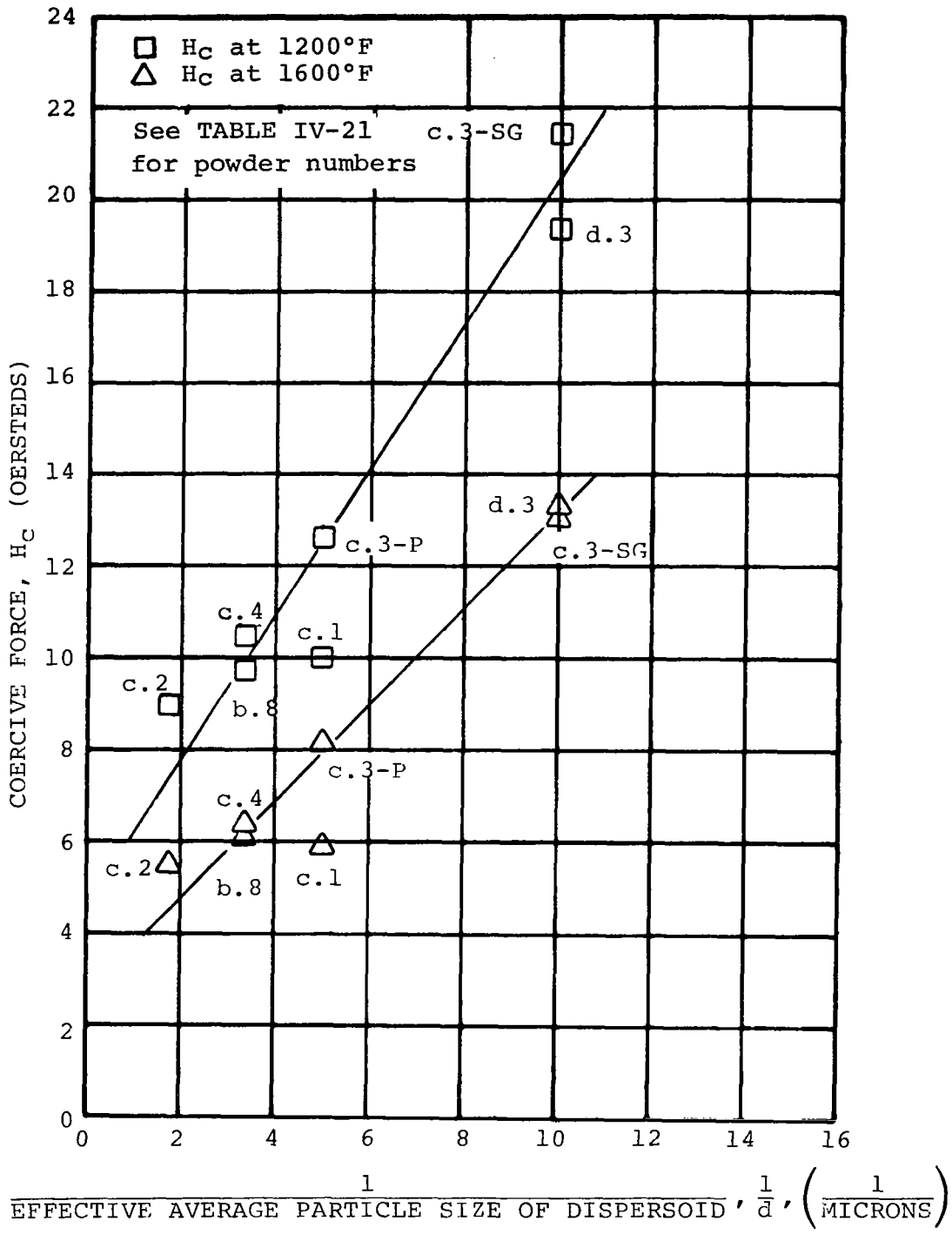

Figure IV-28. Coercive Force at 1200°F and 1600°F of Cobalt + 10 v/o Dispersoid (nominal) Extrusions as a Function of the Inverse of the Particle Size of Dispersoid

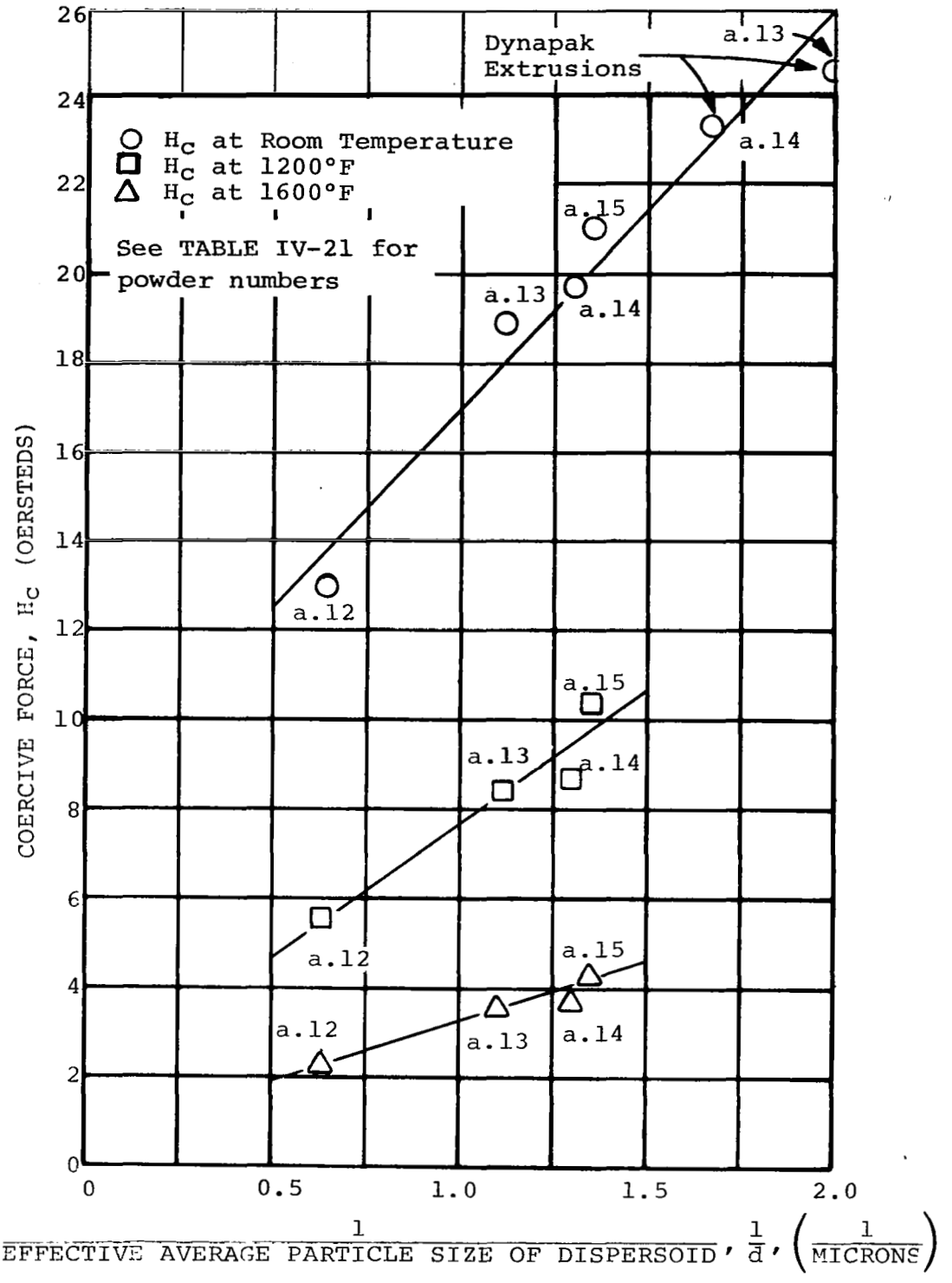

FIGURE IV-29. Coercive Force at Room Temperature, 1200°F and 1600°F of Iron + 27 w/o Cobalt Extrusions with 20 v/o Dispersoid (nominal) as a Function of the Inverse of the Particle Size of Dispersoid

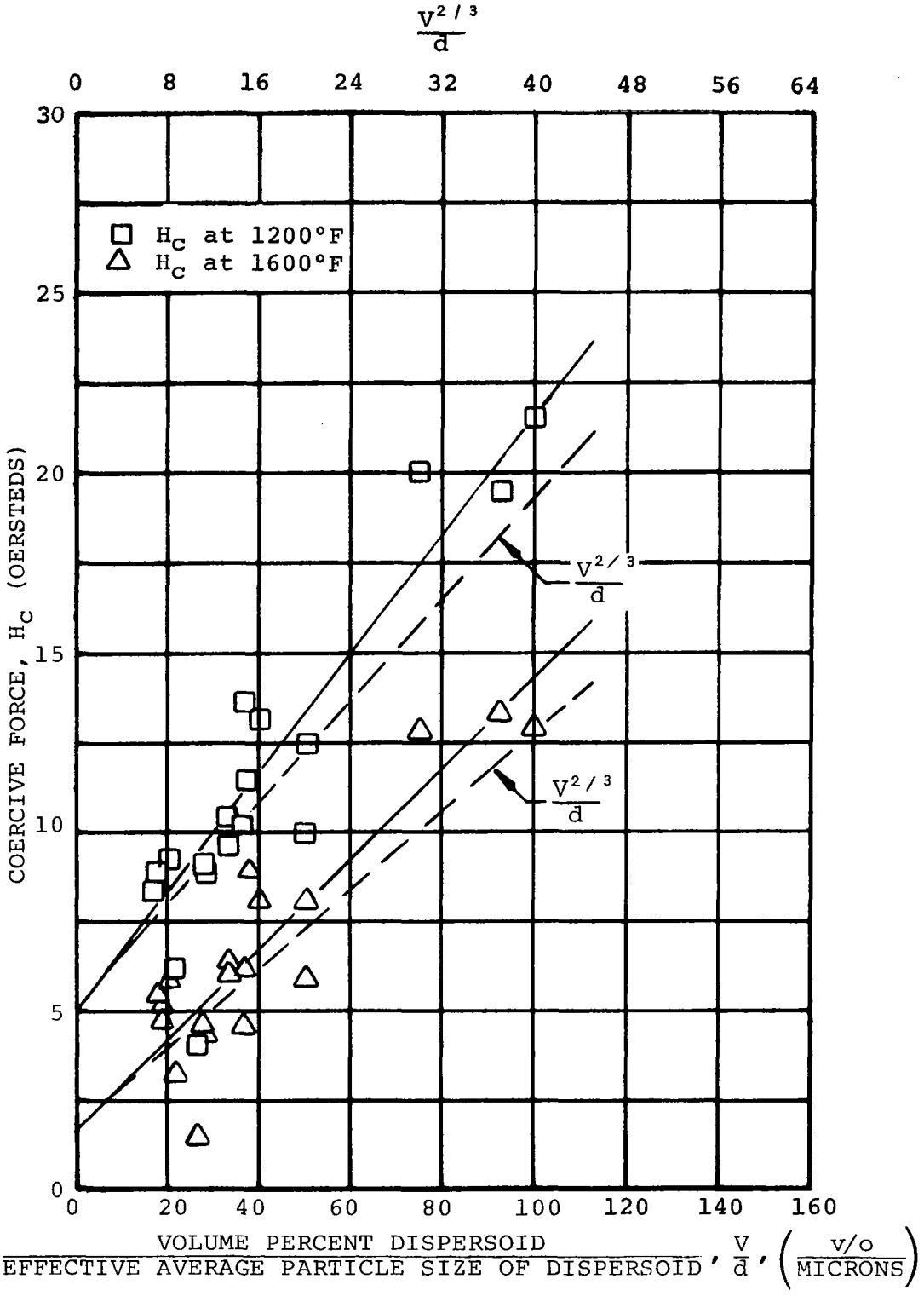

FIGURE IV-30. Coercive Force at 1200°F and 1600°F of Cobalt-Base Hydraulic Extrusions as a Function of the Dispersoid Parameter, $\frac{V}{d}$

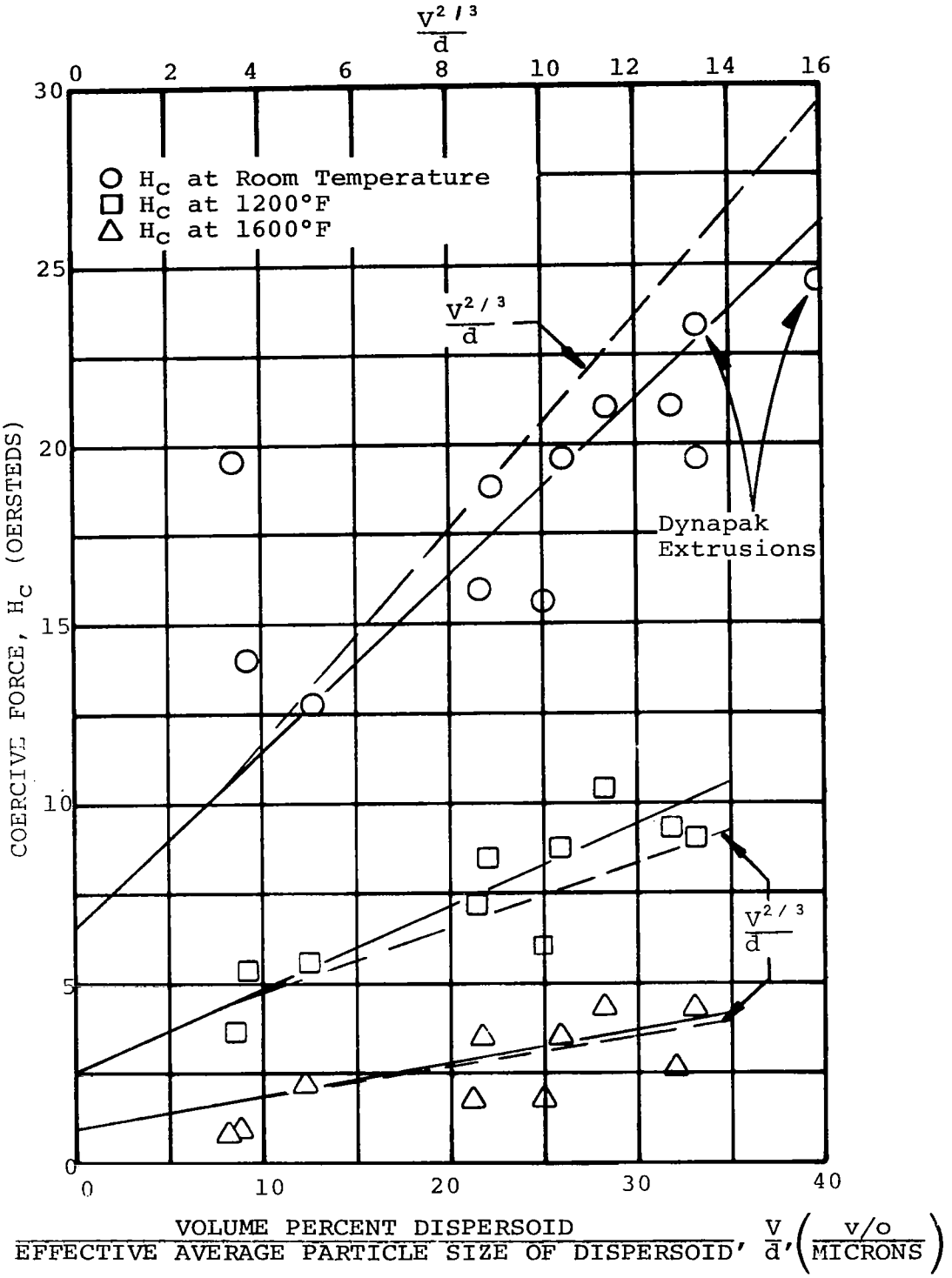

FIGURE IV-31. Coercive Force at Room Temperature, 1200°F, and 1600°F of Iron + 27w/o Cobalt Extrusions as a Function of the Dispersoid Parameter, $\frac{V}{d}$

e. COERCIVE FORCE MEASUREMENTS ON PRELIMINARY SECONDARY WORKED (PHASE 2) HYDRAULIC EXTRUSIONS

During the second phase of the program exploratory secondary working treatments were applied to selected compositional systems at 1500° F and later at lower temperatures. Each cycle of secondary working consisted of one pass of 10 percent reduction by swaging followed by a 10 minute anneal at the swaging temperature. Initially 14 cycles were applied at 1500° F in a four-die swaging machine. When two smaller dies later became available for this machine, 16 cycles were applied.

Coercive force was affected by secondary working as expected, table IV-22. However, in no case did coercive force reach 25 oersteds at 1200° to 1600° F. After 14-16 cycles, the Co+Boride atomized powder compositions Nos. 30 and 5 had much higher values of coercive force at 1200° to 1600° F. On the other hand, the Co+ThO_2 composite powder extrusions showed a smaller but significant change, figure IV-32. It was also established that the matrix structural changes in iron+27 w/o cobalt-base compositions were strongly reflected in coercivity measurements. These observations were exploited in the final phase (phase 3) of the program where measurements of coercive force were employed in a calibration study of secondary working and proof testing of the thermal stability of the matrix grain structure. These will be presented and discussed in later sections of this report.

4. Tensile Properties of Hot-Extruded (Phases 1, 2, and 3) and Preliminary Secondary Worked (Phase 2) Compositions

The longitudinal tensile properties of extrusions and secondary worked rod were determined at room temperature and in vacuum at 1200° and 1600° F after aging 100 hours in vacuum at the elevated test temperature. An aging treatment was applied before testing in order to stabilize the dispersoid and matrix structure. It was decided to use an aging period of 100 hours at the same temperature as the test temperature for all cobalt-base and iron+27w/o cobalt-base compositions in order to provide a common basis for comparison in the initial and intermediate portions of this program. The transformation in Fe+27w/o cobalt-base alloys at 1770° F restricted the possible aging temperature to something below this.

a. TENSILE PROPERTIES OF HYDRAULIC EXTRUSIONS (PHASE 1)

TABLE IV-22. Coercive Force of Hydraulic Extrusions Secondary Worked 14 to 16 Cycles at 1500° F to 1000° F

Powder or Extrusion No.	Nominal Composition (weight percent)	Amount of Dispersed Phase (percent by volume)	Average Size of Dispersed Particles (microns)	Average Inter-particle Spacing (microns)	Secondary Work(a)		Coercive Force, Hc (oersteds)					
					Secondary Working Temp. (°F)	Secondary Working Cycles (No.)	At Room Temp.		At 1200°F	At 1400°F	At 1500°F	At 1600°F
							As Received	After Testing at 1600°F				
a. Prealloyed Atomized Powders												
30	Co+0.8B+3.2Cb	20	0.77	3.1	None	0	19.7	18.2	4.1	2.9	2.3	1.5
30	Co+0.8B+3.2Cb	20	0.77	3.1	1000	16	21.0	17.5	10.8	7.8	6.2	4.5
5	Co+1.0B+4.2Cb	27	0.75	2.0	None	0	47.0	45.5	10.3	8.0	5.9	4.6
5	Co+1.0B+4.2Cb	27	0.75	2.0	1500	14	21.5	21.0	16.3	15.1	13.0	9.9
13	Fe+25.6Co+1.0B+4.2Zr	20	0.90	3.6	None	0	18.8	17.6	8.4	6.4	4.9	3.6
13	Fe+25.6Co+1.0B+4.2Zr	20	0.90	3.6	1500	14	16.0	16.0	6.3	3.8	---	---
13	Fe+25.6Co+1.0B+4.2Zr	20	0.90	3.6	1000	16	28.5	18.3	15.5	6.6	4.5	3.5
13	Fe+25.6Co+1.0B+4.2Zr	20	0.90	3.6	800	14	44.0	17.3	12.6	5.6	4.2	3.2
19	Fe+24.8Co+8.3Zr	6.4(ZrO_2)	0.3	3.0	None	0	15.9	13.9	7.1	4.5	2.9	1.9
19	Fe+24.8Co+8.3Zr	6.4(ZrO_2)	0.3	3.0	1000	16	31.1	21.0	12.5	8.7	7.2	6.0
c. Composite Powders												
13	Co+4.5ThO_2(0.01-0.06$_\mu$), Sherritt Gordon	4	0.1	2.4	None	0	50.5	45.8	13.3	11.0	9.5	8.2
13	Co+4.5ThO_2(0.01-0.06$_\mu$), Sherritt Gordon	4	0.1	2.4	1500	14	45.5	41.5	16.0	12.7	11.5	9.3
13	Co+4.5ThO_2(0.01-0.06$_\mu$), Sherritt Gordon	4	0.1	2.4	1000	16	31.8	31.0	13.2	11.4	9.6	8.4
14	Co+8.4ThO_2(0.01-0.06$_\mu$), Sherritt Gordon	7.5	0.1	1.2	None	0	48.0	43.8	20.0	16.3	15.2	13.0
14	Co+8.4ThO_2(0.01-0.06$_\mu$), Sherritt Gordon	7.5	0.1	1.2	1500	14	43.8	40.2	23.4	19.2	16.9	14.4
14	Co+8.4ThO_2(0.01-0.06$_\mu$), Sherritt Gordon	7.5	0.1	1.2	1250	16	38.6	37.5	21.5	18.4	15.6	13.5
3	Co+11.2ThO_2(0.01-0.06$_\mu$), Sherritt Gordon	10	0.1	0.9	None	0	60.0	58.5	21.5	16.8	15.1	13.0
3	Co+11.2ThO_2(0.01-0.06$_\mu$), Sherritt Gordon	10	0.1	0.9	1500	14	46.2	46.4	21.8	17.3	16.5	13.4

(a) Each cycle of secondary working consisted of approximately a 10-percent reduction in area followed by a 10-minute anneal at the swaging temperature.

TABLE IV-22. Coercive Force of Hydraulic Extrusions Secondary Worked 14 to 16 Cycles at 1500° F to 1000° F (continued)

Powder or Extrusion No.	Nominal Composition (weight percent)	Amount of Dispersed Phase (percent by volume)	Average Size of Dispersed Particles (microns)	Average Inter-particle Spacing (microns)	Secondary Work[a]		Coercive Force, Hc (oersteds)					
					Secondary Working Temp. (°F)	Secondary Working Cycles (No.)	At Room Temp.		At 1200°F	At 1400°F	At 1500°F	At 1600°F
							As Received	After Testing at 1600°F				
c. Composite Powders (Continued)												
3	Co+11.2ThO_2(0.01-0.06$_u$), Chas. Pfizer	10	0.2	1.8	None	0	76.5	76.0	12.4	10.3	9.0	8.2
3	Co+11.2ThO_2(0.01-0.06^u), Chas. Pfizer	10	0.2	1.8	1500	14	70.0	67.3	13.7	11.8	10.5	9.1
3	Co+11.2ThO_2(0.01-0.06$_u$), Chas. Pfizer	10	0.2	1.8	1250	16	37.5	41.7	16.5	13.8	12.0	10.2
15	Fe+24.5Co+9.3ThO_2(0.01-0.06$_u$), Chas. Pfizer	7.5	0.3	3.7	None	0	15.5	15.1	7.4	5.8	4.6	4.1
15	Fe+24.5Co+9.3ThO_2(0.01-0.06^u), Chas. Pfizer	7.5	0.3	3.7	1000	16	25.5	20.0	12.1	9.0	7.5	6.4
11	Fe+23.7Co+12.1ThO_2(0.01-0.06$_u$), Chas. Pfizer	10	0.3	2.7	None	0	19.6	19.2	9.0	6.5	5.3	4.4
11	Fe+23.7Co+12.1ThO_2(0.01-0.06$_u$), Chas. Pfizer	10	0.3	2.7	1500	14	24.0	23.4	13.5	10.8	9.4	8.0

(a) Each cycle of secondary working consisted of approximately a 10-percent reduction in area followed by a 10-minute anneal at the swaging temperature.

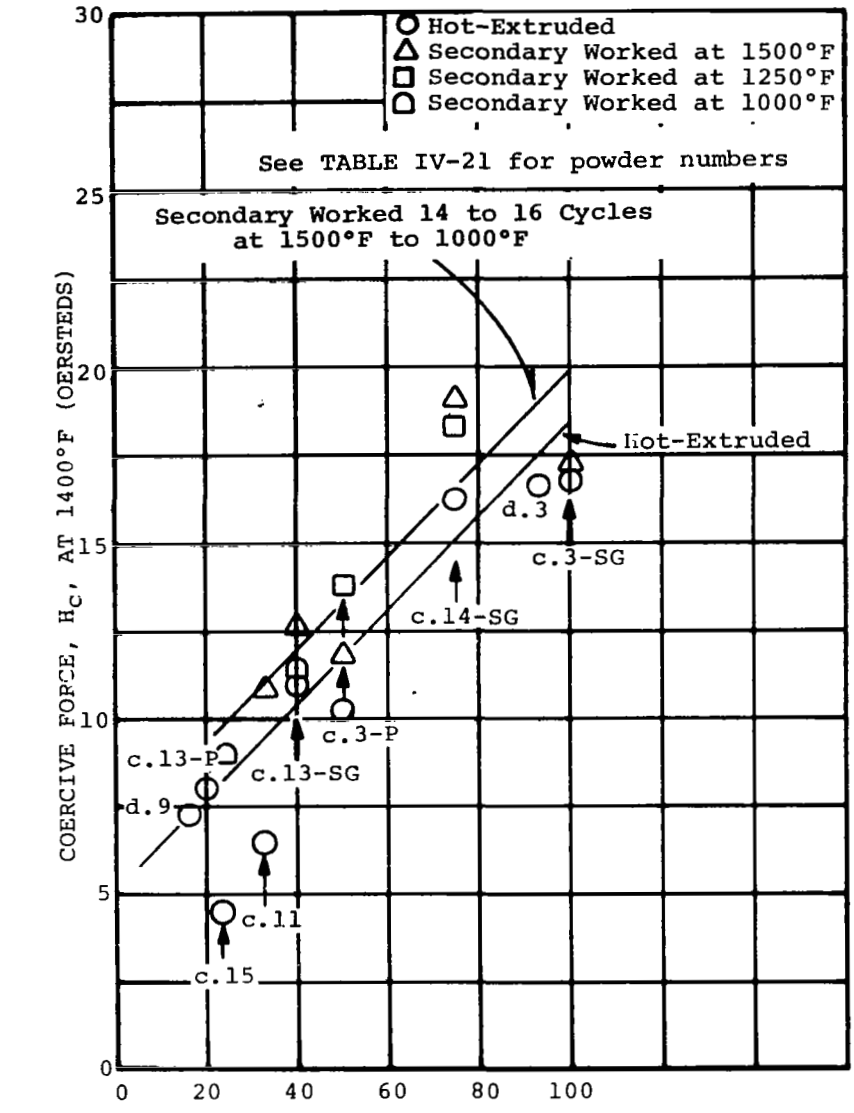

NOTE: Each cycle of secondary working consisted of approximately a 10-percent reduction in area followed by a 10-minute anneal at the swaging temperature.

FIGURE IV-32. Coercive Force at 1400° F of Cobalt + Thoria Alloys in the As-Extruded and Secondary Worked Conditions. Comparative data shown for two Iron + 27w/o Cobalt Alloys, Nos. c.11 and c.15.

The tensile properties of hydraulic as-extruded rod at room and elevated test temperatures are listed in table IV-23 for compositions obtained for the initial evaluation effort (phase 1). The properties of Nivco alloy and DuPont's TD Nickel are given at the bottom of table IV-23 for comparison. The tensile data for Nivco alloy 5/8-inch diameter forged and heat treated bar were obtained on specimens of the same size as for the experimental compositions. The data for TD Nickel bar were obtained from ref. IV-37.

The cobalt-base alloys with boron additions made from prealloyed atomized powder Nos. 3 to 6, containing 26 to 32 v/o dispersed phase, and the iron+cobalt-base alloys made from atomized powder Nos. 12 to 15, containing 20 and 21 v/o dispersoid, tended to have the highest strength at room temperature in comparison with the other compositions made by other methods and containing lesser amounts of dispersoid.

At 1200° F the same alloys, Nos. 3 to 6 and 12 to 15, tended to retain their strength advantage, although their yield strength levels were approached by some of the extrusions of internally oxidized and composite powders. The tensile elongation and reduction of area values were high for extrusions of prealloyed atomized powders. This was related to the rather coarse average particle size (0.73 to 1.6 microns) and large average interparticle spacing (2.0 to 6.4 microns) of the dispersed phase, table IV-15.

The tensile tests at 1600° F revealed the Co+1.0w/oB+4.2w/oCb alloy extruded from prealloyed atomized powder No. 5 had the highest ultimate strength (41,100 psi) and highest yield strength (22,600 psi) combined with high elongation (66%) and reduction in area (61%).

The extrusions of powders made by other methods containing dispersions of thoria and alumina tended to have lower values of elongation and reduction in area at all test temperatures than the prealloyed atomized powder products. In this respect, the oxide-strengthened extrusions behaved more like conventional dispersion-strengthened material. Fracture of the test specimens occurred in some instances before reaching the yield strength at 0.2% offset, and the measured elongation was approximately zero. Some of these materials would be expected to be notch sensitive.

The supplier extrusion No. 3, Co+11.2w/oThO_2 (9.3v/o ThO_2) had low strength at 1200° and 1600° F in spite of a relatively fine, uniform dispersion of ThO_2. This was believed to be related to the high oxygen content (0.21w/o other than as ThO_2) and the high sulphur content (0.028 w/o).

The effect of increasing the amount of dispersoid on the yield strength of cobalt-base extrusions at 1200° F and 1600° F is illustrated in figure IV-33. There was a general tendency for strength to increase with increasing volume percent of dispersed phase. (In this type of plot the influence of the size of the dispersed particles and their interparticle spacing have been neglected.)

Decreasing the average distance between dispersed particles in the matrix tended to raise the yield strengths of extrusions at 1200° and 1600° F, as shown in figure IV-34. This decrease in average interparticle spacing was achieved by decreasing the particle size for a given volume percent of dispersoid, or by increasing the volume percent dispersoid while holding the particle size constant.

b. TENSILE PROPERTIES OF DYNAPAK EXTRUSIONS (PHASE 1)

A comparison of the tensile properties of extrusions made with a hydraulic press and Dynapak, table IV-24, showed that the one cobalt-base and two iron+27w/o cobalt-base compositions of prealloyed atomized powders had significantly higher strengths at 1200° F when extruded by Dynapak. On the other hand, there was no significant improvement in strength at 1600° F.

As mentioned earlier, the purpose of employing the Dynapak was to enable extrusions to be made at a lower temperature (1600° F billet) than used for conventional hydraulic extrusions (2000° F). The boride dispersed particles were smaller in the Dynapak extrusions, as shown earlier in table IV-20, and led to higher strengths in the specimens tensile tested at 1200° F (after aging 100 hours at 1200° F). The lack of improvement in strength at 1600° F (after aging the specimens 100 hours at 1600° F) was attributed to the coarsening of the boride particles at that temperature. This latter feature suggested a limitation on strength stability by dispersed boride phases of these particular chemical compositions.

TABLE IV-23. - Tensile Properties of Hydraulic

Powder or Extrusion No.	Nominal Composition (weight percent)	At Room Temperature			
		Ultimate Strength (1000 psi)	0.2% Offset Yield Strength (1000 psi)	Elongation in 4D (percent)	Reductio in Area (percen
a. Prealloyed Atomized Powders (Extruded)					
3	Co+1.0B+2.2Ti	123.1	117.0	6.0	2.1
4	Co+1.0B+4.2Zr	162.4	144.3	1.0	0.7
5	Co+1.0B+4.2Cb	172.8	116.2	10.0	4.1
6	Co+1.0B+8.3Ta	175.6	136.1	9.8	8.4
12	Fe+26.1Co+1.0B+2.2Ti	132.1	87.8	7.0	6.3
13	Fe+25.6Co+1.0B+4.2Zr	147.1	88.9	10.0	11.8
14	Fe+25.6Co+1.0B+4.2Cb	146.5	101.5	10.0	9.1
15	Fe+24.5Co+1.0B+8.3Ta	129.0	79.3	8.0	7.8
b. Internally Oxidized Powders (Extruded)					
8	Co+4.7Al_2O_3	111.5	106.2	0.5(d)	2.1(
9	Co+3.6BeO	117.7	99.3	5.0	4.1
17	Fe+25.6Co+5.1Al_2O_3	95.8	60.1	5.0	8.9
18	Fe+26.0Co+3.9BeO	113.9	92.6	15.0	11.1
c. Composite Powders (Extruded)					
3	Co+11.2ThO_2 (0.01-0.06 μ), Sherritt Gordon	85.8(e)	(c)	0.0	0.0
11	Fe+23.7Co+12.1ThO_2 (0.01-0.06 μ) Vitro Labs	102.4	80.9	8.0	6.2
1	Co+4.75Al_2O_3(0.01-0.06 μ), Chas. Pfizer	102.4	93.5	1.0	1.8
2	Co+4.75Al_2O_3(0.1-0.6 μ), Chas. Pfizer	-	-	-	-
3	Co+11.2ThO_2(0.01-0.06 μ), Chas. Pfizer	109.6	106.3	3.0	1.5
4	Co+11.2ThO_2(0.1-0.6 μ), Chas. Pfizer	-	-	-	-
11	Fe+23.7Co+12.1ThO_2(0.01-0.06 μ), Chas. Pfizer	118.3	87.4	6.0	4.9
d. Supplier Extrusions of Dispersion-Strengthened Cobalt					
3	Co+11.2ThO_2(0.01-0.06 μ ThO_2)	129.4	97.3	0.2	0.0
9	Co+2.3ThO_2(0.01-0.06 μ ThO_2)	120.5	82.5	3.5	10.6
9(b)	Co+2.3ThO_2(0.01-0.06 μ ThO_2)	104.6	80.8	1.3	3.8
e. Comparison Materials					
	Nivco 5/8 in. dia. Forged and Heat Treated Bar(f)	175.4	116.6	37	23.5
	TD Nickel 1-1/4 in. dia. Bar (Secondary Worked)	90	80	25	80

(a) Specimens aged 100 hours in vacuum (pressure of 1 x 10^{-5} torr or less) at the elevated tensile test temperature before testing in vacuum (pressure of 1 x 10^{-5} torr or less), except for TD Nickel.

(b) Cold reduction in area of 85 percent by swaging after hot extrusion. All other material tested in hot extruded condition.

Extrusions Obtained for Initial Evaluation Effort (Phase 1)

At 1200°F[a]				At 1600°F[a]			
Ultimate Strength (1000 psi)	0.2% Offset Yield Strength (1000 psi)	Elongation in 4D (percent)	Reduction in Area (percent)	Ultimate Strength (1000 psi)	0.2% Offset Yield Strength (1000 psi)	Elongation in 4D (percent)	Reduction in Area (percent)
51.2	26.4	27.0	24.6	20.7	6.3	42.0	30.0
75.7	38.9	20.0	24.2	30.3	10.1	52.0	51.1
80.3	41.9	23.0	26.9	41.1	22.6	66.0	61.0
73.6	42.0	24.0	24.8	34.1	12.1	64.0	57.7
56.4	27.6	50.0	52.5	17.5	8.5	86.0	70.0
62.1	31.5	40.0	44.0	18.5	10.0	82.0	69.5
67.2	31.5	34.0	34.2	17.7	7.3	48.0	69.5
62.8	31.5	34.0	27.7	16.6	8.4	76.0	57.7
38.0	30.4	17.0	14.9	20.9	11.7	15.0	11.2
32.5	20.7	78.0	39.6	13.3	7.0	28.0	27.2
42.4	23.7	30.0	25.0	11.8	5.4	26.0[d]	22.8[d]
47.7	30.5	24.0	21.1	11.6	3.7	36.0	22.9
25.7	25.6	4.0[d]	0.0[d]	12.9	(c)	0.0[d]	0.0[d]
29.8	16.8	4.0	7.3	6.9	2.7	7.0[d]	14.1[d]
28.5	21.6	4.0[d]	7.4[d]	15.2	10.9	1.0	1.3
28.5	21.4	15.0	10.0	7.6	7.0	1.5	0.6
30.1	24.4	8.0	3.5	20.4	15.9	3.0	1.8
27.5	20.7	1.0	2.1	12.6	11.9	2.0	0.6
34.6	22.0	4.0[d]	14.3[d]	20.3	12.2	38.0	26.9
25.1	18.3	4.0	2.1	8.4	(c)	2.0[d]	-[d]
25.8	13.8	30.0	23.6	14.5	6.7	23	16.3
30.5	19.4	7.0	5.4	15.5	9.9	4.0[d]	0.2[d]
97.1	74.3	30.0	51.5	24.9	9.5	124	93.4
38	33	14	29	26	22	10	19

(c) Failed before reaching 0.2% offset.
(d) Broke outside gage length.
(e) Broke in threads.
(f) Heat treated 1725±25°F for 1 hour, water quenched, then air aged at 1225±5°F for 50 hours.

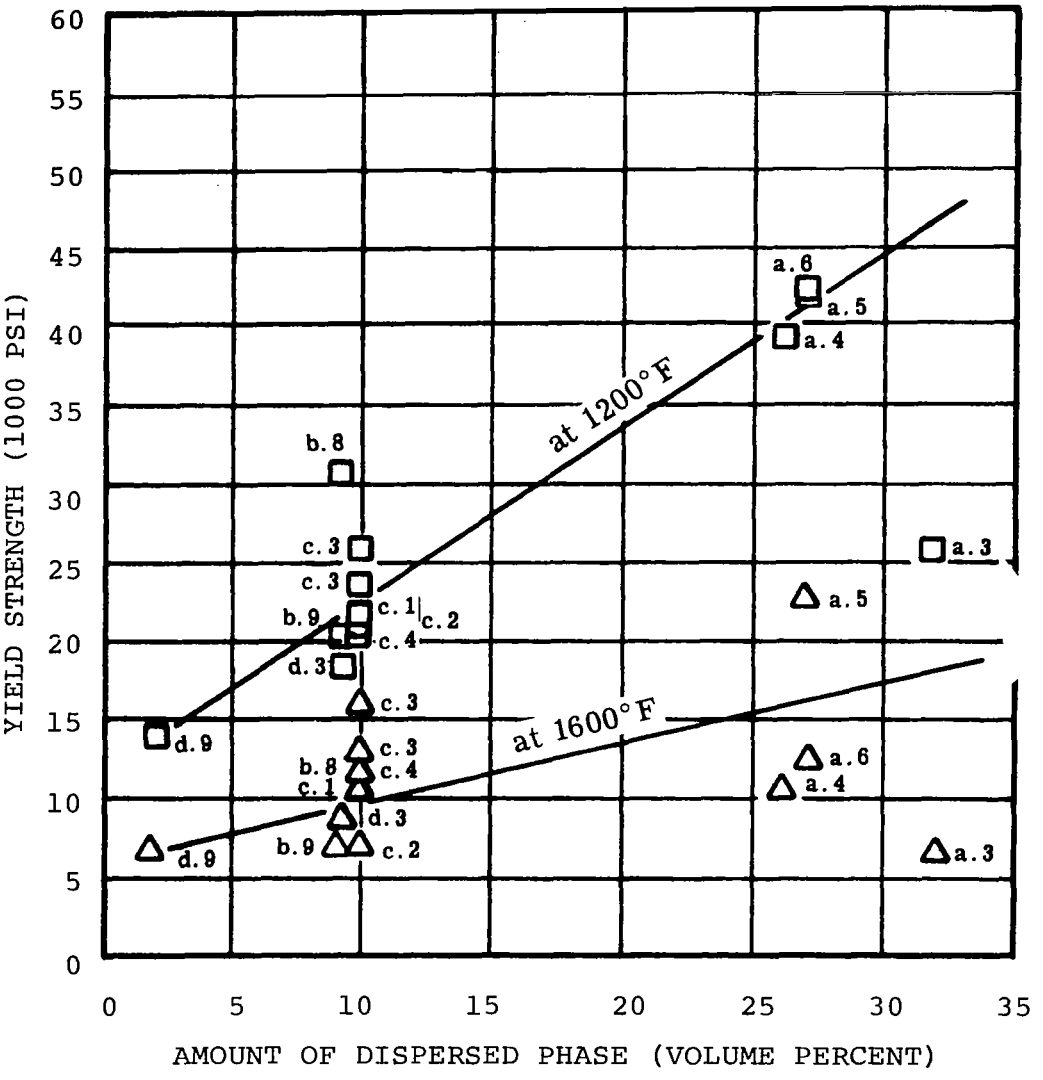

Note: Data points for the various compositions are identified by powder or extrusion numbers listed in tables IV-15 and IV-23.

FIGURE IV-33. Effect of Amount of Dispersed Phase in Cobalt As-Extruded Rod on the Yield Strength at 1200° and 1600° F

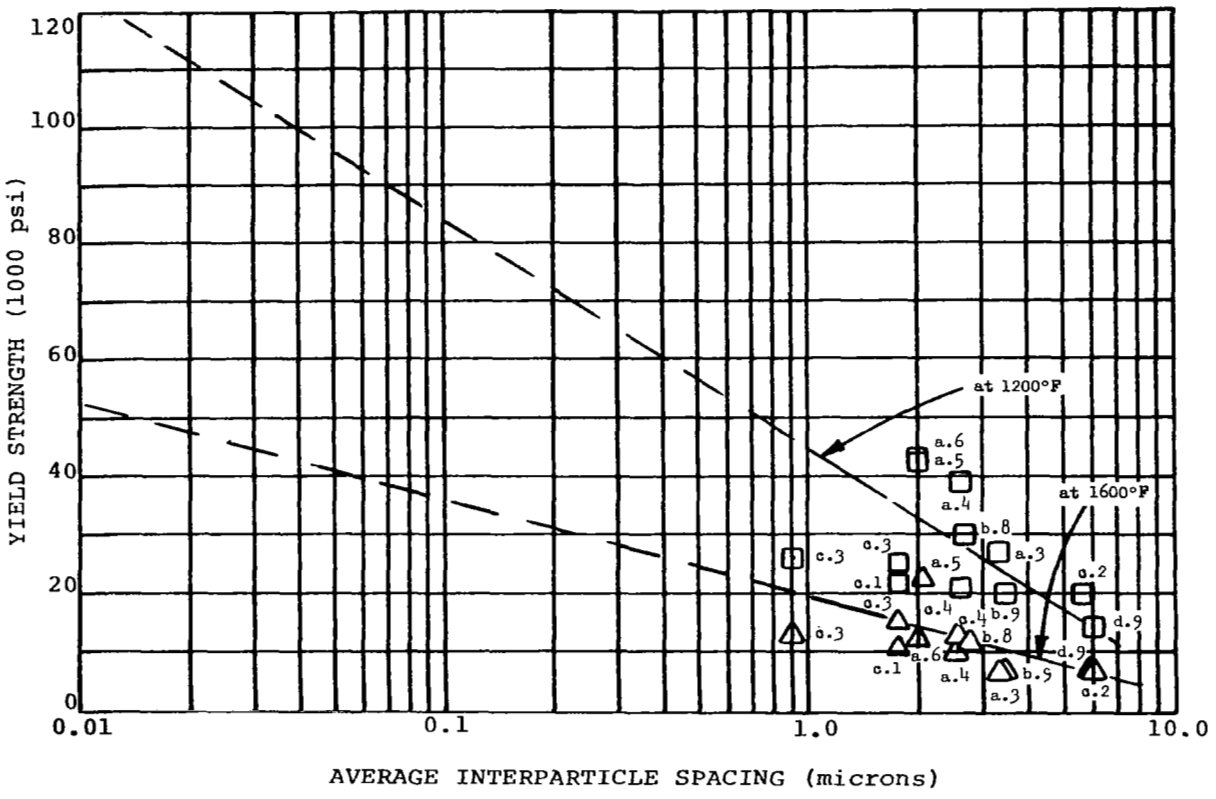

Note: Data points for the various compositions are identified by Powder or Extrusion numbers listed in tables IV-15 and IV-23.

FIGURE IV-34. Effect of Distance Between Dispersed Particles (Approximate Values) in Cobalt As-Extruded Rod on Yield Strength at 1200° and 1600° F

TABLE IV-24. Comparison of Elevated Temperature Tensile Properties of Extrusions Made with a Conventional Hydraulic Press and Dynapak

Powder or Extrusion No.	Nominal Composition (weight percent)	Extrusion Method	Test Temperature (°F)	Tensile Properties[a]		
				Ultimate Tensile Strength (1000 psi)	Yield Strength, 0.2% Offset (1000 psi)	Elongation in 4D (percent)
4	Co+1.0B+4.2Zr	Hydraulic	1200	75.7	38.9	20.0
4	Co+1.0B+4.2Zr	Hydraulic	1600	30.3	10.1	52.0
4	Co+1.0B+4.2Zr	Dynapak	1200	82.9	48.4	30.0
4	Co+1.0B+4.2Zr	Dynapak	1600	24.6	6.1	114.0
13	Fe+25.6Co+1.0B+4.2Zr	Hydraulic	1200	62.1	31.5	40.0
13	Fe+25.6Co+1.0B+4.2Zr	Hydraulic	1600	18.5	10.0	82.0
13	Fe+25.6Co+1.0B+4.2Zr	Dynapak	1200	70.7	42.3	44.0
13	Fe+25.6Co+1.0B+4.2Zr	Dynapak	1600	18.1	10.2	62.0
13	Fe+25.6Co+1.0B+4.2Zr	C.W. 65%[b]	1200	80.2	38.5	2.0[c]
14	Fe+25.6Co+1.0B+4.2Cb	Hydraulic	1200	67.2	31.5	34.0
14	Fe+25.6Co+1.0B+4.2Cb	Hydraulic	1600	17.7	7.3	48.0
14	Fe+25.6Co+1.0B+4.2Cb	Dynapak	1200	71.0	36.7	52.0
14	Fe+25.6Co+1.0B+4.2Cb	Dynapak	1600	19.8	9.8	118.0

(a) All tensile specimens aged 100 hours in vacuum (pressure of 1×10^{-5} torr or less) at the elevated test temperature before testing in vacuum of 1×10^{-5} torr.
(b) Dynapak extrusion was given a 65 percent cold reduction in area by swaging.
(c) Low elongation probably resulted from longitudinal crack present at one end of tensile specimen.

A short length of the Fe+25.6w/oCo+1.0w/oB+4.2w/oZr Dynapak extruded rod was cold reduced 65 percent by swaging. Cold working did not greatly affect the tensile and yield strengths at 1200° F. The low elongation, 2.0 percent, at 1200° F probably was related to a longitudinal crack present near one end of the tensile specimen which became apparent after final machining. The cracked condition may have originated from the extrusion defect located near the back of the extrusion, although precautions were taken to avoid this. Dispersion-strengthened products fabricated for an actual application would be subjected to inspection by radiographic and ultrasonic methods. These test methods would reveal such defects.

All of the Fe+27w/oCo-base extrusions in table IV-24 had a recrystallized structure, both hydraulic and Dynapak. The higher strengths of the Dynapak extrusions at 1200° F were related to the smaller size of dispersed particles and, hence, smaller interparticle spacing in the matrix mentioned earlier.

c. TENSILE PROPERTIES OF HYDRAULIC EXTRUSIONS (PHASES 1, 2, AND 3) WITH AND WITHOUT PRELIMINARY SECONDARY WORKING (PHASE 2)

Compositions extruded during the intermediate evaluation (phase 2) and included in table IV-25 were prealloyed atomized powder No. 19, Fe+24.8w/oCo+8.3w/oZr (6.4v/oZrO_2); powder No. 9A, Co+3.6w/oBeO(8.3v/oBeO) which was given a 1/2 hour internal oxidation treatment; and composite powder Nos. 13 and 14, Co+4.5w/o ThO_2 and Co+8.4w/oThO_2 with 4v/o and 7.5v/oThO_2, respectively, from both Sherritt Gordon and Chas. Pfizer. These compositions were more dilute than many of the compositions investigated in phase 1. There was evidence in the literature that strength levels might be maintained or even increased by reducing the amount of dispersoid. It has been reported for one dispersion-hardening model (ref. IV-28) that maximum strength of hot-extruded materials would be expected with between 4 and 15 v/o dispersed phase and a particle radius between 30 and 50 Å. Nickel + thoria sheet secondary worked by alternate cycles of rolling and annealing showed a maximum tensile strength at approximately 3v/o of 50 to 150Å thoria (ref. IV-39). The tendency to form clusters and the size of the clusters increased with increasing thoria content. In cobalt + thoria rod secondary worked by swaging the tensile strength increased with increasing thoria content in the range investigated, 0.5v/o to 4v/o (refs. IV-69 and IV-70).

The Rockwell C hardness values measured on transverse sections of rod half-way between edge and center, and the longitudinal tensile properties are presented in table IV-25 for hydraulic extrusions with and without secondary working, which was applied at 1500° F for 14 cycles in the initial study.

In the hot-extruded condition, the Fe+24.8w/oCo+8.3w/o Zr composition containing 6.4v/oZrO_2 and 14v/o coarse, elongated particles of Fe-Co-Zr constituent obtained on phase 2 had a slightly higher yield strength at 1200° F and a slightly lower yield strength at 1600° F than the phase 1 composition from which it was derived, Fe+25.6w/oCo+1.0w/oB+4.2w/oZr. The Co+3.6w/oBeO powder composition No. 9A internally oxidized for 1/2 hour, had a higher yield strength at 1600°F, but the same yield strength at 1200° F, in comparison with the same powder material internally oxidized for 2 hours. This was due to the fact that the fineness of the dispersoid was not significantly increased with the shorter internal oxidation time.

TABLE IV-25. - Tensile Properties of Hydraulic Extrusions Obtained for Initial and Intermediate

Powder or Extrusion No.	Nominal Composition (weight percent)	Secondary Work(f)			Rockwell C Hardness (g) (R_C)	At Room	
		Secondary Working Temp. (F)	Secondary Working Cycles (No.)	Cumulative Reduction in Area (percent)		Ultimate Strength (1000 psi)	0.2% Offset Yield Strength (1000 psi)
a. Prealloyed Atomized Powders (Extruded)							
5	Co+1.0B+4.2Cb	None	0	0	41.2	172.8	116.2
5	Co+1.0B+4.2Cb	1500	14	75	46.5	--	--
13	Fe+25.6Co+1.0B+4.2Zr	None	0	0	30.5	147.1	88.9
13	Fe+25.6Co+1.0B+4.2Zr	1500	14	75	--	--	--
19	Fe+24.8Co+8.3Zr	None	0	0	29.5	156.3	105.3
b. Internally Oxidized Powders (Extruded)							
9	Co+3.6BeO (2 hr.)	None	0	0	--	117.7	99.3
9A	Co+3.6BeO (1.2 hr.)	None	0	0	--	121.2	92.4
9A	Co+3.6BeO (1.2 hr.)	1500	14	75	--	--	--
c. Composite Powders (Extruded)							
13	Co+4.5ThO_2 (0.01-0.06μ), Sherritt Gordon	None	0	0	37.6	157.9	141.7
14	Co+8.4ThO_2 (0.01-0.06μ), Sherritt Gordon	None	0	0	41.6	170.0	--
14	Co+8.4ThO_2 (0.01-0.06μ), Sherritt Gordon	1500	14	75	38.4		
3	Co+11.2ThO_2 (0.01-0.06μ), Sherritt Gordon	None	0	0	39.6	85.8(e)	--
3	Co+11.2ThO_2 (0.01-0.06μ), Sherritt Gordon	1500	14	75	39.1	--	--
13	Co+4.5ThO_2 (0.01-0.06μ), Chas. Pfizer	None	0	0	--	115.5	88.9
13	Co+4.5ThO_2 (0.01-0.06μ), Chas. Pfizer	1500	14	75	--	--	--
14	Co+8.4ThO_2 (0.01-0.06μ), Chas. Pfizer	None	0	0	--	115.2	109.2
14	Co+8.4ThO_2 (0.01-0.06μ), Chas. Pfizer	1500	14	75	--	--	--
3	Co+11.2ThO_2 (0.01-0.06μ), Chas. Pfizer	None	0	0	36.5	109.6	106.3
3	Co+11.2ThO_2 (0.01-0.06μ), Chas. Pfizer	1500	14	75	34.8	--	--
11	Fe+23.7Co+12.1ThO_2 (0.01-0.06μ), Chas. Pfizer	None	0	0	25.4	118.3	87.4
11	Fe+23.7Co+12.1ThO_2 (0.01-0.06μ), Chas. Pfizer	1500	14	75	31.6	--	--
d. Comparison Materials							
	Nivco 5 8 in. diam Forged and Heat Treated Bar(h)	--	--	--	--	175.4	116.6
	TD Nickel 1-1 4 in. diam Bar (Secondary Worked)	--	--	--	--	90	80

(a) Specimens aged 100 hours in vacuum (pressure of 1 x 10^{-5} torr or less) at the elevated tensile test temperature before testing in vacuum (pressure of 1 x 10^{-5} torr or less), except for TD Nickel.
(b) Tested at a strain rate of 0.005 in. in. minute from Yield to fracture instead of 0.05 in. in. minute.
(c) Failed before reaching 0.2 percent offset.
(d) Broke outside gage length.
(e) Broke in threads.

With and Without Secondary Working (14 Cycles)

Evaluation Efforts (Phases 1 and 2)

Temperature		At 1200°F[a]				At 1600°F[a]			
Elongation in 4D (percent)	Reduction in Area (percent)	Ultimate Strength (1000 psi)	0.2% Offset Yield Strength (1000 psi)	Elongation in 4D (percent)	Reduction in Area (percent)	Ultimate Strength (1000 psi)	0.2% Offset Yield Strength (1000 psi)	Elongation in 4D (percent)	Reduction in Area (percent)
10.0	4.1	80.3	41.9	23.0	26.9	41.1	22.6	66.0	61.0
--	--	124.4	103.4	7.8	4.0	44.5	27.5	40.0	38.9
10.0	11.8	62.1	31.5	40.0	44.0	18.5	10.0	82.0	69.5
--	--	70.0	37.6	35.0	39.0	19.8	10.5	70.0	55.1
14.0	13.6	74.7	34.7	22.0	32.6	20.8	9.5	110.0	99.8
5.0	4.1	32.5	20.7	78.0	39.6	13.3	7.0	28.0	27.2
10.0	15.9	22.8[b]	20.4	14.9	17.2	21.6	9.9	29.0	22.0
--	--	36.6	23.8	19.0	34.0	20.9	11.5	14.0	11.0
2.0	6.3	19.3[b]	19.1	4.4	4.2	12.4	5.8	15.0	10.8
3.0	0.9	21.9[b]	21.9	1.5	0.8	10.3	8.4	2.0	0.7
		36.7	26.2	6.0	2.2	14.6	(c)	2.0	5.0
0.0	0.0	25.7	25.6	4.0	0.0	12.9	(c)	0.0[d]	0.0[d]
--	--	37.6	30.6	8.0	5.5	17.9	17.9	2.0	2.0
8.0	12.2	21.7[b]	20.3	11.9	11.1	18.3	10.1	28.0	9.3
--	--	30.2	19.9	17.0	16.9	17.3	7.1	9.0	9.3
2.0	0.6	23.7[b]	22.6	5.7	3.8	17.5	9.3	12.0	4.7
--	--	30.5	20.2	14.0	6.5	18.8	9.2	5.0	2.5
3.0	1.5	30.1	24.4	8.0	3.5	20.4	15.9	3.0	1.8
--	--	30.1	24.4	10.0	12.6	23.7	19.2	5.0	4.6
6.0	4.9	34.6	22.0	4.0	14.3	20.3	12.2	38.0	26.9
--	--	43.9	26.1	16.0	16.2	15.0	7.5	8.0	7.8
37	23.5	97.1	74.3	30.0	51.5	24.9	9.5	124	93.4
25	80	38	33	14	29	26	22	10	19

(f) Each cycle of secondary working consisted of approximately a 10-percent reduction in area followed by a 10-minute anneal at the swaging temperature.

(g) R_C hardness values measured on transverse sections of rod halfway between edge and center.

(h) Heat treated 1725±25°F for 1 hour, water quenched, then air aged at 1225±5°F for 50 hours.

The extrusions of the new cobalt-base composite powders No. 13 and 14 containing 4v/o and 7.5v/oThO_2 were weaker than the old extrusions from Sherritt Gordon and Chas. Pfizer powder No. 3 containing 10 v/oThO_2. However, the more dilute compositions tended to have more ductility.

The room temperature hardness of the Co+Boride extrusion No. 5 was increased significantly by the secondary working conditions used, while the Co+ThO_2 compositions tested actually showed a slight decrease. On the other hand, the thoriated iron-cobalt extrusion No. 11 increased in hardness.

The yield strength at 1200° and 1600° F of the Co+Boride extrusion No. 5 having an interparticle spacing of approximately 2.0 microns was improved substantially by secondary working at 1500° F. The extrusion of the Co+3.6w/oBeO internally oxidized powder (1/2 hour) having an interparticle spacing of approximately 3.3 microns showed an increase in yield strength at 1200° F and 1600° F of a little less than 20 percent. The response of the thoriated cobalt-base extrusions to secondary working at 1500° F was also dependent on the interparticle spacing. Of those alloys which received secondary working, the Co+8.4w/oThO_2 and Co+11.2w/o ThO_2 extrusions from Sherritt Gordon powders, and the Co+11.2w/oThO_2 from Chas. Pfizer powder were definitely stronger in the secondary worked condition. Also, the tensile elongation was improved. It appeared that the average interparticle spacing had to be approximately 2 microns or less in order for the material to show a strength response to secondary working, at least under these conditions.

Smith (ref. IV-67) has indicated that the anchoring force of an insoluble inclusion on a grain boundary is proportional to V/d. Ashby (ref. IV-68) developed a theoretical equation which indicated the strength of dispersion-strengthened materials was proportional to the volume percent of dispersoid (V) divided by the mean particle diameter (d) all to the 1/2 power. The V/d ratio has been used to interpret the strengthening effect in nickel + thoria (ref. IV-39) and cobalt + thoria (ref. IV-69) dispersion-strengthened materials.

The Rockwell C hardness at room temperature, yield strength at 1200° F, and coercive force at 1200° F for the Co+ThO_2 alloys in the hot-extruded and secondary worked conditions are shown as a function of the dispersoid parameter (V/d) in figure IV-35. All of these

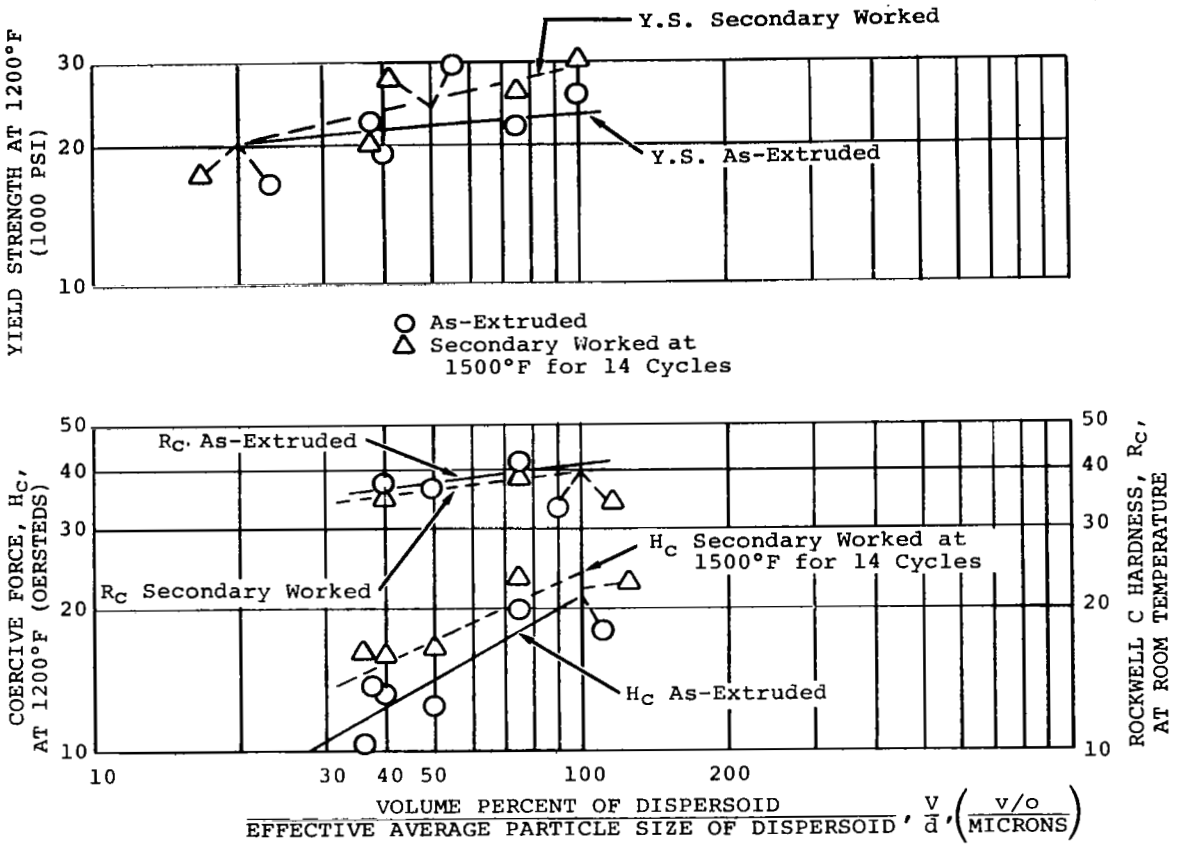

FIGURE IV-35. Coercive Force and Yield Strength at 1200° F and Rockwell C Hardness at Room Temperature of Co + ThO_2 Alloys in the As-Extruded and Secondary Worked (14 Cycles at 1500° F) Conditions

properties increased with V/d ratio. Only at the larger values of V/d (smaller values of interparticle spacing), was the yield strength increased by secondary working substantially above that of the as-extruded condition.

In the case of the Fe+25.6w/oCo+1.0w/oB+4.2w/oZr extrusion from atomized powder No. 13 in table IV-25, secondary working for 14 cycles at 1500° F provided a 19 percent increase in yield strength at 1200° F and a 5 percent increase at 1600° F. Secondary working of the Fe+23.7w/oCo+12.1w/oThO_2 extrusion increased the yield strength by 19 percent at 1200° F, but decreased the yield strength by 39 percent at 1600° F.

The secondary working temperature of 1500° F was above the recrystallization temperature of these Fe+27w/oCo-base compositions. An elongated, recrystallized grain structure was produced by secondary working, as compared with the equiaxed structure present in the original extruded stock. The elongated grain structure was changed through grain growth to a more equiaxed type by aging the tensile specimens 100 hours at 1600° F. Those aged 100 hours and tested at 1200° F retained the elongated grain structure. The fact that recrystallization and grain growth occurred in these materials, but not in the Co-base, at 1500° F and above suggested that the Fe+Co-base had serious high-temperature limitations because of the thermal instability of the matrix structure. It was not possible to obtain for evaluation Fe+Co-base powder compositions for this investigation with really small interparticle spacings (2 microns or less), because the effective particle size of the dispersoid was always rather coarse. The atomized powder composition No. 13 (20v/o dispersoid) and the composite powder composition No. 11 (10v/o dispersoid) had interparticle spacings of approximately 3.6 and 2.7 microns, respectively. In order to achieve finer interparticle spacings, the volume percent dispersoid would have had to be increased substantially. This was not done in order to avoid further dilution of the saturation magnetization values.

The extrusion of atomized powder composition No. 19 in table IV-25 had 6.4v/o of ZrO_2 dispersoid (0.3 micron effective particle size) and 14v/o of coarse, elongated Fe-Co-Zr constituent particles. Although too coarse for dispersion-strengthening, it was believed that the elongated Fe-Co-Zr constituent particles would act as effective barriers to lateral grain growth in the secondary worked condition, giving a smaller grain size and improved thermal stability.

5. Creep Properties of Hydraulic Extrusions (Phases 1, 2, and 3) with and without Preliminary Secondary Working (Phase 2)

The vacuum creep properties obtained at 1400° F after aging the specimens in vacuum for 100 hours at 1400° F or 2 hours at 1830° F are indicated in table IV-26. The creep strain was measured on the specimens after cooling to room temperature. Also included in table IV-26 are the vacuum tensile properties calculated for 1400° F by averaging the 1200° F and 1600° F tensile properties, and the measured values of coercive force and saturation magnetization at 1400° F.

The Co+1.0w/oB+4.2w/oCb composition extruded from atomized powder No. 5 had better creep resistance in the hot-extruded condition than in the secondary worked conditions used (16 cycles maximum). This was also true for the Fe+27w/oCo-base atomized powder compositions Nos. 13 and 19. However, the creep resistance of the Co+1.0w/oB+4.2w/oCb rod in the secondary worked condition showed some improvement at 16 cycles at 1250° F over 14 cycles at 1500° F.

The relatively coarse dispersoid particles (0.75 micron average size) in atomized powder extrusion No. 5 were too large to effectively anchor the grain boundaries developed during secondary working even though the interparticle spacing was 2.0 microns. As a result, the secondary worked grain structure developed with 14 to 16 cycles tended to be more unstable under stress in the creep tests than did the original hot-extruded structure. The same type of problem was encountered with the secondary worked Fe+Co-base atomized powders Nos. 13 and 19.

On the other hand, the Co+11.2w/oThO_2 (10v/oThO_2) composite powder No. 3 from Chas. Pfizer showed a substantial improvement in creep resistance with secondary working. After 16 cycles at 1250° F, a creep strain of 0.22 percent was obtained after 100 hours at 15,000 psi stress at 1400° F. The Co+8.4w/oThO_2 (7.5v/oThO_2) composite powder No. 14 from Sherritt Gordon showed significant improvement in creep resistance as the secondary working temperature was decreased from 1500° to 1250° F. The addition of 0.25w/oZr to the composite powder in combination with a high temperature aging treatment (2 hours at 1830° F) was beneficial in improving creep resistance.

All of the materials listed in table IV-26 had a coercive force well under the tentative limit of 25 oersteds at 1400° F, and a saturation magnetization above 12.0 kilogauss, except for atomized powder No. 5 which had a saturation of only 10.1 kilogauss.

TABLE IV-26. - Short-Term Vacuum Creep Properties of Hydrauli

Obtained for Initial and Intermediat

Powder or Extrusion No.	Nominal Composition (weight percent)	Amount of Dispersed Phase (percent by volume)	Average Effective Size of Dispersed Particles (microns)	Average Inter-particle Spacing (microns)	Secondary Work(d	
					Secondary Working Temp. (°F)	Seconda Worki Cycle (No.
a. Prealloyed Atomized Powders (Extruded)						
5	Co+1.0B+4.2Cb	27	0.75	2.0	None	0
5	Co+1.0B+4.2Cb	27	0.75	2.0	1500	14
5	Co+1.0B+4.2Cb	27	0.75	2.0	1250	16
13	Fe+25.6Co+1.0B+4.2Zr	20	0.90	3.6	None	0
13	Fe+25.6Co+1.0B+4.2Zr	20	0.90	3.6	1500	14
13	Fe+25.6Co+1.0B+4.2Zr	20	0.90	3.6	1250	16
13	Fe+25.6Co+1.0B+4.2Zr	20	0.90	3.6	1000	16
19	Fe+24.8Co+8.3Zr	$6.4ZrO_2$	0.3	3.0	None	0
19	Fe+24.8Co+8.3Zr	$6.4ZrO_2$	0.3	3.0	1250	16

(a) Specimens aged 100 hours at 1400°F in vacuum (pressure of 1×10^{-5} torr or less) before creep testing in vacuum (pressure of 1×10^{-6} torr or less) except for TD Nickel and one as noted.

(b) No tests made at 1400°F. Average of 1200°F and 1600°F tensile properties. Specimens aged 100 hours in vacuum (pressure of 1×10^{-5} torr or less) at the tensile test temperature before tensile testing in vacuum (pressure of 1×10^{-5} torr or less) except for TD Nickel.

Extrusions With and Without Secondary Working (14 to 16 Cycles)

Evaluation Efforts (Phases 1 and 2)

Cumulative Reduction in Area (percent)	At 1400°F[a] Short Term Vacuum Creep Properties: Creep Strain in 100 Hours (percent) At 10,000 psi Stress	At 1400°F[a] Short Term Vacuum Creep Properties: Creep Strain in 100 Hours (percent) At 15,000 psi Stress	At 1400°F[b] Vacuum Tensile Properties: Ultimate Tensile Strength (1000 psi)	At 1400°F[b] Vacuum Tensile Properties: 0.2% Offset Yield Strength (1000 psi)	At 1400°F[b] Vacuum Tensile Properties: Elongation in 4D (percent)	At 1400°F Magnetic Properties: Coercive Force, H_c (oersteds)	At 1400°F Magnetic Properties: Saturation Magnetization, B_s (kilogauss)
0	0.21	0.92	60.7	32.3	44.5	8.0	10.1
75	--	9.6	84.5	65.5	23.9	15.1	10.1
82	--	6.5	--	--	--	--	10.1
0	0.17	Failed in 64 hrs, 16.7% strain	40.3	20.8	61.0	6.4	15.0
75	--	Failed in 11.5 hrs, 32.8% strain	44.9	24.1	52.5	3.8	15.0
82	--	Failed in 5.7 hrs, 11.4% strain	--	--	--	--	15.0
82	--	Failed in 7.2 hrs, 14.2% strain	--	--	--	6.6	15.0
0	0.00	Failed in 17.5 hrs, 53.2% strain	47.8	22.1	66.0	4.5	15.0
82	--	Failed in 2.6 hrs, 103.0% strain	--	--	--	8.7	15.0

(c) Specimen aged 2 hours at 1830°F in vacuum (pressure of 1×10^{-5} torr or less) before creep testing instead of 100 hours at 1400°F.

(d) Each cycle of secondary working consisted of approximately a 10 percent reduction in area followed by a 10 minute anneal at the swaging temperature.

TABLE IV-26. - Continued. Short-Term Vacuum Creep Properties

Working (14 to 16 Cycles) Obtained for Initial and

Powder or Extrusion No.	Nominal Composition (weight percent)	Amount of Dispersed Phase (percent by volume)	Average Effective Size of Dispersed Particles (microns)	Average Inter-particle Spacing (microns)	Secondary Work(d)	
					Secondary Working Temp. (°F)	Secondary Working Cycles (No.)
b. Internally Oxidized Powders (Extruded)						
8	Co+4.7Al_2O_3	9.8	0.3	2.8	None	0
9	Co+3.6BeO	8.3	0.3	3.3	None	0
18	Fe+26.0Co+3.9BeO	9.6	0.3	2.8	None	0
c. Composite Powders (Extruded)						
13	Co+4.5ThO_2 (0.01-0.06μ), Sherritt Gordon	4	0.1	2.4	None	0
13	Co+4.5ThO_2 (0.01-0.06μ), Sherritt Gordon	4	0.1	2.4	1000	16
14	Co+8.4ThO_2 (0.01-0.06μ), Sherritt Gordon	7.5	0.1	1.2	None	0
14	Co+8.4ThO_2 (0.01-0.06μ), Sherritt Gordon	7.5	0.1	1.2	1500	14
14	Co+8.4ThO_2 (0.01-0.06μ), Sherritt Gordon	7.5	0.1	1.2	1250	16
14	Co+8.4ThO_2+0.25Zr	7.5	0.1	1.2	1250	16
14	Co+8.4ThO_2+0.25Zr	7.5	0.1	1.2	1250	16

(a) Specimens aged 100 hours at 1400°F in vacuum (pressure of 1 x 10^{-5} torr or less) before creep testing in vacuum (pressure of 1 x 10^{-6} torr or less) except for TD Nickel and one as noted.

(b) No tests made at 1400°F. Average of 1200°F and 1600°F tensile properties. Specimens aged 100 hours in vacuum (pressure of 1 x 10^{-5} torr or less) at the tensile test temperature before tensile testing in vacuum (pressure of 1 x 10-5 torr or less) except for TD Nickel.

of Hydraulic Extrusions With and Without Secondary

Intermediate Evaluation Efforts (Phases 1 and 2)

Cumulative Reduction in Area (percent)	At 1400°F[a] Short Term Vacuum Creep Properties: Creep Strain in 100 Hours (percent) At 10,000 psi Stress	At 1400°F[a] Short Term Vacuum Creep Properties: Creep Strain in 100 Hours (percent) At 15,000 psi Stress	At 1400°F[b] Vacuum Tensile Properties: Ultimate Tensile Strength (1000 psi)	At 1400°F[b] Vacuum Tensile Properties: 0.2% Offset Yield Strength (1000 psi)	At 1400°F[b] Vacuum Tensile Properties: Elongation in 4D (percent)	At 1400°F Magnetic Properties: Coercive Force, H_c (oersteds)	At 1400°F Magnetic Properties: Saturation Magnetization, B_s (kilogauss)
0	0.40	Failed in 10.8 hrs, 2.6% strain	29.5	21.1	16.0	8.0	12.6
0	Failed in 11.8 hrs, 2.7% strain	--	22.9	13.9	53.0	6.4	12.9
0	Failed during loading, 6.5% strain	--	29.7	17.1	30.0	4.9	16.4
0	--	--	15.9	12.5	9.7	11.0	13.6
82	--	Failed in 20 hrs, 0.84% strain	--	--	--	11.4	13.6
0	--	--	16.1	15.2	1.8	16.3	13.3
75	--	0.94	25.7	20.4	4.0	19.2	13.3
82	--	0.55	--	--	--	18.4	13.3
82	--	0.75	--	--	--	--	13.3
82	--	0.21[c]	--	--	--	--	13.3

(c) Specimen aged 2 hours at 1830°F in vacuum (pressure of 1 x 10^{-5} torr or less) before creep testing instead of 100 hours at 1400°F.

(d) Each cycle of secondary working consisted of approximately a 10 percent reduction in area followed by a 10 minute anneal at the swaging temperature.

TABLE IV-26. - Concluded. Short-Term Vacuum Creep Properties

Working (14 to 16 Cycles) Obtained for Initial and

Powder or Extrusion No.	Nominal Composition (weight percent)	Amount of Dispersed Phase (percent by volume)	Average Effective Size of Dispersed Particles (microns)	Average Inter-particle Spacing (microns)	Secondary Work[d]	
					Secondary Working Temp. (°F)	Secondary Working Cycles (No.)
c. Composite Powders (Extruded)(continued)						
3	Co+11.2ThO_2 (0.01-0.06μ), Sherritt Gordon	10	0.1	0.9	None	0
3	Co+11.2ThO_2 (0.01-0.06μ), Sherritt Gordon	10	0.1	0.9	1500	14
3	Co+11.2ThO_2 (0.01-0.06μ), Chas. Pfizer	10	0.2	1.8	None	0
3	Co+11.2ThO_2 (0.01-0.06μ), Chas. Pfizer	10	0.2	1.8	1500	14
3	Co+11.2ThO_2 (0.01-0.06μ), Chas. Pfizer	10	0.2	1.8	1250	16
11	Fe+23.7Co+12.1ThO_2 (0.01-0.06μ), Chas. Pfizer	10	0.3	2.7	None	0
d. Comparison Alloys						
	Nivco Alloy 5/8 in. dia. Forged and Heat Treated Bar (e)	--	--	--	--	--
	TD Nickel 1-1/4 in. dia. Bar (Secondary Worked)	--	--	--	--	--

(a) Specimens aged 100 hours at 1400°F in vacuum (pressure of 1 x 10^{-5} torr or less) before creep testing in vacuum (pressure of 1 x 10^{-6} torr or less) except for TD Nickel and one as noted.

(b) No tests made at 1400°F. Average of 1200°F and 1600°F tensile properties. Specimens aged 100 hours in vacuum (pressure of 1 x 10^{-5} torr or less) at the tensile test temperature before tensile testing in vacuum (pressure of 1 x 10^{-5} torr or less) except for TD Nickel.

of Hydraulic Extrusions With and Without Secondary

Intermediate Evaluation Efforts (Phases 1 and 2)

	At 1400°F[a] Short Term Vacuum Creep Properties		At 1400°F[b] Vacuum Tensile Properties			At 1400°F Magnetic Properties	
Cumulative Reduction in Area (percent)	Creep Strain in 100 Hours (percent) At 10,000 psi Stress	Creep Strain in 100 Hours (percent) At 15,000 psi Stress	Ultimate Tensile Strength (1000 psi)	0.2% Offset Yield Strength (1000 psi)	Elongation in 4D (percent)	Coercive Force, H_c (oersteds)	Saturation Magnetization, B_s (kilogauss)
0	0.24	Failed in 0.15 hrs, 0.33% strain	19.3	19.3	2.0	16.8	12.8
75	--	Failed in <0.1 hrs, 0.22% strain	27.8	24.3	5.0	17.3	12.8
0	0.21	Failed in 7.5 hrs, 0.40% strain	25.3	20.2	5.5	10.3	12.9
75	--	0.57	27.4	21.8	7.5	11.8	12.9
82	--	0.22	--	--	--	13.8	12.9
0	Failed in 9.5 hrs, 4.5% strain	--	27.5	17.1	21.0	6.5	16.2
--	0.40	3	50	30	60	5.5	8.1
--	0.0	0.0-0.1	32	27	12	Non-Magnetic	Non-Magnetic

(c) Specimen aged 2 hours at 1830°F in vacuum (pressure of 1×10^{-5} torr or less) before creep testing instead of 100 hours at 1400°F.

(d) Each cycle of secondary working consisted of approximately a 10 percent reduction in area followed by a 10 minute anneal at the swaging temperature.

(e) Heat treated 1725±25°F for 1 hour, water quenched, then air aged at 1225±5°F for 50 hours.

6. Final Evaluation Effort (Phase 3)

Based on the combination of magnetic, creep, and tensile properties of compositions obtained in the initial and intermediate evaluation efforts, three iron+27w/o cobalt-base and three cobalt-base compositions were selected for the final evaluation effort (phase 3). This involved calibration studies of the effect of secondary working over a range which included a larger number of cycles to improve thermal stability, and proof testing of the thermal stability of the matrix grain structure so produced. Based on the information developed here, the secondary working treatments were chosen for final application to hot-extruded rod of two iron+27w/o cobalt-base and one cobalt-base composition in order to provide the most suitable material for creep and tensile tests. Electron micrographs showing the structures of these compositions in the secondary worked condition were presented in an earlier section on microstructure.

a. CALIBRATION STUDIES OF SECONDARY WORKING

The Rockwell C hardness measurements at room temperature and the coercive force measurements at room and elevated temperatures are presented in table IV-27 for three Fe+27w/oCo-base and three Co-base compositions in the form of 7/8-inch diameter extruded rod. The calibration studies included the application of up to 36 cycles of secondary work at 800°, 1000°, or 1250° F (below the recrystallization temperature). The maximum number of cycles which could be applied before the rod cracked severely and broke up during swaging was dependent on the composition and the temperature of secondary working. The secondary working temperature had to be raised from 1000° to 1250° F in order to achieve the maximum number of cycles with every composition.

(1) Iron+27w/o Cobalt-Base Alloys

The prealloyed atomized powder composition Fe+25.6 w/oCo+1.0w/oB+4.2w/oZr was secondary worked first at 800° F and 1000° F as a guide for all of the Fe+ 27w/oCo-base systems. Only 14 cycles could be applied at 800° F before the rod cracked severely and broke up. The 800° F secondary working temperature was abandoned in future work because of the following reasons:

a) the maximum number of working cycles which could be applied was too low for calibration purposes.

b) the hardening effect as indicated by Rockwell C hardness at room temperature was essentially the same for secondary working at 1000° F as at 800° F.

c) the coercive force values in the 1200° to 1600° F range, which reflected the level of internal stress retained on re-heating, were actually higher for the material secondary worked 16 cycles at 1000° F than for 14 cycles at 800° F.

d) the coercive force at room temperature before and after heating to 1600° F (approximately 10 minutes at 1600° F) showed a smaller change (ΔH_c of 10.2 oersteds) for the 16 cycles at 1000° F than for the 14 cycles at 800° F (ΔH_c of 26.7 oersteds), indicating greater thermal stability was achieved with the former.

The Rockwell C hardness values for the three Fe+27w/oCo-base compositions are plotted as a function of 1/N, where N is the number of cycles of secondary working, in figure IV-36. The hardness of the prealloyed atomized powder compositions Fe+25.6w/oCo+1.0B+4.2w/oZr and Fe+24.8w/oCo+8.3Zr increased steadily with the 16 secondary working cycles applied at 1000° F. When the temperature was necessarily raised to 1250° F and 28 cycles were applied, the hardness decreased, indicating that there had been a return to a lower level of work-hardening. The Fe+24.8w/oCo+8.3w/oZr composition apparently underwent a slight increase in work-hardening at 1250° F from 28 to 32 cycles. The Fe+24.5w/oCo+9.3w/oThO_2 composition had lower hardness than the others and did not show significant work-hardening beyond 4 cycles at 1000° F. When the working temperature was increased to 1250° F, the hardness at 28 cycles was lowered.

The level of internal stress, as indicated by coercive force tests at elevated temperatures, that was retained in the 1200° to 1600° F range on re-heating increased with the number of cycles of secondary work in all Fe+27w/oCo-base alloys. This is illustrated in figure IV-37 for the Fe+24.8w/oCo+8.3w/oZr composition.

TABLE IV-27. - Calibration Study of Secondary Working-Coercive

Powder or Extrusion No.	Nominal Composition (weight percent)	Amount of Dispersed Phase (percent by volume)	Average Effective Size of Dispersed Particles (microns)	Average Inter-particle Spacing (microns)	Secondary Work[d]	
					Secondary Working Temp. (°F)	Secondary Working Cycles (No.)
Fe+27w/oCo-Base Powders:						
Atomized No.						
13	Fe+25.6Co+1.0B+4.2Zr	20	0.90	3.6	None	0
13	Fe+25.6Co+1.0B+4.2Zr	20	0.90	3.6	1000	4
13	Fe+25.6Co+1.0B+4.2Zr	20	0.90	3.6	1000	8
13	Fe+25.6Co+1.0B+4.2Zr	20	0.90	3.6	1000	16
13	Fe+25.6Co+1.0B+4.2Zr	20	0.90	3.6	1250[a]	28
13	Fe+25.6Co+1.0B+4.2Zr	20	0.90	3.6	800	4
13	Fe+25.6Co+1.0B+4.2Zr	20	0.90	3.6	800	8
13	Fe+25.6Co+1.0B+4.2Zr	20	0.90	3.6	800	14
Atomized No.						
19	Fe+24.5Co+8.3Zr	6.4 ZrO_2[b]	0.3	3.0	None	0
19	Fe+24.5Co+8.3Zr	6.4 ZrO_2[b]	0.3	3.0	1000	4
19	Fe+24.5Co+8.3Zr	6.4 ZrO_2[b]	0.3	3.0	1000	8
19	Fe+24.5Co+8.3Zr	6.4 ZrO_2[b]	0.3	3.0	1000	16
19	Fe+24.5Co+8.3Zr	6.4 ZrO_2[b]	0.3	3.0	1250[a]	28
19	Fe+24.5Co+8.3Zr	6.4 ZrO_2[b]	0.3	3.0	1250[a]	32
19	Fe+24.5Co+8.3Zr	6.4 ZrO_2[b]	0.3	3.0	1250[a]	36
Composite No.						
15	Fe+24.5Co+9.3ThO_2 (0.01-0.06 μ), Chas. Pfizer	7.5	0.3	3.7	None	0
15	Fe+24.5Co+9.3ThO_2 (0.01-0.06 μ), Chas. Pfizer	7.5	0.3	3.7	1000	4
15	Fe+24.5Co+9.3ThO_2 (0.01-0.06 μ), Chas. Pfizer	7.5	0.3	3.7	1000	8
15	Fe+24.5Co+9.3ThO_2 (0.01-0.06 μ), Chas. Pfizer	7.5	0.3	3.7	1000	16
15	Fe+24.5Co+9.3ThO_2 (0.01-0.06 μ), Chas. Pfizer	7.5	0.3	3.7	1250[a]	28

(a) The secondary working temperature had to be increased from 1000°F to 1250°F in order to achieve the indicated number of cycles.

(b) Also present was 14 v/o of large, elongated particles of Fe-Co-Zr constituent.

Force and Hardness of Fe+27 w/o Co-Base and Co-Base Alloys

umulative teduction in Area percent)	Hardness at Room Temperature (Rockwell C)	At Room Temp.		Coercive Force, Hc (oersteds)						
		As Received	After Testing at 1600°F	At 800°F	At 1000°F	At 1200°F	At 1250°F	At 1400°F	At 1500°F	At 1600°F
0	30.5	20.6	18.5	14.8	12.5	9.9	9.0	6.7	5.4	4.1
32	38.1	32.0	16.5	25.0	22.8	13.7	10.5	5.0	3.3	2.6
56	40.3	33.0	16.7	25.0	22.3	14.0	10.0	4.7	3.5	2.8
82	41.7	28.5	18.3	22.5	20.3	15.5	12.7	6.6	4.5	3.5
95	36.4	24.8	24.4	17.2	14.4	12.3	11.2	9.0	7.1	5.3
	38.2	45.3	16.5	36.5	20.5	14.5	12.1	7.0	3.2	2.8
	39.8	46.3	16.5	36.5	21.5	13.3	11.1	4.4	3.2	2.6
	40.5	44.0	17.3	36.8	24.0	12.6	11.3	5.6	4.2	3.2
0	29.5	15.9	13.9	11.1	9.6	7.1	6.2	4.5	2.9	1.9
32	38.7	46.5	20.4	34.8	28.0	14.3	12.6	9.0	7.7	6.5
56	39.4	37.5	19.6	27.9	23.7	13.3	11.5	8.9	7.4	6.0
82	41.5	31.1	21.0	24.3	22.4	12.5	11.6	8.7	7.2	6.0
95	37.5	27.2	25.6	18.9	16.0	13.3	12.9	10.7	9.4	6.7
97	38.6	25.5	--	--	--	--	--	--	--	--
98	(c)	26.5	25.8	18.9	16.2	13.6	12.8	10.5	8.9	8.5
0	21.2	15.5	15.1	11.0	9.2	7.4	6.9	5.8	4.6	4.1
32	30.5	29.3	17.4	23.7	17.8	10.8	9.8	7.5	6.2	5.5
56	31.5	25.8	18.0	20.6	17.2	11.2	10.2	8.2	6.9	5.9
82	30.6	25.5	20.0	19.8	17.4	12.1	11.2	9.0	7.5	6.4
95	26.7	21.0	21.3	14.8	13.4	11.1	10.5	8.8	7.7	6.3

(c) No accurate measurements obtained because of small diameter of core material in steel-clad rod.
(d) Each cycle of secondary working consisted of approximately a 10-percent reduction in area followed by a 10-minute anneal at the swaging temperature.

TABLE IV-27. - Continued. Calibration Study of Secondary Workin

Powder or Extrusion No.	Nominal Composition (weight percent)	Amount of Dispersed Phase (percent by volume)	Average Effective Size of Dispersed Particles (microns)	Average Inter-particle Spacing (microns)	Secondary Work(	
					Secondary Working Temp. (°F)	Second Worki Cycle (No.)
Co-Base Powders:						
Composite No.						
13	Co+4.5ThO_2(0.01-0.06 μ), Sherritt Gordon	4	0.1	2.4	None	0
13	Co+4.5ThO_2(0.01-0.06 μ), Sherritt Gordon	4	0.1	2.4	1000	4
13	Co+4.5ThO_2(0.01-0.06 μ), Sherritt Gordon	4	0.1	2.4	1000	8
13	Co+4.5ThO_2(0.01-0.06 μ), Sherritt Gordon	4	0.1	2.4	1000	16
13	Co+4.5ThO_2(0.01-0.06 μ), Sherritt Gordon	4	0.1	2.4	1250(a)	22
Composite No.						
14	Co+8.4ThO_2(0.01-0.06 μ), Sherritt Gordon	7.5	0.1	1.2	None	0
14	Co+8.4ThO_2(0.01-0.06 μ), Sherritt Gordon	7.5	0.1	1.2	1250(a)	4
14	Co+8.4ThO_2(0.01-0.06 μ), Sherritt Gordon	7.5	0.1	1.2	1250(a)	8
14	Co+8.4ThO_2(0.01-0.06 μ), Sherritt Gordon	7.5	0.1	1.2	1250(a)	16
14	Co+8.4ThO_2(0.01-0.06 μ), Sherritt Gordon	7.5	0.1	1.2	1250(a)	28
Atomized No.						
30	Co+0.8B+3.2Cb	20	0.77	3.1	None	0
30	Co+0.8B+3.2Cb	20	0.77	3.1	1000	4
30	Co+0.8B+3.2Cb	20	0.77	3.1	1000	8
30	Co+0.8B+3.2Cb	20	0.77	3.1	1000	16
30	Co+0.8B+3.2Cb	20	0.77	3.1	1250(a)	22

(a) The secondary working temperature had to be increased from 1000°F to 1250°F in order to achieve t indicated number of cycles.
(b) Also present was 14 v/o of large, elongated particles of Fe-Co-Zr constituent.

oercive Force and Hardness of Fe+27 w/o Co-Base and Co-Base Alloys

umulative ;eduction n Area percent)	Hardness at Room Temperature (Rockwell C)	At Room Temp.		Coercive Force, Hc (oersteds)						
		As Received	After Testing at 1600°F	At 800°F	At 1000°F	At 1200°F	At 1250°F	At 1400°F	At 1500°F	At 1600°F
0	37.6	50.5	45.8	21.0	16.0	13.3	12.6	11.0	9.5	8.2
32	36.7	38.3	37.0	21.0	17.0	14.5	13.9	12.0	10.0	8.4
56	37.8	29.5	28.5	19.3	17.5	15.0	14.0	11.4	9.7	7.0
82	37.1	31.8	31.0	18.9	15.5	13.2	12.8	11.4	9.6	8.4
91	29.1	27.0	27.2	14.3	12.6	10.8	10.4	8.9	7.7	6.3
0	41.6	48.0	43.8	28.0	24.5	20.0	18.8	16.3	15.2	13.0
32	40.0	42.5	40.5	29.4	25.5	22.5	21.3	19.0	16.0	13.3
56	41.1	42.0	39.5	29.5	26.0	22.5	21.0	18.0	16.0	13.5
82	39.0	38.6	37.5	27.5	25.0	21.5	21.0	18.4	15.6	13.5
95	34.9	26.3	26.9	17.2	15.9	14.5	13.8	12.0	10.4	8.7
0	32.3	19.7	18.2	9.2	5.7	4.1	3.8	2.9	2.3	1.5
32	35.6	32.8	32.9	21.0	19.2	12.5	11.7	9.1	7.3	5.1
56	39.4	28.8	18.8	21.4	19.9	16.3	15.6	10.2	8.1	5.3
82	43.8	21.0	17.5	15.0	13.0	10.8	10.1	7.8	6.2	4.5
91	43.2	19.0	18.3	15.4	14.7	13.7	13.3	10.5	7.8	5.6

:) No accurate measurements obtained because of small diameter of core material in steel-clad rod.
i) Each cycle oi secondary working consisted of approximately a 10-percent reduction in area followed by a 10-minute annealat the swaging temperature.

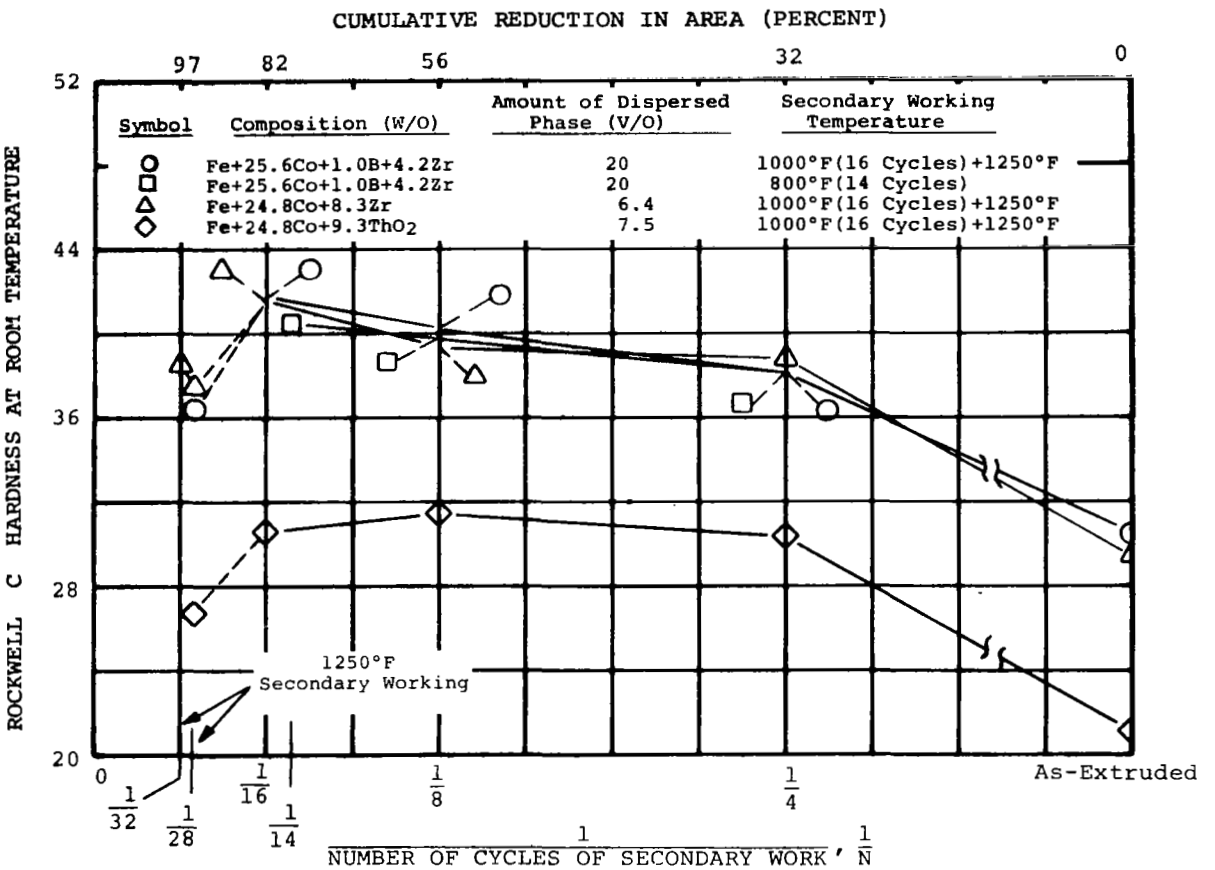

NOTE: Each cycle of secondary working consisted of approximately a 10-percent reduction in area followed by a 10-minute anneal at the swaging temperature.

FIGURE IV-36. Effect of Number of Cycles of Secondary Working on Hardness at Room Temperature of Fe+27w/o Co-Base Alloys

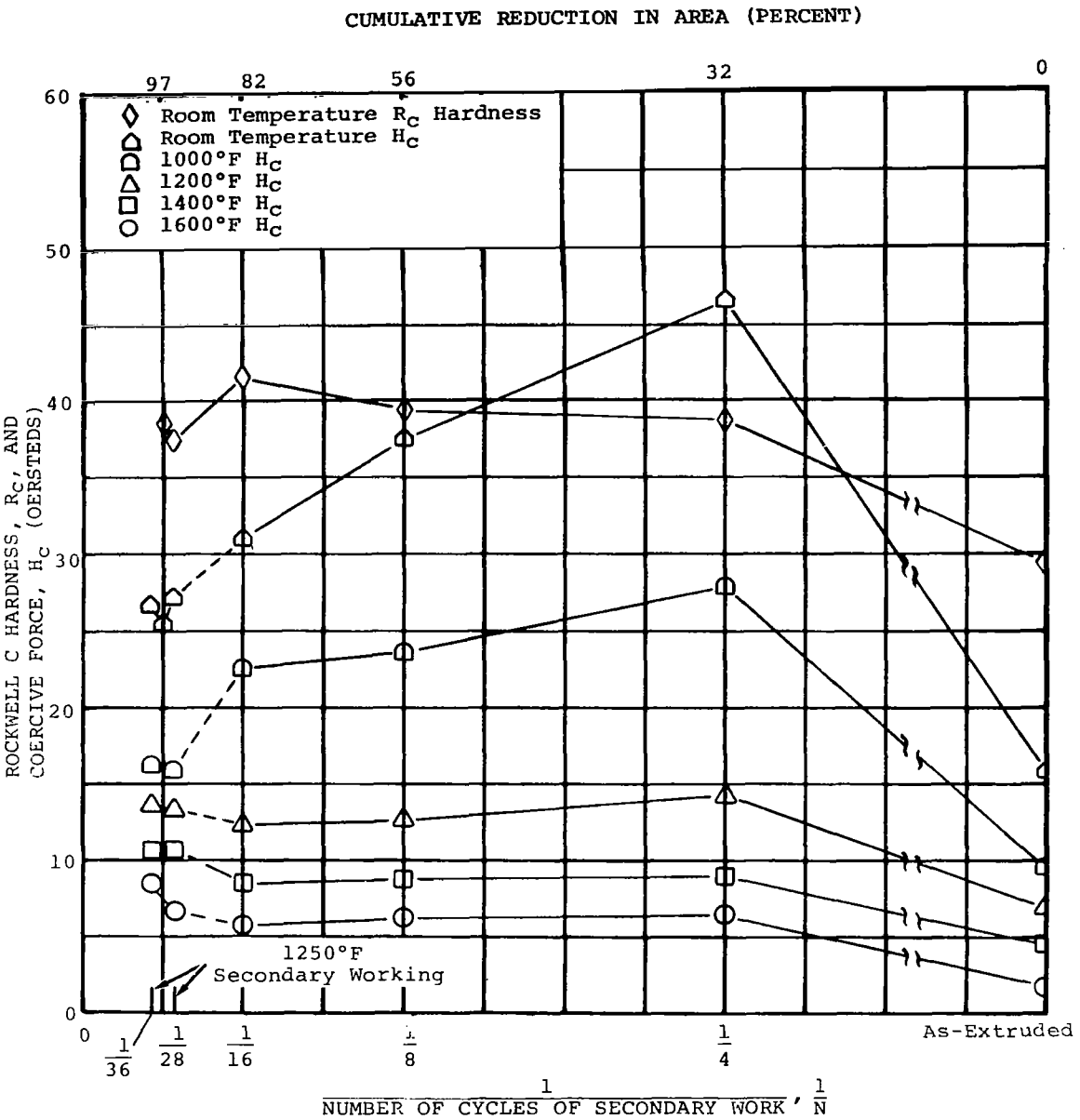

NOTE: Each cycle of secondary working consisted of approximately a 10-percent reduction in area followed by a 10-minute anneal at the swaging temperature.

FIGURE IV-37. Hardness at Room Temperature and Coercive Force at Room and Elevated Temperatures of Fe+24.8w/o Co+8.3w/o Zr Composition Secondary Worked at 1000°F for 16 Cycles and Remainder at 1250°F.

The thermal stability of the matrix grain structure was improved also by increasing the number of cycles of secondary work, as shown by the fact that the coercive force values at room temperature before and after heating to 1600° F were more nearly the same, (ΔH_c diminished), figure IV-38.

(2) Cobalt-Base Alloys

The Rockwell C hardness values for the three cobalt-base compositions are plotted against 1/N, where N is the number of cycles of secondary working, in figure IV-39.

The hardness of the composite powder compositions No. 13, Co+4.5w/oThO_2, and No. 14, Co+8.4w/oThO_2, stayed approximately constant or decreased very slightly with up to 16 cycles of secondary working at a constant temperature, either 1000° or 1250° F. However, when the number of cycles was increased beyond 16 to 22 or 28 there was a significant decrease in hardness. The hardness changes were due to a decrease in the relative amount of hexagonal cobalt present at room temperature. As a result of secondary working, the high temperature cubic form of cobalt was stabilized. Also, when the temperature was increased from 1000° to 1250° F after 16 cycles in order to reach 22 cycles with the Co+4.5w/oThO_2 composition, part of the hardness decrease was probably due to a net reduction in the level of internal stress.

The hardness of the atomized powder composition No. 30, Co+0.8w/oB+3.2w/oCb, increased continuously with 16 cycles of secondary working at 1000° F. However, when the temperature was raised to 1250° F and a total of 22 cycles were applied, the hardness remained essentially the same as at 16 cycles. This reflected no net gain in work-hardening.

The coercive force values in the 1200° to 1600° F range for the Co+4.5w/oThO_2 composition and Co+8.4w/oThO_2 composition changed very little with increasing number of cycles of secondary working up to 16. Data for the latter alloy are presented in figure IV-40. This was believed to be associated with the relatively small effective particle size of the dispersoid (0.1 micron) and interparticle spacings (2.4 and 1.2 microns) in the thoriated cobalt materials. This tended to promote the development of cell or subgrain boundaries in the matrix which were

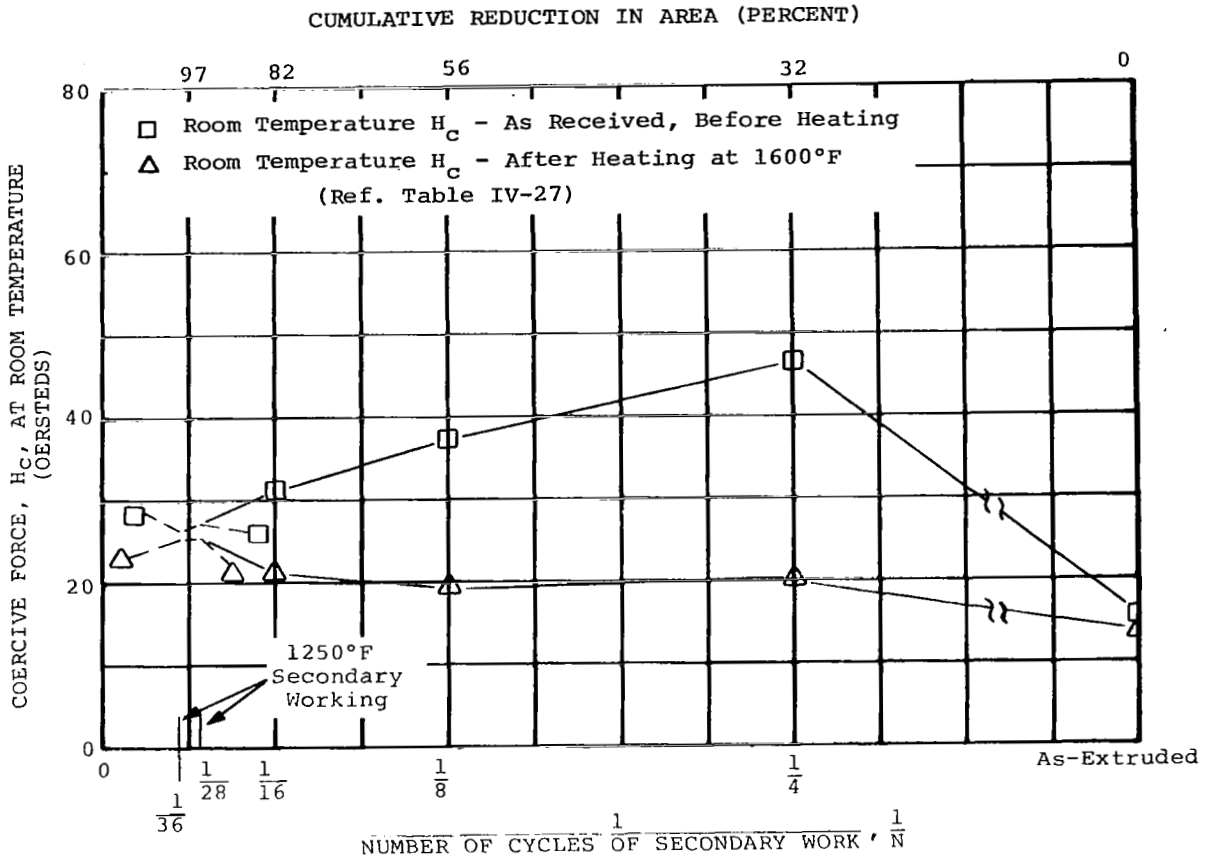

NOTE: Each cycle of secondary working consisted of approximately a 10-percent reduction in area followed by a 10-minute anneal at the swaging temperature.

FIGURE IV-38. Coercive Force at Room Temperature of Fe+24.8w/o Co+8.3w/oZr Composition Secondary Worked at 1000° F for 16 Cycles and Remainder at 1250° F before and after Heating 10 Minutes at 1600° F

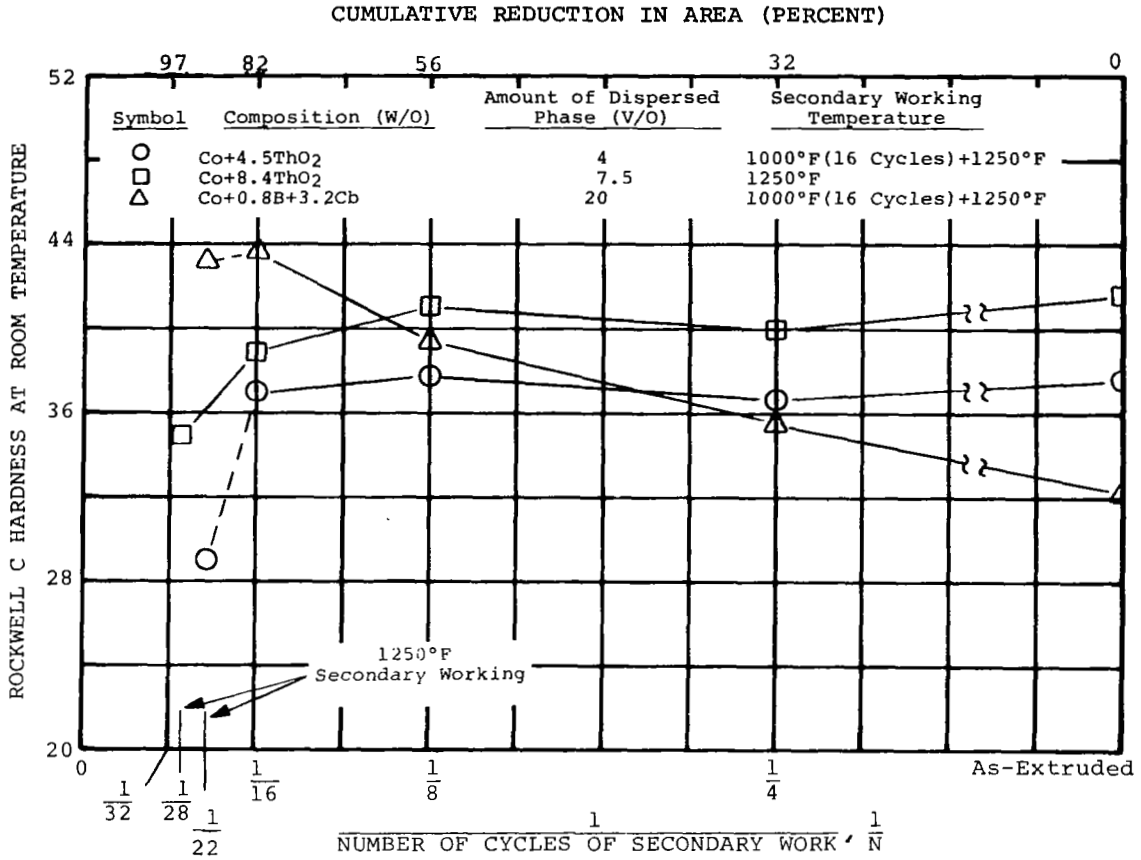

NOTE: Each cycle of secondary working consisted of approximately a 10-percent reduction in area followed by a 10-minute anneal at the swaging temperature.

FIGURE IV-39. Effect of Number of Cycles of Secondary Working on Hardness at Room Temperature of Co-Base Alloys

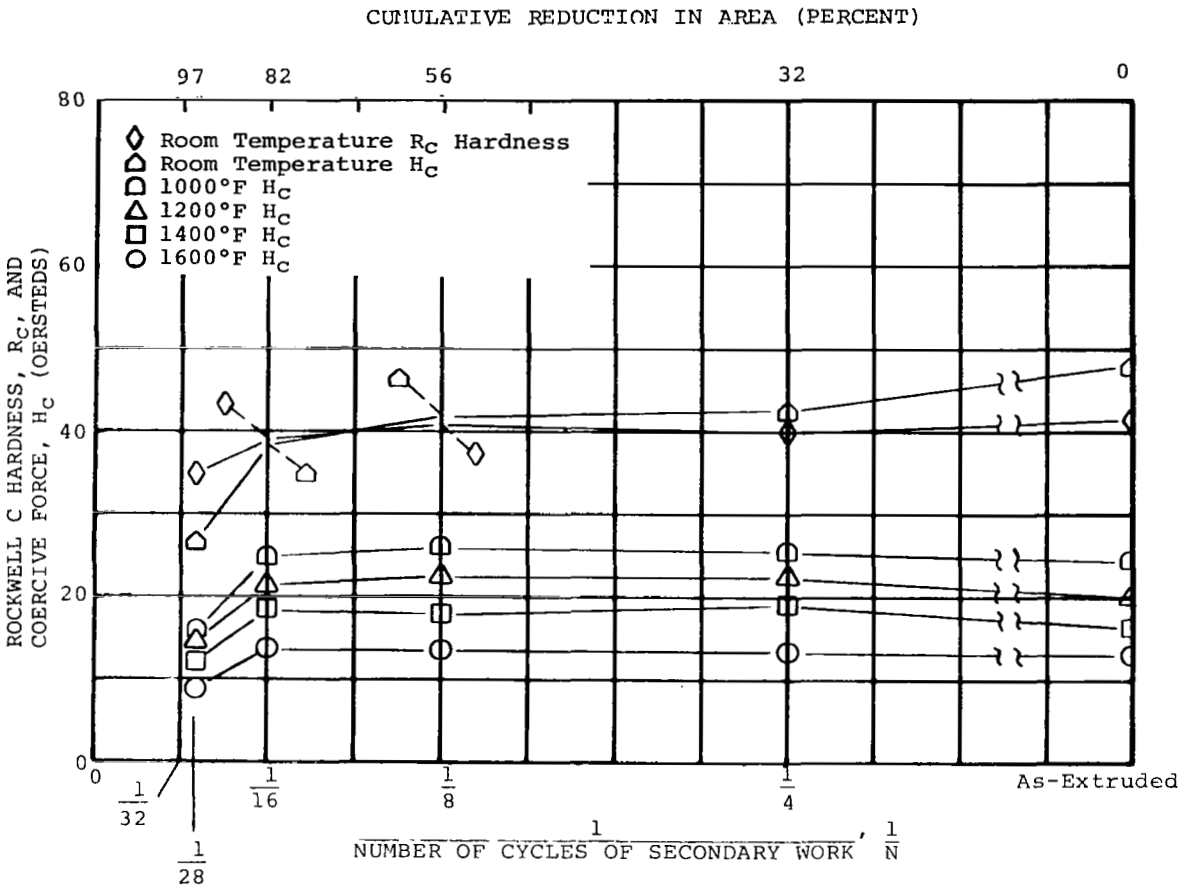

NOTE: Each cycle of secondary working consisted of approximately a 10-percent reduction in area followed by a 10-minute anneal at the swaging temperature.

FIGURE IV-40. Hardness at Room Temperature and Coercive Force at Room and Elevated Temperatures of Co+8.4w/o ThO_2 Composition Secondary Worked at 1250° F

anchored by thoria particles. As a result of secondary working, the dislocations tended to be associated with the boundary walls rather than existing as dislocation tangles in the matrix. Furthermore, the dislocations remained aligned in walls during subsequent heating rather than moving about within the subgrains.

Secondary working of the thoriated cobalt compositions for 22 or 28 cycles at 1250° F reduced the coercive force in the 1200° to 1600° F range. This was interpreted to mean that a relatively greater portion of the dislocations present were aligned in boundary walls, and there was a net reduction in the dislocation tangles or isolated dislocations present within the cell bodies.

The atomized powder composition No. 30, Co+0.8w/o B+3.2w/oCb, had coercive force values in the 1200° to 1600° F range which were much higher after secondary working than in the as-extruded condition, secondary work cycle No. 0. This meant that the level of internal stress (dislocation tangles) in the matrix was greatly increased by secondary working and largely retained at 1200° to 1600° F. The effective particle size of the dispersoid (0.77 microns) and interparticle spacing (3.1 microns) were too large for the development and stabilization of subgrain boundaries such as occurred in the thoriated cobalt system.

The thermal stability of the matrix grain structure of all three cobalt-base alloys was improved by increasing the number of cycles of secondary work. The coercive force measurements at room temperature before and after heating to 1600° F were more nearly the same, (ΔH_c decreased). This is illustrated in figure IV-41 for the Co+8.4w/o ThO_2 rod. The lowest values of coercive force at room temperature were obtained with the maximum number of working cycles. This indicated that the high-temperature cubic form of cobalt had been stabilized and retained at room temperature, while the hexagonal form of cobalt had been essentially eliminated.

b. CALCULATIONS OF COERCIVE FORCE FROM THEORY AND COMPARISON WITH MEASURED VALUES

The most comprehensive equations developed for the calculation of coercive force are those by Néel (refs. IV-

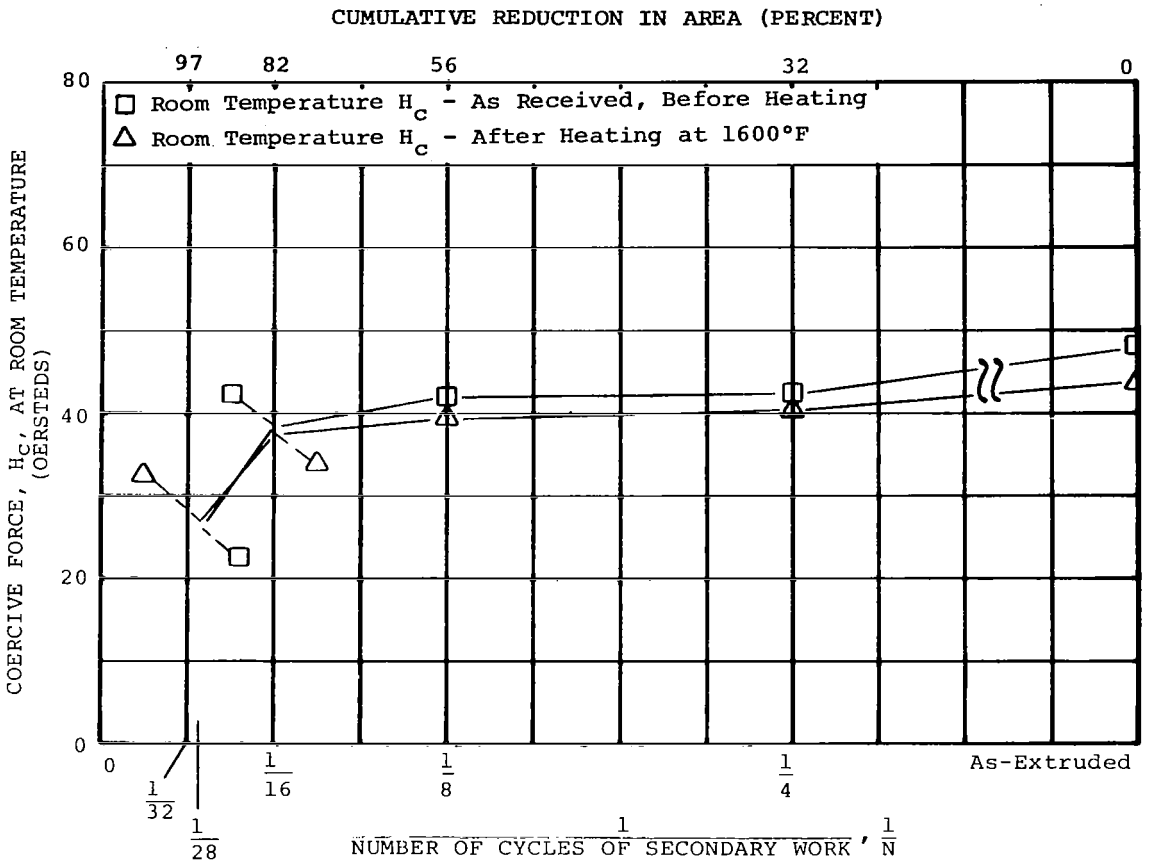

NOTE: Each cycle of secondary working consisted of approximately a 10-percent reduction in area followed by a 10-minute anneal at the swaging temperature.

FIGURE IV-41. Coercive Force at Room Temperature of Co+8.4w/o ThO_2 Composition Secondary Worked for N Cycles at 1250° F Before and After Heating 10 Minutes at 1600° F

66, IV-71, IV-72) who considered both the magnetic poles around large inclusions and the change in magnetization as a result of variations in internal stress. Dijkstra and Wert (ref. IV-62) modified some of these equations for the effect of particle size. They showed that a maximum in the curve of H_c versus particle size of inclusions occurred when particle size approached domain wall thickness. Furthermore, the coercive force decreased with increasing particle size for particles larger than the domain wall thickness, and with decreasing particle size for particles smaller than the domain wall thickness.

For purposes of the present discussion, only the equations developed by Néel will be considered. The three equations and the prevailing conditions for which they were developed are as follows:

$$H_{c_1} = 1.035(f)\frac{\lambda_s\sigma}{I_s}\left[1.386+1/2\ \ln\left(\frac{6.8\ I_s^2}{3/2\ \lambda_s\sigma}\right)\right], \text{ for } \lambda_s\sigma >> K$$

$$H_{c_2} = \frac{9}{15\pi}(f)\frac{\lambda_s^2\sigma^2}{KI_s}\left[1.386+1/2\ \ln\left(\frac{2\pi I_s^2}{K}\right)\right], \text{ for } \lambda_s\sigma << K$$

$$H_{c_3} = \frac{2}{\pi}(V)\frac{K}{I_m}\left[0.386+1/2\ \ln\left(\frac{2\pi I_m^2}{K}\right)\right], \text{ for non-magnetic inclusions}$$

H_c = coercive force

f = volume fraction of the material subject to a large disturbing stress

σ = internal stress

V = volume fraction of inclusions

λ_s = magnetostriction constant

K = crystalline anisotropy constant

I_s = saturation intensity of magnetization

I_m = mean value of saturation intensity magnetization (for dispersion-strengthened materials)

In order to illustrate the application of these equations, figure IV-42 shows the computed curves of coercive force versus temperature for nickel (ref. IV-71). The H_{c_1} curve displays a maximum which both decreases and shifts toward higher temperatures with decreasing internal stress (from $\sigma = 10^9$ dynes/cm^2 to 10^8 dynes/cm^2 or from 14,500 psi to 1,450 psi). The H_{c_2} curve refers to the case where the K value is relatively very high and, therefore, has a limited applicability. The H_{c_3} curve, which considers primarily the effect of inclusions, shows a steep decrease in slope with increasing temperature, mainly because of a decrease in the value of crystalline anisotropy (K). The additive effects of internal stress (or strain) and inclusion contributions to coercive force are indicated in figure IV-43, (ref. IV-72). In most practical cases, combinations of only two curves occur. In the case of cobalt and iron+27w/o cobalt-base materials, the contributions of H_{c_1} and H_{c_3} are important, reflecting the effects of both internal stress and inclusions, while H_{c_2} gives very low values.

The present investigation included: (a) calculation of the coercive force versus temperature relationship for a cobalt-base and an iron+27w/o cobalt-base alloy, both with 7.5v/o thoria, and a comparison of calculated with measured data, and (b) an analysis of these data, particularly with respect to the effect of processing conditions on the structure of both composite materials. The curves for both calculated and measured H_c values are shown in figures IV-44 and IV-45. For theoretical calculations the following conditions were assumed: (a) the internal stress (σ) equaled 20 percent of the yield strength, and (b) the volume fraction (f) of the material subject to a large disturbing stress amounted to 0.10. Obviously it is difficult to make precise estimates of σ and f. The values selected were in agreement with what is known about the stress distributions in these materials and what others have used in similar calculations. The volume fraction (V) of inclusions was 0.075. Since the temperature dependence of crystalline anisotropy and magnetostriction of iron+27w/o

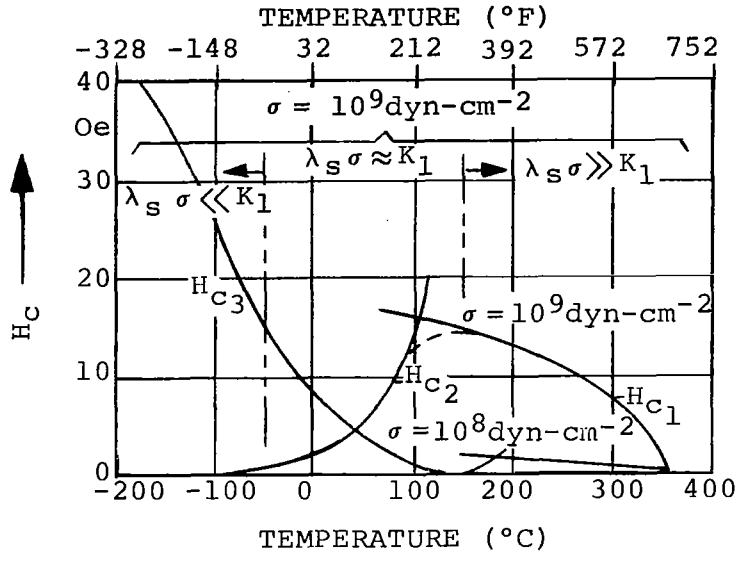

FIGURE IV-42. Temperature dependence of coercive force (Hc) of nickel, calculated using Néel's equations. Two stress levels (σ) assumed: 10^9 dynes/cm^2 and 10^8 dynes/cm^2. Volume fraction of dispersoid (V) as well as volume fraction of strained matrix (f) assumed to be 0.1.

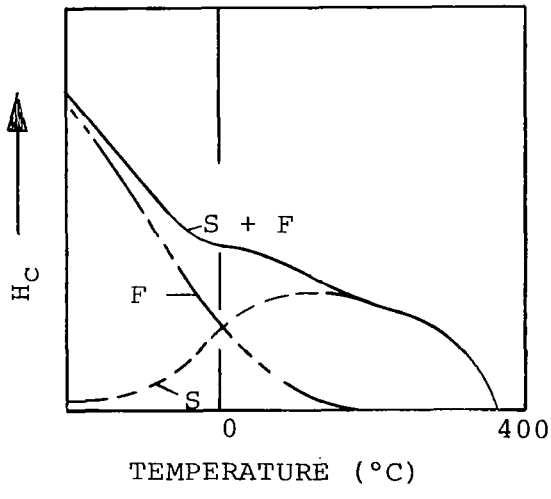

FIGURE IV-43. Additive effects of internal strain (S) and non-magnetic particle (F) contributions to the calculated coercive force versus temperature curve (schematic).

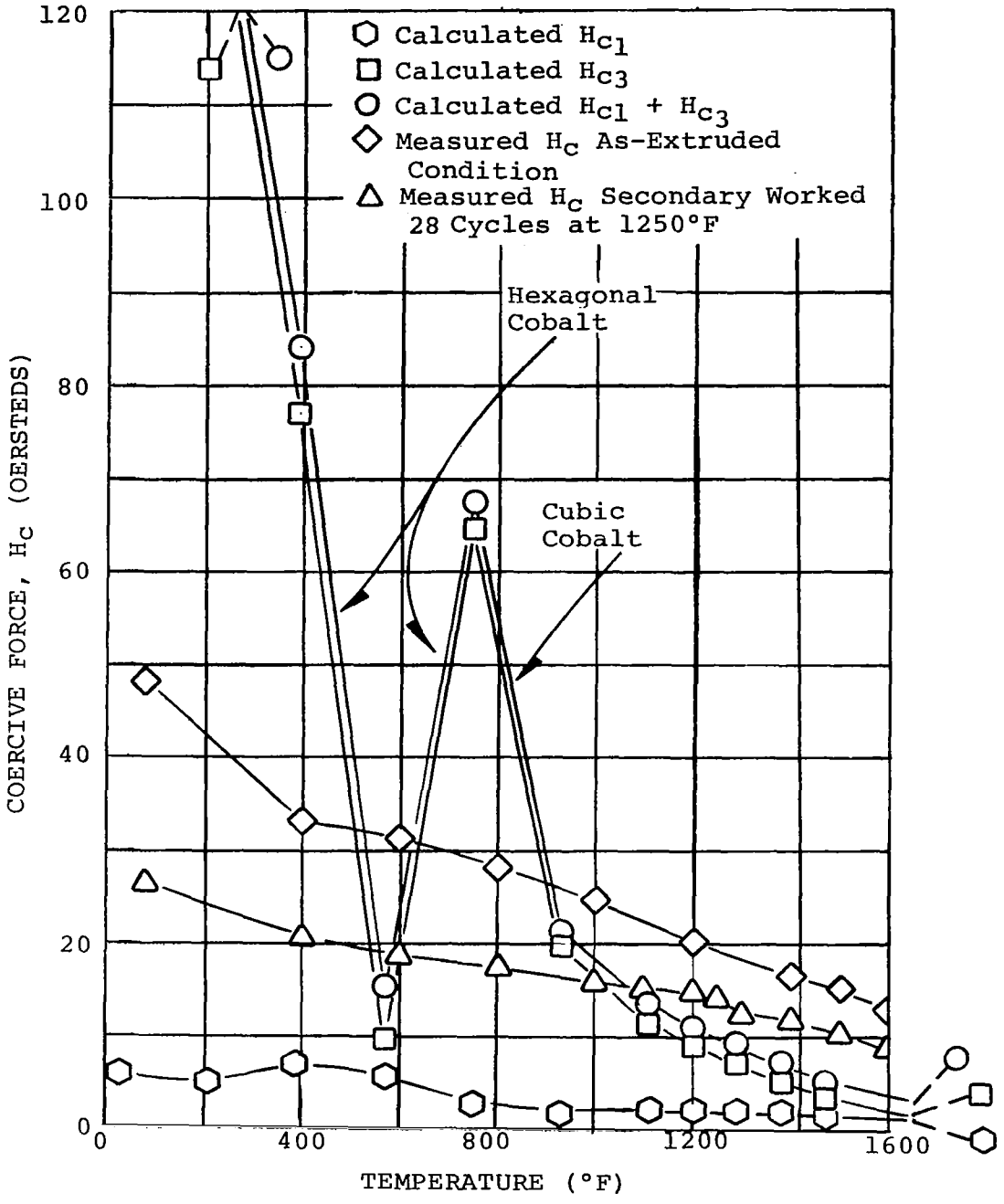

FIGURE IV-44. Calculated Coercive Force ($H_{c_1} + H_{c_3}$) from Néel's Equations and Measured Coercive Force in As-Extruded and Secondary Worked Conditions as a Function of Temperature for Co+8.4w/o ThO_2 Composition

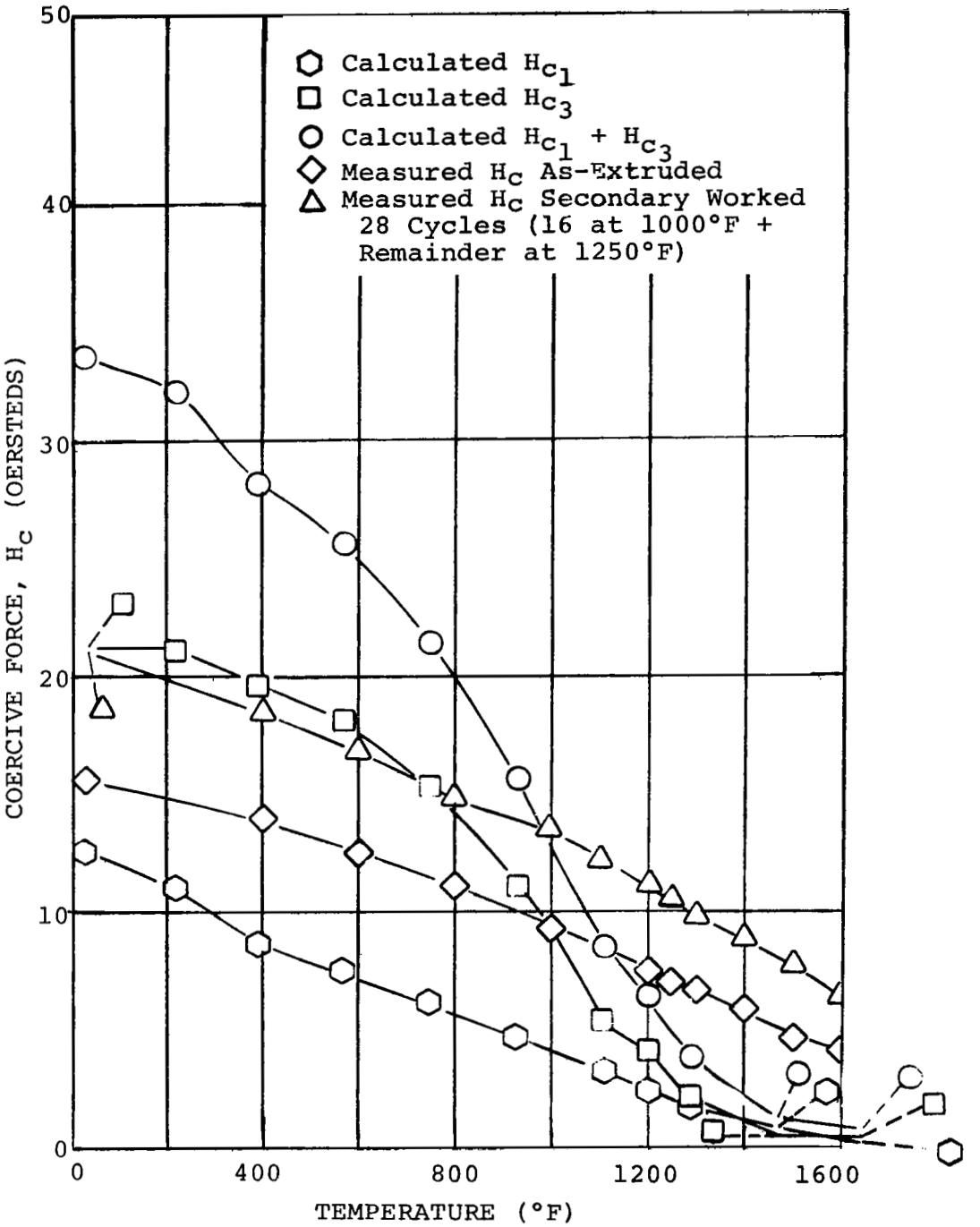

FIGURE IV-45. Calculated Coercive Force ($H_{c_1} + H_{c_3}$) from Néel's Equations and Measured Coercive Force in As-Extruded and Secondary Worked Conditions as a Function of Temperature for Fe+24.5w/oCo+9.3w/o ThO_2 Composition

cobalt material has not been measured, the "power law" (ref. IV-73 and IV-74) was used to calculate values from the following equations:

$$K_{(T)} = K_{(O)} \left[\frac{I_{s\,(T)}}{I_{s\,(O)}}\right]^{10}$$

$$\lambda_{s\,(T)} = \lambda_{s\,(O)} \left[\frac{I_{s\,(T)}}{I_{s\,(O)}}\right]^{3}$$

where the subscripts (T) and (O) refer to the values of K, λ_s and I_s at the absolute temperature (T) in °Kelvin and at absolute zero (O).

Even with the best estimated and measured values for the parameters in the Néel equations, there was rather poor agreement between the calculated ($H_{c_1}+H_{c_3}$) and measured coercive force versus temperature curves, figures IV-44 and IV-45. Considering the lack of accurate data for the temperature dependence of magnetostriction and crystalline anisotropy of both materials, and the level of internal stress and its distribution, this was not surprising. Also, the allotropic transformation in cobalt at 783° F complicated the structure, figure IV-44. These results illustrated the difficulties in trying to calculate coercive force from theory and why it was necessary to employ an experimental approach on this program.

As can be seen from the calculated curve ($H_{c_1}+H_{c_3}$) in figure IV-44, hexagonal cobalt (low-temperature phase) and cubic cobalt (high-temperature phase) exhibited distinctly different behaviors with temperature. This separation of phases was not apparent in the curve representing the measured data because the Co+8.4w/oThO_2 sample in the as-extruded condition contained a substantial proportion of cubic cobalt which resulted in much lower measured values of coercive force than those calculated for all-hexagonal cobalt. The cubic form of cobalt was further stabilized at low temperatures by secondary working, resulting in still lower values of coercive force.

In figure IV-45, the calculated ($H_{c_1}+H_{c_3}$) coercive force for Fe+27w/oCo-base material was high in the low-temperature region, but showed more satisfactory agreement with that measured on the Fe+27w/o Co-base, single phase (body centered cubic) material than was the case with cobalt.

In the present program, the high-temperature region of the coercive force versus temperature curve was of more importance than the low-temperature region. Firstly, it was the region in which the subject materials would find primary application and, secondly, the effect of internal stress could make a relatively greater contribution to coercive force than in the low temperature region. The level of internal stress was expected to be largely associated with the effect of processing conditions on the matrix structure.

In the case of the cobalt-base material in the as-extruded condition, figure IV-44, the matrix was unrecrystallized and the grains tended to be more equiaxed than elongated. Numerous dislocation tangles would be expected within the grains, thus raising the level of internal stress and contributing to a high coercive force in the 1200° to 1600° F range. On the other hand, after secondary working for 28 cycles at 1250° F, the dislocation tangles within the grain bodies were greatly reduced, the dislocations being mainly aligned in grain and subgrain boundaries forming a cellular structure. In the latter condition, the measured coercive force approached more closely the calculated ($H_{c_1}+H_{c_3}$) coercive force with the assumptions used.

Turning to the Fe+27w/o Co-base material in figure IV-45, the matrix structure in the as-extruded condition consisted of recrystallized, equiaxed grains which were relatively free of internal stress in comparison with the cobalt-base material in the same condition. Therefore, the coercive force in the 1200° to 1600° F range was relatively low, but still above that calculated under the assumptions used. In the secondary worked condition, which had the finer, elongated grain structure and substructure with a higher density of dislocations (mainly aligned in walls), the measured coercive force was greater at all temperatures.

c. PROOF TESTING OF THERMAL STABILITY OF MATRIX IN SECONDARY WORKED CONDITION

Proof testing of the thermal stability of the matrix grain structure was conducted on three Fe+27w/o Co-base and three Co-base compositions in the form of rod which had been secondary worked for at least 28 cycles (or the maximum number of cycles obtained before the rod broke up). For comparison purposes, the proof tests were also conducted on material secondary worked for 16 cycles. Table IV-28 shows the results of proof testing which involved comparison of room temperature coercive force values determined before and after heating secondary worked rod specimens 0.25-inch diameter (or the maximum possible diameter if under 0.25 inch) by 1-inch long for 5 hours at 1400°, 1500°, and 1600° F in a vacuum of $1x10^{-5}$ torr. Since coercive force is a very structure-sensitive property, comparison of coercive force values was used as a method for indicating stability.

The proof test results in table IV-28 indicated through decreasing change in coercive force (ΔH_c) that thermal stability of the matrix grain structure was improved in secondary worked material by increasing the number of cycles beyond 16. For example, the Fe+24.8w/oCo+8.3w/oZr composition had ΔH_c values of -9.2 oersteds at 16 cycles and -1.5 oersteds at 36 cycles in the proof test which involved heating for 5 hours at 1400° F. The Co+4.5w/oThO_2 composition had ΔH_c values of -3.0 oersteds at 16 cycles and +0.6 oersteds at 22 cycles in the same proof test. (A maximum variation of approximately $\pm$1.0 oersteds in ΔH_c values in table IV-28 would be expected from systematic errors.)

In the Fe+27w/o Co-base series, which are prone to undergo recrystallization and grain growth above approximately 1300° F, stability was achieved in the proof test at 1400° F with the Fe+24.8w/oCo+8.3w/oZr material after 32 to 36 cycles and with the Fe+24.5w/oCo+9.3w/oThO_2 after 28 cycles. On the other hand, the Fe+25.6w/oCo+1.0w/oB+4.2w/oZr rod secondary worked for 28 cycles was not stable at 1400° F (ΔH_c of -5.1 oersteds). In the Co-base series, the thoriated cobalt materials were more stable than the Co+0.8w/oB+3.2w/oCb composition. Figure IV-46 shows graphically that thermal stability was improved, ΔH_c became smaller, with secondary working beyond 16 cycles for the three Fe+27w/o Co-base and three Co-base compositions proof tested for 5 hours at 1400° F. Also, the Co-base series, which included a wide range of dispersoid parameter V/d, indicated thermal stability tended to increase with larger values of V/d.

TABLE IV-28. Proof Testing - Room Temperature Coercive Force of Fe+27w/o Co-Base and Co-Base Alloys Before and After Heating

Powder or Extrusion No.	Nominal Composition (weight percent)	Amount of Dispersed Phase (percent by volume)	Average Effective Size of Dispersed Particles (microns)	Average Inter-particle Spacing (microns)	Secondary Work[d]		Coercive Force At Room Temperature				
					Secondary Working Temp. (°F)	Secondary Working Cycles (No.)	Original Coercive Force As Secondary Worked, H_c (oersteds)	Change in Coercive Force From Original Value: After Heating 5 Hours at 1400°F, ΔH_c (oersteds)	After Heating 5 Hours at 1500°F, ΔH_c (oersteds)	After Heating[b] 10 min. at 1600°F, ΔH_c (oersteds)	After Heating 5 Hours at 1600°F, ΔH_c (oersteds)
Fe-27 w/o Co-Base Powders:											
Atomized No.											
13	Fe-25.6Co-1.0B-4.2Zr	20	0.90	3.6	1000	16	28.3	-10.8	--	-10.2	--
13	Fe-25.6Co-1.0B+4.2Zr	20	0.90	3.6	1250[a]	28	24.6	- 5.1	-7.3	- 0.4	--
19	Fe-24.8Co-8.3Zr	6.4 ZrO_2[c]	0.3	3.0	1000	16	29.0	- 9.2	--	-10.1	--
19	Fe-24.8Co-8.3Zr	6.4 ZrO_2[c]	0.3	3.0	1250[a]	24	25.6	- 2.2	-4.9	- 1.6	--
19	Fe-24.8Co-8.3Zr	6.4 ZrO_2[c]	0.3	3.0	1250[a]	32	25.5	- 0.9	-1.4	--	--
19	Fe-24.8Co-8.3Zr	6.4 ZrO_2[c]	0.3	3.0	1250[a]	36	26.6	- 1.5	-2.1	- 0.7	--
Composite No.											
15	Fe-24.5Co-9.3 ThO_2	7.5	0.3	3.7	1000	16	24.7	- 4.7	--	- 5.5	--
15	Fe-24.5Co-9.3 ThO_2	7.5	0.3	3.7	1250[a]	28	23.2	- 1.0	-2.9	+ 0.3	-2.9
Co-Base Powders:											
Composite No.											
13	Co-4.5 ThO_2	4	0.1	2.4	1000	16	30.0	- 3.0	--	- 0.8	-2.1
13	Co-4.5 ThO_2	4	0.1	2.4	1250[a]	22	24.0	+ 0.6	--	+ 0.2	+2.0
14	Co-8.4 ThO_2	7.5	0.1	1.2	1250[a]	16	37.0	0.0	--	- 1.1	+1.0
14	Co-8.4 ThO_2	7.5	0.1	1.2	1250[a]	28	28.7	- 1.2	--	+ 0.6	-2.5
Atomized No.											
30	Co-0.8B-3.2Cb	20	0.77	3.1	1000	16	24.1	- 5.1	--	- 3.5	-8.7
30	Co-0.8B-3.2Cb	20	0.77	3.1	1250[a]	22	18.3	- 1.9	--	- 0.7	-1.9

(a) The secondary working temperature had to be increased from 1000°F to 1250°F in order to achieve the indicated number of cycles.
(b) After determination of coercive force at 1600°F.
(c) Also present was 14 v/o of large, elongated particles of Fe-Co-Zr constituent.
(d) Each cycle of secondary working consisted of approximately a 10-percent reduction in area followed by a 10-minute anneal at the swaging temperature.

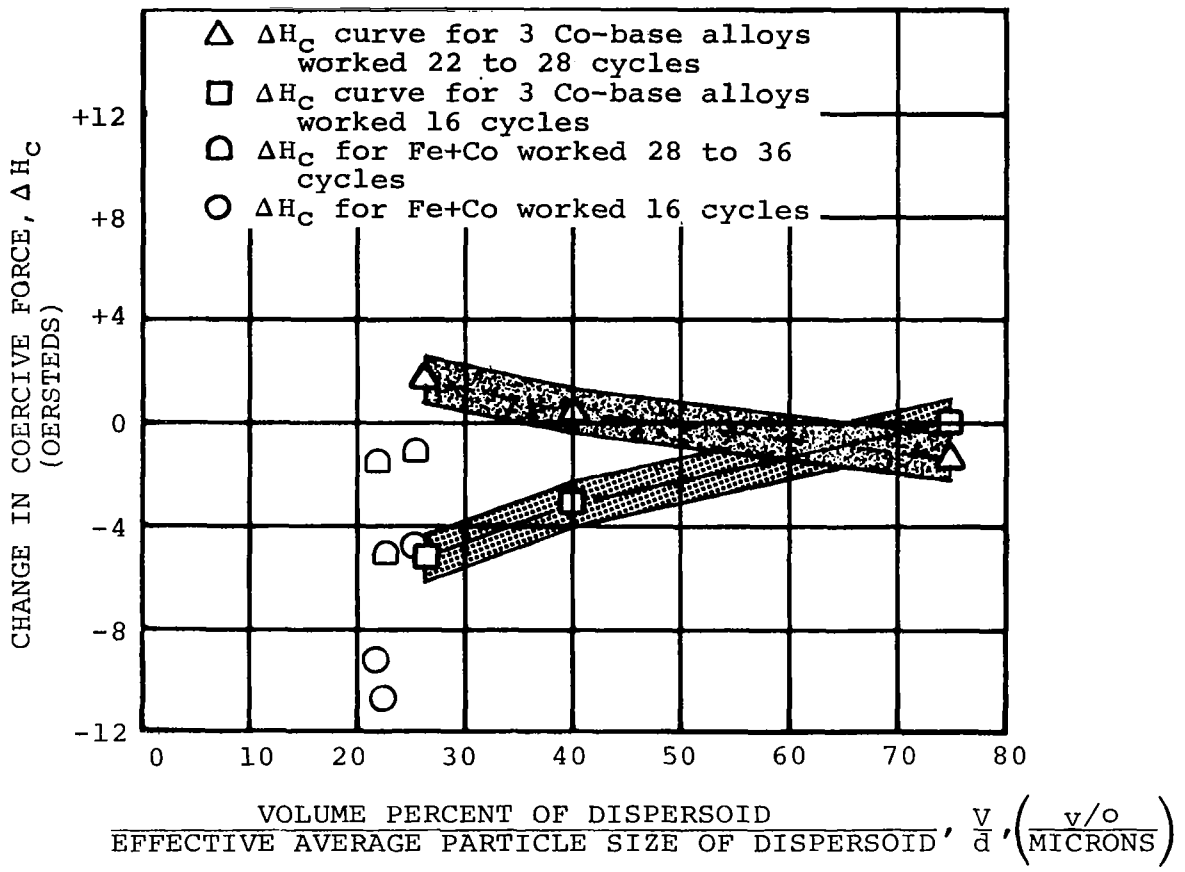

FIGURE IV-46. Change in Coercive Force at Room Temperature of Three Fe+27w/o Co-Base and Three Co-Base Alloys Secondary Worked for 16 Cycles and the Maximum Number of Cycles Before and After Heating 5 Hours at 1400°F in Proof Test

A metallographic examination under the light microscope indicated no change in grain structure before and after heating 5 hours at 1400°F in the proof test for the Fe+24.8w/oCo+8.3w/oZr and the Fe+24.5w/oCo+9.3w/oThO_2 compositions which received 36 and 28 cycles of secondary working, respectively. The Fe+25.6w/oCo+1.0B+4.2 w/oZr composition secondary worked 28 cycles underwent a small amount of grain growth in the proof test. On the other hand, the three Co-base compositions secondary worked for 22 to 28 cycles, did not show a change in grain structure before and after heating 5 hours at 1600° F in the proof test. Because of the obvious limitation on resolution with the light microscope, the fine details of grain structure and subgrain structure were investigated with an electron microscope, and these results were presented in an earlier section of this report on microstructure, figures IV-15, IV-18, and IV-20.

d. CREEP AND TENSILE PROPERTIES OF FINAL COMPOSITIONS AFTER SECONDARY WORKING 28 CYCLES

Based on the response to secondary working, as determined during the calibration study, and the thermal stability of the matrix grain structure achieved by the application of 28 to 36 cycles, as determined by proof testing, the following compositions were selected for short-term creep and tensile testing in vacuum:

1) Prealloyed Atomized Powder No. 19, Fe+24.8 w/oCo+8.3w/oZr

2) Composite Powder No. 15, Fe+24.5w/oCo+9.3w/o ThO_2 (0.01-0.06 micron ThO_2), Chas. Pfizer

3) Composite Powder No. 14, Co+8.4w/oThO_2 (0.01-0.06 micron ThO_2), Sherritt Gordon

The above compositions were the most thermally stable after 28 cycles of secondary working. However, the Fe+24.8w/oCo+8.3w/oZr composition had to be worked beyond 28 cycles to 32 to 36 in order to achieve thermal stability. The minimum size of creep and tensile specimens that could be machined and tested required that specimens be taken after 28 cycles. The 32 to 36 cycle material could not be tested mechanically, but coercive force measurements were made.

The short-term (100-hour maximum) creep properties and tensile properties of rod secondary worked 28 cycles are listed in table IV-29. These may be compared with

TABLE IV-29. Short-Term Creep Properties and Tensile Properties of Final Compositions Secondary Worked for 28 Cycles

Powder or Extrusion No.	Nominal Composition (weight percent)	Amount of Dispersed Phase (percent by volume)	Effective Size of Dispersed Particles (microns)	Average Inter-particle Spacing (microns)	Secondary Work[f]		Short Term Vacuum Creep Properties[a] Creep Strain in 100 Hours (percent)		
					Secondary Working Temp. (°F)	Secondary Working Cycles (No.)	At 1300°F Under 10,000 psi Stress	At 1400°F Under 10,000 psi Stress	At 1400°F Under 15,000 psi Stress
Fe+27 w oCo-Base Powders:									
Atomized No 19	Fe+24.8Co+8.3Zr	6.4ZrO_2[e]	0.3	3.0	None	0	--	0.00	Failed in 17.5 hrs, 53.2% strain
19	Fe+24.8Co+8.3Zr	6.4ZrO_2[e]	0.3	3.0	1250	16	--	--	Failed in 2.6 hrs, 103.0% strain
19	Fe+24.8Co+8.3Zr	6.4ZrO_2[e]	0.3	3.0	1250	28	7.1	--	--
Composite No. 15	Fe+24.5Co+9.3ThO_2	7.5	0.3	3.7	1250	28	Failed in 2.5 hrs, 4.3% strain	--	--
Co-Base Powder:									
Composite No. 14	Co+8.4ThO_2	7.5	0.1	1.2	None	0	--	--	--
14	Co+8.4ThO_2	7.5	0.1	1.2	1250	16	--	--	0.55
14	Co+8.4ThO_2+0.25Zr	7.5	0.1	1.2	1250	16	--	--	0.75
14	Co+8.4ThO_2+0.25Zr	7.5	0.1	1.2	1250	16	--	--	0.21[b]
14	Co+8.4ThO_2+0.25Zr	7.5	0.1	1.2	1250	28	--	--	0.20[b]
Comparison Materials:									
Nivco 5/8 in. diam Forged and Heat Treated Bar[g]					--	--	--	0.40	3
TD Nickel 1-1/4 in. diam Bar (Secondary Worked)					--	--	0.0	0.0	0.0-0.1

(a) Specimens aged 100 hours in vacuum (pressure of 1 x 10^{-5} torr or less) at the test temperature before creep testing in vacuum (pressure of 1 x 10^{-6} torr or less) or tensile testing in vacuum (pressure of 1 x 10^{-5} torr or less) except for TD Nickel.
(b) Specimens aged 2 hours at 1830°F in vacuum (pressure of 1 x 10^{-5} torr or less) before creep testing in vacuum (pressure of 1 x 10^{-6} torr or less) or tensile testing in vacuum (pressure of 1 x 10^{-5} torr or less).
(c) Interpolated values from 1200°F and 1600°F properties.
(d) Tested at a strain rate of 0.005 in./in. minute from yield to fracture instead of 0.05 in./in. minute.
(e) Also contained 14 v/o of coarse, elongated particles of Fe-Co-Zr constituent.
(f) Each cycle of secondary working consisted of approximately a 10 percent reduction in area followed by a 10 minute anneal at the swaging temperature.
(g) Heat treated 1725±25°F for 1 hour, water quenched, then air aged at 1225±5°F for 50 hours.

TABLE IV-29. Short-Term Creep Properties and Tensile Properties of Final Compositions Secondary Worked for 28 Cycles (Continued)

Powder or Extrusion No.	Nominal Composition (weight percent)	Secondary Work[f]		Vacuum Tensile Properties[a]								Saturation Magnetization, B_S (kilogauss) At 1400°F
				At 1300°F				At 1400°F				
		Secondary Working Temp. (°F)	Secondary Working Cycles (No.)	Ultimate Tensile Strength (1000 psi)	0.2% Offset Yield Strength (1000 psi)	Elongation in 4D (percent)	Reduction in Area (percent)	Ultimate Tensile Strength (1000 psi)	0.2% Offset Yield Strength (1000 psi)	Elongation in 4D (percent)	Reduction in Area (percent)	
Fe+27 w/o Co-Base Powders:												
Atomized No. 19	Fe+24.8Co+8.3Zr	None	0	61.3[c]	28.4[c]	44.0[c]	49.4[c]	47.8[c]	22.1[c]	66.0[c]	66.2[c]	15.0
19	Fe+24.8Co+8.3Zr	1250	16	--	--	--	--	--	--	--	--	15.0
19	Fe+24.8Co+8.3Zr	1250	28	34.7	17.2	88.5	67.4	--	--	--	--	15.0
Composite No. 15	Fe+24.5Co+9.3ThO_2	1250	28	19.8	15.9	10.2	25.7	--	--	--	--	16.6
Co-Base Powder:												
Composite No. 14	Co+8.4ThO_2	None	0	19.0[c]	18.6[c]	1.6[c]	0.8[c]	16.1[c]	15.2[c]	1.8[c]	0.8[c]	13.3
14	Co+8.4ThO_2	1250	16	--	--	--	--	--	--	--	--	13.3
14	Co+8.4ThO_2+0.25Zr	1250	16	--	--	--	--	--	--	--	--	13.3
14	Co+8.4ThO_2+0.25Zr	1250	16	--	--	--	--	--	--	--	--	13.3
14	Co+8.4ThO_2+0.25Zr	1250	28	--	--	--	--	39.4[b,d]	38.5	0.6	7.8	13.3
Comparison Materials:												
Nivco 5/8 in. diam Forged and Heat Treated Bar[g]		--	--	73.0[c]	50.0[c]	40[c]	55[c]	50.0[c]	30.0[c]	60[c]	60[c]	8.1
TD Nickel 1-1/4 in. diam Bar (Secondary Worked)		--	--	35	30	13	27	32	27	12	24	Non-magnetic

(a) Specimens aged 100 hours in vacuum (pressure of 1 x 10^{-5} torr or less) at the test temperature before creep testing in vacuum (pressure of 1 x 10^{-6} torr or less) or tensile testing in vacuum (pressure of 1 x 10^{-5} torr or less) except for TD Nickel.
(b) Specimens aged 2 hours at 1830°F in vacuum (pressure of 1 x 10^{-5} torr or less) before creep testing in vacuum (pressure of 1 x 10^{-6} torr or less) or tensile testing in vacuum (pressure of 1 x 10^{-5} torr or less).
(c) Interpolated values from 1200°F and 1600°F properties.
(d) Tested at a strain rate of 0.005 in./in./minute from yield to fracture instead of 0.05 in./in./minute.
(e) Also contained 14 v/o of coarse, elongated particles of Fe-Co-Zr constituent.
(f) Each cycle of secondary working consisted of approximately a 10 percent reduction in area followed by a 10 minute anneal at swaging temperature.
(g) Heat treated 1725±25°F for 1 hour, water quenched, then air aged at 1225±5°F for 50 hours.

TABLE IV-29. Short-Term Creep Properties and Tensile Properties of Final Compositions Secondary Worked for 28 Cycles (Concluded)

Powder or Extrusion No.	Nominal Composition (weight percent)	Secondary Work(f)		Vacuum Tensile Properties(a) At 1600°F				Saturation Magnetization, Bs (kilogauss) At 1600°F
		Secondary Working Temp. (°F)	Secondary Working Cycles (No.)	Ultimate Tensile Strength (1000 psi)	0.2% Offset Yield Strength (1000 psi)	Elongation in 4D (percent)	Reduction in Area (percent)	
Fe+27 w/oCo-Base Powders:								
Atomized No. 19	Fe+24.8Co+8.3Zr	None	0	20.8	9.5	110.0	99.8	12.5
19	Fe+24.8Co+8.3Zr	1250	16	--	--	--	--	12.5
19	Fe+24.8Co+8.3Zr	1250	28	--	--	--	--	12.5
Composite No. 15	Fe+24.5Co+9.3ThO_2	1250	28	--	--	--	--	14.2
Co-Base Powder:								
Composite No. 14	Co+8.4ThO_2	None	0	10.3	8.4	2.0	0.7	11.6
14	Co+8.4ThO_2	1250	16	--	--	--	--	11.6
14	Co+8.4ThO_2+0.25Zr	1250	16	--	--	--	--	11.6
14	Co+8.4ThO_2+0.25Zr	1250	16	--	--	--	--	11.6
14	Co+8.4ThO_2+0.25Zr	1250	28	33.2(b,d)	31.9	1.1	6.0	11.6
Comparison Materials:								
Nivco 5/8 in. diam Forged and Heat Treated Bar(g)		--	--	24.9	9.5	124	93.4	4.3
TD Nickel 1-1/4 in. diam Bar (Secondary Worked)		--	--	26	22	10	19	Non-magnetic

(a) Specimens aged 100 hours in vacuum (pressure of 1 x 10^{-5} torr or less) at the test temperature before creep testing in vacuum (pressure of 1 x 10^{-6} torr or less) or tensile testing in vacuum (pressure of 1 x 10^{-5} torr or less) except for TD Nickel.
(b) Specimens aged 2 hours at 1830°F in vacuum (pressure of 1 x 10^{-5} torr or less) before creep testing in vacuum (pressure of 1 x 10^{-6} torr or less) or tensile testing in vacuum (pressure of 1 x 10^{-5} torr or less).
(c) Interpolated values from 1200°F and 1600°F properties.
(d) Tested at a strain rate of 0.005 in./in./minute from yield to fracture instead of 0.05 in./in./minute.
(e) Also contained 14 v/o of coarse, elongated particles of Fe-Co-Zr constituent.
(f) Each cycle of secondary working consisted of approximately a 10 percent reduction in area followed by a 10 minute anneal at swaging temperature.
(g) Heat treated 1725±25°F for 1 hour, water quenched, then air aged at 1225±5°F for 50 hours.

properties of the same composition in the as-extruded condition (0 cycles) and after 16 cycles, where available. Also, the properties of precipitation hardened Nivco alloy and TD Nickel are included for comparison.

In the case of the two Fe+27w/oCo-base alloys secondary worked for 28 cycles, the creep resistance and tensile properties were low. Although thermal stability of the matrix grain structure was achieved, or at least closely approached, under no load conditions, the average interparticle spacing was too large, 3.0 to 3.7 microns, (V/d ratio too small, 21 to 25) to stabilize the fine, elongated grain structure (figures IV-15 and IV-20) under applied stress and provide resistance to plastic strain. In fact, the data for the Fe+24.8w/oCo+8.3w/oZr composition in the hot-extruded condition, where the grain structure was coarser and equiaxed, showed that it was much more creep resistant and had higher tensile properties.

By contrast, the Co+8.4w/oThO_2+0.25w/oZr composition which had an average interparticle spacing of 1.2 microns and a V/d ratio of 75 did have the greatest creep resistance after 28 cycles of secondary work. The stability of the grain structure developed by secondary working was high under external stress, being enhanced by the 0.1 micron dispersoid, figure IV-18. The yield strengths at 1400° and 1600° F were 2 to 4 times that of the Co+8.4w/oThO_2 (without Zr) composition in the hot-extruded condition and exceeded that of Nivco alloy and TD Nickel by substantial amounts.

E. CONCLUSIONS AND RECOMMENDATIONS

1. Conclusions

a) The feasibility of achieving soft-magnetic properties in the 1200° to 1600° F temperature range in creep-resistant dispersion-strengthened cobalt-base and iron+27w/o cobalt-base materials was established on small diameter extruded and secondary worked rod.

b) The coercive force, which is a structure-sensitive property and an indicator of the degree of magnetic "softness", was substantially less than 25 oersteds at 1200° to 1600° F for all compositions and worked conditions investigated. Coercive force decreased as the average effective particle size of the dispersoid increased in the range investigated (0.1 to 1.5 microns). The coercive force

increased rather rapidly to a maximum value in the vicinity of 0.1 micron in cobalt, which was believed to be the approximate thickness of the magnetic domain boundaries. Coercive force decreased with decreasing V/d ratio, where V is the volume percent and d is the particle size of dispersoid.

c) The saturation magnetization, which is a structure-insensitive property, was lowered in direct proportion to the volume percent of non-magnetic dispersoid present. Saturation magnetization values in the 1200° to 1600° F range were at least 43 percent higher for all iron+27w/o cobalt-base compositions than for Nivco alloy. Even the iron+27 w/o cobalt-base composition containing 21 volume percent of dispersoid had a saturation magnetization greater than 12.0 kilogauss in the 1200° to 1600° F range. In order to maintain a level of 12.0 kilogauss with the cobalt-base alloys, however, the dispersoid content had to be limited to approximately 4v/o at 1600° F and 10v/o at 1500° F.

d) The tensile properties of cobalt-base and iron+27 w/o cobalt-base alloys in the hot-extruded or secondary-worked conditions tended to increase with increasing volume percent dispersoid and decreasing interparticle spacing. It was necessary to provide an average interparticle spacing of approximately 2 microns or less in order to obtain a substantial dispersion-strengthening effect with or without secondary working.

e) The fineness and uniformity of the dispersoid distribution in the final fabricated product were predominately influenced and limited by the degree of dispersion in the original cobalt or iron+cobalt-base powder. Clustering and segregation of dispersoid in the powder had to be minimized. The dispersoid distribution in the hot-extruded rod made with extrusion ratios of 11 to 1 or 8 to 1 was not markedly changed or refined by subsequent secondary working.

f) In the case of the cobalt-base alloys, secondary working for 14 to 28 cycles at 1000° to 1500° F refined the matrix grain structure into elongated grains and tended to stabilize this grain structure and the cubic form of cobalt with increasing number of cycles. Thermal stability of the matrix grain structure at 1400° to 1600° F was improved with average interparticle spacings of less than

approximately 2 microns and large V/d ratios. The Co+8.4w/oThO_2 (7.5v/oThO_2) composition with an interparticle spacing of 1.2 microns, thoria average effective size of 0.1 micron, and V/d of 75 was an example of this.

g) In order to attain a high degree of creep resistance in cobalt-base alloys, the interparticle spacing should be well under 2 microns, the dispersoid size 0.1 micron or less, and the V/d ratio 50 or more. Creep resistance improved by extending the number of cycles beyond 14 or 16 to 28 and keeping the secondary working temperature as low as possible. Satisfactory creep resistance was not achieved in the cobalt-base systems in the hot-extruded condition.

h) The Co+8.4w/oThO_2+0.25w/oZr (7.5v/oThO_2) composition extruded from Sherritt Gordon composite powder with Zr added and the Co+11.2w/oThO_2 (10v/o ThO_2) composition extruded from Chas. Pfizer powder which were secondary worked for 16 to 28 cycles at 1250° F had high creep resistance in short-term tests. These materials showed promise of being able to sustain 10,000 psi stress for 10,000 hours with less than 0.4 percent creep strain at a temperature within the 1200° to 1600° F range.

i) In the case of the iron+27w/o cobalt-base alloys, which are prone to undergo recrystallization and grain growth above approximately 1300° F, thermal stability of the elongated grain structure at 1400° F (under no applied stress) was achieved in secondary worked material only after the application of a very large number of cycles, 28 to 36. The interparticle spacing in the iron+27w/o cobalt-base material exceeded 2 microns, the smallest effective size of dispersoid was 0.3 micron, and the largest V/d ratio was only 25. As a result, the matrix grain boundaries in the secondary worked condition were not anchored by the dispersoid. Plastic strain occurred much more readily under applied stress than in cobalt.

j) The iron+27w/o cobalt-base alloys were actually less creep resistant in the secondary worked condition than in the hot-extruded condition. This was related to the fact that the dispersoids in these materials were too coarse to stabilize (under applied stress) the finer, elongated grain structure developed by secondary working from the

coarser, equiaxed grain structure in the original extrusion. Finer dispersoids in the original powder than are available would be necessary to improve creep resistance in iron+27w/o cobalt in the secondary worked condition, and retard recrystallization and grain growth.

k) In the iron+27w/o cobalt series, the hot-extruded prealloyed atomized powders Fe+24.8Co+8.3Zr and Fe+25.6Co+1.0B+4.2Zr had the highest creep resistance.

2. Recommendations

a) Despite the existence of a transformation temperature at 1770° F and the tendency towards recrystallization and grain growth above approximately 1300° F, iron+27w/o cobalt-base dispersion-strengthened material is favored over cobalt-base for future development primarily because of the 25 percent higher values of saturation magnetization at 1200° to 1600° F that can be achieved in the former.

b) An iron+27w/o cobalt-base powder should be developed having a finer and more uniform distribution of thoria particles than obtained on the present program. The powder should contain approximately 3v/o thoria and, after consolidation, should have an interparticle spacing of 0.5 - 1.0 micron and an average effect particle size of 0.01 - 0.03 micron. This should improve thermal stability, retard recrystallization and grain growth, and provide a creep resistant material in the secondary worked condition.

c) The fabricating procedure for making a solid rotor 8 to 28 inches diameter by 8 to 28 inches long must accomodate numerous cycles of secondary working. The possibility of fabricating the rotor directly as a monolithic piece is remote because of the need to work the piece with about 10 percent reduction per cycle uniformly and thoroughly throughout the entire cross section. Instead, the rotor should be built up from transverse sections as a laminated product. Compacted and sintered powder billets of rectangular shape and approximately one inch thickness should be given a minimum of 16 and preferably 28 cycles of secondary working. Each cycle would consist of rolling with a maximum reduction of 10 percent per pass followed by a stress

relief anneal. Secondary working should be performed at the lowest temperature at which the material can be rolled without excessive cracking. The sheet should be as flat as possible. The secondary-worked sheet should be diffusion bonded together to form a laminated rotor with a minimum of reluctance added to the magnetic circuit.

SECTION V

VACUUM CREEP TEST OF NIVCO ALLOY

By M. Spewock, R. P. Shumate, and E. H. VanAntwerp

A. INTRODUCTION

Long-term creep data are needed on high-strength rotor materials suitable for electric alternators. Nivco alloy (23Ni-1.7Ti-0.4Al-0.2Zr-Balance Co) is presently the highest temperature rotor material available. Originally, five thousand hour tests were planned at temperatures to 1150° F in vacuum ($1x10^{-6}$ torr). After a careful analysis of design data requirements it was determined that creep strain data in 10,000 hours and at creep strains above the original 0.20 and 0.40 percent were needed. The total creep of a solid generator rotor is defined as the change in rotor pole tip diameter over the operating life of the machine. Creep, therefore, must be held to as low a value as practicable in order to minimize the amount of clearance that must be provided between the stator bore seal and rotor. A desirable design target for total integrated creep strain in 10,000 hours is 0.20 percent. Using this criterion for example, a 10-inch diameter rotor would require additional running clearance of 0.020-inch. The localized incremental creep might run from 0.20 inches to as low as 0.002 inches in this example because of stress and temperature gradients which exist in different areas of the rotor. These incremental creep strains are then integrated over the rotor diameter to obtain the average value of 0.20 percent creep strain for the rotor.

While the design limits for total creep strain over the rotor diameter may be only 0.20 to 0.40 percent, the localized creep may amount to several percent in typical designs. Therefore, creep testing was extended to as much as five percent creep strain to provide sufficient design information on the Nivco alloy.

B. EXPERIMENTAL PROCEDURES TESTING

The lack of availability of vacuum chambers for creep testing at elevated temperatures in the desired vacuum range of at least 10^{-6} torr dictated the design of a suitable vacumm creep capsule. The design, shown in figure V-1, was the result of a Westinghouse sponsored program where various vacuum chamber designs, pumping systems, and extensometers were evaluated to determine a system which could provide meaningful data at reasonable cost. Included in the extensometer evaluation were measurements using optical methods and the use of strain gages.

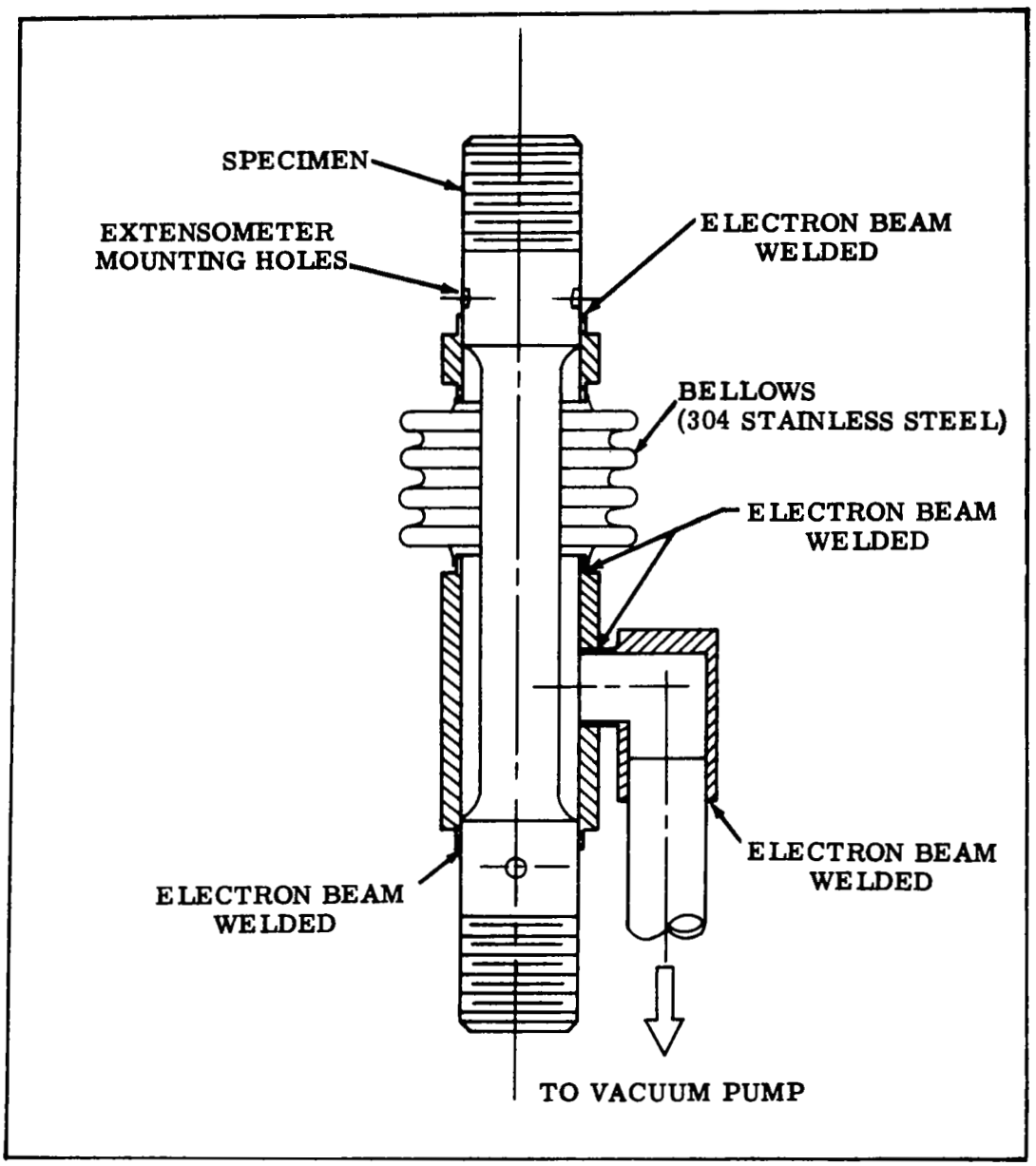

FIGURE V-1. Vacuum Creep Capsule Showing Encapsulated Vacuum Creep Specimen

A series of vacuum measurements were made on the capsule configuration to evaluate pressure losses in the design. These included both hot and cold capsule vacuum measurements at a position on the upper end of the capsule (position of highest pressure) as well as at a position upstream from the vacuum pumps. Because the total capsule is heated, the ionization gage could not be located at the capsule top end; therefore, data were obtained by brazing a 12-inch extension onto the capsule and locating the ionization gage at the top of this extension outside of the hot zone. After a 48-hour bakeout, a cold-trapped oil diffusion pumped capsule at 860° F achieved a pressure of 8.2×10^{-7} torr at the capsule extension.

A similar series of vacuum measurements were made using a four liter per second sputter-ion pump. After 22 hours at 570° F, the pressure at the capsule extension was observed to be 6.1×10^{-7} torr and at the pumping port it was observed as 2.1×10^{-7} torr. After 23 hours and an increase in temperature to 1050° F, the pressure was 5.5×10^{-7} torr at the pump port and 3×10^{-6} torr at the top of the capsule extension. A new sputter-ion pumping system of twice the capacity was procured and used in the test program. This allowed improved vacuum conditions during testing over that observed with the smaller sputter-ion pump. In addition, the removal of the capsule extension reduced the chamber volume being pumped.

During normal operation of the sputter-ion pumping systems, one power supply operating on standard 115 V ac power was used for each pump. These power supplies, however, were designed so that either one could power two pumps simultaneously. Consequently, an automatic power supply switch-over device was designed and successfully tested under the conditions of a simulated failure of one power supply such that both pumps were run from the remaining power supply. In the event of a service power failure, a battery and inverter were wired to cut in immediately thereby preventing a pressure rise. Performance of both safety devices was verified on the complete test capsule and dummy stainless steel specimen. This system was built and operated continuously for 295 hours before being terminated to begin the testing of the Nivco alloy.

The shock of rupture of a specimen in the early phases of the test program shattered the ionization gage and admitted air into the system. The ionization gage mounting was modified to withstand the physical shock of rupture should another unexpected failure occur. Should the gage fail, it is isolated from the capsule by a vacuum valve which is only used until the operating pressure reaches 10^{-5} torr. Ion pump current was used as a measure of pressure below 10^{-5} torr.

As part of a Westinghouse program to determine capsule bellows reliability, one type of 304 stainless steel bellows[1] was held at 1350° F in air for more than 4,000 hours. Twice monthly the bellows was removed from the furnace and leak checked using a mass spectrometer. The bellows remained leak tight. A second bellows was removed from an actual creep test capsule at 2056 hours for metallographic examination. An examination failed to reveal any degree of deterioration in the bellows. No evidence of intergranular penetration by oxygen was present.

C. RESULTS AND EVALUATION

All creep specimens (figure V-2) were rough machined, heat treated and machined to finish dimensions. Heat treatment consisted of a solution anneal in air at 1725° F for one hour, a water quench, and aging in air at 1225° ±5° F for 25 hours. The specimens were electron beam welded into capsules and assembled into the creep machine. The pressure was reduced in the capsule and the temperature increased slowly so that the pressure would not exceed 5×10^{-6} torr. When the pre-determined temperature (1000° to 1150° F) was stabilized and the pressure reached 9×10^{-7} torr the samples were loaded. In all cases, the pressure continued to drop until they reached the 10^{-9} torr range. Table V-1 shows a summary of data of the specimens tested on this program.

The data shown in this report were taken from Nivco alloy heat 10-NO2V-1099 with a grain size of ASTM 7 (approximately 440 grains). The chemical analysis of this heat is shown below:

Heat 10-NO2V-1099 (weight percent)

Ni	23.40	Ti	1.75
Co	72.40	Zr	0.26
Si	0.27	C	0.0038
Mn	0.26	O	0.0009
Al	0.39	Fe	0.27

This grain size and analysis are considered typical of Nivco alloy produced after April 1965. It should be noted that heats produced prior to this time tended to have a larger grain size and the data reported here might not be characteristic of the early heats.

Strain-time plots for the specimens are shown in figures V-3 to V-9. Capsule pressures at the beginning and end of the test are noted on the figures. Early creep specimens had higher than

---

[1]Purchased from Flexonics Division of Calument and Hecla, Inc., Bartlett, Illinois.

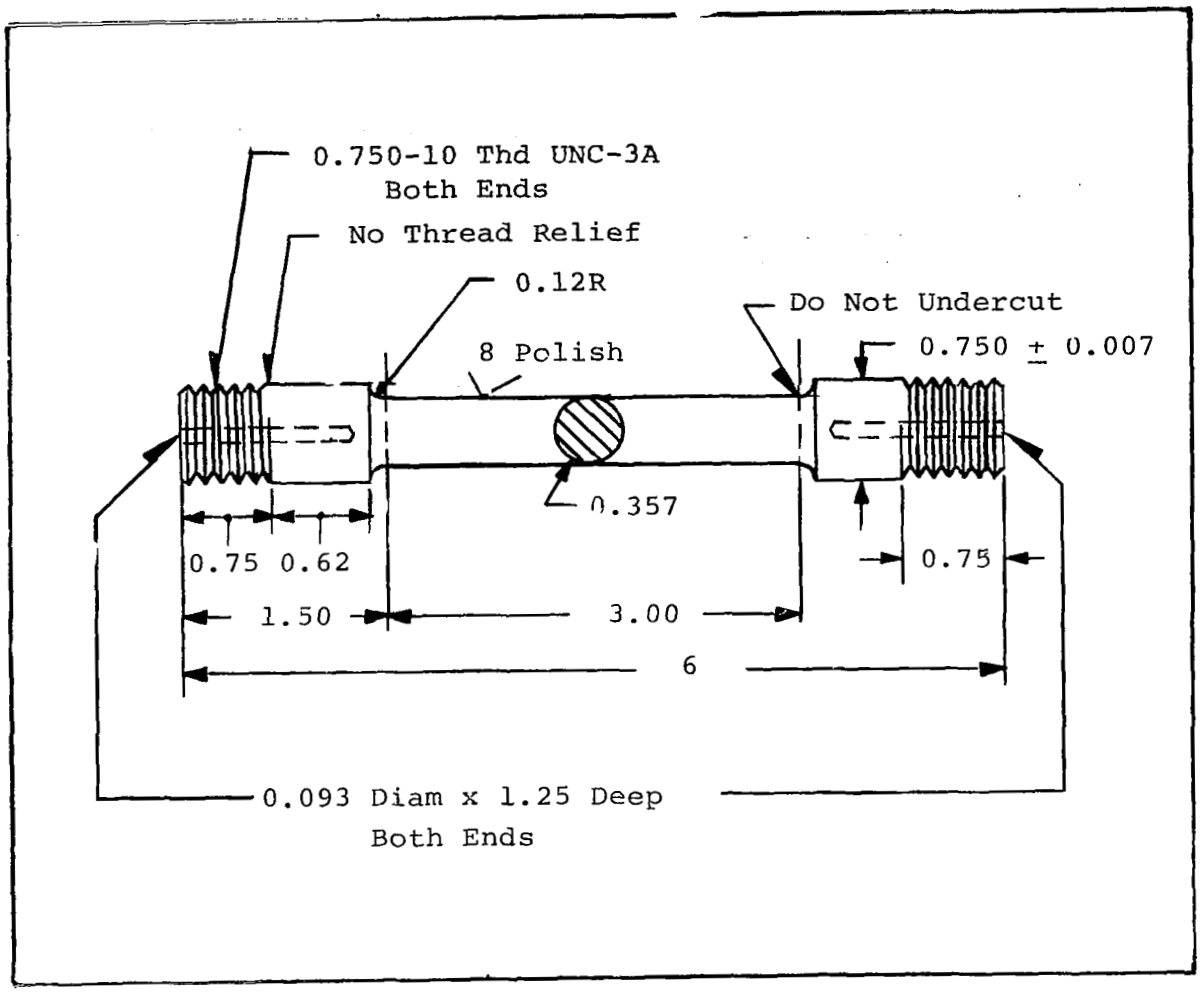

FIGURE V-2. Creep Specimen for Encapsulation

anticipated creep rates. In order to establish a satisfactory long term creep rate two approaches were pursued: (1) the temperature was held constant and the stress reduced, and (2) the temperature was reduced while the stress remained relatively constant. Specimen No. 1 (figure V-3) was removed from test early in the program after 2.4 percent creep strain was attained. However, in order to procure more information about the creep characteristics of Nivco alloy in the 1100° to 1150° F range at various stresses it was decided to leave the later specimens on test until approximately five percent creep strain had been reached. Satisfactory 10,000-hour creep data has been obtained at 1100° F. These data are shown in table V-1, and plotted on figure V-4. At 1150° F the desired 10,000 hours was not obtained within the five percent creep strain limitation.

TABLE V-1. Summary of Data of Nivco Vacuum Creep Tests

	Specimen Number[a]						
	1	2	3	4	5	6	7
Temperature (°F)	1 100	1 100	1 150	1 050	1 150	1 000	1 150
Stress (psi)	50 000	37 500	30 000	50 000	25 000	55 000	15 000
Duration of Test (hours)	3 021	10 007[b]	5 006	10 073[b]	6 744	7 225[b]	3 503[b]
Total Creep Strain (%)	2.41	1.19	5.32	1.75	5.21	0.49	0.27
Time to Cause 0.2% Creep Strain (hours)	65	2 100	150	490	220	1 150	2 320
Time to Cause 0.4% Creep Strain (hours)	275	3 850	460	1 600	590	5 230	extrapolated 6 000
Time to Cause 1.0% Creep Strain (hours)	1 170	8 810	1 550	5 350	2 020	(c)	(c)
Transition Strain (%)	1.58	0.84	1.53	(c)	1.73	(c)	(c)
Transition Time (time in hours beginning of 3rd stage creep)	2 060	7 650	2 520	(c)	3 700	(c)	(c)
Minimum Creep Rate (% per hour)	6.5×10^{-4}	1.15×10^{-4}	5.4×10^{-4}	1.52×10^{-4}	4.2×10^{-4}	4.85×10^{-5}	6.23×10^{-5}
Pressure at Completion of Test (torr)	4.8×10^{-9}	1.0×10^{-9}	2.7×10^{-9}	2.3×10^{-9}	4.4×10^{-9}	2.2×10^{-9}	5.9×10^{-9}
Strain Time Plot Shown in Figure Number	V-3	V-4	V-5	V-6	V-7	V-8	V-9

(a) Nivco Alloy Heat 10N02V-1099. All specimens heat treated before testing at 1725°F for one hour; water quenched then air aged at 1225°F for 25 hours.
(b) Capsules were removed from test at hours shown. Performance at time of removal was still satisfactory.
(c) Not reached during test.

Review of the data presented shows that Nivco alloy exhibits a rapid increase in creep rate as the temperature nears 1100° F. This may be seen in table V-1. The 1000° F specimen showed a creep rate of 0.485×10^{-4} percent per hour at 55,000 psi. The 1050° and 1100° F specimens, while loaded 5000 psi less, had creep rates of 1.5×10^{-4} and 6.5×10^{-4} percent per hour respectively.

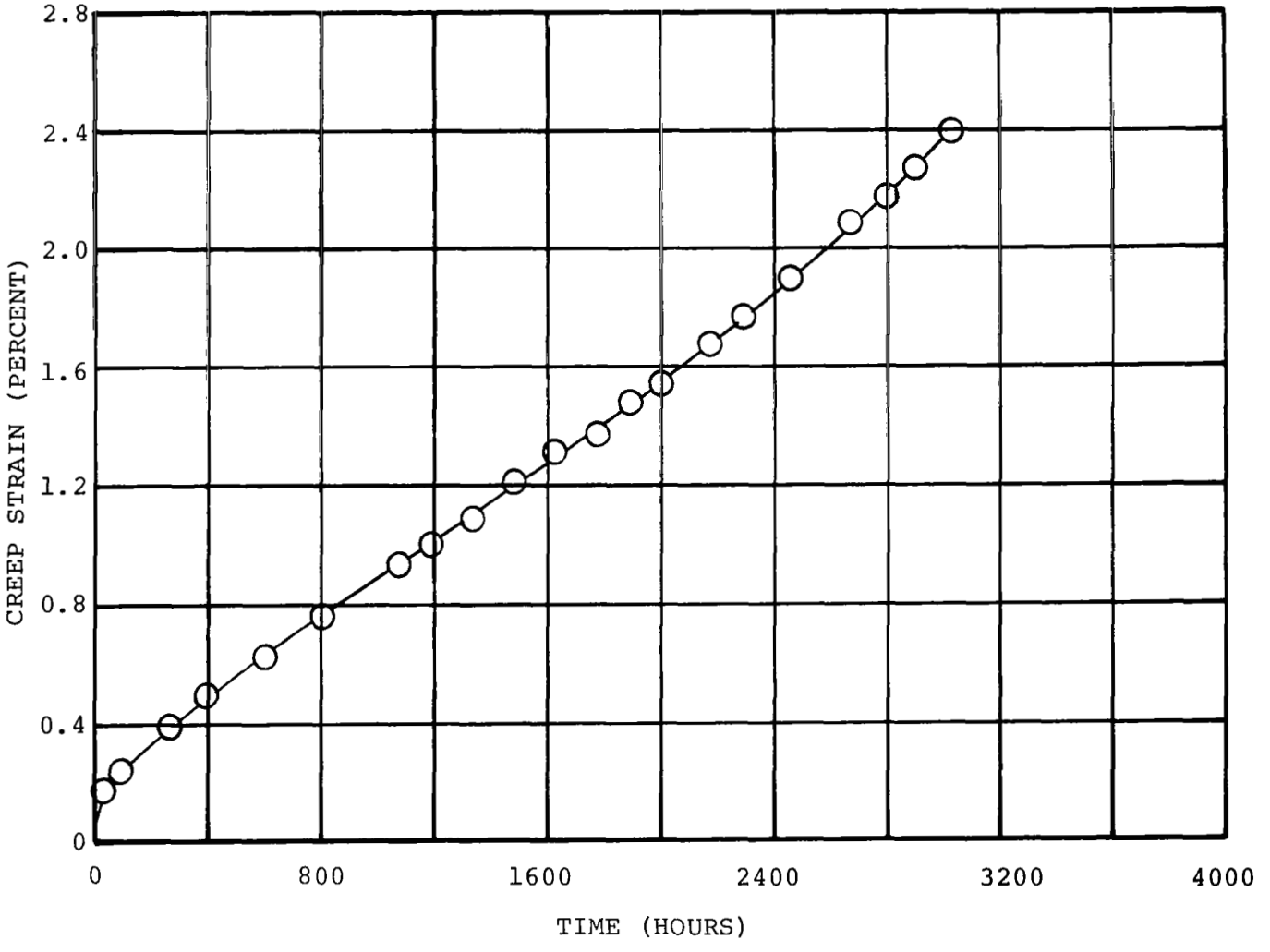

FIGURE V-3. Creep, Nivco Heat 10NO2V-1099, Tested in Vacuum at 1100° F and 50,000 psi. Pressure at Beginning of Test 9.0×10^{-7} torr and at End of Test 4.3×10^{-9} torr (Specimen No. 1)

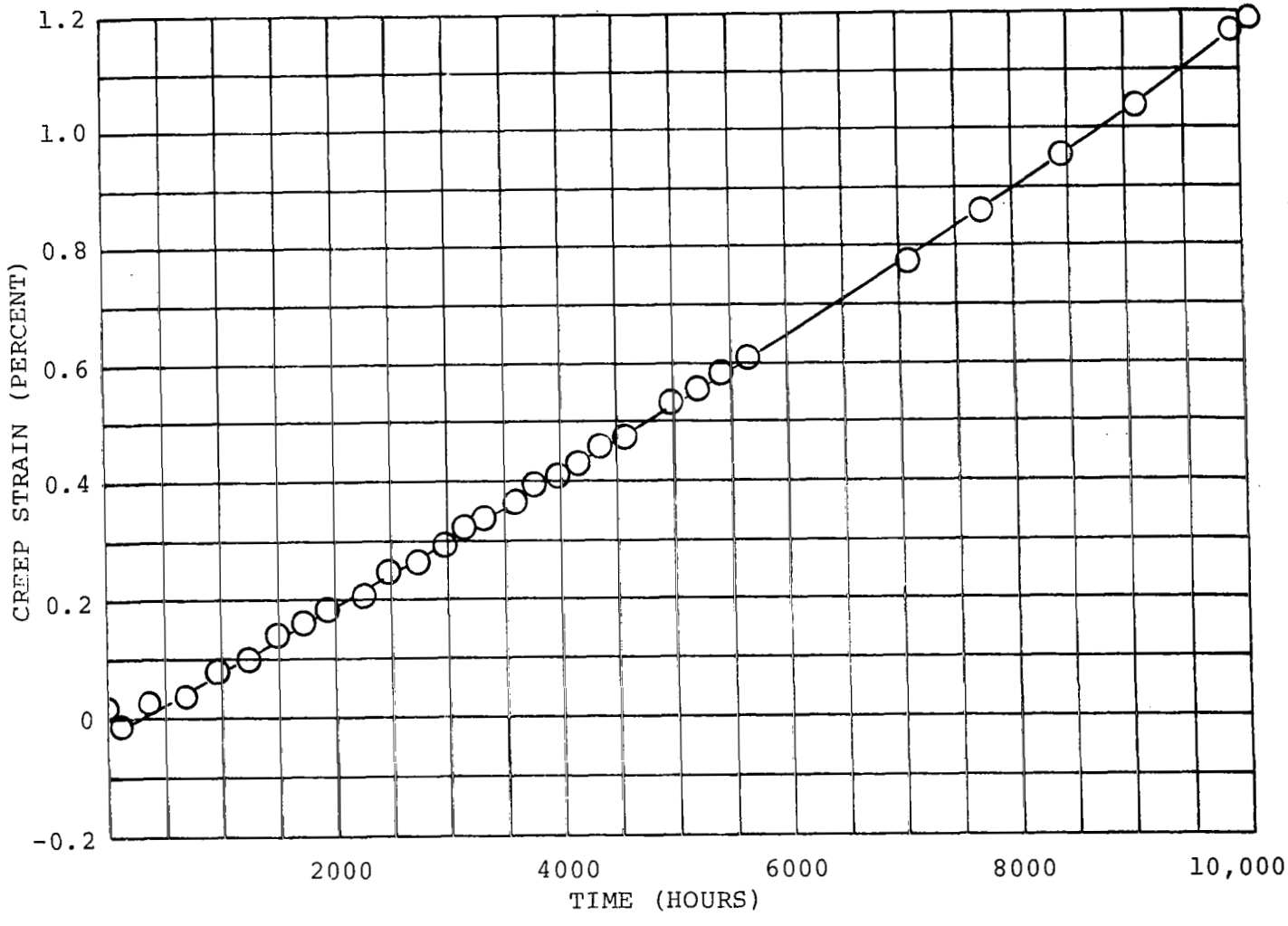

FIGURE V-4. Creep, Nivco Heat 10NO2V-1099, Tested in Vacuum at 1100° F and 37,500 psi. Pressure at Beginning of Test 9.0×10^{-7} torr and at End of Test 1.0×10^{-9} torr (Specimen No. 2)

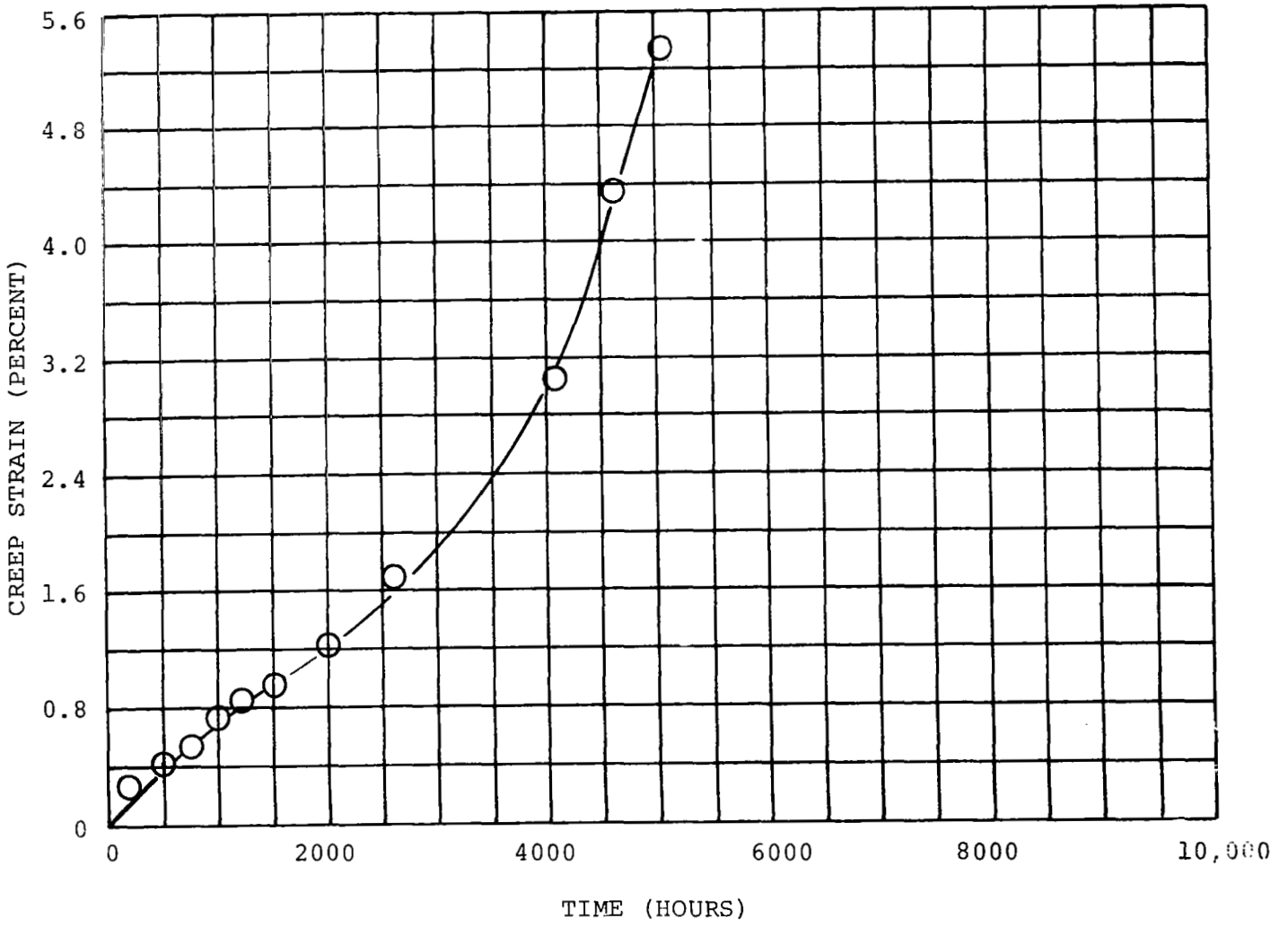

FIGURE V-5. Creep, Nivco Heat 10NO2V-1099, Tested in Vacuum at 1150° F and 30,000 psi. Pressure at Beginning of Test 9.0×10^{-7} torr and at End of Test 2.7×10^{-9} torr (Specimen No. 3)

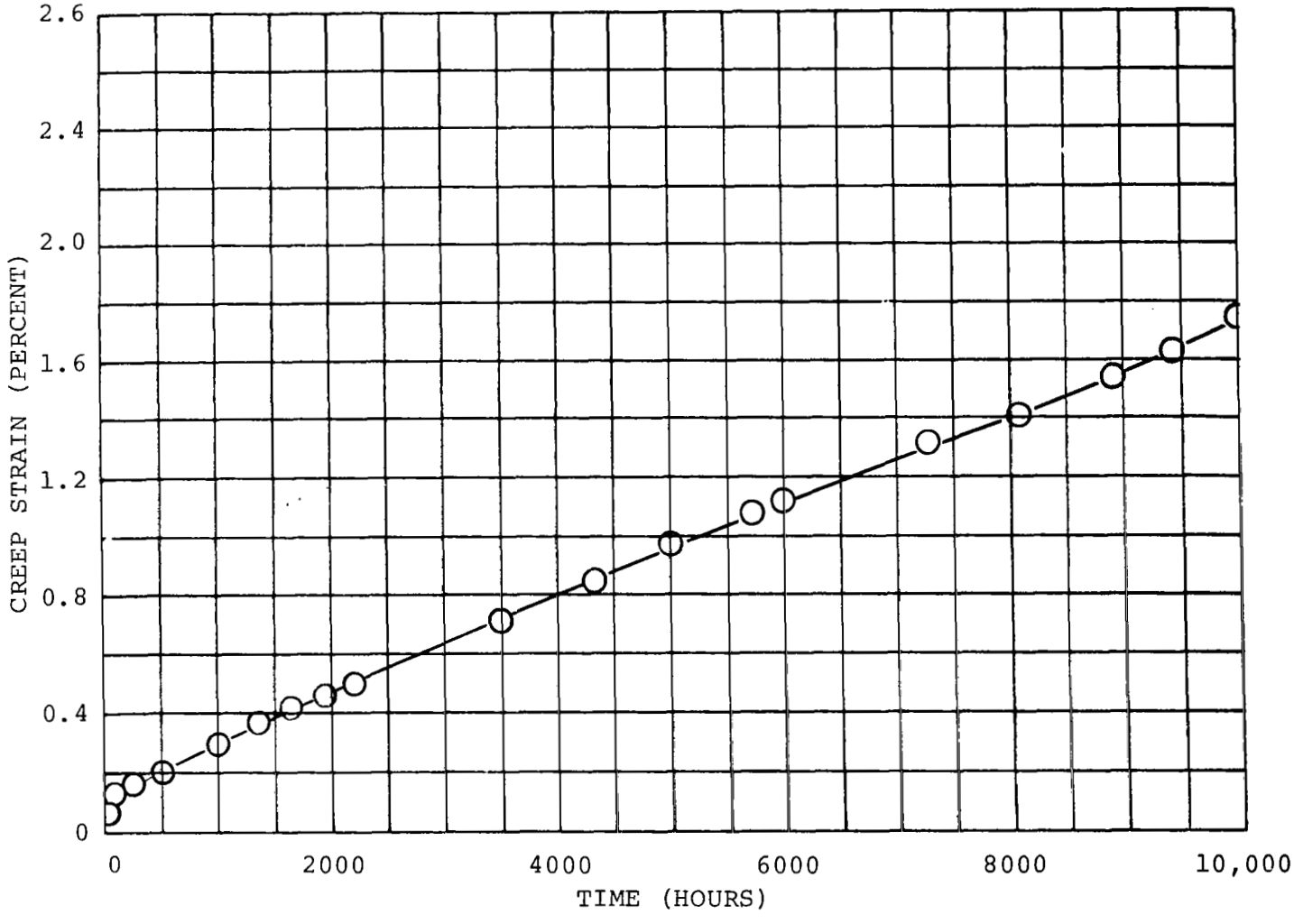

FIGURE V-6. Creep, Nivco Heat 10NO2V-1099, Tested in Vacuum at 1050° F and 50,000 psi. Pressure at Beginning of Test 9.0×10^{-7} torr and at End of Test 2.3×10^{-9} torr (Specimen No. 4)

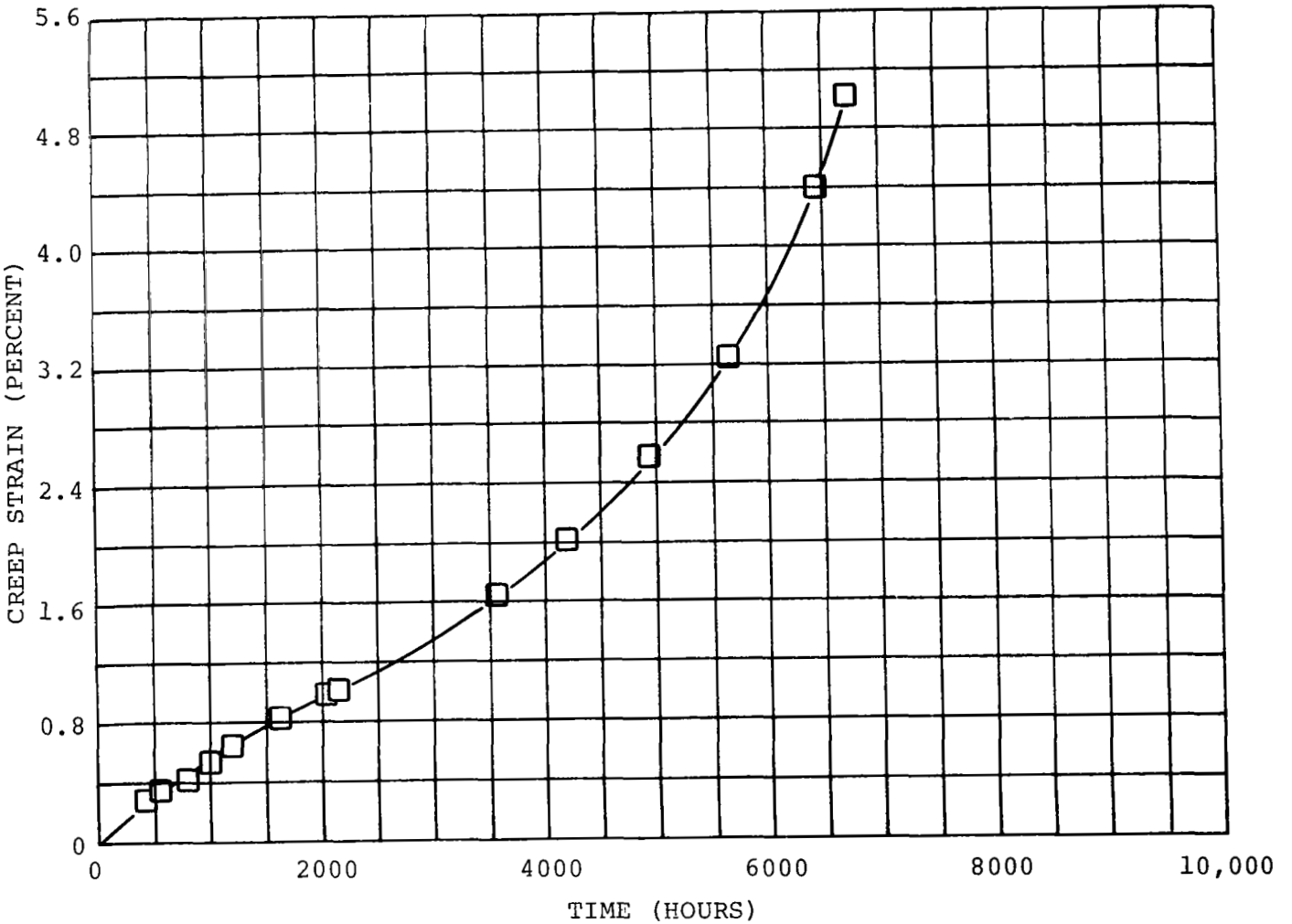

FIGURE V-7. Creep, Nivco Heat 10NO2V-1099, Tested in Vacuum at 1150° F and 25,000 psi. Pressure at Beginning of Test 9.0×10^{-7} torr and at End of Test 4.4×10^{-9} torr (Specimen No. 5)

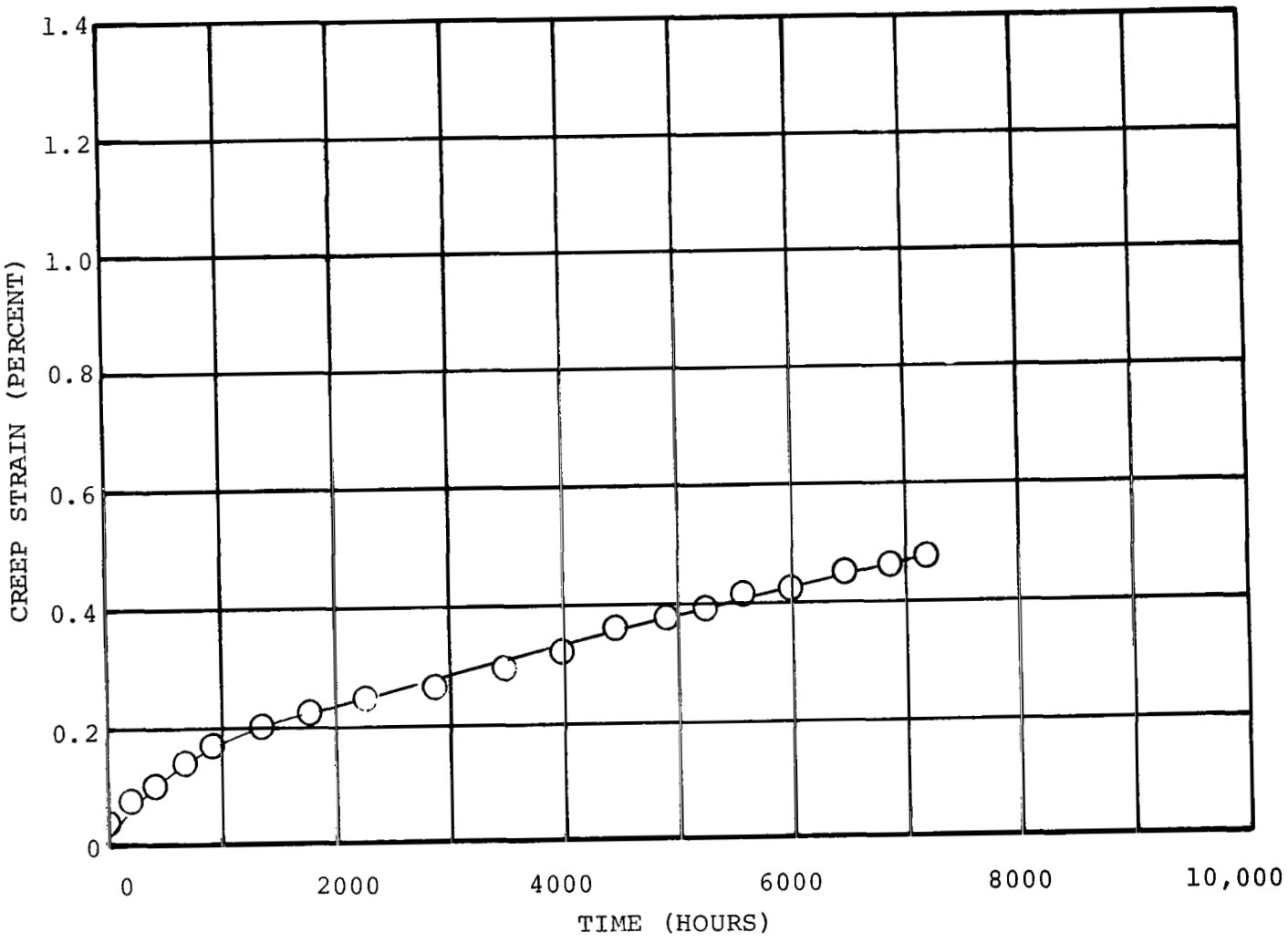

FIGURE V-8. Creep, Nivco Heat 10NO2V-1099, Tested in Vacuum at 1000° F and 55,000 psi. Pressure at Beginning of Test 9.0×10^{-7} torr and at End of Test 2.5×10^{-9} torr (Specimen No. 6)

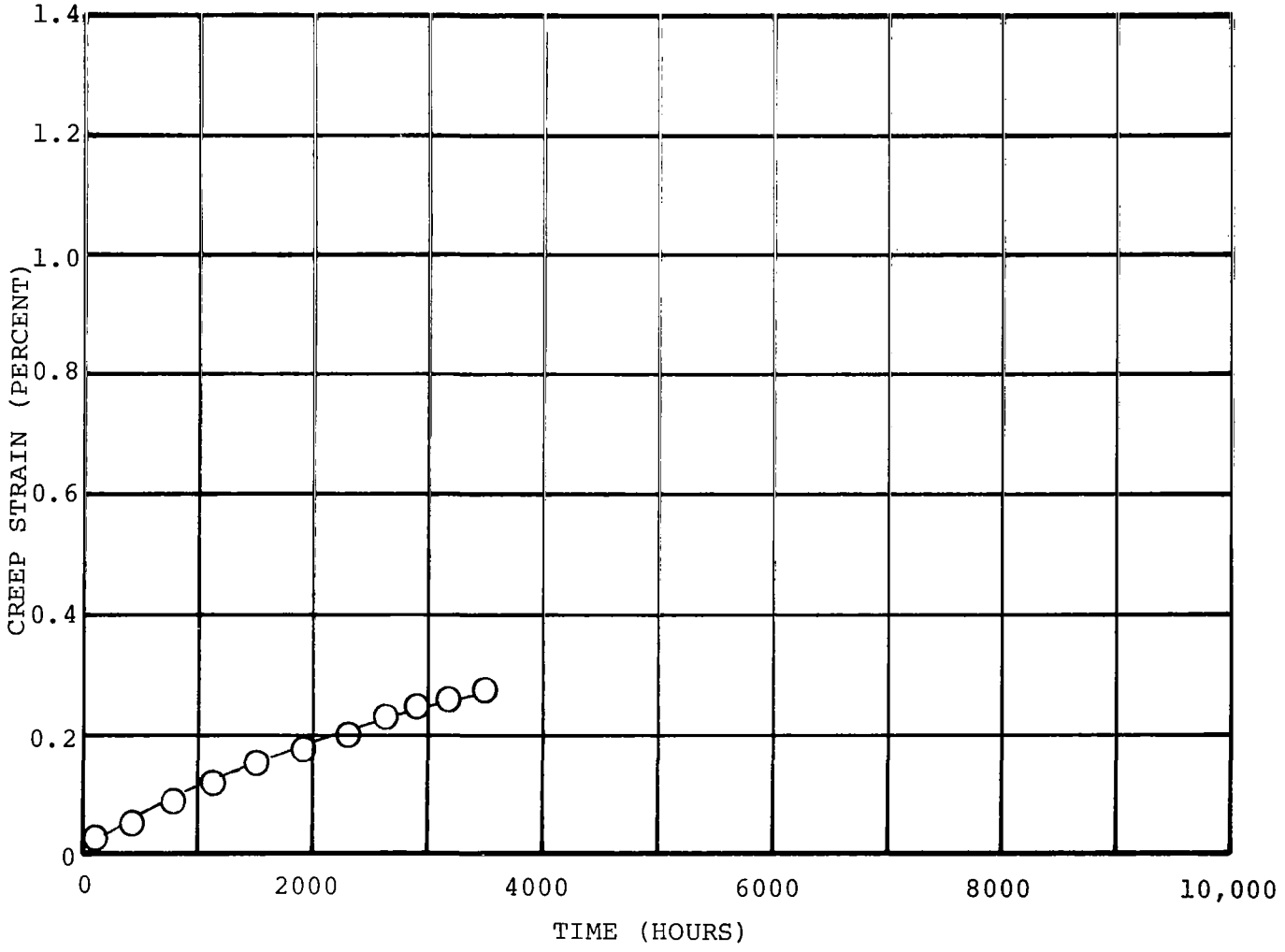

FIGURE V-9. Creep, Nivco Heat 10NO2V-1099, Tested in Vacuum at 1150° F and 15,000 psi. Pressure at Beginning of Test 9.0×10^{-7} torr and at End of Test 5.9×10^{-9} torr (Specimen No. 7)

In a space rotor application the effect of high temperature vacuum on magnetic stability as well as mechanical performance was needed, so the structure sensitive property, coercive force was measured. Table V-2 shows these coercive force measurements taken before and after the vacuum creep tests. An average room temperature coercive force value of 9.2 oersteds was obtained for samples before testing. This value was determined from 36 determinations on 9 specimens. The values ranged from a low value of 8.0 to a high value of 10.4 oersteds. The highest values after test were obtained on the specimens which were creep tested at 1150° F, the Hc in the gage length having increased by a factor of four. The gage length portion of the specimen was under higher stress in the high-vacuum area of the capsule while the ends were outside this area (figure V-1) and at lower stress. Examination shows that time-temperature and stress contribute to the increase in the coercive force after exposure. The data suggest that the peak of the coercive force aging curve had been approached in the 1150° F test and that a change in the material's permeability had resulted. The 1050° and 1100° F tests had not brought about as severe a change, but the coercive force will continue to increase at these temperatures if additional time is accumulated. These data indicate that any study of the aging kinetics of a magnetic rotor alloy must consider its stressed condition as well as the vacuum and temperature environments.

Analyses of interstitial content of Nivco alloy creep specimens were performed before and after creep testing in the vacuum creep capsules (figure V-1). The results of the analyses (table V-3) show that there was no increase in oxygen or nitrogen after testing at 1150° F for 5000 hours or at 1050° F for 10,073 hours. There was an increase in carbon content in both cases; although the absolute value after test remained quite low--100ppm and 75ppm under the two test conditions. The most likely source

TABLE V-2. Coercive Force in Oersteds of Nivco Alloy After Creep Tests Shown in Table V-1 (Room Temperature)

	Specimen Number[a][b]						
	1	2	3	4	5	6	7
End Section	14	18	24	13	25	Not measured	
Gage Section	27	30	49	24	47	Not measured	

(a) Nivco Alloy Heat 10N02V-1099. All specimens heat treated before testing at 1725°F for one hour; water quenched then air aged at 1225°F for 25 hours.
(b) The average coercive force of 9 specimens before test was 9.2 oersteds with a low value of 8.0 and a high value of 10.4.

TABLE V-3. Interstitial Analysis of Nivco Alloy Creep Specimens Before and After Vacuum Creep Tests

Element	Specimen 3		Specimen 2		Specimen 4	
	Content (ppm)		Content (ppm)		Content (ppm)	
	Before Test	After Test of 5006 Hours at 1150°F in Vacuum	Before Test	After Test of 10,007 Hours at 1100°F in Vacuum	Before Test	After Test of 10,073 Hours at 1050°F in Vacuum
Carbon	41	100	40	85	44	75
Oxygen	10	8	9	12	9	8
Nitrogen	6	6	5	6	5	5

of the carbon was back-diffusion from the liquid nitrogen trapped oil diffusion pump which was used to rough-down the system before starting the ion pump. The low level of interstitial pick-up during the 10,000-hour test confirms the suitability of the vacuum creep capsule for creep tests at low pressure.

Spark source mass spectrographic analyses were performed on specimens Nos. 2 and 4 before test and after 10,000-hour creep tests to determine possible variance of chemistry from the center to the edge of the specimen cross-section (table V-4).

Only zirconium chemistry appeared to vary from the center of the specimen cross-section to the edge, but this variance also appeared in the before-test condition.

No conclusive evidence of change in internal chemical composition could be attributed to long-term creep testing.

Metallographic examination of the Nivco long-term creep specimens by light microscopy revealed an approximate ASTM 7 equivalent grain size before testing. The grain size was just slightly larger after 10,000 hours creep test. Figure V-10 shows typical micrographs of Nivco creep specimens before and after creep tests. A rather uniform network of discontinuous (cellular) precipitate had formed at the grain boundaries during the 10,000-hour creep test.

To aid the design engineer in predicting creep performance of Nivco alloy at various temperatures the creep data have been reduced to Larson-Miller Parameters and plotted on figure V-11.

TABLE V-4. Chemical Analysis[a] of Nivco Alloy Heat No. 10NO2V-1099 Before and After Vacuum Creep Tests

Element[b] (Atomic %)	Composition (atomic percent)[b]							
	Specimen 2 Before Test		Specimen 2 after 10,007 Hours Test at 1100°F and 37,500 psi stress		Specimen 4 Before Test		Specimen 4 after 10,073 Hours Test at 1050°F and 50,000 psi stress	
	Center	Edge	Center	Edge	Center	Edge	Center	Edge
Ni	23	23	23	23	23	23	23	23
Ti	1.7	1.7	1.7	1.7	1.7	1.7	1.7-3	3
Mn	0.3	0.3	0.3	0.3	0.3	0.3	0.3	0.3
Zr	0.16	0.17-0.5	0.25	0.2-0.5	0.25	0.2-0.5	0.16-0.5	1.2-1.6
Fe	0.04	0.04	0.04	0.04	0.04	0.04	0.04	0.04
Cu	0.001	0.001	0.001	0.001	0.001	0.001	0.001	0.001-0.01
Si	0.2	0.2	0.2	0.2	0.2	0.2	0.2	0.2
Al	0.3	0.3	0.3	0.3	0.3	0.3	0.3	0.3
Cr	0.003	0.003	0.003	0.003	0.003	0.003	0.003	0.003
V	0.001	0.001	0.001	0.001	0.001	0.001	0.001	0.001

(a) Analysis performed using a Spark source mass spectrograph.
(b) With reference to nickel content of 23 atomic percent, when two values are shown, it indicates a variation in replicate determinations. This in turn reflects a variation distribution of a zirconium-rich phase or precipitate. Variation in titanium was shown in one case.

Two creep tests did not reach 10,000 hours by the end of the program. One of these, at 1150° F, was put on test at a stress level (15,000 psi) low enough to avoid or just approach third stage creep in 10,000 hours. This was done to better define the slope of the Larson-Miller curve (figure V-11). The other was the 1000° F, 55,000 psi specimen which was being run for replication.

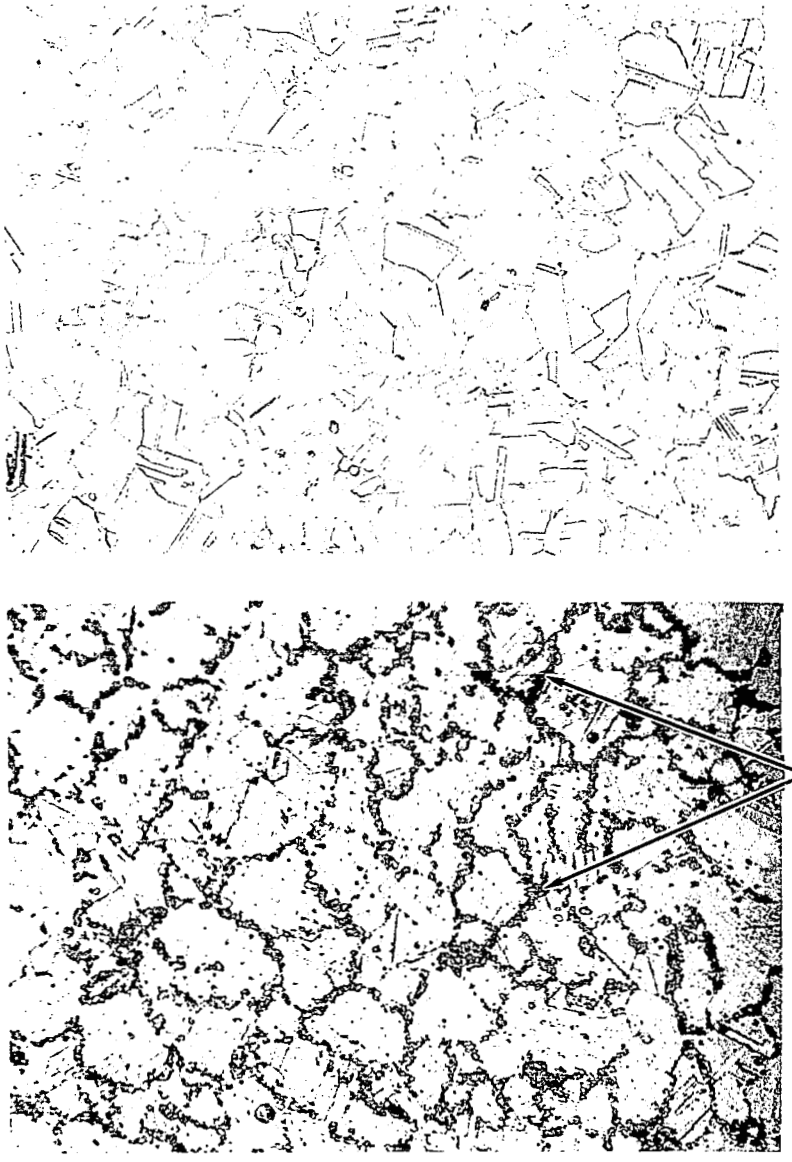

FIGURE V-10. Photomicrographs of Nivco Alloy Before and After 10,000-hour Creep Test. 500X

Etchant: 20 ml Hcl, 40 ml HNO_3, 60 ml glycerine

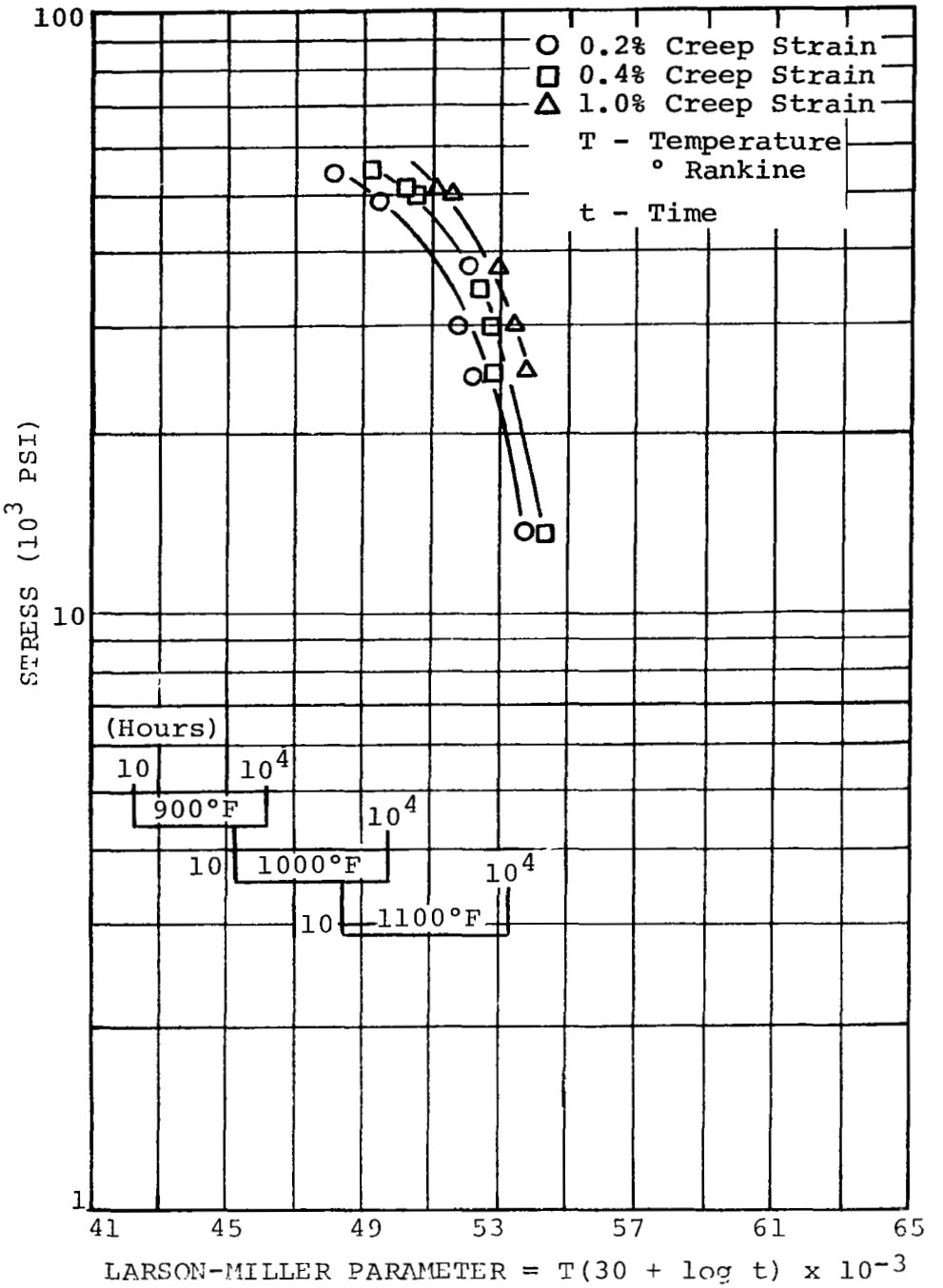

FIGURE V-11. Larson-Miller Plot of Nivco Alloy Bar in Vacuum (10^{-9} torr) Based on 10,000-Hour Test Data

D. CONCLUSIONS

1) Ten-thousand hour vacuum creep data were provided on Nivco alloy, which is a commercially available high-temperature magnetic alloy.

2) At stresses above 37,500 psi, Nivco alloy exhibits a rapid increase in creep rate at temperatures above 1100° F.

3) The vacuum creep capsule provides a good economical method of creep testing for pressure requirements as low as $1x10^{-9}$ torr and at temperatures to 1200° F, with very little increase in oxygen and nitrogen content in the creep specimen.

SECTION VI

REFERENCES

II-1 Bozarth, R. M.: Ferromagnetism, D. VanNostrand Co., Fig. 5-77, p. 162; Fig. 5-80, p. 165, 1951.

II-2 Preuss A.: A Dissertation, Magnetic Properties of Fe-Co Alloys at Different Temperatures, Univ. Zurich, 1912.

II-3 Elmen, G. W.: "Magnetic Alloys of Iron, Nickel and Cobalt," J. Franklin Institute, v. 207, p. 583, 1929.

II-4 Pshchenkova, G. V.; and Skokov, A. D.: "The Temperature Dependence of Magnetic Induction in Fe-Co Alloys," Physics of Metals and Metallography, USSR, v. 14, p. 797, 1962.

II-5 Decker, R. F.; and DeWitt, R. R.: "Trends in High Temperature Alloys," Journal of Metals, v. 17 No. 2, p. 139, 1965.

II-6 Decker, R. F.; and Floreen, S.: Precipitation from Substitutional Iron Base Austenitic and Martensitic Solid Solutions, Symposium; Precipitation from Iron Base Alloys, Intersc. Div., John Wiley, in press.

II-7 Decker, R.F.; Yeo, R.B.; Eash, J.T.; and Bieber, C.G.: "Maraging Steels," Materials in Design Engineering, May 1962.

II-8 Decker, R. F.; Eash, J. T.; and Goldmann, A. J.: "18% Nickel Maraging Steel," Trans. ASM, v. 55, p. 58, 1962.

II-9 Floreen, S.; and Decker, R. F.: "Maraging Steel for 1000° F Service," Trans. ASM, v. 56, p. 403, Sept. 1963.

II-10 Sadowski, E. P.; "Development of 12% Nickel Maraging Steel," ASM, Metals Engrg., v. 5, p. 56, 1965.

II-11 Kueser, P. E.; Pavlovic, D. M.; Lane, D. H.; Clark, J. J.; and Spewock, M.: "Properties of Magnetic Materials for Use in High-Temperature Space Power Systems," NASA SP-3043, 1967.

II-12 Freche, J. C.; Ashbrook, R. L.; and Klima, I. J.: "Cobalt Base Alloys for Space Power Systems," J. Metals, v. 15, p. 928, 1963.

II-13 Cochardt, A.: "Die Anwendung des Magneto-Mechanischen Effectes für Leigerungen mit Hoher Dampfung und Festigkeit," Z. Metallkunde, v. 50, p. 203, 1959.

II-14 Schramm, J.: "Das Dreistoffsystem Nickel-Kobalt-Aluminum," Z. Metallkunde, v. 55, p. 403, 1941.

II-15 Detert, K.; and Pohl, G.: "Untersuchung über die Ausscheidungsvorgänge in Nickel-Kobalt Legierungen mit Aluminum-Titan Zusätzen," Z. Metallkunde, v. 55, p. 35, 1964.

II-16 Detert, K.; and Pohl, G.: "Untersuchungen über die Ausscheidungsvorgänge in Co-Ni Legierungen mit Al and Ti Zusätzen," Z. Metallkunde, v. 57, 1966.

II-17 Hagel, W. C.; and Beattie, H. J.: "High Temperature Aging Structures in ν Hardened Austentic Alloys," Trans. AIME, v. 215, p. 967, 1959.

II-18 Pfiefer, W. A.: Levitation Melting, "A Survey of State-of-the-Art," J. of Metals, v. 17, p. 487, May 1965.

II-19 Detert, K.: "Investigation of the Transformation and Precipitation Process in 15% Maraging Steel," Trans. ASM, v. 59, p. 262, 1966.

II-20 Detert, K.: "Untersuchungen des Ausscheidungsverhaltens in Hochfasten Martensitaushärtenden Nickelstählen," Archiv Eisenhüttenw. v.37, 1966.

II-21 Chen, C. W.: "Temperature Dependence of Magnetic Properties of Silicon-Iron," J. Appl, Phys., v. 29, p. 1337, 1958.

II-22 Bozarth, R. M.: Ferromagnetism, D. VanNostrand Co., p. 160, 1951.

II-23 Mihalisin, J. R.; and Decker, R. F.: "Phase Transformations in Nickel-Rich Nickel-Titanium-Aluminum Alloys," Trans. AIME, v. 218, p. 507, 1960.

II-24 Speich, G. R.: "Cellular Precipitation in an Austenitic Fe-30Ni-6Ti Alloy," Trans. AIME, v. 227, p. 754, 1963.

II-25 Detert, K.; and Pohl, H.: "Investigation of Precipitation Processes in Co-Ni Alloys with Al and Ti additions," Z. Metallkunde, v. 57, 1966.

II-26 Floreen, S.: "Hardening Behavior of Ternary Alloys Based on Iron, 18% Nickel," Trans, ASM, v. 57, p. 38, 1964.

II-27 Floreen, S.; and Speich, G. R.: "Some Observations on the Strength and Toughness of Maraging Steels," Trans. ASM, v. 57, p. 714, 1964.

II-28 Detert, D.; and Pohl, H.: "Untersuchungen über die Ausscheidungsvorgänge in Kobalt-Nickel-Legierungen mit Aluminium and Titan-Zusätzen," Z. Metallkunde, v. 55, p. 36, 1965.

II-29 Detert, K.; and Pohl, H.: "Untersuchungen über die Ausscheidungsvorgänge in Nickel-und Nickel-Kobalt-Legierungen mit Aluminium-Titan-Zusätzen," Z. Metallkunde, v. 55, p. 36, 1965.

II-30 Hornbogen, E.; and Kreye, H.: "Anomale Anderungen des spez. Elektrischen Widerstandes in Nickel-Aluminium-Legierungen," Z. Metallkunde, v. 47, p. 122, 1966.

II-31 Mihalisin, J. R.; and Decker, R. F.: "Phase Transformations in Nickel-Rich Nickel-Titanium-Aluminium Alloys," Trans. AIME, v. 218, p. 507, 1960.

II-32 Mitchell, W. I.: "Über das Auschärtungsverhalten Einer Komplexen Legierung auf Nickel Basis," Z. Metallkunde, v. 55, p. 613, 1955.

II-33 Dragsdorf, R. D.; and Forgen, W. D.: "The Intermetallic Phases in the Co-Ta System," Acta. Cryst., v. 15, p. 531, 1962.

II-34 Miller, G. P.; and Mitchell, W. J.: "Structure of Nickel-Cobalt-Molybdenum Maraging Steels in the Air Cooled Condition," J. Iron Steel Inst., v. 203, p. 899, 1965.

II-35 Mihalisin, J. R.: "Age Hardening and Structure of Iron-Nickel-Cobalt Alloys," ASM Trans. Quart. v. 59, p. 60, 1966.

II-36 Massalski, T. B.: "The Mode and Morphology of Massive Transformations in Cu-Ga, Cu-Zn, Cu-Zn-Ga, and Cu-Ga-Ge Alloys," Acta. Met v. 6, p. 243, 1958.

II-37 Fleetwood, M. J.; Higgonson, G. M.; and Miller, G. P.: "The Identification of Precipitates in Maraging Steels by Electron Microscopy and Electron Probe X-ray Microanalysis," Brit, J. of Appl, Phys., v. 16, p. 645, 1965.

II-38 Hagel, W. C.; and Beattie, Jr., H. J.: "High Temperature Aging Structures in Hardened Austenitic Alloys," Trans. AIME, v. 215, p. 967, 1959.

II-39 Guard, R. W.; and Westbrook, J. H.: "Alloying Behavior of Ni_3Al (γ phase)," Trans. AIME, v. 215, p. 807, 1959.

III-1 Preuss, A.: A Dissertation, Magnetic Properties of Fe-Co Alloys at Different Temperatures, Univ. Zurich, 1912.

III-2 Pscheakova, G. V.; and Skokov, A. D.: "The Temperature Dependence of Magnetic Induction in Fe-Co Alloys," Physics of Metals and Metallography, USSR, v. 14, p. 797, 1962.

III-3 Hansen, M.: Constitution of Binary Alloys, McGraw Hill, 1958.

III-4 Pfiefer, W. A.: "Levitation Melting, A Survey of State-of-the-Art," J. of Metals, v. 17, p. 487, May 1965.

III-5 Masumoto, H.: "On a New Transformation of Cobalt and the Equilibrium Diagrams of Nickel-Cobalt and Iron-Cobalt Alloys," Sci. Rept., Tohoku Univ., v. 15, p. 469, 1926.

III-6 Ellis, W. C.; and Greiner, E. S.: "Equilibrium Relations in the Solid State of the Iron Cobalt System," Trans. ASM, v. 29, p. 415, 1941.

IV-1 Watkinson, J. F.: "Atomization of Metal and Alloy Powders," Powder Metallurgy, No. 1/2, 1958, pp. 13-23.

IV-2 Towner, R. J.: "Atomized Powder Alloys of Aluminum," Metal Progress, May 1958, v. 73, pp. 70-76, 176, 178.

IV-3 Holtz, F. C.: "Development of Improved Cutting Tool Materials," Interim Engineering Progress Report, 25 April 1964 - 24 July 1964, IR-7-714 (VII), pp. 13-21, AD-445024, Contract AF 33(657)-8786, IIT Research Institute, Chicago, Illinois.

IV-4 Reen, O. W.: "Development of Dispersion Hardened Cobalt Alloys from Atomized Powder," 1965 International Powder Metallurgy Conference June 14-17, 1965, New York.

IV-5 Meddings, B.; Kunda, W.; and Mackiw, V. N.: "The Preparation of Nickel-Coated Powders," Powder Metallurgy, Edited by Leszynski, W., pp. 775-798, 1961, Interscience Publishers, Inc., New York.

IV-6 Holmgren, J. D.; Gibson, J. O.; and Sheer, C.: "Some Characteristics of Arc-Vaporized Submicron Particulates," J. Electrochem, Soc., v. III, No. 3, March 1964, pp. 362-369.

IV-7 Bufferd, A. S.; and Grant, N. J.: "Oxide Dispersion Strengthening of Cobalt-Base Alloys," Journees Internationales des Applications du Cobalt, June 9-11, 1964, pp. 1-11.

IV-8 Triffleman, B.: "A New Pre-Alloyed Powder Process and Products," Progress in Powder Metallurgy 1962, v. 18, pp. 156-165, Metal Powder Industries Federation, New York, N. Y.

IV-9 Phelps, R. T.; Gulbransen, E. A.; and Hickman, J. W.: "Electron Diffraction and Electron Microscope Study of Oxide Films Formed on Metals and Alloys at Moderate Temperature," Ind. Eng. Chem., v. 18, June 14, 1946, p. 391.

IV-10 Gulbransen, E. A.; and Andrew, K. F.: "The Kinetics of the Oxidation of Cobalt," J. Electrochem. Soc., v. 98, No. 6, p. 241, June 1951.

IV-11 Preece, A.; and Lucas, G.: "The High-Temperature Oxidation of Some Cobalt-Base and Nickel-Base Alloys," J. Inst. Metals, v. 81, p. 219 1952-1953.

IV-12 Phalnikar, C. A.; Evans, E. B.; and Baldwin, Jr., W. M.: "High Temperature Scaling of Co-Cr Alloys," J. Electrochem. Soc., v. 103, No. 8, pp. 429-438, August 1956.

IV-13 Bridges, D. W.; Baur, J. P.; and Fassell, Jr., W. M.: "Effect of Oxygen Pressure on the Oxidation Rate of Cobalt", J. Electrochem Soc., v. 103, pp. 614-618, 1956.

IV-14 Fisher, B.; and Tannhauser, D. S.: "The Phase Diagram of Cobalt Monoxide at High Temperatures," J. Electrochem. Soc., v. 111, pp. 1194-1196, 1964.

IV-15 Morral, F. R.: "Identification of Corrosion Products on Cobalt and Cobalt Alloys," Corrosion, v. 18, No. 11, pp. 421t-423t, November 1962.

IV-16 Morral, F. R.: "Informative Abstracts on Corrosion of Cobalt and Cobalt Alloys," Cobalt Information Center, Battelle Memorial Institute.

IV-17 Gulbransen, E. A.; Phelps, R. T.; and Hickman, J. W.: "Oxide Films Formed on Alloys at Moderate Temperature," Ind. Eng. Chem., v. 18, p. 640, October 15, 1946.

IV-18 Hickman, J. W.; and Gulbransen, E. A.: "Electron Diffraction Study of Oxide Films Formed on Alloys of Iron, Cobalt, Nickel and Chromium at High Temperatures," Metals Tech., v. 13, No. 7, pp. 1-26, October 1936, TP 2069.

IV-19 Aukrust, E.; and Muan, A.: "Thermodynamic Properties of Solid Solutions with Spinel-Type Structure: II. The Systems Co_3O_4-Fe_3O_4 at 1200° C" Trans. Met. Soc. AIME, v. 230, No. 6, pp. 1395-1399, October 1964.

IV-20 Aukrust, E.; and Muan, A.: "Activities of Components in Oxide Solid Solutions: The Systems CoO-MgO, CoO, and Co-"FeO" at 1200° C," Trans, Met. Soc. AIME, v. 227, No.6, pp. 1378-1380, December 1963.

IV-21 Brazing Manual, American Welding Society, 1963, p. 62.

IV-22 Chang, W. H.: "A Dew Point-Temperature Diagram for Metal-Metal Oxide Equilibria in Hydrogen Atmospheres," Welding Journal, v. 35, No. 12, pp. 662-s to 624-s, December 1956.

IV-23 Preece, A.; and Lucas, G.: "The High-Temperature Oxidation of Some Cobalt-Base and Nickel-Base Alloys," J. Inst. Metals, v. 81, p. 219, 1952-53.

IV-24 Lund, C. H.; and Wagner, H. J.: "Oxidation of Nickel and Cobalt Base Superalloys," DMIC Report 214, March 1, 1965, p. 3.

IV-25 Hagel, W. C.: "The Oxidation of Iron, Nickel, and Cobalt Base Alloys Containing Aluminum," paper presented at the 2nd International Congress on Metallic Corrosion sponsored by the National Association of Corrosion Engineers, New York, N.Y., March 11-15, 1963.

IV-26 Wolf, J. S.; and Evans, E. B.: "Effect of Oxygen Pressure on Internal Oxidation of Nickel-Aluminum Alloys," Corrosion, v. 18, No. 4, pp. 129t-136t, April 1962.

IV-27 Komatsu, N.; Bonis, L. J.; and Grant, N. J.: "Some Features of Internal Oxidation of Dilute Copper and Nickel Alloys for Dispersion Strengthening" Powder Metallurgy, Ed. By W. Leszynski, Interscience Publishers, pp. 343-358, 1961.

IV-28 Preston, O.; and Grant, N. J.: "Dispersion Strengthening of Copper by Internal Oxidation," Trans, Met. Soc. AIME, v. 221, No. 1, pp. 164-172, February 1961.

IV-29 Lewis, M. H.; Seebohm, R. H.; and Martin, J. W.: Powder Metallurgy, No. 10, pp. 87-107, 1962.

IV-30 Gatti, A.: "Iron-Alumina Materials," Trans. Met. Soc. AIME, v. 215, pp. 753-755, October 1959.

IV-31 Haverstraw, R. C.: "Final Report on High Temperature Extrusion Lubricants," Technical Documentary Report NR. ML-TDR-64-256, July 1964, Contract AF 33(657)-9141, Air Force Materials Laboratory, Wright-Patterson Air Force Base, Ohio (AD-606243).

IV-32 Black, T. W.: "Better Forging Lubricants Double Die Life," Machinery, October 1965, pp. 99-102.

IV-33 Perlmutter, I.; and De Pierre, V.: "Extruding Refractory Metals," Metal Progress, November 1963, pp. 90-95, 128-136.

IV-34 Sabroff, A. M.: "Lubricants for High-Temperature Metal-Working Process," Metals Engineering Quarterly, May 1963, v. 3, No. 2, pp. 31-35.

IV-35 "Product Information - Glass Lubricants for Metal Forming," Bulletin IC-18, June 15, 1961, Corning Glass Works, Corning, New York.

IV-36 Adachi, M.; and Grant, N. J.: "The Effects of Stored Energy and Recrystallization on the Creep Rupture Properties of Internally Oxidized Copper-Alumina and Copper-Silica Alloys," Trans. Met. Soc. AIME, v. 218, October 1960, pp. 881-887.

IV-37 TD Nickel, Dispersion-Strengthened Nickel, Du Pont Metal Products, Production Information A-41076, E. I. du Pont de Nemours & Co., Wilmington, Delaware.

IV-38 Tracey, V. A.; and Worn, D. K.: "Some Observations on the Cold-Drawing and Annealing Behavior of Nickel Containing a Dispersed Phase of Thoria." Powder Metallurgy, no. 10, 1962, pp. 34-48.

IV-39 Fraser, R. W.; Meddings, B.; Evans, D. J. I.; and Mackiw, V. N.: "Dispersion-Strengthened Nickel by Compaction and Rolling of Powder Produced by Pressure Hydrometallurgy," International Powder Metallurgy Conference, June 14-17, 1965, New York, N.Y.

IV-40 White, J. E.; and Carnahan, R. D.: "A Microplasticity Study of Dispersion Strengthening in TD-Nickel," Trans, Met. Soc. AIME, v. 230, October 1964, pp. 1298-1306.

IV-41 Doble, G. S.; and Quigg, R. J.: "Effects of Deformation on the Strength and Stability of TD Nickel," Trans. Met. Soc. AIME, v. 233, February 1965, pp. 410-415.

IV-42 Sims, C. T.: "Structural Stability in Ni-2 ThO_2 Alloy," Trans. Met. Soc. AIME, v. 227, December 1963, pp. 1455-1457.

IV-43 Inman, M. C.; Zwilsky, K. M.; and Boone, D. H.: "Recrystallization Behavior of Cold Rolled TD-Nickel," Trans. ASM, v. 57, 1964, pp. 701-713.

IV-44 Mincher, A. L. and Klingler, L. J.: "Research on Dispersion-Strengthened Cobalt-Base Alloys," Third Quarterly Progress Report under AF 33(615)-1680, September 1, 1965 to December 1, 1965.

IV-45 Bufferd, A. S.: Sc. D. Thesis, Dept. of Metallurgy, Massachusetts Institute of Technology, 1965.

IV-46 Howard, R. T.; and Cohen, M.: "Quantitative Metallography by Point Counting and Lineal Analysis," Trans. AIME, v. 194, 1947, pp. 413-426.

IV-47 Smith, C. S.: "Microstructure," Trans. ASM, v. 45, 1953, pp. 533-575.

IV-48 Norris, L. F.; Reinhardt, G.; and Cremens, W. S.: "Comparison of Selected Submicron Powder Blending Methods for Dispersion Alloys," NASA TD D-3834, February, 1967.

IV-49 Barrett, C. S.: Structure of Metals, Second Edition, 1952, McGraw-Hill, p. 86.

IV-50 Taylor, A.: X-ray Metallography, 1961, John Wiley & Sons, p. 663.

IV-51 Förster, F.: "Production Unit for the Rapid and Accurate Measurement of the Coercive Force and Its Temperature Dependence," Zeit Metallkunde, v. 46, No. 4, 1955, p. 359.

IV-52 Hoselitz, K.: Ferromagnetic Properties of Metals and Alloys, Oxford, Clarendon Press, 1952, p. 131.

IV-53 Pauthenet, R.: "Magnetic Properties of Cobalt and of Some Cobalt Alloys and Ionic Compounds," Cobalt, No. 26, March 1965, pp. 3-9.

IV-54 Brandstedt, S. B.: "Other Iron and Nickel Base Alloys in Powder Metallurgy," Stainless Steel Powder Seminar, Detroit, Michigan, Feburary 25, 1965, sponsored by Hoeganaes Sponge Iron Corp., Riverton, New Jersey.

IV-55 Fischer, G. W., et. al.: "Complex Shapes by Slip Casting," Interim Progress Report Phase I, May 1964-August 1964, Contract AF 33(657)-1366, General Electric Company, Cincinnati, Ohio AD 444008.

IV-56 Farrell, K.: "Sintering of Atomized Superalloys and a Hardenable Stainless Steel," Int. J. Powder Met., v. 1, no. 3, July 1965, pp. 26-36.

IV-57 Farrell, K.: "Forging Sintered Inconel 713C Powder Compacts," Int. J. Powder Met., v. 2, no. 1, January 1966, pp. 3-5.

IV-58 Stadelmaier, H. H.: "Ternary Borides with the Cubic Chromium Carbide Structure," Met. Soc. AIME, Nuclear Metallurgy, v. 10, 1964, pp. 159-166.

IV-59 Stadelmaier, H. H.; and Hofer, G.: "Cobalt-Rich Corner of the Cobalt-Tantalum-Boron Systems and the Co_{21}-Ta_2B_6 Phase," Metall., v. 18, No. 5, May 1964, pp. 460-462.

IV-60 Stadelmaier, H. H.; and Schobel, J. D.: "Die Kobalteckeim Driestoffsystem Kobalt-Niob-Bor," Metall., v. 20, No. 1, January 1966, pp. 31-32.

IV-61 Tripp, H. P.; and King, B. W.: "Thermodynamic Data on Oxides at Elevated Temperature," J. Am. Cer. Soc., v. 38, no. 12, December 1, 1965, pp. 432-437.

IV-62 Dijkstra, L. J.; and Wert, C.: "Effect of Inclusions on Coercive Force of Iron," Phys. Rev., v. 79, no. 6, September 15, 1950, pp. 979-985.

IV-63 Dijsktra, L.J.: "Relation of Magnetic Properties to Microstructure," Relation of Properties to Microstructure, 1954, pp. 209-232, American Society for Metals, Cleveland.

IV-64 Kerr, J.; and Wert, C.: "Effect of Nitrides on the Coercive Force of Iron," J. Appl. Phy., v. 26, no. 9, September 1955, pp. 1147-1151.

IV-65 Nix, W. D.; and Huggins, R. A.: "Coercive Force of Iron Resulting from the Interaction of Domain Boundaries with Large Nonmagnetic Inclusions," Phys. Rev., v. 135, no. 2A, July 20, 1964, pp. A401-A407.

IV-66 Bozorth, R. M.: Ferromagnetism, pp. 825-828, 1951, D. Van Nostrand Co., Inc., New York.

IV-67 Smith, C. S.: "Grains Phases and Interfaces; An Interpretation of Microstructure," AIME Trans., v. 175, 1948, p. 47.

IV-68 Ashby, M.: "The Hardening of Metals by Non-Deforming Particles," Z. Metallkunde, v. 55, no. 1, 1964, pp. 5-17.

IV-69 Mincher, A. L.; Pollock, W. I.; and Klingler, L. J.: "Research on Dispersion Strengthened Cobalt Base Alloys," Second Quarterly Progress Report under AF33(615)-1680, June 1, 1965 to September 1, 1965.

IV-70 Mincher, A. L.: "Dispersion-Strengthened Cobalt Alloys," Cobalt No. 32, September 1966, pp. 119-123.

IV-71 Kneller, E.: "A Contribution to the Temperature Dependence of the Properties Affecting the Technical Magnetization Curve of Nickel," Beiträge Zur Theorie des Ferromagnetismus und der Magnetisierungskurve," W. Köster, Ed., 1956, pp. 127-130, Springer - Verlag, Berlin.

IV-72 Kneller, E.: Ferromagnetismus, 1962, Springer-Verlag, Berlin.

IV-73 Zener, C.: "Classical Theory of the Temperature Dependence of Magnetic Anisotropy Energy," The Physical Review, v. 96, no. 5, December 1, 1954, pp. 1335-1337.

IV-74 Carr, Jr., W. J.: "Secondary Effects in Ferromagnetism," Handbuch der Physik, Encyclopedia of Physics, S. Flugge, E., v. 18, No. 2, pp. 322, 326 and 327.

Reports published on this program are:

Kueser, P. E., et al: "Development and Evaluation of Magnetic and Electrical Materials capable of Operating in the 800° to 1600° F Temperature Range", First Quarterly Report, NASA-CR-54354, March 1965.

Kueser, P. E., et al: "Development and Evaluation of Magnetic and Electrical Materials Capable of Operating in the 800° to 1600° F Temperature Range", Second Quarterly Report, NASA-CR-54355, June 1965.

Kueser, P. E., et al: "Development and Evaluation of Magnetic and Electrical Materials Capable of Operating in the 800° to 1600° F Temperature Range", Third Quarterly Report, NASA-CR-54356, September 1965.

Kueser, P. E., et al: "Development and Evaluation of Magnetic and Electrical Materials Capable of Operating in the 800° to 1600° F Temperature Range", Fourth Quarterly Report, NASA-CR-54357, December 1965.

Kueser, P. E., et al: "Development and Evaluation of Magnetic and Electrical Materials Capable of Operating in the 800° to 1600° F Temperature Range", Fifth Quarterly Report, NASA-CR-54358, March 1966.

Kueser, P. E., et al: "Development and Evaluation of Magnetic and Electrical Materials Capable of Operating in the 800° to 1600° F Temperature Range", Sixth Quarterly Report, NASA-CR-54359, June 1966.

Kueser, P. E., et al: "Development and Evaluation of Magnetic and Electrical Materials Capable of Operating in the 800° to 1600° F Temperature Range", Seventh Quarterly Report, NASA-CR-54360, September 1966.

APPENDIX

PROCUREMENT INFORMATION

FOR

NIVCO COBALT ALLOY BAR

December 26, 1967

Prepared For

THE NATIONAL AERONAUTICS AND SPACE ADMINISTRATION

Contract NAS3-6465

Materials Development Section
Systems Research and Development Department
Aerospace Electrical Division
Westinghouse Electric Corporation
Lima, Ohio 45802

Procurement Information for Nivco Cobalt Alloy Bar

1. This specification covers vacuum melted "Nivco" cobalt alloy bar.

2. PROCESS: The alloy shall be vacuum melted.

3. CONDITION: The bars shall be hot rolled, solution and precipitation treated.

4. HEAT TREATMENT: The bars shall be solution treated by heating to 927° - 954°C (1700° - 1750°F), holding at temperature for one hour and quenching in water. Material shall then be precipitation treated by heating to 649° - 677°C (1200° - 1250°F), holding at temperature for 50 hours and cooling in air.

5. QUALITY: The bars shall be uniform in quality and condition, clean, sound, and free from foreign materials and from internal and external defects detrimental tc fabrication or performance of parts.

6. CHEMICAL COMPOSITION: The bars shall conform to the following requirements as to chemical composition:

			Check Analysis	
			Under Min	Over Max
Carbon, Max	0.05	Percent	-	0.005
Manganese	0.20 - 0.50	"	0.03	0.03
Silicon, Max	0.25	"	-	0.02
Phosphorus, Max	0.01	"	-	0.002
Sulfur, Max	0.02	"	-	0.003
Nickel	22.50 - 24.00	"	0.20	0.20
Titanium	1.60 - 1.80	"	0.05	0.05
Zirconium	0.15 - 0.30	"	0.05	0.05
Aluminum	0.15 - 0.45	"	0.03	0.03
Iron, Max	0.30	"	-	0.05
Cobalt	Remainder		-	-

7. CHECK ANALYSIS: (7.1) Check analyses may be made by the purchaser on finished material representing each lot, using an analytical procedure as agreed upon by the purchaser and the manufacturer.

(7.2) The chemical composition thus determined shall conform to the requirements specified in Section 6.

8. MECHANICAL PROPERTIES: (8.1) The bars shall conform to the following requirements for mechanical properties at room temperature:

Tensile Strength, Psi, Min	150,000
Yield Strength, Psi, Min	95,000
Elongation in 4D, Percent, Min	20
Reduction of Area, Percent, Min	22
*Brinell Hardness, Min	255

*Or equivalent Rc

(8.2) The mechanical properties shall be determined in accordance with ASTM A-370 using the 0.2 percent offset method when determining yield strength.

9. STRESS RUPTURE STRENGTH: A combination plain and notched stress rupture test specimen as shown in Figure 1, maintained continuously at 621°C ± 2°C (1150°F ± 3°F) while an axial load of 55,000 pounds per square inch or greater is applied continuously, shall not rupture in less than 100 hours. The test shall be continued until rupture occurs and the plain bar elongation after rupture shall not be less than 5 percent when measured at room temperature. If the test piece fails in the notch section during any part of the test, or in the smooth section in less than 100 hours, the lot or bars represented by the test piece is not acceptable.

10. GRAIN SIZE: (10.1) The bars shall have an average grain size of ASTM No. 6 or finer.

(10.2) The grain size shall be determined after solution treatment at a magnification of 100 X using either Method A or Method B of ASTM E-112 as follows:

Method A: Count the number of grains in 1 square inch at 100 X and solve for n using the following formula: Number of grain per square inch = 2^{n-1}

where : n = ASTM grain size number.

Method B: Count the number of grains intercepted by a 5-inch line at 100 X and solve for n using the following formula:

n = 3.9 plus 6.64 log (y-1)

where : n = ASTM grain size number

y = Number of grains intercepted by a 5-inch line at 100 X

(10.3) Heat treated bars shall not contain more than 5 percent, by number, of abnormally large grains, i.e., grains more than two ASTM numbers coarser than the average, as determined by microscopic examination of a typical area.

11. REJECTIONS: Materials not conforming to this specification or to authorized modifications will be subject to rejection.

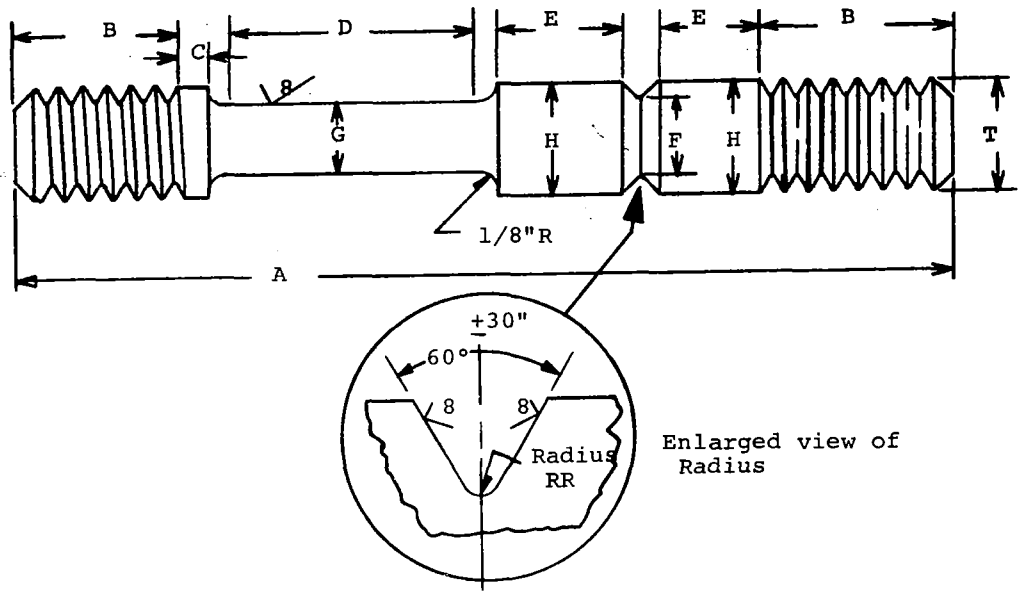

Center Gage Diameter G, Inch	C	D	E	F	H	RR
0.357	1/8	1.5	3/8	0.357	0.500	0.010
0.505	1/8	2.0	3/8	0.505	0.750	0.015
Tolerance ±0.001	+1/32 -0	--	+1/32 -0	+0.001	+0.003	+0.005

NOTES:

1. Surface marked $\sqrt{8}$ finish to 8 microinches or better.
2. The difference between dimensions "F" and "G" shall not exceed 0.001 inch.
3. Taper gage length "D" to center so that diameter "G" at the ends of the gage length exceeds diameter diameter "G" at the center of the gage length by not less than 0.0005 nor more than 0.0015 inch.
4. All sections shall be concentric about the specimen axis within 0.001 inch.
5. Thread size "T" shall be equal to or greater than "H".
6. Dimensions "A" and "B" are not specified.

FIGURE A-1. Combination Smooth-Notch Stress Rupture Test Specimen